Linking Large-Scale Meteorological Conditions to Floods in Mesoscale Catchments

Von der Fakultät Bau- und Umweltingenieurwissenschaften der Universität Stuttgart
zur Erlangung der Würde eines Doktor- Ingenieurs (Dr.-Ing.)
genehmigte Abhandlung

von

Fulya Filiz

aus Adana, Türkei

Hauptberichter: Prof. Dr. rer. nat. Dr.-Ing. habil. András Bárdossy
Mitberichter: Prof. Dr.-Ing. Axel Bronstert

Tag der mündlichen Prüfung: 14. Juni 2004

Institut für Wasserbau der Universität Stuttgart
2005

Heft 137

Linking Large-Scale Meteorological Conditions to Floods in Mesoscale Catchments

von
Dr.-Ing.
Fulya Filiz

Eigenverlag des Instituts für Wasserbau der Universität Stuttgart

D93 Linking Large-Scale Meteorological Conditions to Floods in Mesoscale Catchments

Titelaufnahme der Deutschen Bibliothek

Filiz, Fulya:

Linking Large-Scale Meteorological Conditions to Floods in Mesoscale Catchments / von Fulya Filiz. Institut für Wasserbau, Universität Stuttgart. – Stuttgart: Inst. für Wasserbau, 2005

(Mitteilungen / Institut für Wasserbau, Universität Stuttgart: H. 137)
Zugl.: Stuttgart, Univ., Diss., 2005
ISBN 3-933761-40-9

Herausgegeben 2005 vom Eigenverlag des Instituts für Wasserbau

Druck: Sprint-Digital-Druck GmbH, Stuttgart

Preface

This work is the result of the research project SPHERE (Systematic Palaeoflood and Historical Data for the Improvement of Flood Risk Estimation) sponsored by the European Commission.

The goal of the project was to improve our knowledge on discharge extremes using palaeoflood and historical information. The task of the research group of the Institute of Hydraulic Engineering was to find a link between atmospheric conditions and floods. This extremely difficult problem was investigated by Fulya Filiz during the last 4 years. She developed an interesting new model for downscaling extreme discharges directly from atmospheric conditions, both for present, past and future conditions, using GCM output. Case studies in France and Spain demonstrate the applicability of the method.

Stuttgart, 15.03.2005 Prof. Dr. rer. nat. Dr.-Ing. András Bárdossy

Danksagung

Die vorliegende Dissertationsschrift entstand während meiner Tätigkeit als wissenschaftliche Mitarbeiterin am Institut für Wasserbau der Universität Stuttgart. Die Arbeit wurde im Rahmen des von der Europäischen Union geförderten Forschungsprojektes Systematic Palaeoflood and Historical Data for the Improvement of Flood Risk Estimation (SPHERE) durchgeführt.

Mein herzlicher Dank gilt Herrn Prof. Dr. András Bárdossy für die Übernahme des Hauptberichts und für seine wertvolle Zeit, die er für meine Dissertation investiert hat. Im Rahmen unseres EU-Projektes durfte ich eine hervorragende internationale Zusammenarbeit erfahren, welche mir sehr viel Freude bereitet hat.

Herrn Prof. Dr. Axel Bronstert danke ich besonders dafür, dass er trotz seiner vielfältigen Verpflichtungen sofort bereit war den Mitbericht zu übernehmen. Seine Unterstützung war von großer Bedeutung.

Für die freundliche und warme Atmosphäre möchte ich mich bei allen Mitarbeitern des Instituts bedanken. Ein großes Dankeschön an Prof. Dr.-Ing. Erwin Zehe. Seine Anregungen und Ratschläge kamen stets an der richtigen Stelle und zum richtigen Zeitpunkt. Besonderer Dank gilt ebenso an Dipl.-Ing. Frank Zöller, Dr.-Ing. Uwe Ehret, Dipl.-Geoökol. Fridjof Schmidt und Dr.-Ing. Arne Färber.

Schließlich möchte mich noch bei meinen Eltern Selma und Atilla Filiz, meinem lieben Bruder Çağatay Filiz von ganzem Herzen bedanken, die mir mein Studium in Deutschland durch ihren für mich sehr wichtigen Beistand unterstützt haben.

Table of Contents

List of Figures

List of Tables

List of Symbols

Symbol	Description
α	Stochastic parameter in a statistical downscaling model
α_b	Beta distribution parameter
β_b	Beta distribution parameter
β_w	Weibull distribution parameter
Γ	Gamma function
ε	Independent random component of regional climate in a statistical downscaling model
$\Delta Q(\Delta t)$	Difference in discharge within the time window Δt [m^3/s]
$\Delta Q^+(\Delta t)$	Increase in discharge [m^3/s]
$\Delta Q^-(\Delta t)$	Decrease in discharge [m^3/s]
Δt	Concentration time/ lag time [day]
λ_w	Weibull distribution parameter
μ	All trainings points including {1,.., P}
$\mu(g)$	Membership function
$\mu_k(t)$	Membership grade corresponding to rule k
$\mu^*_k(t)$	Membership grade corresponding to rule k after the reclassification
μ_m	Membership function of the anomalies
μ_m	Membership grade
A	Contribution of the discharge increases within a given CP [%]
A/HH	Wetness index: the ratio between contribution of discharge increases for a given CP and its occurrence rate (high values indicate wet CPs) [-]
c(**x**)	Class label for a given trainings point
CP(t)	CP on a given day
CP(Δt)	CP of the previous day(s)
d^{μ}	Distance between two points
d_E	Euclidean distance
d_M	Mahalanobis distance
D	Dataset

DOF	Degree of fulfillment
F(X)	Relative frequency [%]
g(i t)	Normalized anomalie of gridded pressure data
h(i,t)	Gridded pressure data
$\bar{h}(i,t)$	Mean annual cycle smoothed
HH	Relative occurrence frequency of a CP for a given time period [%]
H_k	The observed frequency of the CP *k*
H_k^*	Corrected frequency of the CP *k* after reclassification
i	Gridpoint. The order of observed data - i^{th} observation
I	Number of gridpoints for which data are available
$I_1(t)$	Bernoulli random variable
$I_2(t)$	Bernoulli random variable
J	Jackknife estimator
k_r	Recession constant dependent on the catchment [-]
k_0	The fuzzy rule selected with the highest DOF value
K	Total number of fuzzy rules
L	Climate parameter
m	Mean discharge increases on a wet day for a given CP [m^3/s]
m	Fuzzy class describing the location of the pressure center. Total number of stochastic parameters in a statistical downscaling model
M	Number of attempt changes in simulated annealing algorithm
$N_{k,m}$	Number of gridpoints which are assigned to class *m* in rule *k*
n	Sample size
O_1	First objective function of the classification
O_2	Second objective function of the classification
O^*	The actual value of the objective function in simulated annealing algorithm
p	Number of variables. Dimension of observations
p_m	Exponents in the DOF function
P	Number of training points
P(X)	Probability of exceedance [%]
P(t)	Precipitation time series
$p(CP(t))$	Probability of a discharge increase on a day with a given CP [%]

$p_{x_0}(z(CP(t))$	Probability of occurrence of increase in discharge with a given CP
$\overline{p}_{z_0}$	Probability of an increase in discharge
q_s	Annealing temperature
q_0	Initial annealing temperature
Q_{max}	Maximum flow [m^3/s]
$Q(t)$	Discharge on a given day [m^3/s]
$Q(t_0)$	Flow where recession starts [m^3/s]
$Q(t-\Delta t)$	Discharge of the previous day(s) [m^3/s]
Q(t)	Discharge time series
R	Regional climate parameter
s	Standard deviation of discharge increases total on a wet day for a given CP [m^3/s]
s(i,t)	Standard deviation for a given date at gridpoint *i*
S^{-1}	Inverse of S (the covariance matrix)
t	Time [days]
t_0	Time where recession starts [days]
t_n	Estimator of a parameter based on sample size of *n*
T	Total number of days
T(t)	Temperature time series
T(X)	Recurrence interval [years]
v	Triangular fuzzy number
v^*	The actual fuzzy class in simulated annealing algorithm
ν_k	Correction factor for the rule *k* obtained by using an optimization method for the reclassification of historical CPs
V	Fuzzy rule system
v(i,k)	Index of the membership function corresponding to selected locations
w_1	Weight for the objective function O_1
w_2	Weight for the objective function O_2
x	Discharge value before transformation
x	Training point
$\mathbf{x}^\mu$	Trainings points within {1,…,P}
x_t	Transformed discharge value [m^3/s]

x	Observations of air pressure [mbar]. A random variable in a model
x_0	Discharge threshold value [m³/s]
$\mathbf{x}(t)$	Vector of air pressure
$\mathbf{y}(t)$	Vector of air temperature
$X(t)$	Beta distributed random variable in $[0, x_0]$
y	Observations of air temperature [°C]
$Y(t)$	Weibull distributed random variable with parameters depending on CP
$\bar{z}$	Mean increase in discharge on an arbitrary day [m^3/s]
z_0	Given threshold limit for discharge [m³/s]
$Z(t)$	Variable for positive discharge differences [m³/s]
$\overline{z(CP(t))}$	Mean increase in discharge with a given CP

Acronyms and Abbreviations

AGCM	Atmospheric General Circulation Model
BALTEX	BALTic Sea Experiment
CA	Cluster Analysis
CEDEX	Centro de Estudios y Experimentación de Obras Públicas, Spain
CFC	Chloroflourcarbon
CP	Circulation pattern
CSIRO-Mk2	Climate Model devepoled at Commonwealth Scientific and Industrial Research Organisation, Australia
DOE	Department of Energy, USA
ECHAM4/OPYC	Climate Model developed at Max Planck Institut für Meteorologie (MPI) and the Deutsches Klimarechenzentrum (DKRZ)
EFAS	European Flood Alert System
GEV	Generalized Extreme Value
GCM	General Circulation Model
GWL	Großwetterlagen
H	Anticyclone (High)
HadCM3	Climate Model developed at Hadley Centre for Climate Prediction and Research, UK
HBV	Hydrologiska Byråns Vattenbalansavdelning (water balance section of the hydrological bureau of the Swedish Meteorological and Hydrological Institute)
HGF	Helmholtz Gemeinschaft Deutscher Forschungszentren
IMPROVE	Improved understanding of past climatic variability from early daily European instrumental sources
IPCC	Intergovernmental Panel on Climate Change
IWS	Institute of Hydraulic Engineering, University of Stuttgart
L	Cyclone (Low)
LAM	Limited Area Models
LARSIM	Large Area Runoff Simulation Model
LSHM	Landscape Scale Hydrologic Model
KIHZ	Natürliche Klimavariationen in Historischen Zeiten bis 10000 Jahre von heute (Natural Climate Variations from 10000 years to the present day)
KS	Kolmogorov-Smirnov Goodness Test
MM	Method of Moments
MLM	Maximum Likelihood Method
MOS	Model Output Statistics
NCAR	National Center for Atmospheric Research, USA
NCEP	National Center for Environmental Research, USA
NN	Nearest Neighbor Method
OGCM	Ocean General Circulation Model
pdf	Probability density function
RCM	Regional Climate Model
REMO	Regional Model
SA	Simulated Annealing
SLP	Sea Level Pressure
SST	Sea Surface Temperature

SPHERE	Systematic Palaeoflood and Historical data improvEment for flood Risk Estimation
Tc	Tropical continental air mass
Tm	Tropical maritime air mass
Pc	Polar continental air mass
Pm	Polar maritime air mass
Am	Arctic maritime air mass
TOPMODEL	Semi-Distributed Topographic Model
USCE	United States Corps of Engineers

Abstract

In recent years, several severe floods with high social and economical impact occurred in many parts of the world including Europe. New and innovative hydrometeorological methods are required for the investigation of the flood phenomenon and for explaining the governing relationships between climate and floods.

The present study aims to provide a better understanding and insight of flood causing weather conditions and to explain the links between climate and floods. Furthermore, the main goal was to establish a stochastic link between large-scale atmospheric information and local-scale variables (i.e. discharge) in mesoscale catchments.

For the investigation of flood-prone weather conditions in the Study Areas, a fuzzy rule-based classification method was used. The objective of the classification was to define circulation patterns which explain the relationships between large-scale atmospheric circulation and the surface climate. The fuzzy rules were optimized with a simulated annealing algorithm.

A stochastic discharge downscaling model was developed in order to establish a *direct link* between circulation patterns and the discharge in the selected basins. Modeling discharge differences instead of discharge enabled the linkage of discharge increases to circulation patterns at a daily time resolution. Thus, increases in discharge were considered as a result of changing weather conditions. Based on the deterministic reaction of the catchment, the discharge decreases were modeled by the linear reservoir approach.

The approach delivered promising results. The critical circulation patterns were identified both for the instrumental and historical period using sea level pressure observations. The downscaling model showed that discharge observations can be successfully used to explain flood conditions. Based on the historical climate reconstructions, the occurrence frequency of possible past floods indicated high variability within the simulation period.

Zusammenfassung

Einleitung

Hochwasser entsteht als Folge extremer Wettersituationen und zählt zu den häufigsten auftretenden Katastrophen weltweit. In den letzten Jahren wurde in vielen Teilen der Welt von einer Vielzahl von Hochwasserereignissen mit großen Schäden berichtet. Im Zeitraum von 1980 bis 2002 haben sich auch in Europa viele Flutkatastrophen ereignet. Die häufigsten Hochwasserereignisse traten in Frankreich, Italien und Großbritannien auf (22 %, 17 %, bzw. 17 % der in Europa gemessenen Ereignisse, Innovation-Report). Im Hinblick auf wirtschaftliche Folgen waren in erster Linie Deutschland und Italien betroffen, beide mit einem Schadensumfang von 11 Milliarden Euro, gefolgt von Spanien und Großbritannien mit einer Schadenshöhe von 6 Milliarden Euro.

Die aktuellen Hochwasserereignisse gaben Anlass zu der Spekulation, dass der anthropogene Treibhauseffekt zu einem Anstieg der Auftrittsrate derartiger Extremereignisse im Klimasystem führe. Der gegenwärtige Wissensstand der Klimaforschung kann einen derartigen direkten Zusammenhang nicht belegen. In heutigen Klimamodellen, die das reale Klima in mathematischen Modellen abbilden, sind einige klimarelevante Prozesse noch nicht zufriedenstellend dargestellt, z.B. die Wirkung von Wolken, Aerosolen oder die veränderliche solare Strahlung. Aus diesem Grund werden verbesserte Klimamodelle benötigt, um konkrete Aussagen über die eventuellen Auswirkungen des Klimawandels zu ermöglichen.

Bronstert (2000) berichtet, dass der Mensch durch Eingriffe in die Natur über verschiedene Faktoren die Entstehung von Hochwasser begünstigen könne. Die anthropogen bedingte Klimaänderung sowie das veränderte Landnutzungsverhalten des Menschen haben das Schadenspotential des Hochwassers deutlich erhöht.

In der vorliegenden Arbeit soll im Folgenden der Zusammenhang zwischen Klima und Hochwasser untersucht werden. Dafür soll ein Link zwischen großräumigen atmosphärischen Variablen (z.B. Druckfelder) und den lokalen, hydrologisch relevanten Parameter (z.B. Niederschlag, Temperatur, Strahlung, hier: Abfluss) in mesoskaligen Einzugsgebieten

hergestellt werden. Dieser Zusammenhang ist von besonderer Bedeutung etwa bei der Abschätzung der Folgen von Klimaänderungen auf das Hochwassergeschehen.

Hochwasserereignisse sind meistens die Folge von ungewöhnlichen Wettergeschehnissen. Um die Entstehung von Hochwasser erklären zu können, wurden bereits zahlreiche Untersuchungen über den Zusammenhang zwischen Klima und Hochwasser durchgeführt. Bei gemäßigtem Klima führen hohe Niederschlagsmengen, die in mesoskaligen Einzugsgebieten innerhalb von kurzer Zeit fallen, in der Regel zu Hochwasser. Es ist offensichtlich, dass es einen engen Zusammenhang zwischen atmosphärischer Zirkulation und klimatischen Variablen gibt. Darauf wurde bereits von vielen Autoren hingewiesen (Bürger, 1958, Lamb, 1977). Es wird in der Regel versucht, die Wettervariablen (Niederschlag, Temperatur) mit den großräumigen, atmosphärischen Variablen, wie Druckfeldern oder anderen abgeleiteten Indizien (Wirbelstromstärke, Stromrichtung), zu verbinden. Wilby et al. (1998) geben einen guten Überblick über die verschiedenen Methoden.

In Duckstein et al. (1993) folgern die Autoren, dass es bestimmte Wetterlagen gibt, die statistisch betrachtet eindeutig öfter vor den Hochwasserereignissen vorkommen als an anderen Tagen. Nach Caspary (1996) ist das Winterhochwasser in Südwestdeutschland die Folge der Zonal-Zirkulationen. Bárdossy (1993), Stahl und Demuth (1999) und viele andere Autoren haben das Auftreten von bestimmten Großwetterlagen (GWL) mit der Niederschlagsmenge in einem bestimmten Einzugsgebiet verknüpft. Im Gegensatz dazu wurde bislang sehr wenig über die Zusammenhänge zwischen großräumigen atmosphärischen Variablen und Abflussmengen geforscht (Duckstein et al., 1993). Diese sollen in der vorliegenden Arbeit mit Hilfe verschiedener Methoden eingehend untersucht werden.

Methodik

Downscaling Methoden für Niederschlag und Temperatur basieren auf der Überlegung, dass tägliche Wettervariablen mit den atmosphärischen Zirkulationen desselben Tages in Verbindung gebracht werden können. Dies ist nicht der Fall für den Abfluss, da der Abfluss meistens aus dem Wetter der vergangenen Tagen resultiert. Das Hauptproblem der Anknüpfung von atmosphärischer Zirkulation an den Abfluss auf täglicher Basis ist vielfältig begründet:

- Die Reaktion des Abflusses im Einzugsgebiet kann sich aufgrund der Konzentrationszeit verzögern.
- Zusätzliche Faktoren im Bezug auf den Zustand des Einzugsgebietes, wie vorhergehende Feuchtigkeit oder Niederschlag sowie die Vegetation, können den Abfluss beträchtlich beeinflussen.
- Hohe Abflüsse können sowohl auf der ansteigenden als auch auf der fallenden Seite der Abfluss-Kurve vorkommen.

Aus diesen oben genannten Gründen ist eine *direkte Verbindung* zwischen atmosphärischer Zirkulation und Abfluss nicht möglich. Um eine direkte Verbindung zu ermöglichen, wurden deshalb im Rahmen dieser Arbeit anstatt die Abflußwerte, die Anstiege im Abfluss mit der atmosphärischen Zirkulation gekoppelt.

Der Anstieg (positive Änderung) im Abfluss ist die Folge des Niederschlags (oder der Schneeschmelze). Der Rückgang (negative Änderung) im Abfluss ist die natürliche Reaktion des Einzugsgebiets, um das Übermaß an Abfluss aus dem Gebiet zu leiten (siehe Abbildung 1). Infolgedessen sind hauptsächlich die Tage mit den Anstiegen für die Hochwasseranalyse interessant. In der vorliegenden Arbeit werden die Anstiege des Abflusses, welche vom Wetter verursacht werden, an die aktuelle atmosphärische Zirkulation gekoppelt. Die negativen Änderungen sind die Folge der deterministischen Reaktionen des Einzugsgebietes auf Überschuss an Abfluss.

Die Schwierigkeit der Anknüpfung von atmosphärischer Zirkulation an Abfluss in großen Einzugsgebieten besteht darin, dass die Wirkung des Niederschlags auf den Abfluss durch die längeren Konzentrationszeiten erst an den folgenden Tagen erkennbar wird. Dennoch kann die Methode in den mesoskaligen Einzugsgebieten mit kurzen Konzentrationszeiten verwendet werden. Darüber hinaus tendieren Großwetterlagen dazu, einige Tage vorzuherrschen, wodurch eine Vereinfachung der Identifikation von kritischen Großwetterlagen entsteht.

Im Rahmen dieser Arbeit sollen die *kritischen* Großwetterlagen in den ausgewählten Einzugsgebieten bestimmt werden. Dafür wird eine Klassifikationsmethode angewendet, welche auf Fuzzy-Logik beruht. Die Details können aus Bardossy et. al (1995) entnommen werden. Die Fuzzy-Regeln wurden nicht von Experten bestimmt, anstatt dessen wurde ein

Optimierungsalgorithmus mit Simulated Annealing (SA) verwendet. Weitere Informationen sind in Bárdossy (2002) zu finden.

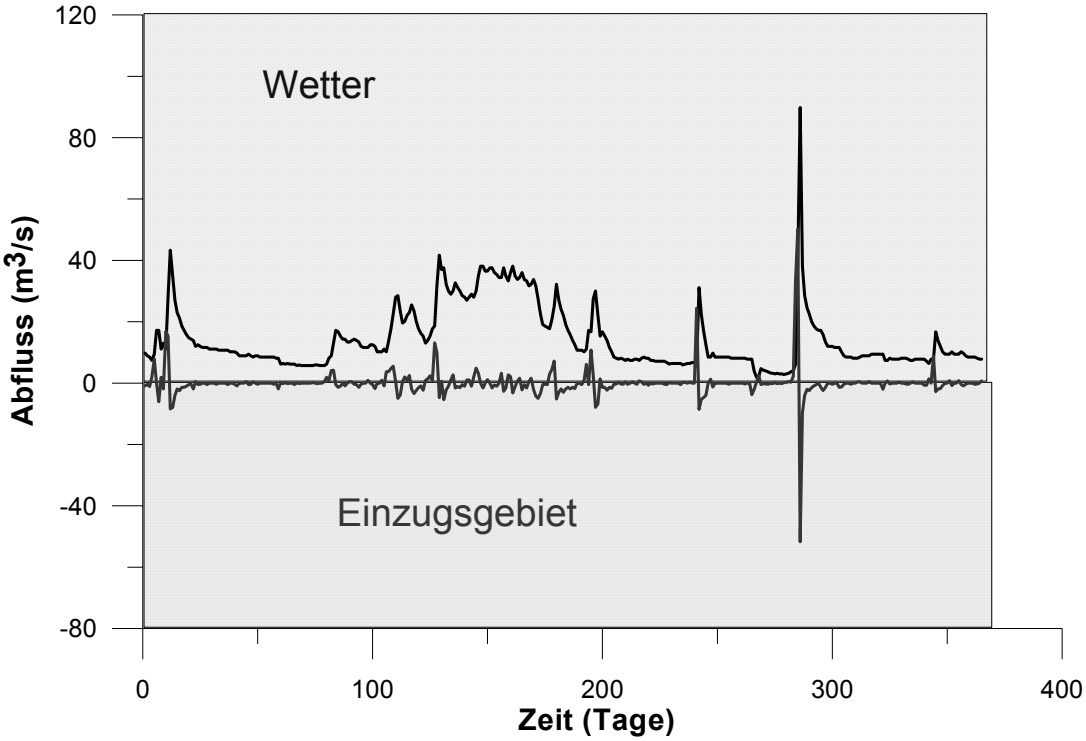

Abbildung 1 Tägliche Differenzen des Abflusses in Ardèche (St.Martin). Anstiege im Abfluss sind die Folge des Wetters wobei die Rückgange als die natürliche Reaktion des Einzugsgebietes betrachtet werden

Die Klassifikation besteht aus einer Datentransformation, der Bestimmung der Fuzzy-Regeln und der Klassifizierung der beobachteten Daten. Bei der Klassifikation werden Bodenluftdruckdaten oder Daten zur Geopotentialhöhe verwendet. Die Voraussetzung hierfür ist die Verfügbarkeit deren täglichen Rasterdaten. Daraus werden die normierten Anomalien berechnet. Für jede Großwetterlage wird eine Fuzzy-Regel bestimmt, so dass jedem Rasterpunkt eine Fuzzy-Zugehörigkeitsfunktion zugewiesen werden kann. Es gibt folgende Möglichkeiten: Die Anomalie an der Stelle (am Gitterpunkt) ist:

- stark positiv
- mittel positiv
- mittel negativ
- stark negativ
- irrelevant (für die Wetterlage)

Zur Klassifikation der Bodenluftdruckkarte wird zunächst die tägliche Bodenluftdruckkarte zu einer täglichen Anomaliekarte transformiert, weiter wird dann für jede Regel der jeweilige Erfüllungsgrad berechnet. Die Regel mit dem höchsten Erfüllungsgrad wird dann angenommen. Anschließend wird dieser Index der Großwetterlage zugewiesen.

Die Qualität der Klassifikation soll dazu dienen, die optimalen Regeln zur Beschreibung der hochwasserverursachenden Wetterlagen zu finden. Das Ziel der Klassifikation ist die Identifizierung eines Regelwerksystems, welches diese kritischen Großwetterlagen optimal beschreibt. Die kritischen Großwetterlagen in den ausgewählten Einzugsgebieten werden in Abbildung 3 und Abbildung 4 dargestellt.

Aus den untersuchten Einzugsgebieten hochwasserrelevante Aussagen ableiten zu können, werden in der Regel atmosphärische Variablen an Niederschlag und Temperatur gekoppelt (Regionalisierungsverfahren) und dann weiter als Input für ein Niederschlag-Abfluss-Modell verwendet. Dies soll die Untersuchung der Abflusscharakteristiken des Einzugsgebietes ermöglichen. Die Probleme dieses Vorgehens liegen in der Unsicherheit und Ungenauigkeit der GCMs und des Downscalings, da weiterhin hydrologische Modelle nur ungenaue Nachbildungen der Natur sein können und somit bei der Berechnung des Abflusses weitere Fehler verursachen. Die Fehler, die bei der Berechnung der Hochwasser entstehen, sind oft am gravierendsten. Da aber Hochwasserereignisse selten auftreten, wird in diesen Fällen viel Aufwand für die Zeiten zwischen den Hochwasserereignissen betrieben, was sich für die Extremwertstatistik als irrelevant herausstellt.

Eine alternative Methode, die im Rahmen dieser Arbeit vorgestellt wird, stellt einen direkten Zusammenhang zwischen dem großräumigen atmosphärischen Geschehen und dem Hochwasser her. Auf der Basis dieser Zusammenhänge zwischen den großräumigen atmosphärischen Variablen und den lokalen Parametern wird ein Abfluss-Downscaling Modell erarbeitet. Dieses dient zur Generierung von Abfluss-Reihen in täglicher Auflösung, welche auf beobachteten Bodenluftdruckdaten oder aus GCM stammenden Klimaszenarien basiert. Somit kann ein direkter Link zwischen groß- und kleinräumigen Variablen in mesoskaligen Einzugsgebieten erstellt werden.

Ein möglicher Vorteil der Betrachtung des Abflusses ist, dass er die gefallene Niederschlagsmenge auf einer großen Fläche aufsummiert, und das bedeutet, dass es weniger von der lokalen Variabilität des Niederschlags beeinflusst werden kann.

Das Abfluss-Modell besteht aus stochastischen Parametern, welche die Differenzen im Abfluss modellieren. Die Anstiege im Abfluss werden durch zwei verschiedene Verteilungsfunktionen modelliert, deren Parameter von GWL abhängig sind. Die Rückgange im Abfluss werden einem linearen Speichermodell nachgebildet. Die generierten Abfluss-Reihen wurden mit dem Kolmogorov-Smirnov Test (KS) getestet. Außerdem wurden die statistischen Parameter wie Mittelwert, Standardabweichung und verschiedene Quantile zwischen Beobachtungen und Simulationen miteinander verglichen. Die Untersuchung lieferte interessante Ergebnisse die im Folgenden erläutert werden.

Anwendung und Ergebnisse

Die oben beschriebene Methodik wurde auf zwei Einzugsgebiete angewandt: Ardèche in Frankreich und Llobregat in Spanien. Ardèche ist ein Nebenfluss der Rhône mit einer Einzugsgebietsgröße von 2350 km². Llobregat fließt durch die Stadt Barcelona zum Mittelmeer. Seine Einzugsgebietsgröße beträgt 4984 km². Abbildung 2 stellt die geographische Lage der beiden Einzugsgebiete dar.

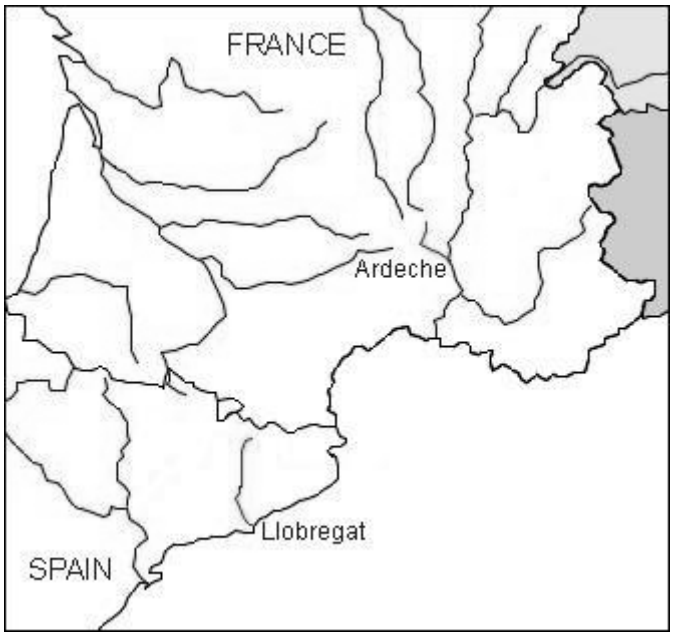

Abbildung 2 Einzugsgebiete Ardèche (Frankreich) und Llobregat (Spanien)

10 Großwetterlagen für Ardèche und 12 Großwetterlagen für Llobregat wurden in der Klassifikation festgestellt und nach der Split Sampling Methode validiert.

Zur Bestimmung des Regelwerksystems wurden Abflussdaten für 10 Jahre (1981-1990) im Optimierungsalgorithmus benötigt. Dieses Regelwerksystem wurde dann in einer Kontrollperiode (1951-1980) geprüft, um zu sehen, ob das Regelwerksystem wichtige Charakteristiken erkennen ließ. Die Werte der Zielfunktion in der Kontrollperiode wurden mit den Werten in der Lernperiode verglichen. In allen Fällen konnte kein erheblicher Unterschied in der Statistik zwischen Lern- und Validierungsperiode festgestellt werden. Dies zeigt, dass das Regelwerksystem die wichtigen Abflusscharakteristiken des Einzugsgebietes wiedergeben konnte.

Tabelle 1 enthält die Ergebnisse des Ardèche Einzugsgebietes in der Periode von Oktober bis April, in der die meisten Hochwasser aufgetreten sind. Hierfür wurde der Anstieg im Abfluss in Zusammenhang mit der herrschenden Großwetterlage betrachtet.

Tabelle 1 Statistik des Anstieges im Abfluss in Zusammenhang mit der herrschenden Großwetterlage in Ardèche Einzugsgebiet (Oktober-April, 1955-1997)

GWL	Häufigkeit des Anstieges	Wahrscheinlichkeit des Anstieges	Anteil	Anteil/HH Feuchtigkeits-index	Mittelwert m^3/s	Stabw. m^3/s
GWL01	7.33	51.13	31.82	**4.34**	113.8	224.6
GWL02	2.27	31.71	2.56	1.13	47.7	189.4
GWL03	5.20	29.43	1.47	0.28	12.9	26.2
GWL04	8.55	47.95	33.73	**3.95**	110.3	216.4
GWL05	1.57	43.53	4.25	**2.71**	83.4	121.7
GWL06	3.93	23.94	1.97	0.50	28.0	53.0
GWL07	15.04	28.10	5.94	0.39	18.8	52.7
GWL08	21.11	25.44	4.98	0.24	12.4	36.1
GWL09	11.11	29.07	4.23	0.38	17.5	50.6
GWL10	19.84	26.79	7.03	0.35	17.7	44.3
nicht definiert	4.04	34.25	2.01	0.50	19.5	40.3

Der Feuchtigkeitsindex einer Wetterlage ist das Verhältnis zwischen dem relativen Anteil der Häufigkeit einer Wetterlage und dem Anteil des Anstiegs, welcher bei der Wetterlage erfolgt. Je höher dieser Index ist, desto höher ist der Anstieg, welcher durch die Wetterlage verursacht wurde.

- Feuchtigkeits-Index < 1 entspricht trockener Wetterlage
- Feuchtigkeits-Index ≈ 1 neutral – weder trocken noch nass
- Feuchtigkeits-Index > 1 nasse Wetterlage

Nach der oben dargestellten Tabelle 1 sind GWL01, GWL04 und GWL05 relevant für den starken Anstieg im Abfluss, wobei GWL01 und GWL04 bzgl. des Hochwassergeschehens eine wichtigere Rolle spielen als GWL05. 70 % der Anstiege haben sich durch diese Wetterlagen (GWL01 und GWL04) ereignet. GWL01 ist äußerst nass, was 434 % des Anstiegs im Vergleich zu einem durchschnittlichen Tag ausmacht (siehe Abbildung 3).

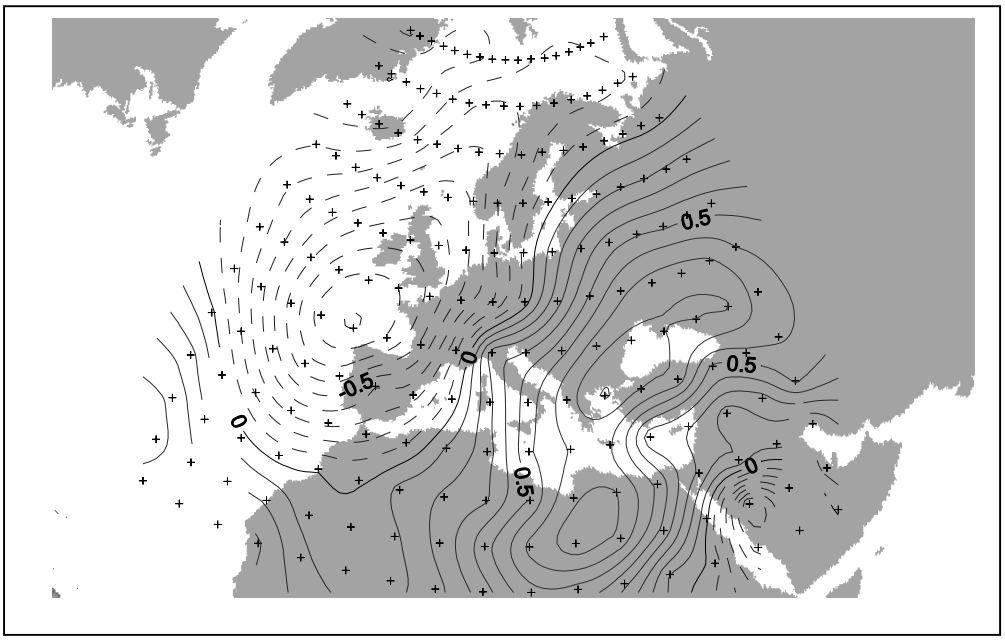

Abbildung 3 Anomalie Karte für den normierten Bodenluftdruck in Ardèche (GWL01). Positive Anomalie (gestrichelte Linie), negative Druckanomalie (durchgezogene Linie)

In Einzugsgebiet Llobregat ist eine einzige Wetterlage für die meisten Anstiege verantwortlich. Die Anstiege, die von anderen Wetterlagen verursacht werden, bleiben stets unter den Durchschnitt. Abbildung 4 stellt eine Karte der Bodenluftdruckanomalien der nassen, hochwasserverursachenden Wetterlage aus dem Llobregat Einzugsgebiet dar.

Die Verteilung der Jahresextreme nach Wetterlagen für das Einzugsgebiet Ardèche wird in Abbildung 5 gezeigt. Daraus wird ersichtlich, dass die bereits als nass eingestuften Wetterlagen GWL01 und GWL04 das Hochwasser verursacht haben. Für die Quantifizierung der Auswirkung von Klimaänderungen auf das Hochwassergeschehen sollte auf das Auftreten und Verhalten dieser Wetterlagen geachtet werden.

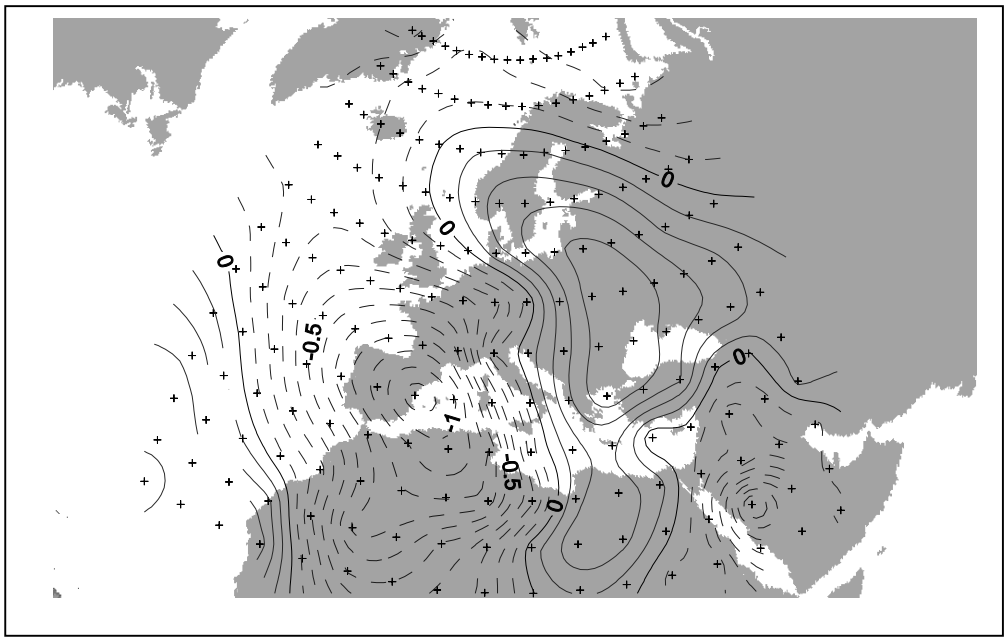

Abbildung 4 Nasse Großwetterlage (GWL09) für das Einzugsgebiet Llobregat

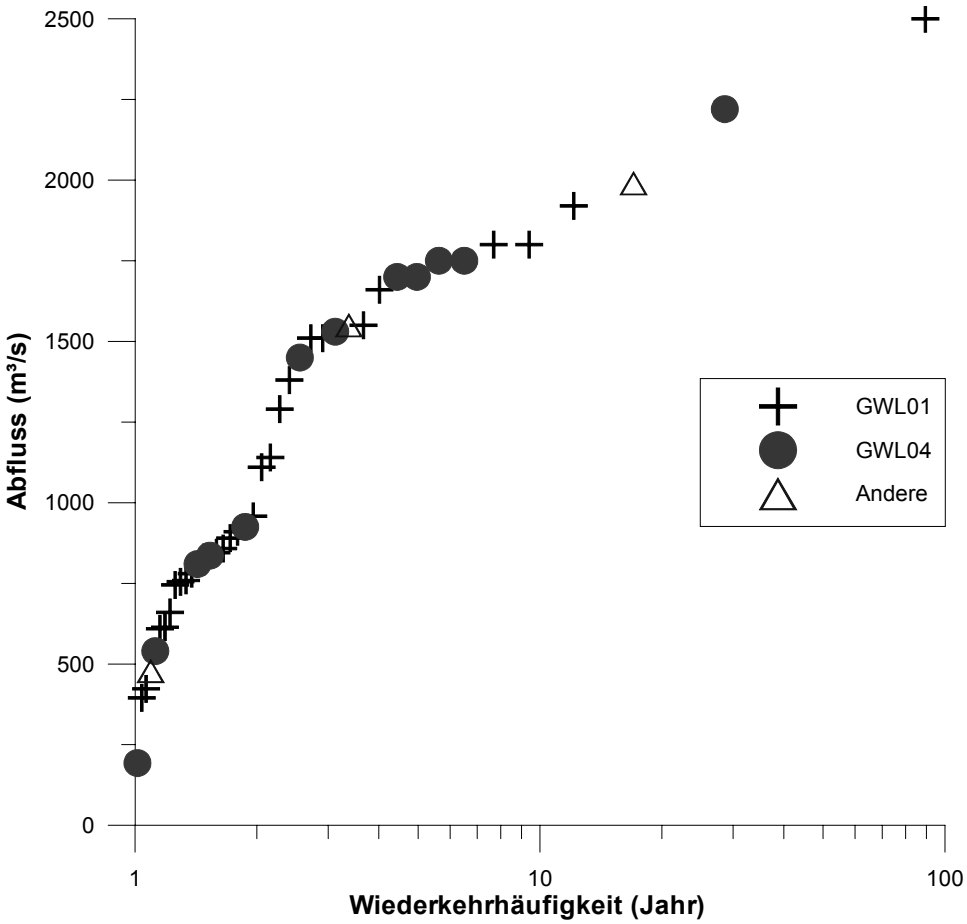

Abbildung 5 Verteilung der Jahresextreme nach verursachender Wetterlage für die Ardèche (St.Martin)

Diskussion und Folgerung

Eine Methodik zur Identifizierung der hochwasserrelevanten Wetterlagen wurde für mesoskalige Einzugsgebiete entwickelt. Die Ergebnisse weisen darauf hin, dass die Anstiege im Abfluss als Indikator zur Identifizierung der hochwasserrelevanten Wetterlagen in mesoskaligen Einzugsgebieten von Bedeutung sind. Eine mögliche Ursache dafür ist der enge Zusammenhang zwischen dem Niederschlag und dem Abfluss in den ausgewählten Einzugsgebieten. Diese Methodik dient u.a. dazu, die Zusammenhänge zwischen meteorologischen Situationen und hydrologischen Reaktionen besser verstehen zu können. Aufgrund der Verzögerung in der hydrologischen Reaktion in großen Einzugsgebieten sollte das Zeitfenster auf die längere Konzentrationszeit entsprechend angepasst werden.

In beiden Einzugsgebieten konnten typische hochwasserrelevante Großwetterlagen identifiziert werden. Das Auftreten dieser Großwetterlagen müsste nicht unbedingt zum Hochwasser führen, dennoch wurde festgestellt, dass alle Hochwasserereignisse durch diese Großwetterlagen verursacht worden sind.

Zwischen Hochwasserereignissen liegen häufig mehrere Jahre. Daher werden für deren Analyse lange Beobachtungsreihen benötigt, um möglichst viele Ereignisse untersuchen zu können. In dieser Arbeit wurden lange Reihen der Bodenluftdruckdaten (NCEP-Reanalysen) untersucht (1899-2003).

GCM Szenarien, welche aus dem KIHZ Projekt resultieren, wurden für die Klassifikation der historischen Großwetterlagen für die letzten 500 Jahre verwendet (1500-1990). Außerdem wurden tägliche Druckfelder mit Hilfe der Bodenluftdruck- und Temperaturdaten aus dem IMPROVE Projekt mit der Nearest Neighbor Methode rekonstruiert (1774-1990). Die Häufigkeit der kritischen GWL hat auf keinen klaren Trend hingewiesen.

Das Downscaling Modell kann für dessen Anwendung in Einzugsgebieten erweitert werden, in denen Schneeschmelze eine bedeutende Rolle bei der Entstehung von Hochwasser spielt. Hierfür müssen Temperaturanstiege in der Klassifikation der GWL berücksichtigt werden.

Basierend auf künftigen Klimaszenarien kann die Vorgehensweise ebenfalls für die Prognose der künftigen Hochwasserereignisse verwendet werden.

Chapter 1

Introduction

Floods are one of the most important catastrophic consequences of extreme weather conditions which might lead to considerable losses of property and life. In recent years, several major floods having high social impact occurred in many parts of the world including Europe. Nearly every year during the last few decades major flooding has happened somewhere on the European continent. For the period 1980-2002, the greatest number of floods occurred in France (22 %), Italy (17 %) and the UK (12 %). The highest number of fatalities occurred in Italy (38 %), followed by Spain (20 %) and France (17 %) (Innovations Report online). The greatest economic losses occurred in Germany and Italy (both € 11 billion), followed by Spain and the UK (both around € 6 billion). These floods which have an average recurrence interval of between 100 and 500 years (USCE, 1996) caused the highest level of damage on record.

In the last decade, much effort has been put into flood risk assessment, flood hazard and risk mapping, flood forecasting and preventative land use planning. For example, the EU Commission is currently developing a European Flood Alert System (EFAS).

Recent flooding highlights the specific need to evaluate societal vulnerability to the response of flooding to global change and climatic vulnerability. Floods becoming a part of our lives incited a new hazard culture – namely, a *living with flood* attitude - which is based on a more integrated approach including measures such as prevention, insurance, forecasting, warning and evacuation, and land use planning. In addition, flood risk education and awareness increased in importance.

The term *flood* is difficult to define. A possible definition of the term could be the inundation caused by a period of unusually large discharge in a river, but even this is quite inaccurate as flooding may occur from sources other than rivers (e.g. the sea and lakes), and the definition of “unusual” is difficult to specify, particularly within a timeframe.

There are many reasons why a river becomes flooded and they almost always relate back to the processes that are a part of the hydrological cycle. Fundamentally rivers flood when there is too much rain to cope with. The extent and size of the flood can often be related to the scale of the basin and other contribution factors that increase the effect of high rainfall such as antecedent soil moisture, deforestration, urbanization, river channel alterations, land drainage and climate change. Other causes of floods are individual events like dam breaks, jökulhlaups (ice-dam bursts) or snowmelt.

1.1 Motivation and Goals

The main scope of the study is to provide a better understanding and insight of flood causing weather conditions and to explain the links between climate and floods in the mesoscale catchments with a size of a few hundreds up to a few thousand square kilometers. The present research was carried out as a part of the SPHERE Project (Systematic, Palaeoflood and Historical data for the improvEment of flood Risk Estimation) funded by the European Union. The project duration was between March 2000 and July 2003. The Institute for Hydraulic Engineering (IWS) at the University of Stuttgart was one of the project partners responsible for the investigation of the links between floods and climate. Within this task, IWS identified the flood-prone large-scale meteorological conditions in the Study Areas – Ardèche in France and Llobregat in Spain – and developed a discharge downscaling method which enables the analysis of possible past and future floods to estimate the flood risk. For the analysis of present and past floods NCEP Re-analysis Data (gridded sea level pressure), past GCM scenarios (KIHZ Project) and historical Point Sea Level Pressure and Temperature data from several stations in Europe (IMPROVE Project) were obtained.

For the purposes of the current study, the identification of the short- and long-term relationships between climatic variability and flooding (on timescales of decades and centuries) is of great importance. Furthermore, the investigation of the changes in frequencies of flood-causing weather conditions and the identification of possible trends might help in the assessment of future flood frequency projections. The following question concerning the increasing frequency of flooding in the recent years, arose in the scientific community:

"*Can we detect any non-stationarity related to anthropogenic effects within the recent flooding or is it just a part of the natural variability of our climate?*"

The answer to this question is *unknown* since the available instrumental climatic and hydrologic data are woefully inadequate for providing concrete answers. All we can indicate is that the anthropogenic factors such as urbanization, changes in the land use and land cover, deforestration and alterations in the river channels and the climate change may have increased the propensity for flooding. Further, the palaeoflood hydrology in Europe consistently shows that the largest floods recorded in the instrumental record were not the largest witnessed by a particular river (i.e. Llobregat and Ardèche). It also provides evidence of past periods, or clusters, of increased flood frequency, e.g. Little Ice Age and Bronze/Iron Age transition (Benito et al., 2003).

The performance of the climatic and hydrologic models has improved considerably in the last decades. Despite the high number of sophisticated models developed, new ideas, more applications and challenging approaches are still sought. New and innovative hydrometeorological methods are required for the investigation of the flood phenomenon and for explaining the complex relationships and interactions in the nature. This work implies *a first application* as well.

The aim of this dissertation is to present a new method to explain flood-prone weather conditions by using *discharge* information observed in the selected basin. Discharge includes significant information in terms of floods, since it is regarded as one of the end- products of precipitation. Hence, it can be integrated into the investigation of flood-causing weather conditions. An automated identification procedure based on fuzzy rules is developed for flood-producing weather situations based on the large-scale observations.

In order to establish a daily link between circulation patterns and flood events, investigation of discharge increases instead of discharge is suggested. This approach is useful in mesoscale catchments with short concentration times.

A new downscaling method, different from conventionally-used downscaling methods, was developed to generate daily discharge time series directly from large-scale atmospheric information. The common way of linking large-scale information to local-scale variables is

usually downscaling of precipitation and temperature from large-scale atmospheric features and to link them to discharge with a rainfall-runoff model. In this work, a stochastic discharge simulation was developed to downscale discharge from atmospheric circulation directly.

The research delivers interesting and promising results. The investigation in both Study Areas provided successful outcomes concluding that there is a strong link between the occurrence of certain circulation patterns and the occurrence of floods in the Studied Regions.

The thesis is structured in seven chapters as follows.

In the following section, Section 1.2, the Study Areas and their characteristics are introduced.

Chapter 2 gives a brief overview of the governing meteorological factors of the flood-producing mechanisms. The principles of weather, climate and global water cycle are revisited here. This is followed by an explanation of the occurrence of precipitation and floods. Finally, a statistical analysis of flood peaks will be discussed.

The context of Chapter 3 is based on the linkage of large-scale information to local-scale parameters in general. It comprises the frequently used methods of classification techniques of circulation patterns and summarizes the broad downscaling methods that are in use. This part concludes with the assessment of consequences of climatic factors at the river basin scale including examples of the conventional approach to downscaling.

Chapter 4 presents the fuzzy rule-based classification method in detail. The principle of CP definition and the critical circulation patterns identified for each basin are presented.

Chapter 5 discusses the discharge downscaling method developed and introduces the results for each basin. The application of the model to historical climate scenarios is covered in Chapter 6.

Chapter 7 concludes the thesis with a discussion and conclusions.

1.2 Study Areas

Two mesoscale study areas have been selected in France and Spain (see Figure 1.1). The first area studied is the Ardèche River, a Rhone tributary with a catchment area of 2350 km², located in the southeastern part of France.

Extreme rainfall intensities in the east part of Massif Central (Cévennes), due to orographical precipitations and simultaneous Mediterranean and oceanic influences, produce extreme floods on the Ardèche River during the autumn season. It is common that high rainfalls producing extraordinary floods in this river affect the southern part of France.

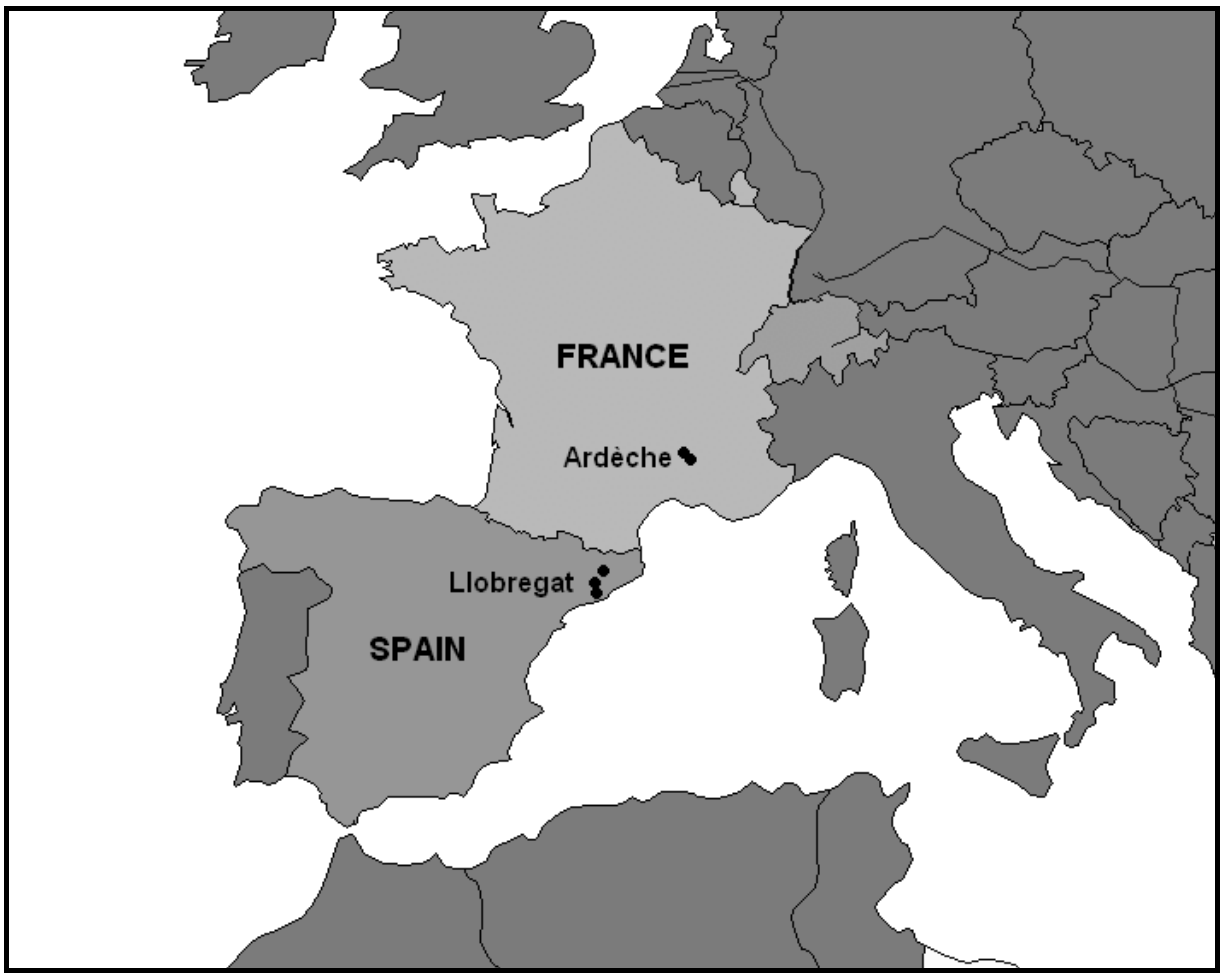

Figure 1.1 Location of Ardèche and Llobregat Rivers.

The second Study Area is the Llobregat Basin in Spain, which is a medium river with a catchment size of 4984 km². It flows to the Mediterranean Sea through the city of Barcelona

passing by the city´s industrial area. It has a typical Mediterranean regime with extreme floods occurring during the autumn season due to very heavy convective storms that mostly contribute to the flood risk in the Llobregat.

In Figure 1.2 the location map of the Ardèche Basin is illustrated.

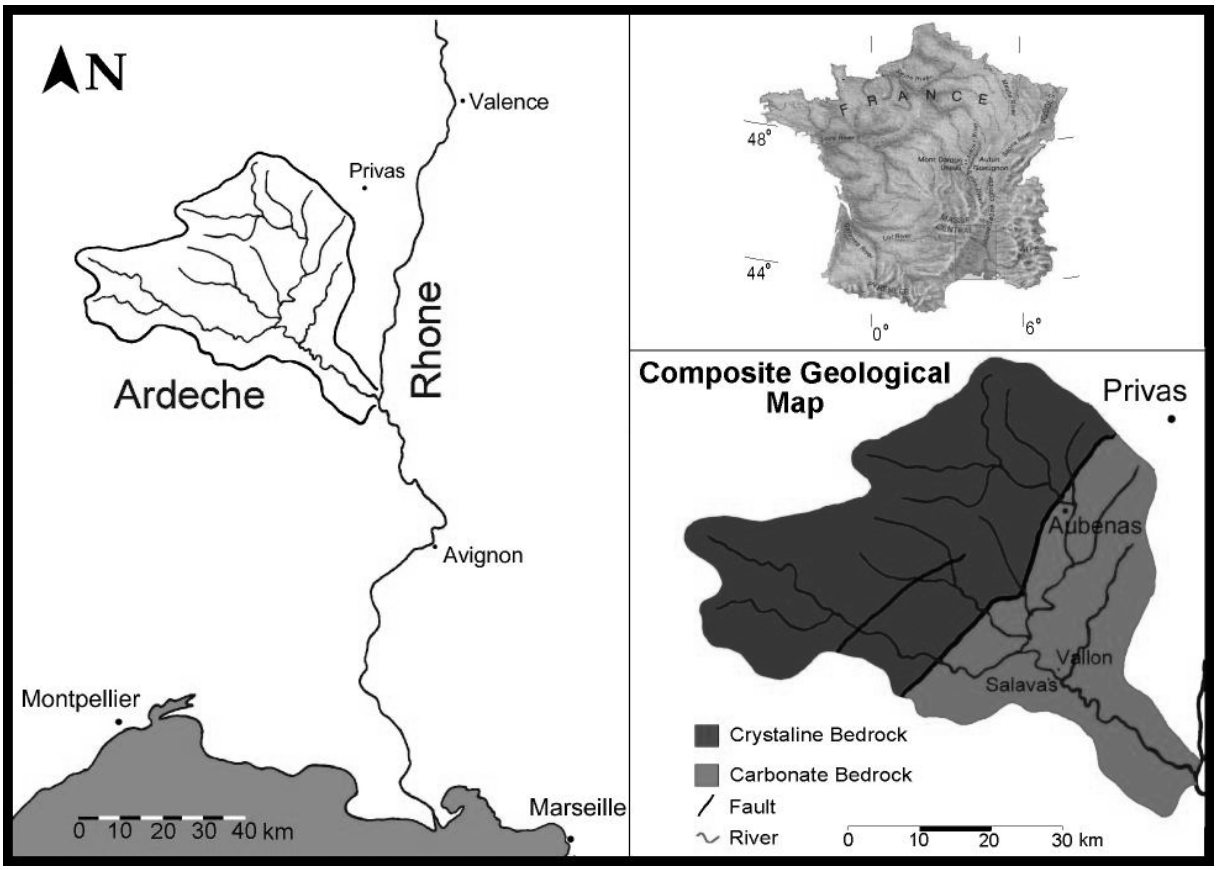

Figure 1.2 Location map of the Ardèche Catchment.

These basins have been selected because they are sensitive to different flood-producing storms which can be easily identified. There are Atlantic and Mediterranean influences within these basins, and therefore the basins are under the influence of different hydroclimatological regimes. In methodological terms, they can represent a wide range of western European areas. Furthermore, extreme floods in these basins affect large urbanized areas (in the case of the Llobregat River, the 5 million inhabitants of Barcelona; the Ardèche River the 150,000 inhabitants of Aubenas).

The Ardèche River has experienced severe floods in the past. Figure 1.3 shows the Ardèche River at Pont d´Arc in Summer 2000 and Figure 1.4 depicts the 1890-flood at the same place. The arc can hardly be recognized due to the enormous amount of water.

Figure 1.3 Ardèche at Pont d´Arc in Summer 2000.

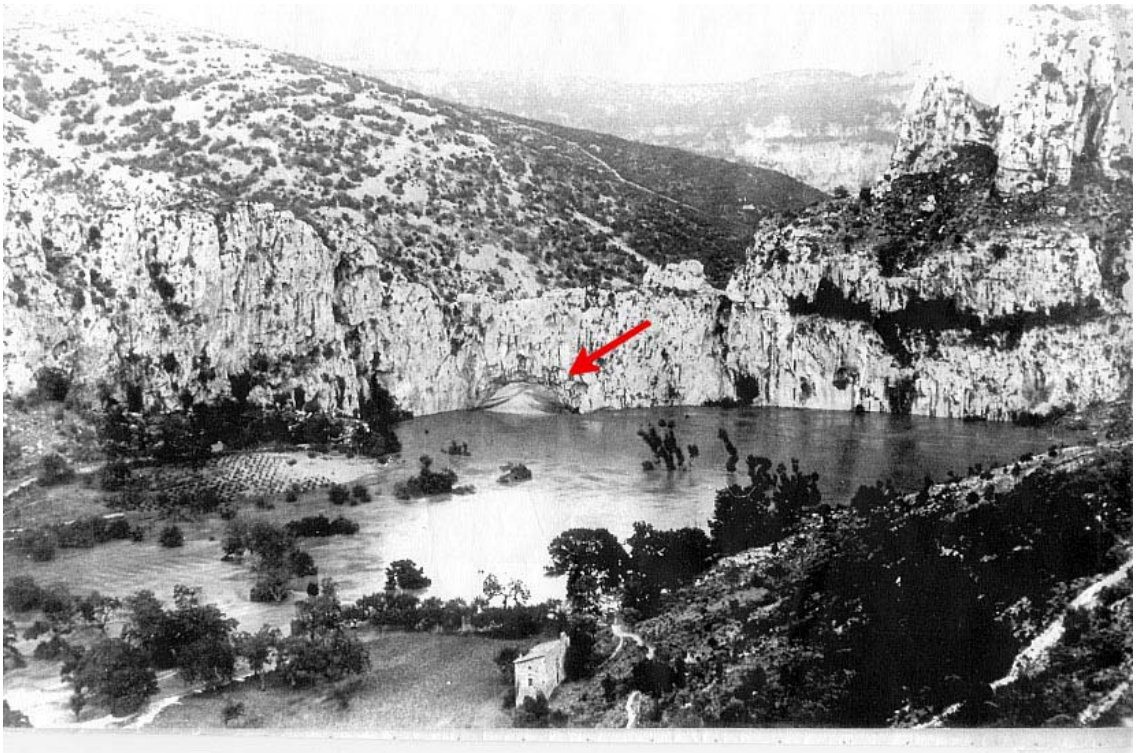

Figure 1.4 Ardèche at Pont d´Arc in 1890-flood. The arrow points at the arc.

Llobregat faces similar flooding frequencies. High intensity-short duration rainfall events result in severe floods in the region. The following figure (Figure 1.5) shows the location map of Llobregat on the left side, and on the right, the Llobregat is photographed in Summer 2000 (photos on right-top and right-bottom). However, the photo at the bottom is *during* the 2000-flood. One can hardly imagine that both photos originate from the same river.

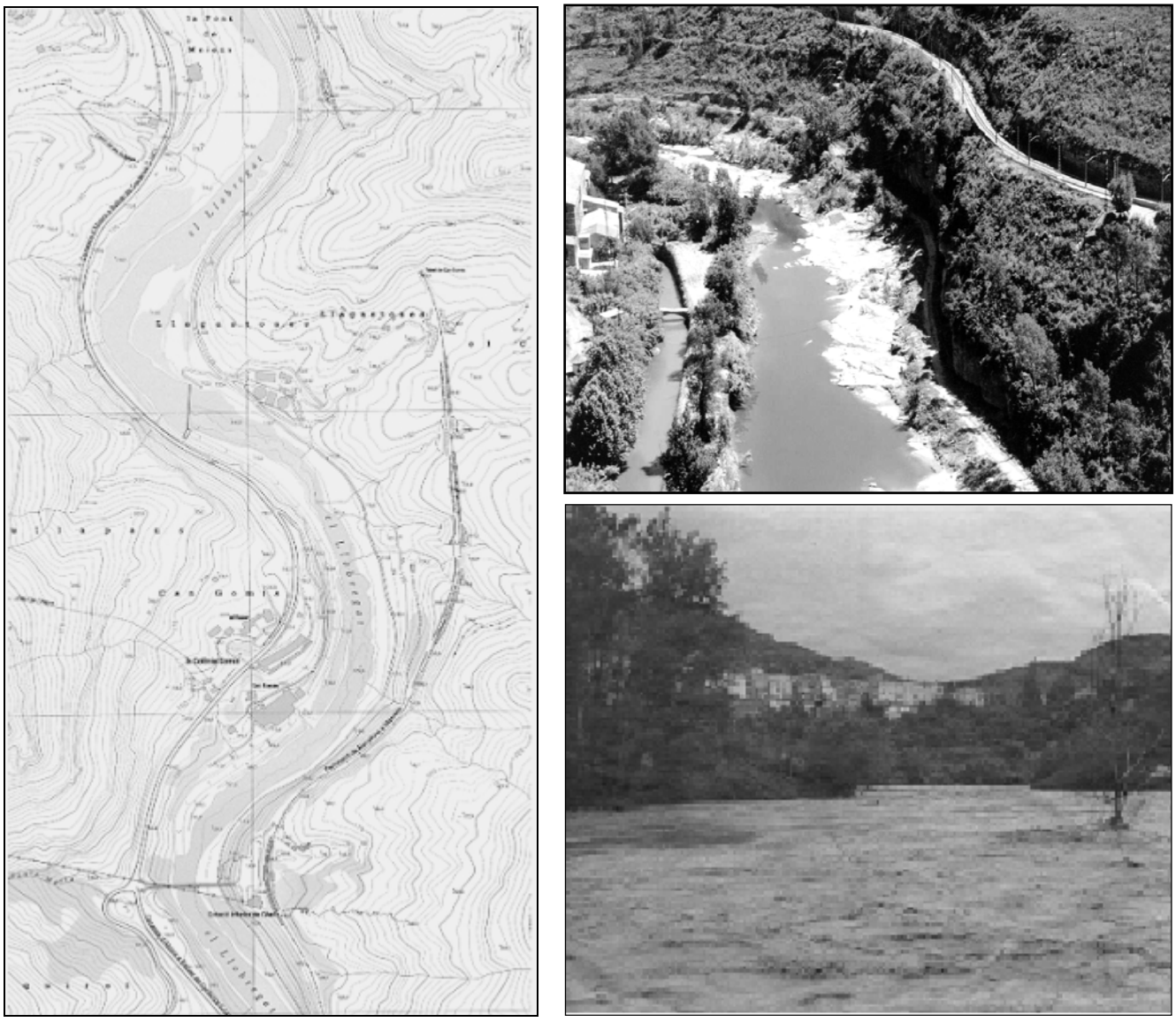

Figure 1.5 Map of Llobregat River at Monistrol (left). The Llobregat River in summer 2000 (right-top) and Llobregat photographed during the flood event of June 10th, 2000 (right-bottom).

The following photos give an impression of the dimension of floods in the Llobregat Region. The photos (see Figure 1.6 and 1.7) are taken at the same location (see the bridge), Figure 1.7 depicting a flood on 20th September 1971.

Figure 1.6 The Llobregat River.

Figure 1.7 Flood in the Llobregat River on 20th September 1971.

From the hydrological point of view, it is important to observe the seasonal variability of the average discharge during a year, as it indicates the wet and dry periods in a basin. Figure 1.8 demonstrates the average daily discharge amounts in the Ardèche at Saint Martin during the observation period (1955-1997). One can clearly see from the diagram that in the Ardèche the aveage discharge level is very low between May and September (very dry summer period) whereas from October to April the average discharge becomes much higher (winter). Therefore, the flood season was chosen to be between October-April and the investigation of the floods was restricted to this period.

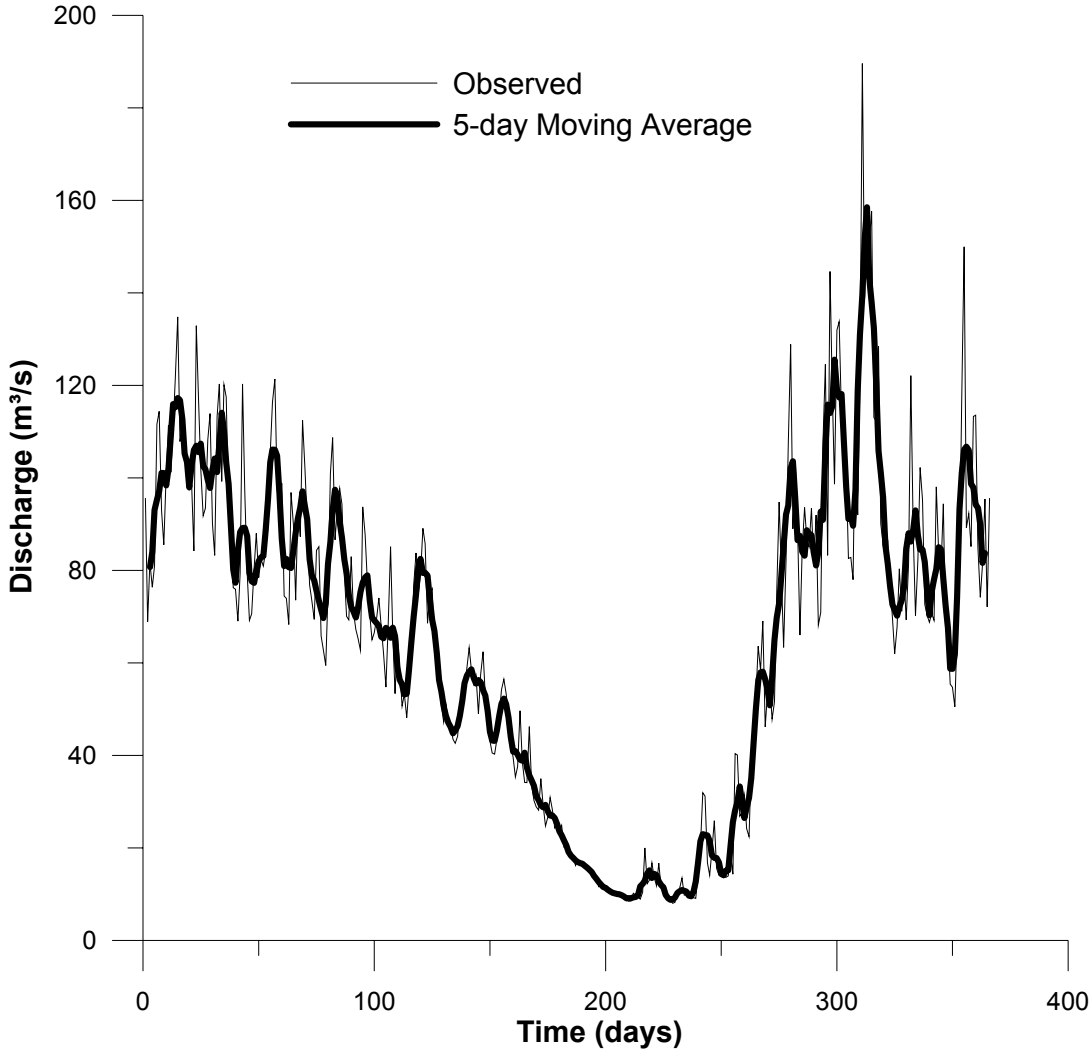

Figure 1.8 Hydrograph of daily average discharge at Ardèche-Saint Martin over one year.

Llobregat shows small differences in the average daily discharge behavior. Here, the magnitude of the seasonal fluctuations in the discharge is much lower than in the Ardèche. Still, the summer and winter seasons can be clearly inferred from the diagram in Figure 1.9. In the Llobregat, the wet winter period begins in September and ends in May according to average daily discharges observed between 1912-1990 at Martorell.

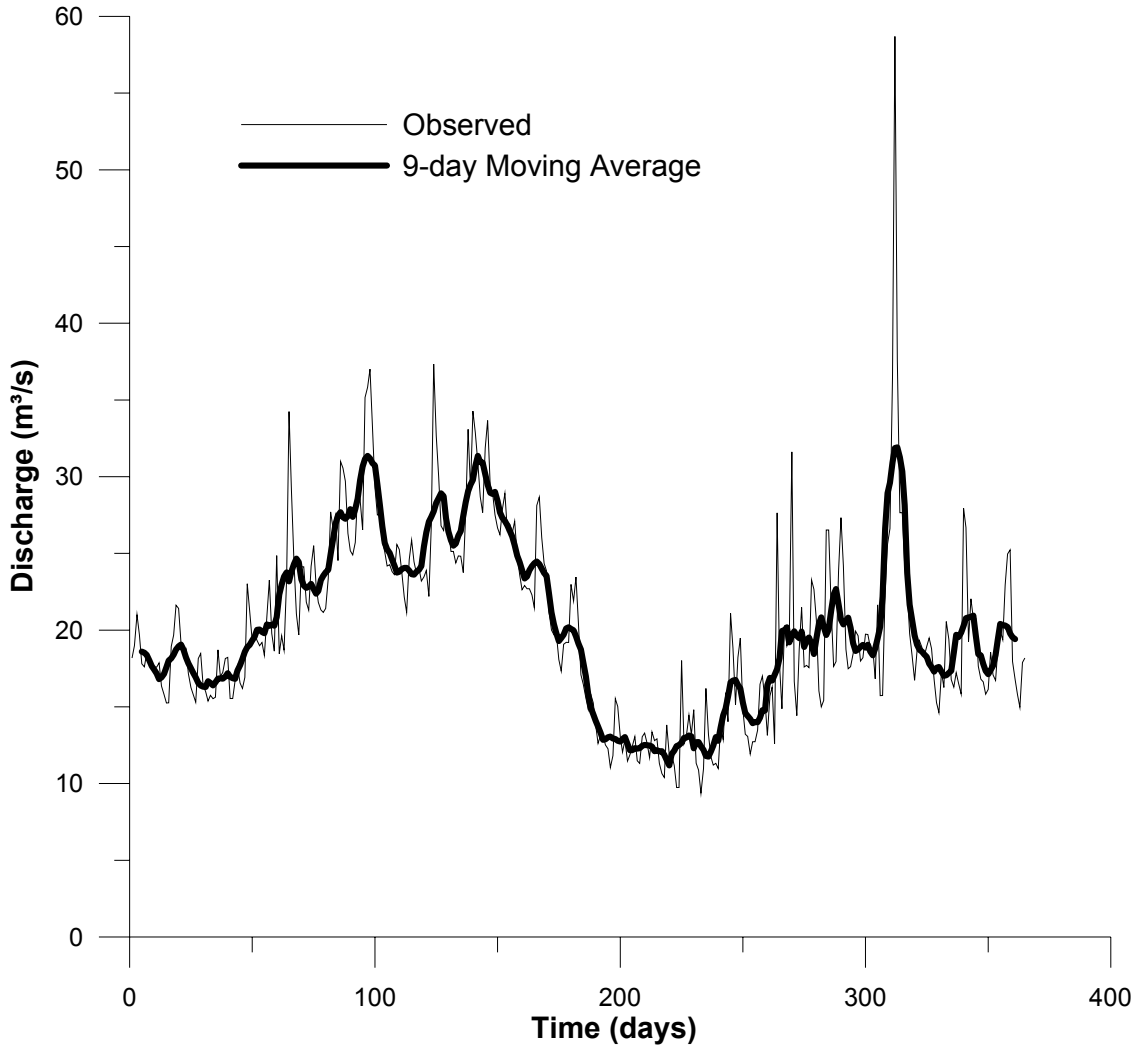

Figure 1.9 Hydrograph of daily average discharge at Llobregat-Martorell over one year.

In both catchments, intense rainfall causes a fast increase of discharge and leads to occasional floods. The concentration times are short, and both rivers flow naturally without being significantly affected by artificial influences. Water management activities usually do not cause sudden substantial increase of discharge, thus they do not have a significant effect on the analysis related to floods in this study. In the next chapter, an overview on the meteorological factors related to flood-producing mechanisms will be considered.

Chapter 2

Meteorological Influences on Flood-Producing Mechanisms

2.1 Introduction

In our dynamic world, the basic and the most important elements for humans like air, water and heat are in motion as well. The most important reason for this dynamic characteristic is the permanently changing weather which is comprised of a cycle of events. The interactions between the meteorological elements such as solar radiation, the atmosphere, water vapor and wind maintain the continuous variability of weather, which in turn helps sustain life on Earth. Due to the spatio-temporal differences in the aforementioned elements, the driving forces evolve which take place to reach the desired equilibrium state.

For the definition and the identification of the flood-prone atmospheric conditions which will be discussed in Chapter 4, it is of major importance to review the essential terms and mechanisms related to weather, climate and floods. In the following, a brief overview on weather and climate, the elements of weather, global water cycle and precipitation will be presented. Later, the scope will be restricted to floods and the statistical analysis of extremes.

2.2 Weather and Climate

Weather systems, which produce the variety of instantaneous states of the atmosphere, differ in their size and lifespan. Four scales are commonly recognized: *microscale systems*, such as turbulent eddies near the surface up to a diameter of ten meters; *mesoscale systems*, such as thunderstorms, which extend some 10 km horizontally and have a duration of a few hours; *synoptic scale systems*, like midlatitude cyclones and tropical storms which have a diameter of

a few thousand km and a lifetime of a few days; and *planetary scale* waves in the atmospheric circulation span 5000-10000 km and usually persist for several weeks.

General atmospheric circulation consists of large scale, three-dimensional turbulent air movements which determine the distribution of energy, and mass and the air mixture. Circulation plays an important role in terms of heat transport in the atmosphere, preventing places with heat excess from becoming warmer and regions with heat deficit from cooling even more. Seasonal air displacements affect the circulation processes.

Due to air circulation natural and anthropogenic gases are transported long distances and advection of certain air masses takes place. Within the climatic processes, atmospheric circulation plays an important role. The global circulation takes place due to the differences in warming of the atmosphere and the spatial distribution of the air pressure.

Climate introduces the longer time scales operating in the atmosphere (global scale). A recent view of climate, which has emerged over the past twenty years, envisions a climate system involving interactions between the atmosphere, oceans, land surface, snow and ice cover, and biosphere. Climate refers to the average weather in terms of the mean and its variability over a certain timespan and a certain area. Climate in a wider sense is the state of the climate system including a statistical description i.e. mean, variance, extremes, distribution functions, and frequency analysis of each climatic component.

The term *climate change* refers to statistically significant variations in either the mean state of the climate or in its variability. Climate change might occur due to natural internal processes or external forcings or to persistent anthropogenic changes in the composition of the atmosphere or in landuse (IPCC, 2001).

2.2.1 The Weather Elements (Climatic Elements)

The Sun is the ultimate source of heat energy of the Earth, keeping its surface temperature relatively constant in a certain range (-51 to 49 °C). Due to solar radiation, the atmosphere is heated primarily from the surface by the absorption of the terrestrial radiation and by turbulent heat transfer. The atmosphere absorbs a significant amount of infrared radiation (due to the presence of water vapor, carbon dioxide, and other trace gases). Once the air above the

surface becomes warmer, it starts to expand, and as a result of decreasing density, it rises. As the rising warm air moves further away from the land, it cools due to the decreasing temperature with height and sinks.

The distribution of solar radiation is not geographically uniform. The equator receives solar radiation from directly overhead, and is thus hot. The poles, in contrary to the equator, are cold due to the fact that the sun rays impact the Earth at shallower angles.

Related to the uneven distribution of solar radiation, differences in the air pressure evolve. This is the most important driving force in terms of changes in weather which depends on the weight of the air in the atmosphere pressing down to Earth. When air rises due to increasing temperatures, it leaves an area of lower pressure behind (the upward movement of air reduces the pressure). The opposite – an increase in the air pressure – happens when air is sinks back down. Due to uneven surface heating, there are many areas of high and low pressure above the Earth´s surface. These inequalities produce differences in air pressure which generate winds: horizontal movements of air and heat (advection) and vertical movements of air (convection). In order to eliminate the pressure differences, the pressure gradient force pushes the air to flow from areas with high pressure to low pressure fields. The greater the pressure gradient between high and low pressure areas is, the higher the wind speed is.

The heat is greater in equatorial areas, which means that air rises above the equator producing low pressure. Winds come into the area to try to keep the pressure as equal as possible, which means that this area is referred to as the ITCZ: Inter-Tropical Convergence Zone. Air moves to North (N) and South (S) from here, eventually falling again at around 30 degrees N and S outside the tropics.

80 % of heat transfer from ITCZ is done by winds, remaining 20 % by ocean currents. There is also an important role played by major tropical storms such as hurricanes, which originate over warm waters and then move away from these source regions, eventually running out of energy.

An air mass is a body of air whose physical properties, especially temperature, moisture content and lapse rate, are more or less uniform horizontally for hundreds of kilometres. Once they move out of their source area, they become subject to modification, with the major changes occurring at the boundaries between air masses.

There are five main air masses that affect Europe:

- Tropical continental (Tc) – warm and dry
- Tropical maritime (Tm) – warm and moist
- Polar continental (Pc) – cold and dry
- Polar maritime (Pm) – cool and moist
- Arctic maritime (Am) – cold and moist

An air mass may be heated from below either by passing from a cold to a warm surface, or by solar heating of the ground over which the air mass is located. It can also therefore be cooled from below.

Heating from below acts to increase the instability of the air mass, so that the effect may be felt through a considerable thickness of air, whereas surface cooling often produces a temperature inversion, which limits the vertical extent of cooling.

One of the most important advances in meteorology was the realisation that many of the day to day changes in weather are associated with the formation and movement of boundaries between air masses: fronts. The term front was developed by Bergeron, Bjerknes and Solberg, and the name was taken from the term used for armies meeting: the Western front etc.

It was observed that the typical geometry of the air mass interface takes on the form of a *wave*. Frontal waves in the atmosphere are unstable i.e: they grow, and then dissipate. The instabilities on the polar front are the main reason for the evolution of cyclones in the mid-latitudes.

Cyclones, also called *low pressure systems* (L), are regions with a lower air pressure relative to their surroundings. The low pressure center corresponds to the lowest air pressure value measured. Therefore, horizontal motion in any horizontal within a cyclone means an increase in the air pressure. The negative deviations of the atmospheric pressure from the normal value (1000 mb) were identified as barometric minima (lows) by H.W. Brandes at the beginning of 19^{th} century who initiated the first air pressure map of West and Central Europe. Low pressure fields are usually associated with wet, cloudy weather and decreasing temperature.

Anticyclones, also named *high pressure systems* (H), correspond to pressure fields having a higher pressure compared to the surroundings (above normal). The pressure measured is highest at the center of the high pressure field. Therefore, moving away from the center of a high pressure system indicates a decrease in the air pressure. When compared with low

pressure systems, highs pressure systems tend to cover a greater area, move more slowly and have a longer duration. High pressure fields usually correspond to sunny, dry weather. A typical pattern of low and high pressure regions can be seen in Figure 2.1.

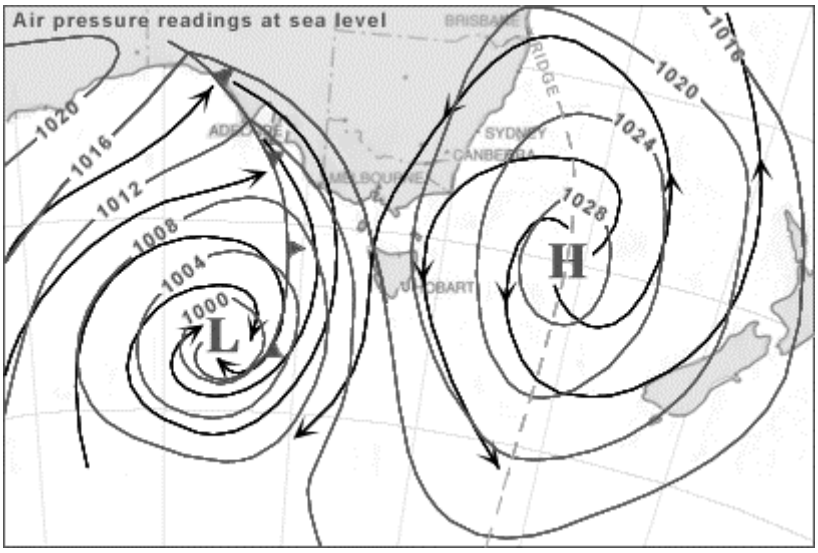

Figure 2.1 A simple weather map showing low (**L**) and high (**H**) pressure regions, wind direction, a ridge of high pressure and a cold front .

Isobars in synoptic weather maps join locations with the same air pressure. Around the pressure center, an isobar is shaped like an ellipse. Isobars are generated from mean sea level pressure reports and are drawn for equal intervals of pressure (i.e. every 4 millibars). Closer isobars indicate higher pressure gradients and thus stronger winds. Where the isobars are elongated around a high pressure system (orange colored line as seen in Figure 2.1), they are referred to as a ridge. An elongated extension of isobars away from a low pressure centre is known as a trough of low pressure. This trough usually contains one or more cold fronts.

Due to the Coriolis force, the winds flow counterclockwise around a cyclone and clockwise around an anticyclone in the Northern Hemisphere; the opposite flow direction apply in the Southern Hemisphere. The Coriolis force arises from the fact that the movement of masses over the Earth´s surface is usually viewed with respect to a moving coordinate system (i.e. the latitude and longitude grid which *rotates* with the Earth). Once the air has been set in motion by the pressure gradient force from a high pressure system towards a low pressure system, it undergoes an apparent deviation from its path, as seen by an observer on the Earth. The air does not actually deviate from its path, but it appears to do so because of the motion of the coordinate system (see Figure 2.2). As the wind gains speed, the deflection increases until the Coriolis force equals the pressure gradient force. At this point, the wind will be blowing

parallel to the isobars and the wind is referred to as *geostrophic wind*. The air moves along a north-south path, or longitudinal line, and will undergo apparent deflection to the right in the Northern Hemisphere and to the left in the Southern Hemisphere. There are two reasons for this phenomenon: first, the Earth rotates eastward; and second, the tangential velocity of a point on the Earth is a function of latitude (the velocity is essentially zero at the poles and attains a maximum value at the equator). More detailed information can be found in Hupfer and Kuttler (1998) and Barry and Chorley (1998).

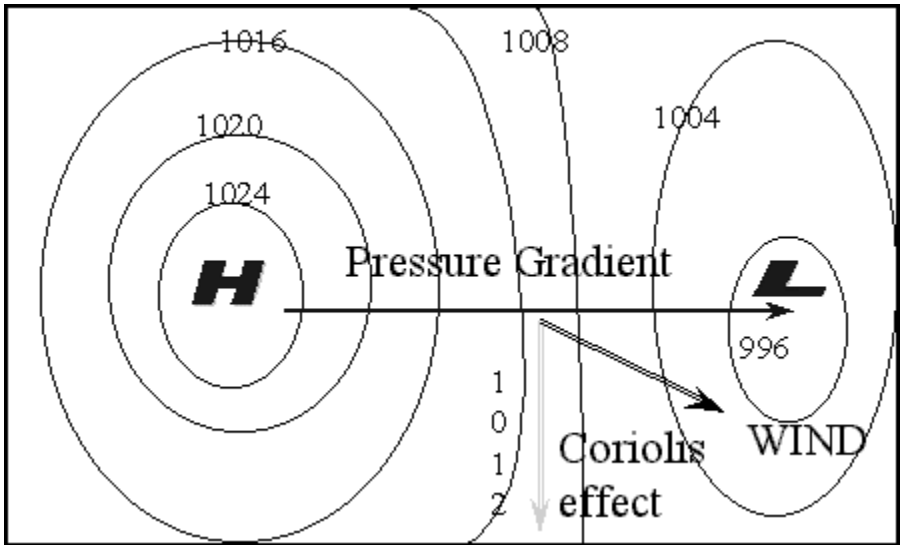

Figure 2.2 Coriolis effect on the direction of winds in the Northern Hemisphere.

Changes in air pressure often signify changes in weather. Rising air pressure usually means fair weather, whereas falling air pressure generally signals stormy weather. This is because a drop in air pressure often indicates that a cyclone, or low pressure system, is moving into an area, bringing clouds and precipitation. A rise in air pressure frequently means that a high pressure system is approaching an area bringing fair weather. Figure 2.3 illustrates an idealized cyclone.

A cyclone is formed by a warm front (see Figure 2.4-left) pushing the moist air to the north and a cold front (Figure 2.4-right) pulling southward. The leading edges of air masses are being wrapped around a center of low pressure or the center of the cyclone.

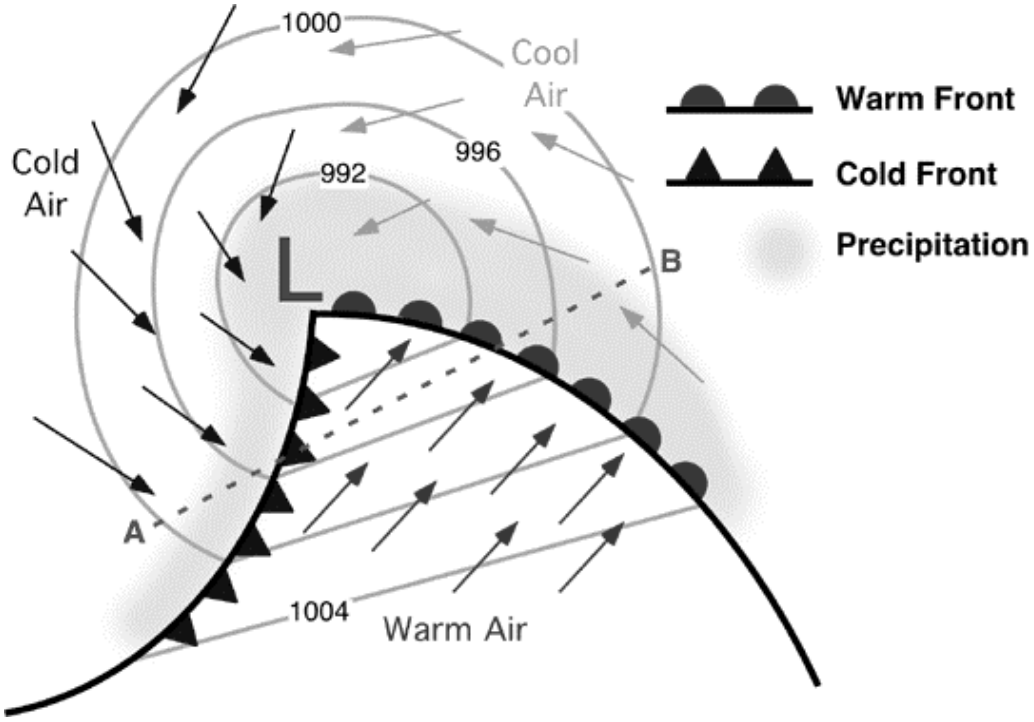

Figure 2.3 Fronts, wind patterns, pressure patterns, and precipitation distribution found in an idealized mature mid-latitude cyclone.

A transition zone where a warm air mass is replacing a cold air mass is called a warm front. Warm fronts generally move from southwest to northeast (due to the Coriolis effect) and the air behind a warm front is warmer and more moist (humid) than the air ahead of it. As shown in Figure 2.3 and Figure 2.4, a warm front is represented by a red solid line with semicircles pointing toward the colder air in the direction of movement. The opposite applies for a cold front. This time colder air mass replaces the warmer air mass. Due to this transition, temperatures might drop more than 15 degrees within the first hour. The direction of the movement is usually from northeast to southwest. The schematic representation of a cold front consists of blue solid lines with triangles along the front pointing the direction of the air movement.

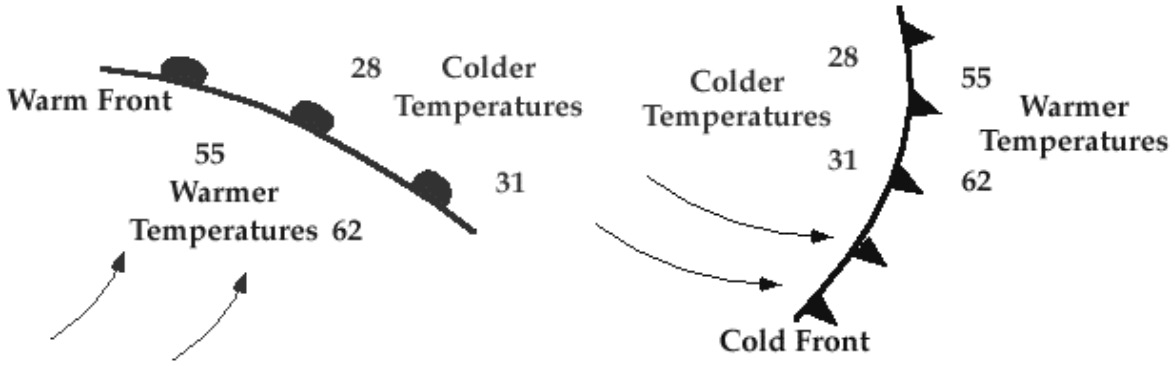

Figure 2.4 Warm and cold fronts (temperatures in degrees Fahrenheit, °F).

While air is in motion, water will be transported in form of water vapor. It is well known that water exists in the atmosphere in three forms: solid, liquid and gas. These are various forms of atmospheric moisture, which plays a significant role in weather when it changes from one state to another. These changes are condensation (cloud, fog, dew and frost) and precipitation (rainfall and snow).

2.2.2 The Global Water Cycle

About 70 % of the Earth is covered with water. The diagram in Figure 2.5 displays the volumes of water contained in oceans, on land and in the atmosphere. The arrows indicate the annual exchange of water between these entities. The oceans, land and atmosphere contain 97.5 %, 2.4 %, and less than 0.001 % of the Earth´s water, respectively; the latter is surprising because water plays such an important role in weather. The annual precipitation for the Earth is more than 30 times the atmosphere's total capacity to hold water. This shows how rapid the recycling of water must occur between the Earth's surface and the atmosphere.

Evaporation is one of the main elements of the hydrologic cycle. Due to solar radiation, water particles in the oceans and lakes reach a certain energy level and become water vapor. Approximately 80 % of all evaporation is from the oceans, with the remaining 20 % coming from inland water and vegetation. Winds transport the evaporated water around the globe, influencing the humidity of the air throughout the world.

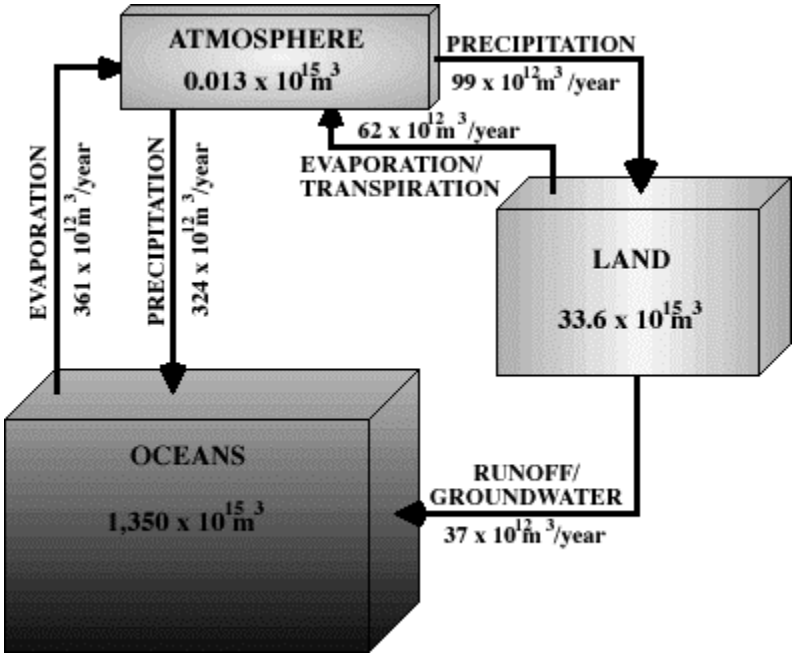

Figure 2.5 Storage and fluxes of the global water budget (*Source: adapted from Peixoto and Kettani, 1973)*.

The other process is condensation, which involves the transition of water vapor to liquid form. It generally occurs in the atmosphere where the sun-heated air rises, cools and loses its capacity to hold water vapor. As a result, excess water vapor condenses to form cloud droplets. The upward motions that generate clouds can be produced by convection in unstable air, convergence associated with cyclones, lifting of air by fronts and lifting over elevated topography such as mountains.

2.2.3 Precipitation

Precipitation occurs as a final result of the aforementioned coupled processes which is the most important and governing factor in the water balance of a region (Ward and Robinson 2000). Its occurrence in its discrete nature and its high spatio-temporal variability within a catchment are important in understanding the water cycle at the catchment scale. To some extent, these factors lead to uncertainties come into play which make the hydrological processes interesting and relevant for research.

There are several precipitation forms other than rain (which is the common form). These include hail, snow, sleet, and freezing rain. Precipitation occurs, when large air masses become cooled down below the dew point. Dew point temperature is defined as the

temperature at which air would have to cool (at constant pressure and constant water vapor content) in order to reach saturation. Dew points provide insight into the amount of moisture in the air. This was addressed at the beginning of the chapter with respect to condensation of water vapor. The process of cooling can take place quickly if the air masses are rapidly lifted up to higher elevations. The way the lifting up of air takes place (initial processes) results in different types of precipitation. These are convective (thermal lifting of an air column to form a thunderstorm cloud), orographic (lifting against a mountain barrier) and cyclonic (lifting of warm air over cold air) rainfall types.

Convective precipitation can be accounted for usually local, brief and often intense rainfall events (i.e. in form of showers). The rising of air columns occur mainly during the day in summer and are probably caused by the increased solar heating of the surface. In terms of hydrologic interaction, convective rainfall is relatively less effective for increasing soil moisture due to its short duration. However, in mid-latitudes it occurs during warm periods and provides high ratios of moisture to cloud cover.

In case of orographic precipitation, the topography plays a significant role. In mid-latitudes, it usually appears as winter snow at higher altitudes. Snowmelt transported as surface flow is an important factor for the runoff contribution.

Cyclonic precipitation is produced by travelling cyclones and anticyclones of mid-latitudes. These storms produce moderate, continuous precipitation over extensive areas. They can show low intensity and long duration characteristics which result more in entering the groundwater systems and being less transported by the surface flow.

2.2.4 Floods

Climate has an important influence on the relationship between precipitation and runoff. Most flooding occurs when the volume of water in a river or stream exceeds the capacity of the channel. Numerous factors affect the streamflow, therefore the potential for flooding. The following factors might contribute to flooding:

- Rainfall intensity and duration
- Topography, anthropogenic factors in terms of land cover and land use

- Soil conditions: state of the catchment such as antecedent moisture content related to previous rainfall
- Ground cover, vegetation
- Contribution of snowmelting/sudden release of water held by ice jams

As the two key elements of flooding are the rainfall intensity and duration related to weather, the scope of this study will be restricted to the investigation of flood prone meteorological conditions which should serve a better understanding of the links between climate, meteorology and hydrology with respect to the flood occurrence in the Studied Regions.

2.3 Statistical Analysis of Flood Peak Discharges

2.3.1 Time Series Analysis

During the last decades Time Series Analysis has become one of the most important and widely used branches of Mathematical Statistics. This type of analysis is especially employed to understand and to structure the underlying forces or mechanisms that produced the observed data related to a process or a phenomenon. The two main goals of time series analysis are:

a) identifying the nature of the phenomenon represented by the sequence of observations
b) forecasting (predicting future values of the time series variable).

At this point, it is worthwhile to allude to John Casti´s statement about the meaning of prediction:

"Can science foretell the future? People get terribly confused about the role of prediction in science. A lot of them have never understood that 'prediction' has two meanings. A theory of earthquakes, for example, can be 'predictive' without being able to predict earthquakes. A theory is predictive if it states that under certain conditions, certain consequences will follow. It is not obliged to state in advance when those conditions will hold." (Casti, 1992)

A *time series* is a sequence of measurements, typically taken at successive points in time. Time series analysis accounts for the fact that data points taken over time may have an internal structure (such as autocorrelation, trend or seasonal variation) which should be taken into account. The underlying pattern of the observed time series is to be identified and formally described for explaining the nature of the phenomenon and to predict future values of the time series. Time series methods generate forecasts by extrapolating the identified pattern on one or more components of a time series. These methods are widely applied in fields such as in astronomy, meteorology, seismology, engineering, signal processing and economics; this list is by no means complete.

As mentioned above, most of the time series patterns can be described in two basic terms - trend and seasonality. A *trend* represents generally a linear or nonlinear component that changes over time and does not repeat (or at least does not repeat within the given range of observed data) whereas *seasonality* repeats itself in systematic time intervals. It can also be the case that the seasonal changes remain constant over time, but still be related to the trend (called multiplicative seasonality) which is a common type of pattern in time series data.

Within the present study, time series analysis was applied to the Study Areas, the Ardéche and the Llobregat, for analysing flood events dependent on time. Among the frequency determination of high magnitude floods, possible trends in the frequencies have been investigated via moving average smoothing (see Box and Jenkins, 1976; Velleman and Hoaglin, 1981).

2.3.2 Extreme Value Analysis

Estimation of extreme flood characteristics is one of the most important hydological tasks related to water resources planning and analysis like flood risk assessments, design of flood control constructions, and dam safety evaluation (McCuen, 1989).

It is well known that floods may cause severe damage. The awareness of this natural disaster has increased in the recent years, especially in industrialized countries. It is widely accepted that life and property have to be protected against the effects of floods. In order to tackle possible future floods and to estimate the damage that they might cause, it is of great interest

to estimate the likelihood of future flood events and their average recurrence intervals (i.e. 10, 20, 50 or 100 years) for a better design flood estimation.

In flood frequency analysis there are three mathematically interrelated terms of interest. These terms are:

- F(X) [%]: The *relative frequency* which is the probability of the flow (Q_{max}) being *less* than a value X.
- P(X) [%]: The *probability of exceedance* is the probability that corresponds to a maximum flow (Q_{max}) over a time period (typically years) which is *greater* or *equal* to a value X. It will be assumed that each flow value (Q_{max}) is independent of each other (see Equation (2.1)).
- T(X) [years]: T(X), the average *recurrence interval*, is a statistical term meaning the probability of exceedance once every T years over a long period. As seen in Equation (2.2), the average recurrence interval also called *return period* is the reciprocal of the probability of exceedance which refers to the average length of time between occurrences. This should not be interpreted as meaning that is exactly how many years are likely between certain size floods. Thus, a flood event with one percent chance of occurring in any year has an annual exceedance probability of 0.01 and a return period of 100 years, and is therefore called a 100-year flood (see Equation (2.2)).

$$P(X) = 1 - F(X) \tag{2.1}$$

$$T(X) = \frac{1}{P(X)} = \frac{1}{1 - F(X)} \tag{2.2}$$

Due to the shortage of observation series and the rarity of extremes, it is difficult to quantify flood probabilities and the associated risks. Thus, realistic extrapolation ways are sought. Extreme value statistics are used primarily to quantify the stochastic behavior of a process at unusually large (or small) values. Particularly, such analyses usually require estimation of the probability of events that are more extreme than any previously observed.

The theory is based on the idea that the maximum or minimum value of independent identically distributed random variables tends to an asymptotic distribution that only depends on the *tail* of the distribution of the basic variable. There are several distribution functions that are used within Extreme Value Statistics. Some of them are parametric distributions such as Gumbel, Fréchet, Weibull, Gamma, Lognormal, Log-Pearson III Distribution, and General Extreme Value Distribution. Alternate models for extreme values include also contagious

distributions based on random counting of extreme events. Details can be found in Fisher and Tippett (1928), Gumbel (1958).

Extreme Value Analysis is an approach which is based on frequency analysis of measured flood peak discharges. The observed values will be fit to a chosen statistical distribution function and the distribution will be extrapolated in order to determine the peak discharges of small exceedance probabilities. Finally a statistical test is applied whether the sample data can be described with the chosen theoretical probability distribution function or not. Extreme Value Analysis is widely used despite of the fact that the method includes several subjective decisions like:

- the selection of sample data (i.e. annual maximum discharge series).
- the selection of the probability distribution function that will be applied to sample data.
- the selection of the estimation procedure for the parameters of the probability distribution function.

Another important point is the correct interpretation of the results. In order to limit the randomness of the results, it is advisable to use different distribution functions and also to analyze the extremes of several number of generated time series. It is of importance that the generated time series include the characteristics of the observations.

In the present study, Extreme Value Analysis has been used to validate the discharge simulation model. The frequency and the magnitude of reproduced peak flood discharges could be compared with the observed ones during the instrumental period in the Study Areas.

Chapter 3

Linking Large Scale Atmospheric Information to Local Scale Parameters

3.1 Classification of Atmospheric Circulation Patterns

3.1.1 Introduction

The Earth´s atmosphere is constantly in motion producing changing winds, weather and cloud patterns. The term *circulation* refers to the movements of air masses resulting from pressure differences and anomalies in the atmosphere that accounts for the driving forces of weather changes.

Atmospheric circulation is the indication of meteorological conditions which dominate over a large area (e.g. central Europe) with a duration of usually a few days. The main features of weather remain mostly constant during this period, which is followed by a rapid transition to another circulation type. Baur et al. (1944) defined a *circulation pattern* as a mean air pressure distribution over a large area such as Europe and the northern Atlantic Ocean. Circulation patterns (CPs) are, in other words, typical synoptical pressure maps which show the pressure configuration in large (continental) scale including the locations of high and low pressure fields. For example, Bardossy (1993) defined the size of the domain for Europe to lie between the coordinates 40°W, 30°N and 60°E, 80°N.

Certain CP types are usually associated with typical weather situations with respect to their characteristics. Related to this, the occurrence of particular CP types and the amount of precipitation in a distinct basin were linked by Bardossy (1993), Stahl and Demuth (1999) and many other authors which can also indicate wet and dry spells. Duckstein et al. (1993) concluded that certain CP types occur statistically significantly before floods. Caspary (1996) stated that winter floods in south Germany are related to zonal circulations. Wilby (1992) used the atmospheric circulation patterns as drought indicators.

European atmospheric circulation patterns (CPs) or "Großwetterlagen" were proposed by Hess and Brezowsky (1969) which consist of three major circulation types, namely: zonal, mixed and meridional circulation types. These are further specified according to the direction of movement of frontal zones, location of high and low pressure centers and cyclonic and anticyclonic rotation. Hess and Brezowsky (1969) obtained 29 classified and one unclassified circulation patterns (see Appendix 1).

In order to comply with the research demand on large scale meteorological phenomena and their consequences in hydrology - especially with respect to floods, further investigation on the links between large scale meteorological conditions and floods is required. The purpose of this study is to focus on the analysis of flood-prone meteorological conditions and to investigate the consequences of the critical CPs at mesoscale catchments regarding floods.

This chapter gives a brief overview of the classification of CPs and summarizes the general downscaling techniques as background information related to this research.

3.1.2 Classification Techniques

One possibility to investigate weather situations is to classify the circulation patterns. There are two main groups of methods for CP classification (Yarnal, 1984, 1993). The first method is subjective classification in which experts in meteorology are involved. The advantage of this method is that the knowledge and the experience of the meteorologist is incorporated. However, the results cannot be objectively reproduced, and the applicability of the method is restricted within certain geographical regions. Many subjective classification methods have been developed for various regions with different scales. Baur et al. (1944) and Hess and Brezowsky (1969) classified circulation patterns for central Europe, Lamb (1972) for the British Isles, Maheras (1988, 1989) for Greece, Dzerdzeevskii (1962) for the extratropical latitudes of the Northern Hemisphere and Krick (1943) and Elliott (1949) for the United States.

The second type of method for CP classification is objective classification. These classification techniques consist of automated algorithms which operate on selected datasets. The classification is fast and reproducible which is necessary for application to climate change scenarios. The objective classification methods include *k*-means clustering (Wilson et

al.1992), a method based on physical quantities (Jenkinson and Collison, 1977); fuzzy classification based on subjectively defined fuzzy rules (Bárdossy et al., 1995, Stehlik and Bárdossy, 2002); principal component clustering (Goodess and Palutikof, 1998); principal component analysis coupled with *k*-means clustering (Bogárdi et al., 1994); and neural-network methods (Cawley and Dorling, 1996). Jones et al. (1993) presents a detailed study including a comparison between Lamb subjective classification and objective classification schemes.

Once the atmospheric circulation patterns have been classified, they need to be linked to the surface variables in order to distinguish the consequences of large-scale phenomena on the local catchment scale in terms of i.e. temperature, precipitation or moisture. The procedure of connecting large-scale parameters to local scale variables is called *downscaling*. The next section provides a brief summary about the necessity of downscaling and different downscaling methods.

3.2 Downscaling Methods

3.2.1 Introduction

Over most of the time on Earth, humans have been affected by climate but have not had any measurable impact on the climate system. Within the last two centuries, humans have begun to alter the climate, first at regional and then at global scales, although the magnitude of their impacts remain uncertain.

"One of the most important – and yet least well understood – consequences of future changes in climate may be alterations in regional hydrologic cycles and subsequent changes in the quantity of regional water resources" (Gleick, 1987:137).

Since the beginning of the Industrial Revolution (mid-18th century) the impact of human activities had consequences on a continental or even a global scale. Human activities, especially those involving the combustion of fossil fuels for industrial or domestic usage and biomass burning produce greenhouse gases and aerosols which affect the composition of the atmosphere. The emission of chlorofluorocarbons (CFCs) and other chlorine and bromine

compounds has not only an impact on the radiative forcing, but has also led to the depletion of the stratospheric ozone layer. Land use change, due to urbanization and agricultural practices, affect the physical and biological properties of the Earth´s surface. Such effects change the radiative forcing and have a potential impact on regional and global climate.

The increase in greenhouse gas and aerosol concentrations in the atmosphere might lead to an average increase of temperature of the surface-troposphere system (see Figure 3.1).

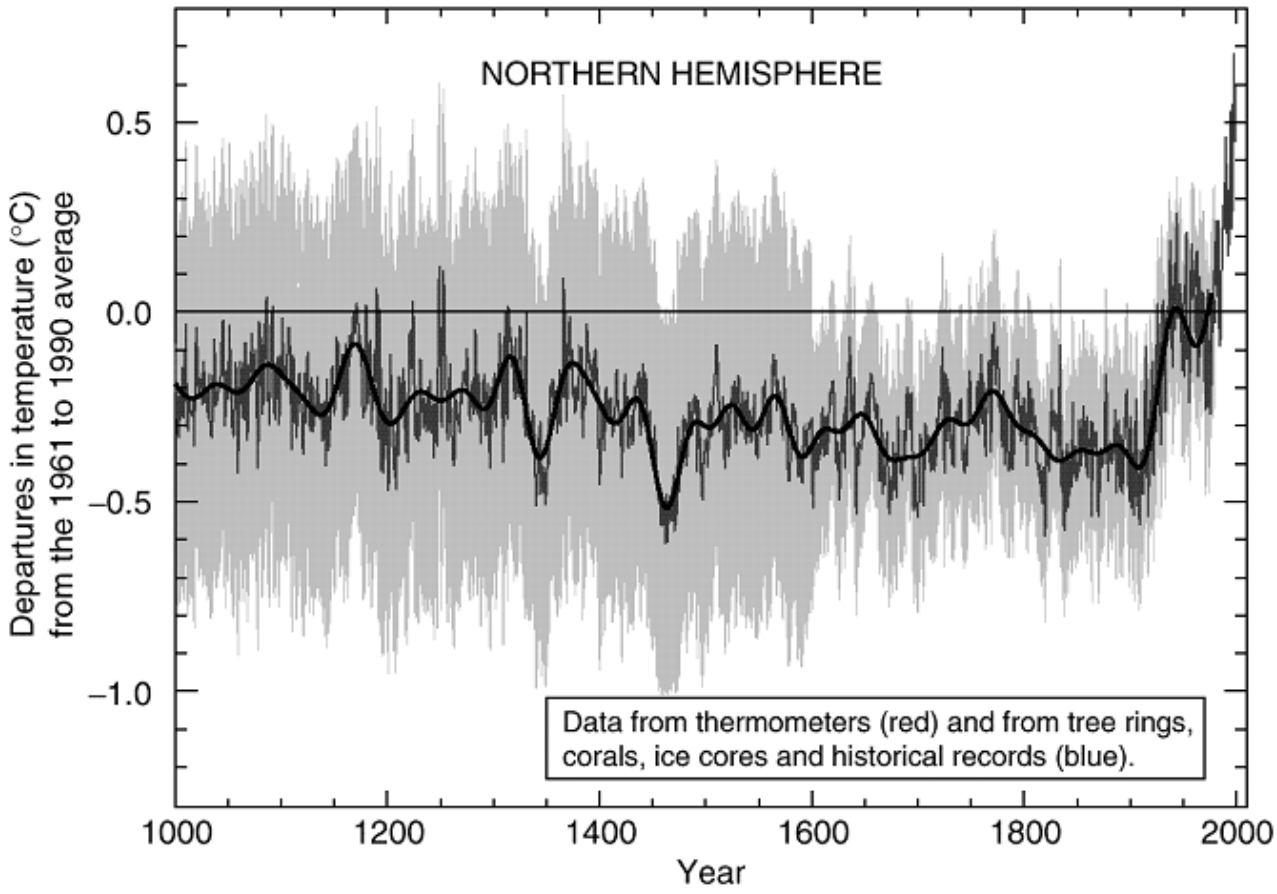

Figure 3.1 Average temperature in the Northern Hemisphere for the past 1000 years. A gradual deviation in temperature is observed since 1961, *Source: IPCC, 2001*.

The response of the stratosphere is quite different. The stratosphere is characterized by a radiative balance between absorption of solar radiation, mainly by ozone, and emission of infrared radiation mainly by carbon dioxide. An increase in the carbon dioxide concentration therefore leads to an increase of the radiative emission and thus to a cooling of the stratosphere (see Figure 3.2.a and 3.2.b). In order to quantify the non-linear climate response, numerical models of the climate system based on well-established physical, chemical and

biological principles, possibly combined empirical and statistical methods have been developed.

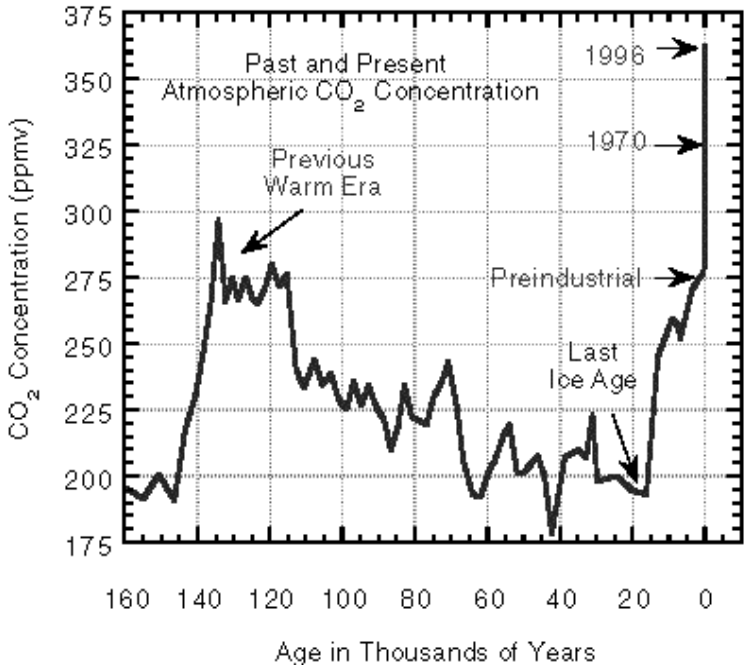

Figure 3.2.a Past and present atmospheric CO_2 concentrations *Source: IPCC, 2001*.

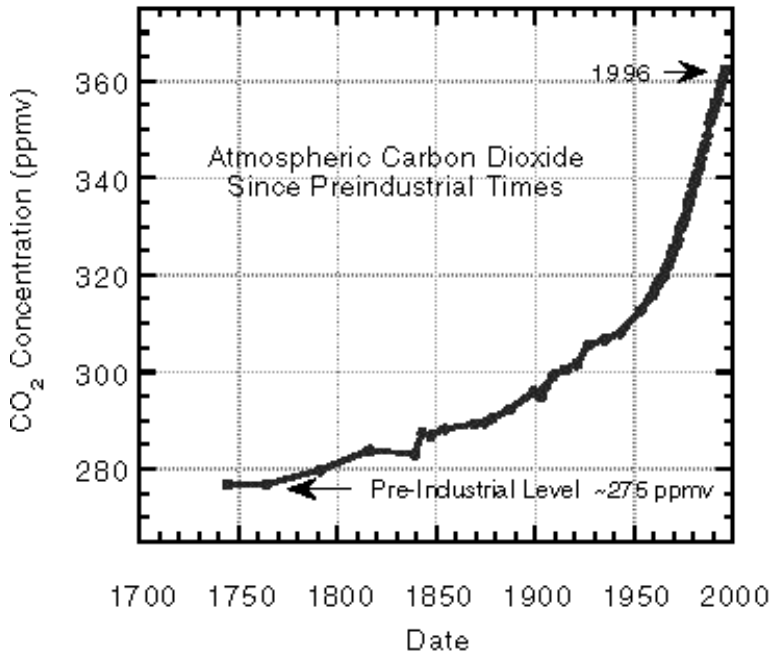

Figure 3.2.b CO_2 concentrations since pre-industrial times *Source: IPCC, 2001*.

The behavior of the climate system, its components and their interactions, can be studied and simulated using tools known as climate models. Today, these models are the primary tools used for studying climate processes and natural climate variability and predicting the response of the climate to human-induced forcing. The most complex atmosphere and ocean models, called General Circulation Models [Atmospheric General Circulation Models (AGCMs) and Ocean General Circulation Models (OGCMs)] are based upon physical laws describing the dynamics and thermodynamics of the atmosphere and oceans with mathematical expressions. They attempt to model the climate system, including internal and external forcing as well its feedback. Due to the size of the climate system (atmosphere, oceans, land) and the time range of climate experiments (several decades to thousand years), the GCMs are spatially and temporally coarse. The current state-of-the-art global climate models are ECHAM4/OPYC (German Climate Research Center), HadCM3 (Hadley Centre for Climate Prediction) and CSIRO-Mk2 (Australia´s Commonwealth Scientific and Industrial Research Organisation). These GCMs operate on horizontal grid resolutions ranging from 100-250 km. Smaller scales cannot be resolved (Robinson and Finkelstein, 1991). Due to the large spatial scales, such climate modifying local geographic factors as topography, land/water-distribution or vegetation type cannot be modeled explicitly. Instead, they are respresented as highly-averaged features. Another source of uncertainty is the need to parameterize sub-grid scale physical phenomena, such as cloudiness and precipitation which are large-scale averages in the GCM output. See Figure 3.3 for the illustration of different input-output scales in GCM, RCM and hydrologic models.

"*Even if global climate models in the future are run at high resolution there will remain the need to "downscale" the results from such models to individual sites or localities for impact studies. Downscaling methodologies are still under development and more work needs to be done in intercomparing these methodologies and quantifying the accuracy of such methods*" (DOE, 1996: 34).

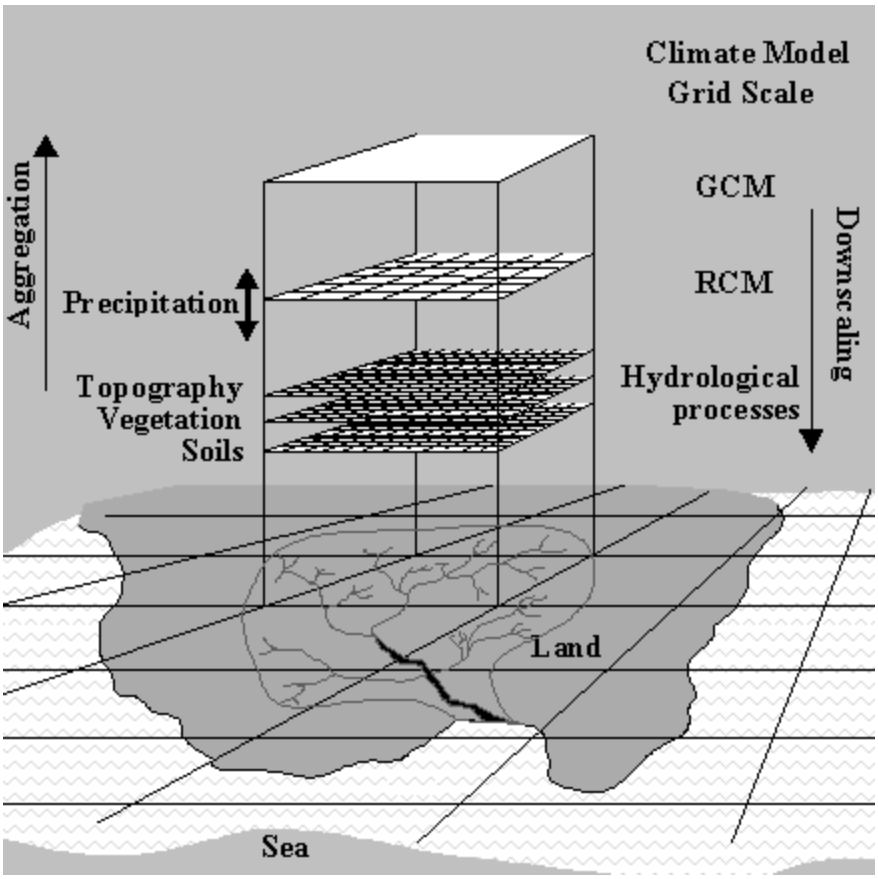

Figure 3.3 Conceptualization of downscaling and aggregation between atmospheric and hydrologic models *Source: Wilby and Wigley (1997)*.

Downscaling techniques have been developed to relate large-scale atmospheric variables to local surface variables. Two broad classes of downscaling approaches exist:

- *Dynamical methods* involving explicit solving of the process-based physical dynamics of the system (e.g. Giorgi and Mearns, 1991; Jones et al. 1995, Jacob et al. 2001)
- *Statistical methods* that use identified system relationships derived from observational data (e.g. Wigley et al. 1990; Wilby, 1995; Hewitson and Crane, 1996, Bürger, 1996)

Downscaling methods are briefly summarized in Zorita and von Storch (1997) and Xu (1999).

3.2.2 Dynamical Downscaling Approaches

Dynamical downscaling methods are used to extract the local scale information from GCM data, so they all produce local scale information based on the GCM results. Three approaches of dynamical downscaling are well known (Rummukainen, 1997), each of which is a sort of a

"time-slice" of a long, coarse-resolution GCM experiment. Dynamical downscaling can be achieved by:

1. running a regional-scale limited area model with the coarse GCM data as geographical or spectral boundary conditions (also known as one-way nesting).
2. performing global scale experiments with high resolution AGCMs (atmospheric GCMs), with coarse GCM data as initial (and partially also as boundary) conditions.
3. using a variable-resolution global model (with the highest resolution over the area of interest).

The goal of dynamical downscaling is achieved by developing and using limited-area models (LAMs) or regional climate models (RCMs).

RCMs have recently been developed that can attain horizontal resolution in the order of tens of kilometers or less over selected areas of interest (i.e. REMO (Jacob and Podzun, 1997)). They have been applied with relative success to numerous regions (e.g. Giorgi and Bates, 1989; Giorgi, 1990; Giorgi and Mearns, 1991; Hostetler and Giorgi, 1992; 1993; Giorgi et al., 1990; 1993; 1994; Jones et al., 1995; Jenkins and Barron, 1997). Jacob (2001) compared different regional climate models within the Baltex area that delivered quite different results for the same region under study.

Compared with GCMs, the resolution of these RCMs is much closer to that of landscape scale hydrologic models (LSHMs) and makes coupling of RCMs and LSHMs potentially suitable for evaluating the effects of hydrologic systems.

Dynamic downscaling operates on some (high-resolution) grid-point scales (i.e. 15 km) and therefore the results will be in the form of spatial averages. These models still cannot meet the demands of spatially explicit models of ecosystems or hydrological systems, and there is still need to downscale the results from such models to individual sites or localities for impact studies.

3.2.3 Statistical Downscaling Methods

The other downscaling approach is statistical downscaling also known as empirical downscaling. In this approach, regional-scale atmospheric predictand variables (such as area averages of precipitation, temperature or moisture) and large scale predictors like circulation patterns or circulation indices such as vorticity and divergence based on the mean sea level pressure are related to station-scale meteorological series (Kim et al., 1984; Karl et al. 1990; Wigley et al., 1990; Hay et al., 1991; 1992). The predictor and the predictands in statistical downscaling are often in form of transient anomalies. The statistics involved can be simple or extensive and some form of regression analysis are typically involved in the final relationships.

Statistical downscaling methods can be classified according to techniques used (Wilby and Wigley, 1997) or according to the chosen predictor variables (Rummukainen, 1997). In Wilby and Wigley´s study, statistical downscaling techniques are described using three categories, namely:

a. regression methods (e.g. Kim et al., 1984; Wigley et al., 1990; von Storch et al., 1993),
b. weather pattern-based approaches (Lamb, 1972, Hay et al., 1991, Bárdossy and Plate, 1992, Bárdossy et al., 1994; Wilby, 1995, Bárdossy and Caspary, 1990),
c. stochastic weather generators (e.g. Richardson, 1981; Wilks, 1992; Gregory et al., 1993; Katz, 1996).

Rummakainen (1997) classified the statistical downscaling methods as follows:

1. *Downscaling with surface variables*:
   This involves the establishment of empirical statistical relationships between large-scale averages of surface variables and local-scale surface variables (e.g. Kim et al., 1984; Wilks, 1989). To develop the relationships, large-scale averages constructed from local time series are used. In practice, the same local scale surface variables will be predictands.
2. *The perfect prognosis (PP) method* (e.g. Zorita et al., 1992):
   This involves the development of statistical relationships between large-scale free tropospheric variables and local surface variables. In this method, both the free atmospheric data and the surface data are from observations.

3. *The model output statistics (MOS) method* (e.g. Karl et al., 1990):
   This is similar to the PP method, except that the free atmospheric variables, which are used to develop the statistical relationships, are taken from GCM output.

In reality, many downscaling approaches consist of the attributes of more than one of these methods and therefore tend to be hybrid in nature.

The statistical downscaling strategy can be formulated in a general way as in Zorita and von Storch (1997) as follows:

Downscaling Model Design

a. Identify regional climate parameter of interest, *R*.
b. Find climate parameter *L* which
   i. controls *R* by $R = F(L,\alpha) + \varepsilon$ with a vector of unknown stochastic parameters $(\alpha_1, ..., \alpha_m)$. The ε represents the part of *R* not described by *F*.
   ii. is reliably simulated in a climate model
c. Use paired samples (*R, L*) from historical records to fit α such that

$$\|\varepsilon\| = \|R - F(L,\alpha)\| = min$$

d. Verify the fitted model $R = F(L,\alpha)$ by means of independent historical data.

Model Application

a. Get the climate parameter *L* from the output of the climate model.
b. Check if the climate model reproduces the link between *R* and *L*.
c. Calculate *R* by $R = F(L,\alpha)$.
d. Use *R* as forcing function i.e for an impact model.

The general limitations, theory and practice of downscaling are well described in the literature (e.g. Grotch and MacCracken, 1991; von Storch et al., 1993; Zorita and von Storch, 1997 and Wilby and Wigley, 1997). A summary of statistical downscaling approaches with respect to their assumptions, uses and limitations is given in Appendix 2 (Xu, 1999).

3.3 Assessment of Consequences of Climatic Factors at the Catchment Scale

There is no doubt about the sensitivity of the hydrological system to changes in the climate. Varying precipitation amounts and intensities affect the timing of runoff generation as well as the frequency of extremes such as floods and droughts. Similarly, changes in temperature influence the evaporation, soil moisture and infiltration mechanisms in a catchment. There is evidence from climate models and hydrological impact studies that flood frequencies are likely to increase with global warming. The extent of increase is uncertain and these uncertainties will vary considerably between catchments for a given change in climate (IPCC, 1996).

For the investigation of the consequences of climate and climate change on individual river basins, it is crucial to perform the downscaling of observed and GCM modeled large-scale information and to evaluate the outcomes at the local scale. To date, the usual way of achieving this task is downscaling precipitation and temperature from GCM simulations and running a rainfall-runoff model to produce results at the catchment scale i.e. discharge for the analysis of extremes.

Current approaches to hydrological modeling for climate change assessments include empirical models, water balance models, conceptual rainfall-runoff models, and physically based distributed models (Leavesley, 1994). As an example, a semi-distributed, topographic model TOPMODEL (e.g. Beven and Kirkby, 1979, Beven et al., 1995) has been used to derive forecasts of hydrological responses to climatic change. The input variables within TOPMODEL are rainfall, temperature, potential evaporation, catchment soil data and the distribution of the topographical index. The outputs are runoff, water equivalent snow (Lepistö and Kivinen, 1997), average amount of soil water, average groundwater depth and the fraction of saturated areas within the catchment.

Bardossy (1999) used a modified version of the HBV model for rainfall-runoff modeling and for calculating the water balance in order to assess the impact of climate change on the hydrological regime of the Upper Neckar catchment in Germany. Downscaling was performed both for observed and GCM modeled large-scale atmospheric variables. The HBV

model uses daily precipitation and temperature data from climate stations to provide daily estimates of areal precipitation, snow accumulation and melt, soil moisture, groundwater level, discharge and routing through lakes.

Another hydrological model coupled with downscaling methods is LARSIM (Large Area Runoff Simulation Model). LARSIM is a partly conceptual and partly physically-based continous model describing the vertical and horizontal water fluxes within the soil. Besides runoff generation in the area of interest, the translation and retention in the river channel and artificial influences of water management systems are included in the model. Lorenz et al. (2003) coupled the atmospheric climate model REMO (Regional Model) and the hydrological model LARSIM within the framework of the BALTic Sea Experiment (BALTEX) and applied it to selected basins in the Baltic Sea as well as in major parts of central Europe.

Much effort has been spent in the last decades to create numerical models to simulate streamflow and simultaneously for simulating all the processes in the hydrological cycle so that estimates can be obtained for many other quantities besides streamflow. However, it is usually the streamflow which is seen as one of the end- products of a model.

Despite the high number of sophisticated hydrological models, new ideas and challenging approaches are sought in order to better explain the complex interactions between climate and local scale variables. This research attempts to link the large-scale information to local-scale *directly* without using rain or rainfall-runoff modeling. An empirical link between the surface variables and the *discharge* will be accomplished in order to investigate the interactions between climate and floods in the Study Areas. The details of the approach will be highlighted in the following chapters.

Chapter 4

Fuzzy Rule-Based Classification

4.1 Introduction

The first stage of the research is based on the classification of circulation patterns for the identification of flood producing weather conditions, and the second phase consists of the application of a new downscaling approach that enables the investigation of possible past, present and future floods at the catchment scale. In this chapter, the application of the fuzzy rule-based classification technique and the results of the classification will be discussed in detail.

A new methodology for the identification of flood producing CPs in mesoscale catchments has been developed since the existing classifications were developed to explain rainfall or temperature conditions, but not directly floods. Existing CP classifications are developed for climatic variables such as precipitation and temperature using subjective or objective classification methods (Goodess and Palutikof 1998, Jones et al., 1993, Stehlik and Bárdossy, 2002) as discussed in Chapter 3. These CP types are not necessarily optimal for explaining flood production because local high precipitation events (affecting only a part of the catchment) might not lead to a substantial increase of the discharge. Therefore a new classification was required in order to classify atmospheric circulation patterns with respect to floods.

The fuzzy rule-based optimization approach used here is an objective classification method. Depending on the surface weather variables to be downscaled (i.e. precipitation, temperature, here discharge increases), the objective of the classification is to define CPs which explain the variability of these surface variables used. Thus, the CPs explain the dependence between large-scale atmospheric circulation and the surface climate (including the spatio-temporal variability). Therefore, the circulation patterns obtained by this classification method are more appropriate to be used as input for downscaling purposes of discharge.

The CPs can be defined by using large scale information i.e. sea level pressure (SLP) data, geopotential heights such as 500 hPa or 700 hPa or other predictor variables such as specific humidity.

As stated above, the goal of the classification in this study is to identify *critical* weather conditions leading to floods by including the discharge information of the distinct catchment in the definition of circulation patterns. Since discharge comprises the effective rainfall which falls down to the catchment, the method promises a better description of the flood-prone weather conditions in the selected basin. Regarding floods, discharge could also be preferred compared to precipitation since it integrates the precipitation falling over a large area, and is thus less influenced by local precipitation variability. This is the reason why discharge can be better linked to large-scale features.

Figure 4.1 illustrates the daily discharge series of Ardèche at Saint Martin in 1970. It can be observed that sudden peaks in the discharge curve are followed by smoother recession limbs in which discharge gradually decreases (excess water flowing out of the catchment). The rising limb in the graph depicting storms reflects the magnitude and duration of the rain event.

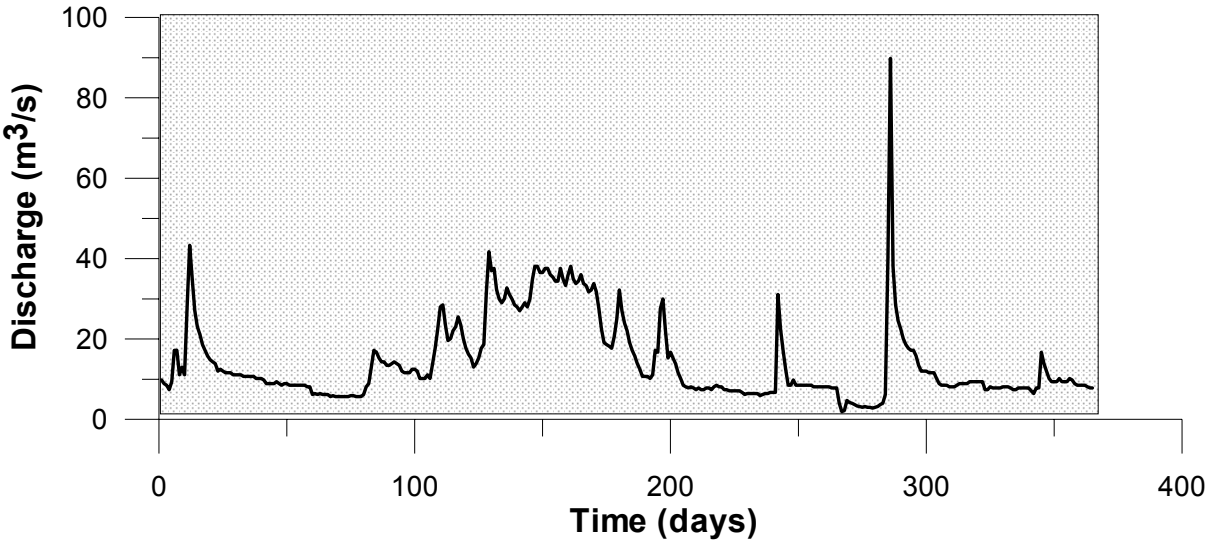

Figure 4.1 Daily discharge series at Ardèche St. Martin in 1970.

Downscaling methods for precipitation and temperature are based on the fact that the surface weather variables on a given day can be directly linked to the atmospheric circulation on the same day. This is not always the case for discharge as high discharge is often the result of weather on the previous days. On a daily time scale, the relationship between large-scale atmospheric features and discharge is difficult to find. The main reasons for this are:

- the delayed reaction of catchment runoff due to the concentration time depending on the size of the basin,
- other influencing factors related to the state of the catchment such as antecedent moisture or previous rainfall, vegetation features,
- high discharges occur both in the rising as in the falling limb of the discharge curve meaning that high discharge might correspond not only to a day with heavy rainfall, but also to a dry day following a flood peak.

In order to link the atmospheric circulation to discharge on daily time scale, instead of discharge values Q(t) on a given day, the differences in discharge ΔQ(t) (discharge increments) were considered as seen in Equation (4.1):

$$\Delta Q(t) = Q(t) - Q(t - \Delta t) \tag{4.1}$$

$\Delta Q(t)$: Difference in discharge within the time window "Δt"
$Q(t)$: Discharge of the day
$Q(t - \Delta t)$: Discharge of the previous day(s)

The discharge time series and the daily differences of discharge (Δt =1 day) of Ardèche-Saint Martin can be seen in Figure 4.2. Obviously, positive changes in discharge are followed by the negative ones.

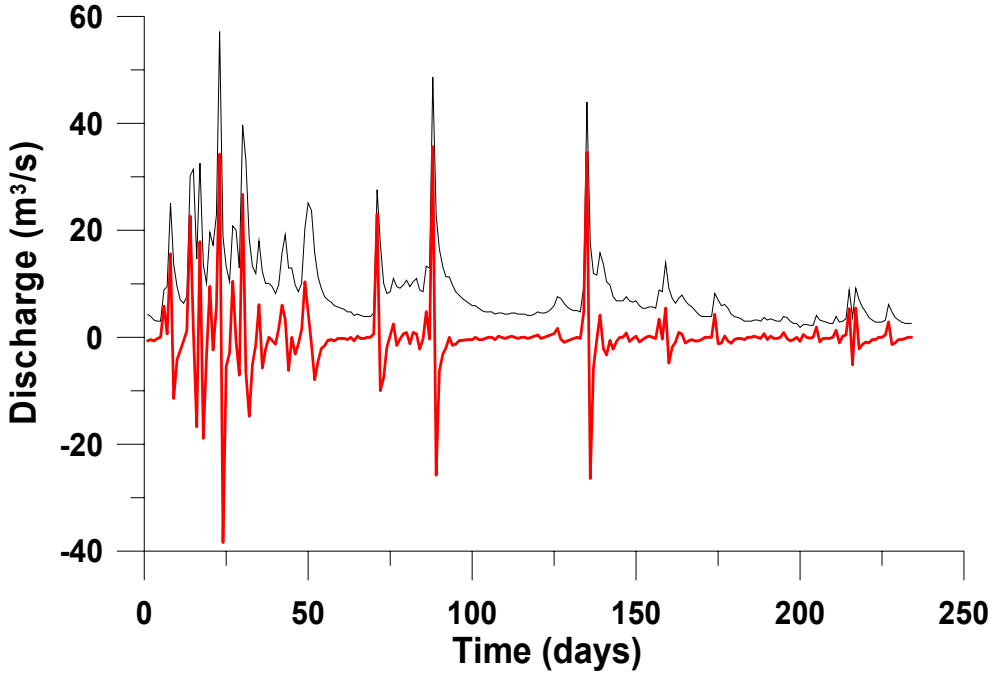

Figure 4.2 Discharge time series of Ardèche-Saint Martin. Black line shows discharge, red line indicates daily differences in discharge.

The time window Δt for the determination of discharge increment series depends on the catchment characteristics and size. For catchments with short concentration times, Δt can be defined as a few hours or one day. For catchments with longer concentration times, Δt might last up to a few days in order to include the lagged relationships.

An increase of the discharge (ΔQ(t) > 0) is usually caused by precipitation (or snowmelt). The decrease (ΔQ(t) < 0) is the natural reaction of the watershed to conduct excess water out of the catchment. Thus, the weather and catchment related components of discharge differences can be distinguished as shown in Figure 4.3.

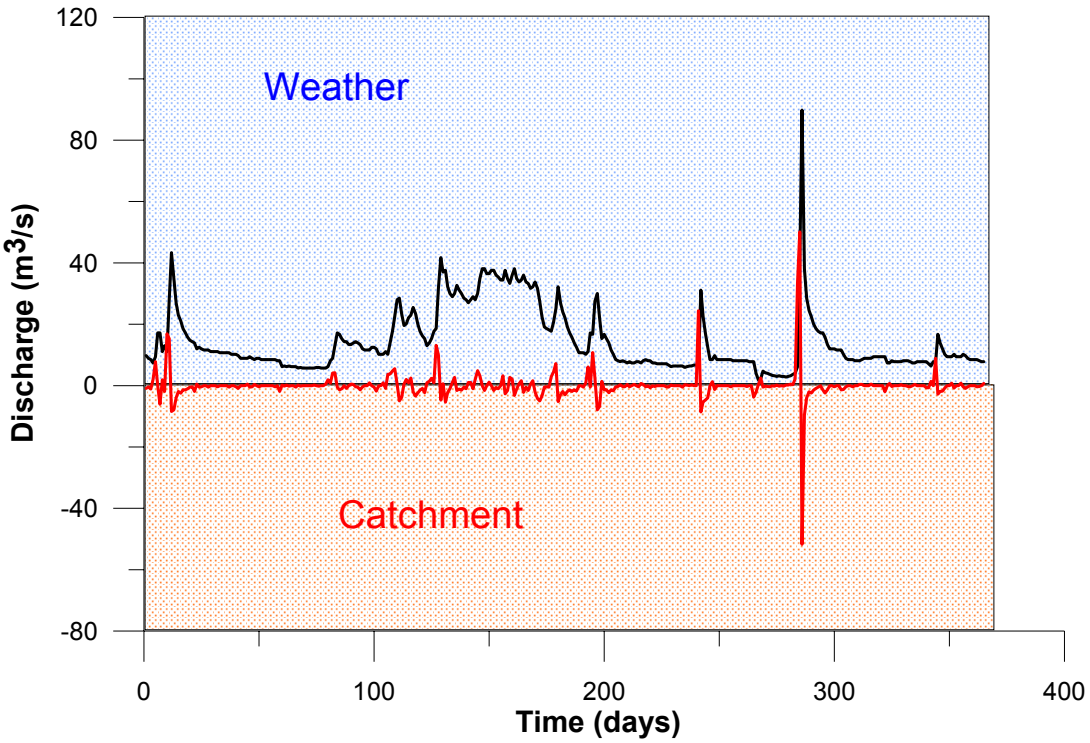

Figure 4.3 The principle of CP definition: Discharge increases are caused by atmospheric circulation patterns whereas the discharge decreases are the natural reaction of the catchment to conduct excess water.

For the analysis of flood producing weather situations, days with positive changes (ΔQ(t) > 0) are interesting since the increases in discharge are the response of the catchment to the atmospheric signal (in form of precipitation). Figure 4.4 demonstrates the discharge increases that are to be explained. Introducing the positive part of ΔQ(t) as new variable Z(t) results from:

$$Z(t) = \begin{cases} \Delta Q(t) & if \quad \Delta Q(t) > 0 \\ 0 & else \end{cases} \tag{4.2}$$

As it can be seen in Figure 4.4 and Figure 4.5, both discharge increases and precipitation show similar characteristics in their discrete nature.

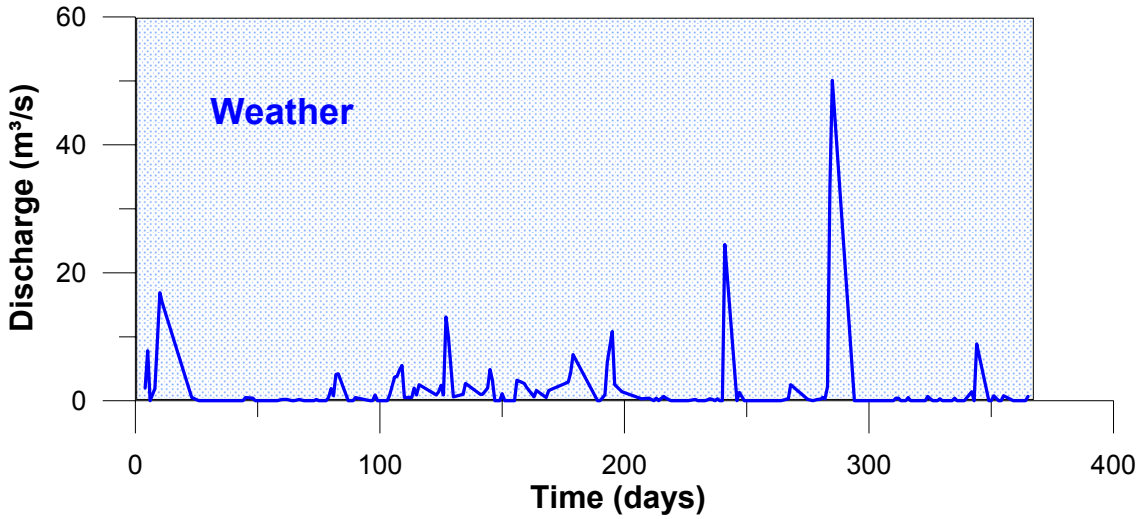

Figure 4.4 Signal to be explained: Positive discharge increments of discharge Z(t) are related to weather.

The problem of linking Z(t) to CPs is that in larger catchments, the effect of rainfall on a given day might also be an increase of the discharge on the subsequent days due to longer concentration times. However, if mesoscale catchments with relatively short flow duration (up to a few days) are considered, the approach is useful.

In addition, CPs tend to prevail for a few days making the identification of critical CPs easier. Further, the linkage of discharge to large-scale meteorological conditions is preferable since discharge is less influenced by local effects.

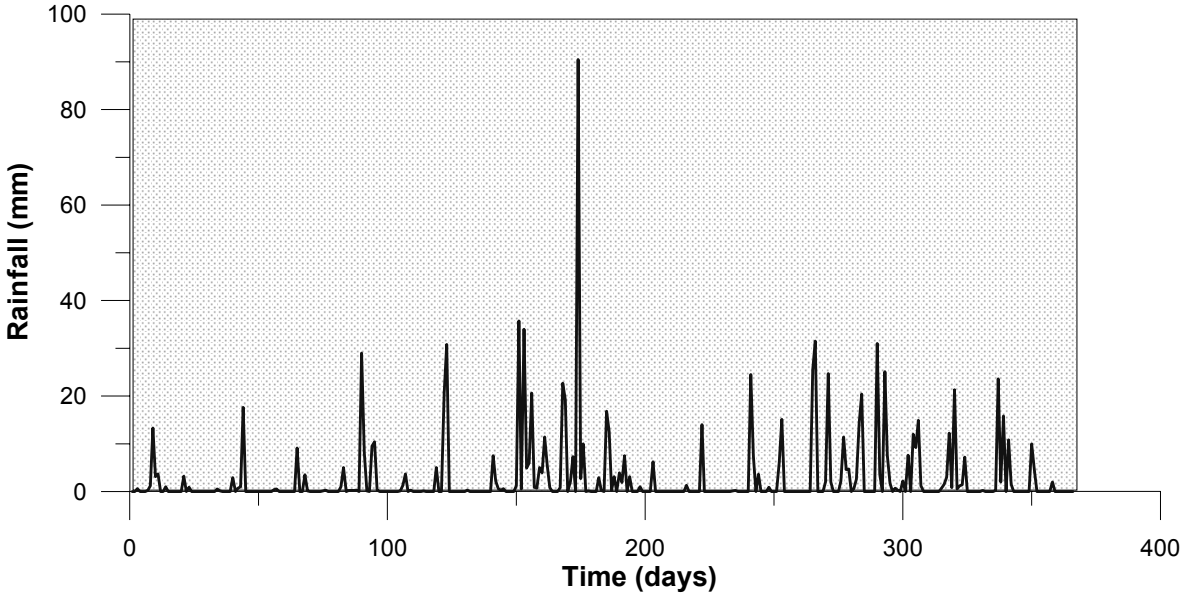

Figure 4.5 Daily precipitation series in Ardèche at Privas in 1970.

The goal of the classification is to obtain CPs which lead to large values of Z(t) indicating high discharge increases. The classification method used is the fuzzy rule-based classification described in detail in Bárdossy et al. (1995) and in Stehlik and Bárdossy (2002). For the identification of flood causing weather situations, the atmospheric circulation patterns (CPs) have to be classified in order to assign one CP to each day. The classification of the circulation patterns is based on the concept of fuzzy sets (Zadeh, 1965) which enables dealing with imprecise statements.

Zadeh stated that "as complexity rises, precise statements lose meaning and meaningful statements lose precision." by referring to the principle of incompatibility in his paper (Zadeh, 1973) which claims that when the complexity of a system exceeds a certain limit, precise and meaningful description of the system´s behavior becomes impossible, and its description must incorporate imprecision. Fuzzy logic enables this imprecision by allowing memberships which define the degree of belonging of a number to an interval or a set instead of the number itself (crisp). Fuzzy theory is a broad theory including fuzzy set theory, fuzzy measure, fuzzy control and others. Fuzziness, as handled in fuzzy logic, is an extension of conventional (binary) logic to handle vagueness mathematically. Details of fuzzy logic can be found in Bárdossy and Duckstein (1995), Tanaka (1997), Zimmermann (1996) and Dubois and Prade (1980).

In the classification of the CPs, each CP is described by a rule containing a set of locations with prescribed pressure anomalies such as low, high pressure, very low, above average etc.

The fuzzy rules are not identified by the expert, but instead, an optimization algorithm called Simulated Annealing (SA) is used as described in Bárdossy (2000). The classification consists of four steps:

- Data transformation (calculation of pressure anomalies),
- Definition of the fuzzy rules,
- Validation of the classification using a split sampling method,
- Classification of observed data.

The transformation of data is done by computing the statistical characteristics of observed data for each time step followed by the standardization.

The basis of the classification are atmospheric data such as SLP or geopotential height fields. In addition to air pressure data, air temperature data can also be involved in the classification. These data are available on a regular grid in daily resolution. The normalized anomalies *g(i,t)* are calculated from the gridded pressure data *h(i,t)* by:

$$g(i,t) = \frac{h(i,t) - \bar{h}(i,t)}{s(i,t)} \tag{4.3}$$

where $i = 1,..,$ I are the gridpoints, $t = 1,..,$ T is the time (in days), $\bar{h}(i,t)$ is the mean annual cycle smoothed (mean over the corresponding Julian date) and *s(i,t)* is the standard deviation for the given date.

Each circulation pattern is defined through a fuzzy rule. These are defined by the location of high and low pressure anomalies. Additionally, for each pattern a large number of locations are considered to be unclassified. To each gridpoint *i*, a fuzzy set membership function is assigned. Five different possibilities are considered as follows:

The anomaly at the location is:

- large positive
- medium positive
- medium negative

- large negative
- arbitrary.

While the first four classes describe the locations of the pressure centers (such as large positive representing points with very high atmospheric pressure etc), the fifth class indicates locations whose anomalies are irrelevant for the CP (unclassified). These five possible classes of anomalies appear to be adequate to describe the main CP features. Thus the *k*-th CP is described with the fuzzy rule *k* represented by a vector

$$v(k) = (v(1,k),....,v(I,k)) \tag{4.4}$$

Here *v(i,k)* is the index (1 to 5) corresponding to gridpoint i for CP *k*. I is the number of gridpoints for which the air pressure data are available. The rule system describing K CPs can be represented by the matrix **V**:

$$\mathbf{V} = \begin{pmatrix} v(1,1) & \dots & v(I,1) \\ . & & . \\ . & & . \\ \\ v(1,K) & \dots & v(I,K) \end{pmatrix} \tag{4.5}$$

The *v(i,k)* -s are the indices (1,…,5) of the membership function corresponding to the selected locations. For the five possible classes membership functions *v* of the rule premises corresponding to previously defined anomalies are defined as triangular fuzzy numbers:

- $v = 1$ very low $(-\infty,-1,-0.2)_T$
- $v = 2$ medium low $(-1.4, -0.6, 0)_T$
- $v = 3$ medium high $(0, 0.6, 1.4)_T$
- $v = 4$ very high $(0.2, 1, +\infty)_T$
- $v = 5$ the membership function is the constant 1.

The membership function of the triangular fuzzy number $(a, b, c)_T$ is defined as:

$$\mu(g) = \begin{Bmatrix} 0 & if & g < a \\ \frac{g-a}{b-a} & if & a \le g < b \\ \frac{g-c}{b-c} & if & b \le g < c \\ 0 & if & g > c \end{Bmatrix} \tag{4.6}$$

The fifth alternative is considered in order to allow any possible pressure anomalies for those locations that have no influence on the circulation pattern. The location and number of such gridpoints depend on the class to be described. Usually most of the gridpoints belong to this class and only characteristic ones are assigned to other classes. The location of these gridpoints might vary for different CPs.

The classification of the pressure map of a given day *t* is done as follows:

- The daily pressure map is transformed to a daily anomaly map according to Equation (4.3)
- For the classification, the membership grades of the pressure anomalies are computed. For a given time *t*, and location *i*, the membership grade $\mu_m = \mu(i,k)$ corresponding to rule *k* is defined as:

$$\mu_m = \mu(i,k) = \mu_{v(i,k)}(g(i,t)) \tag{4.7}$$

- For each rule, the degree of fulfillment (DOF) is calculated as follows:

$$DOF(k,t) = \sum_{m=1}^{4} \left(\frac{1}{N_{k,m}} \sum_{v(i,k)=m} \mu_m(g(i,t))^{p_m} \right)^{\frac{1}{p_m}} \tag{4.8}$$

where $N_{k,m}$ is the number of gridpoints which are assigned to class *m* in rule *k*. μ_m is the membership function of the anomalies corresponding to the five previously defined cases. The exponents p_m are used to account for possible small differences in the exact location of the anomalies. Their role and choice is discussed in Bárdossy et al. (1995).

- The rule k_0 with the highest *DOF(k,t)* is selected, and the corresponding index k_0 is assigned as CP of the day.

The difficulty of this classification method is how to assess the rule vectors. A subjective definition of the rules requires good knowledge of the local meteorological conditions which is often not available. Another possibility for the assessment of the rules is using optimization techniques. Optimized classification means that the rules are assessed for a specific goal such as the best description of local surface variables (here discharge increases). In order to find the *optimal* rules for the description of flood producing weather situations, the performance of the classification has to be defined. Several different functions can be introduced to measure the performance of the classification with regard to identification of flood producing weather conditions. Two measures are used in this study, the *occurrence of positive increments* and a *wetness index*. The performance regarding the probability of the occurrence of a positive increment (a day with increasing discharge) can be measured with:

$$O_1(\mathbf{V}) = \sqrt{\frac{1}{T}\sum_{t=1}^{T} p_{z_0}(z(CP(t)=i)) - \overline{p}_{z_0})^2} \tag{4.9}$$

where $\overline{p_{z_0}}$ is the probability of an increase of the discharge exceeding a given limit $z_0 \geq 0$ on an arbitrary day. $p_{z_0}(z(CP(t)=i)$ is the probability of the occurrence of an increase of the discharge exceeding a given limit $z_0 \geq 0$ on a day with CP of class $i(CP(t)=i)$, and T denotes the total number of days. The value of O_1 is large if there are circulation patterns which often lead to discharge increases that are greater than z_0, and others which seldom or never lead to increase of the discharge exceeding z_0. This means, when the classification is finalized, both wet and dry weather conditions (wet and dry CPs) can be identified.

The second measure is to describe the magnitude of an increase:

$$O_2(\mathbf{V}) = \frac{1}{T}\sum_{t=1}^{T}\left|\frac{\overline{z(CP(t)=i}}{\overline{z}} - 1\right| \tag{4.10}$$

where $\overline{z}$ is the mean increase of the discharge on an arbitrary day. $\overline{z(CP(t)=i)}$ is the mean increase of the discharge on days t with CP $i(CP(t)=i)$. This objective measures the relative performance of the classification compared to no classification. The value of O_2 is large if there are CP types which *regularly* lead to high increases of discharge and others

which do not. This measure is thus related to flood peaks and flood volumes. Both objective functions O_1 and O_2 are calculated for four seasons separately. Higher values indicate a better classification.

The objective of the classification is to identify a rule system **V** which maximizes the two above objective functions (more objective functions are also possible; for example by considering different z_0 values). For this purpose, a weighted sum of the two objectives is used as a single objective function in order to consider both functions simultaneously:

$$O(\mathbf{V}) = w_1 O_1(\mathbf{V}) + w_2 O_2(\mathbf{V}) \tag{4.11}$$

where w_1 and w_2 are weights for the objective functions for O_1 and O_2 respectively. The weights are chosen subjectively according to the importance of the objective functions. In this study, a higher weight is assigned to O_2, since flood peaks and flood volumes are of higher interest than flood occurrences and therefore the focus is on finding CP types which regularly correspond to high discharges and others which do not.

The optimization is done over the set of all possible rule matrices **V**. Due to the complexity of the objective function which has an implicit form, an algorithm based on simulated annealing is used. The following is a summary of the algorithm.

The simulated annealing algorithm (Aarts and Korst, 1989), as its name implies, exploits an analogy between the way in which a metal cools and freezes into a minimum energy crystalline structure (annealing process) and the search for a minimum in a more general system. The algorithm is based upon that of Metropolis et al. (1958), which was originally proposed as a means of finding the equilibrium configuration of a collection of atoms at a given temperature. The connection between this algorithm and mathematical minimization (or maximization depending on the objective) was first noted by Pincus (1970), but it was Kirkpatrick et al. (1983) who proposed it as the basis of an optimization technique for combinatorial (and other) problems. The major advantage of simulated annealing over other methods is its ability to avoid becoming trapped by local minima (or maxima depending on the purpose of the objective function). If the objective function will be maximized, the algorithm employs a random search which not only accepts changes that increase the

objective function, but also some changes that decrease it. The latter are accepted with a certain probability. A flow diagram of the simulated annealing algorithm can be found in Appendix 3. The following elements must be provided for Simulated Annealing:

- A representation of possible solutions
- A generator of random changes in solutions
- A means of evaluating the problem functions
- An *annealing schedule* – an initial temperature and rules for lowering it as the search progresses

The objective of the optimization procedure is to find such fuzzy rules for which the optimization criterion reaches its *maximum* value. This means that the problem can be defined as a combinatorial optimization problem. Due to a given number of fuzzy rules (CPs), it is necessary to consider that each rule has a given number of terms (gridpoints), depending on the size of the pressure window and for each point, one of the five possibilities (fuzzy numbers) can be defined. Since the number of the possible combinations is large, it is not possible to compute the objective function for each combination systematically. The number of all combinations depends on the size of the pressure window and number of CPs to be optimized. In this study, the number of all combinations is approximately 10^{1000} . Therefore, the consideration of all possibilities to find the best result is impossible. For a fixed number of rules, the algorithm for surface variables such as precipitation and temperature as described in Bárdossy et al. (2002) and Stehlik and Bárdossy (2001) can be summarized in several steps as follows:

1. Initialize the rules randomly and evaluate the performance *O*
2. Set the initial "annealing temperature" to q_0
3. Select a rule *k* randomly
4. Select a location *i* randomly
5. Select class v^* randomly
6. If $v(i,k) = v^*$ return to step 2
7. Set $v(i,k) = v^*$ and perform the classification using the modified rule system

8. Calculate performance O^* for the new rules
9. If $O^* > O$ then accept the change
10. If $O^* \leq O$ then with probability $exp\left(\frac{O - O^*}{q_s}\right)$ accept the change
11. If the change is accepted, take $v(i,k) = v^*$ else reset to its previous value
12. Repeat steps 2-10 M times (M refers to number of attempted changes)
13. Decrease the "annealing temperature" by setting $q_{s+1} < q_s$
14. Repeat steps 2-12 until the portion of accepted changes becomes smaller than a predefined threshold.

The initial annealing temperature q_0 is selected so that 50 to 80 % of the attempted changes are accepted. During the first few iterations, the program adjusts it in the way that the above condition is fulfilled. The reason for this choice is to allow strong deviations from the initial rules. The number of attempted changes M, at a given annealing temperature q_s, should be at least as much as the number of arguments multiplied by the number of rules. The algorithm makes it possible to accept negative changes. Accepting these changes depends on the "annealing temperature" which will be decreased during the optimization procedure. It must be considered that the initial classification does not influence the appearance of the resulting optimized CPs in any manner. The optimization process adjusts any initial classification resulting with an "*optimal*" solution.

Once the rules for the CPs have been assessed, the classification has to be validated. A split sampling approach was used for the optimization and validation of the CP classification to determine the classification performance objectively. The objective functions used for the optimization can also be applied as measures of the classification quality.

4.2 Application of Fuzzy Rule-Based Classification to the Study Areas

The fuzzy rule-based classification method described above was applied to several regions of Europe. Here, the results of the classifications for the Ardèche River in France and the Llobregat River in Spain will be presented.

For the assessment of the circulation patterns, a sequence of observed daily sea level pressure distributions was used. This was achieved by using daily gridded sea level pressure data representing large-scale atmospheric information and discharge observations with daily temporal resolution for the indication of floods in the Studied Regions.

Figure 4.6 shows the location of gridpoints of the SLP data used for the classification. The gridded sea level pressure data that represent the observations originate in the National Center for Environmental Research (NCEP) analysis provided by National Center for Atmospheric Research (NCAR, USA). The resolution of data is 5° x 5°. SLP data were preferred to produce long CP time series, since the daily SLP data set is available for the time period 1899-2003 in contrast to geopotential heights (500 hPa, 700 hPa) data for which exist since the mid-20th century.

For the present study, it was essential to involve long time series of data in order to analyze the flood events which are discrete and rare in their occurrence. It should also be noted that for some cases, the geopotential height might come out to be a better predictor than SLP data. For such investigations where the length of the time series does not play an essential role (i.e for precipitation/temperature downscaling), it would be recommendable to compare the quality of the classification based on several pressure datasets. Stehlik and Bárdossy (2003) generated several classifications for basins in Europe using different predictors and compared the classification performances.

The daily discharge time series of the French catchment Ardèche at Saint Martin and Vogue gauges were obtained from Météo France. Complementary to discharge data, daily precipitation data from 2 Stations (Aubenas, Privas) were also provided for 1960-2000 and 1969-2000 respectively. For the Spanish catchment Llobregat at Martorell, Castellvell and Vilumara gauges, the daily discharge observations were provided by Centro de Estudios

Hidrográficos within CEDEX. Due to the availability of longer discharge series at Saint Martin in the Ardèche and at Martorell in the Llobregat, more importance was assigned to these stations than for the others. Longer data series should deliver more reliable outcomes.

The classification of gridded SLP data is done specifically for each catchment. For the Ardèche Catchment I = 84 gridpoints in total were used and K = 10 rules leading to 10 CPs were assessed whereas for the Llobregat Catchment, K = 12 rules were determined leading to 12 CPs to represent the typical weather situations.

For assessing the performance of the classification by using a split sampling approach, 10 years of discharge data (1981-1990) called the "learning period" were used in the optimization algorithm to identify the matrix **V**. Then the rule system was applied to a "control period" (1951-1980) to see whether the rule system captured the main features of discharge correctly (decision parameters are given on the next page). The objective function values for this control period (also named validation period) were compared to those of the learning period. In all cases, there were no significant differences between the obtained values of the statistics corresponding to the learning and the validation period. This indicates that 10 years of discharge data were sufficient to capture the main discharge characteristics in the Study Areas.

Any classification that defines probability $p(CP(t))$ and mean $\bar{z}(CP(t))$ of a discharge increase on a selected station for a single day *t* referring to the classification of the same day can be measured by the indices identical with the objective functions O_1 and O_2. In order to allow a seasonal difference of behavior for the classes (i.e. dry in summer and wet in winter), the indices are usually calculated for winter and summer or for all four seasons separately if necessary.

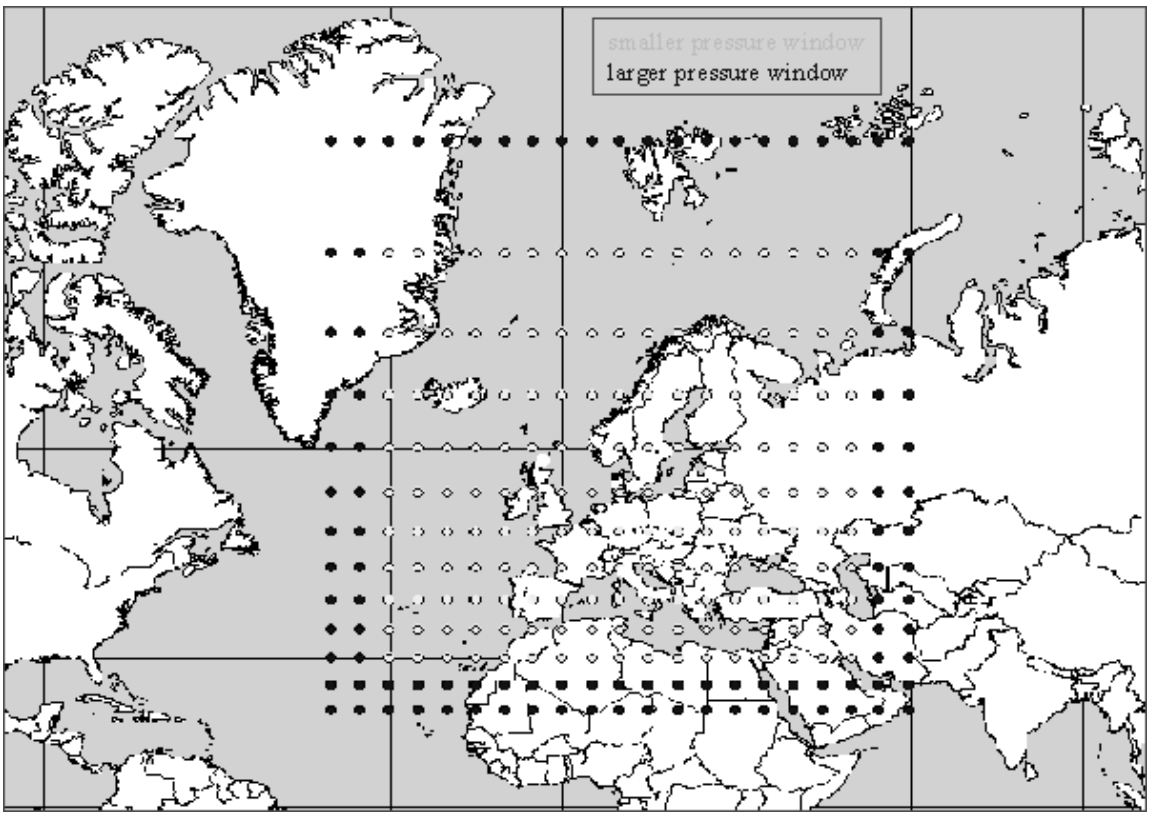

Figure 4.6 Locations of gridpoints used for SLP classification. Light color indicates the smaller pressure window, dark color the larger pressure window.

Parameters to evaluate the performance of the classification presented here are based on the following quantities that are calculated for each season:

HH [%]	Relative occurrence frequency of a CP for a given time period (CP occurrence rate: number of days with a given CP / total number of days)
p(CP(t)) [%]	Probability of a discharge increase on a day with a given CP
A [%]	contribution of the discharge increases within a given CP (ratio of percentage of discharge increases for a given CP to the total discharge increases for a given time period)
A/HH [-]	Wetness index: the ratio between contribution of discharge increases for a given CP and its occurrence rate (high values indicate wet CPs)
m [m³/s]	Mean discharge increases total on a wet day for a given CP
s [m³/s]	Standard deviation of discharge increases total on a wet day for a given CP

In Table 4.1, the results for the Ardèche Catchment at Saint Martin for the time period from October to April (1955-1997) are shown. All considerable flood events occurred in that time period of the year; the evaluation is therefore also restricted to this time interval.

The frequencies of the different CPs, the conditional frequency of discharge increases on days with a given CP, the relative contribution of the CP to the total discharge increases are given in Table 4.1. The higher the wetness index (A/HH), the more the increase caused by the CP. One can indicate the wet and dry CPs according to the wetness index as follows:

Wetness index < 1 indicates a dry CP
Wetness index ≈ 1 neutral
Wetness index > 1 wet CP

The conditional mean and the standard deviation of Z(t) are also shown in Table 4.1. According to the table three CPs – CP01, CP04, and CP05 (wet CPs are highlighted) – cause stronger discharge increases than normal (see also Figure 4.7 showing the occurrence frequency of the CP and its conribution to discharge increases in Ardèche-Saint Martin). By comparing the frequency and the wetness index of these CPs, it can be concluded that CP01 and CP04 are more important than CP05. They contribute to 70 % of all discharge increases. CP01 is extremely wet causing 434 % increase compared to an average day. Due to the fact that CPs might cause precipitation leading to a discharge increase on the following day, the contribution of days following CP01 or CP04 was also calculated. These days bring 10 % of the total increase, so 80 % of the total increase can be considered as a consequence of CP01 and CP04.

Table 4.1 Statistics of Z(t) for different CPs for the Ardèche Catchment.

Ardèche - St. Martin (October – April)						
CP	Frequency HH [%]	Probability of increase p(CP(t)) [%]	Contribution A [%]	Contribution/HH *wetness index* A/HH [-]	Mean m [m^3/s]	Standard Deviation s [m^3/s]
CP01	7.33	51.13	31.82	**4.34**	113.8	224.6
CP02	2.27	31.71	2.56	1.13	47.7	189.4
CP03	5.20	29.43	1.47	0.28	12.9	26.2
CP04	8.55	47.95	33.73	**3.95**	110.3	216.4
CP05	1.57	43.53	4.25	**2.71**	83.4	121.7
CP06	3.93	23.94	1.97	0.50	28.0	53.0
CP07	15.04	28.10	5.94	0.39	18.8	52.7
CP08	21.11	25.44	4.98	0.24	12.4	36.1
CP09	11.11	29.07	4.23	0.38	17.5	50.6
CP10	19.84	26.79	7.03	0.35	17.7	44.3
Unclassified	4.04	34.25	2.01	0.50	19.5	40.3

In order to see the precipitation behavior of the region conditioned on the CPs, the statistics corresponding to the station Privas in the Ardéche Catchment for the same period (October-April) between 1960-2000 were calculated. The results are shown in Table 4.2.

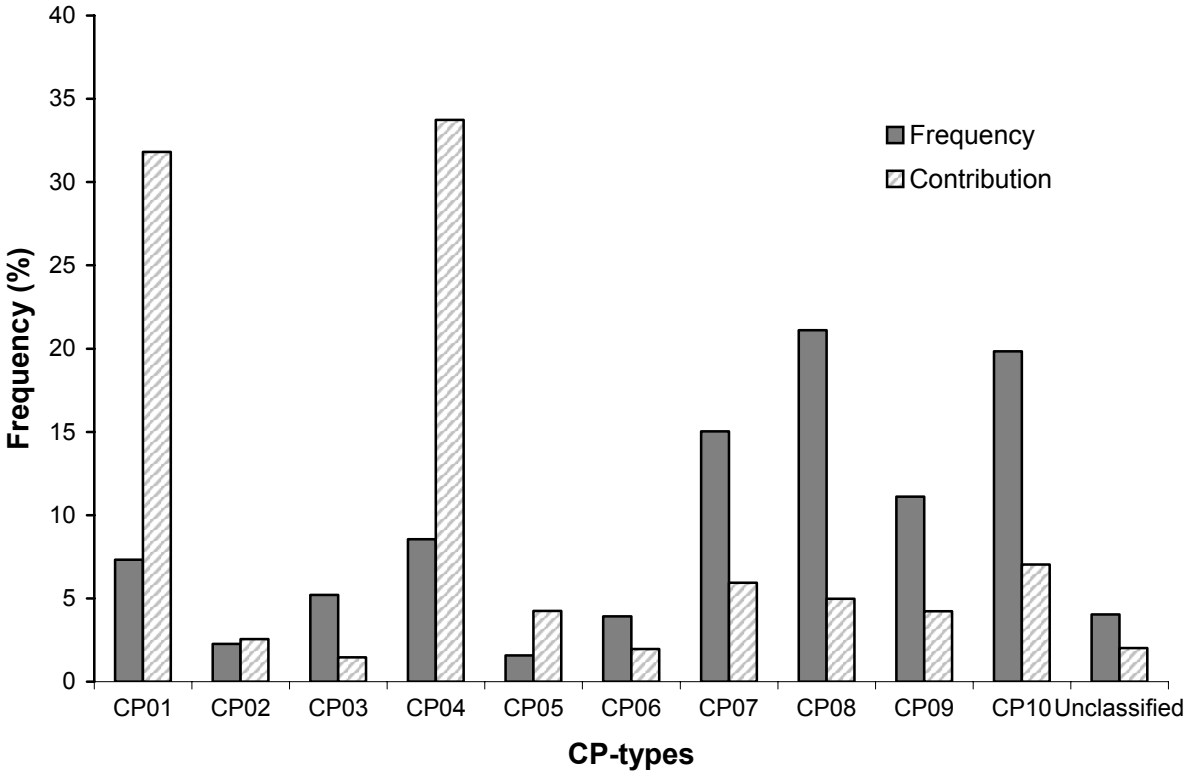

Figure 4.7 Diagram showing the occurrence frequency of CPs and their contribution to discharge increases at Ardèche-St. Martin (1955-1997).

Consequently, the same patterns cause high precipitation as discharge increases. The relative contribution of patterns CP01 and CP04 deviates slightly less from normal for precipitation than for discharge increase (direct discharge = effective rainfall). A possible explanation for this outcome is that precipitation might also occur on days with other CPs without causing considerable changes in discharge.

Figure 4.8 shows the normalized anomalies of the SLP for the *wettest* circulation pattern CP01 in the Ardèche. This CP is characterized by a low pressure anomaly on the Atlantic northwest from the Iberian Peninsula and a high pressure anomaly over the eastern Mediterranean region. The cyclone is shown by blue dashed lines and anticyclone is indicated by red solid lines. Between these two lines, warm and moist air originating from southwest of Africa is transported to the European region over the Mediterranean Sea and then is blocked and diverted counterclockwise to the Atlantic. Due to the temperature loss, water vapor condenses resulting in high precipitation.

Table 4.2 Statistics of precipitation for different CPs for the station Privas (Ardèche).

Privas - Ardèche (October – April)						
CP	Freq. HH [%]	Probability of Precipitation p(CP(t)) [%]	Contribution A [%]	Contribution/HH *wetness index* A/HH [-]	Mean m [m³/s]	Standard Deviation s [m³/s]
CP01	7.32	70.78	27.13	**3.71**	15.06	18.92
CP02	2.27	36.59	3.70	1.63	12.82	15.63
CP03	5.18	38.43	3.45	0.66	4.98	9.55
CP04	8.46	62.75	22.70	**2.68**	12.30	16.21
CP05	1.57	64.71	5.02	**3.20**	14.23	17.64
CP06	3.95	35.51	3.94	1.00	8.09	11.27
CP07	15.10	19.41	6.71	0.44	6.58	9.48
CP08	21.24	16.32	5.97	0.28	4.95	8.84
CP09	11.08	28.45	5.69	0.51	5.19	8.54
CP10	19.78	22.74	11.84	0.60	7.57	10.19
Unclassified	4.06	45.00	3.87	0.95	6.09	10.00

As shown in Table 4.1, this pattern (CP01) is responsible for most of the discharge increases, and thus is leading to floods. The wet CPs do not necessarily lead to floods, but most floods were related to them. In order to see to what extent the wettest CPs might explain floods, the series of observed annual maximum discharge was investigated. CPs prior to discharge maxima corresponding to major increases of discharge were identified. In Figure 4.9, the observed annual maximum discharge and the corresponding return periods and CPs are shown for the Ardèche basin. One can see that only three of the annual maxima of the period 1955-

1997 were not caused by CP01 and CP04. Two of the three were related to CP05 which was also identified as a wet pattern. Only the 1955- event which ranks 14th, was caused by a different CP, namely CP10.

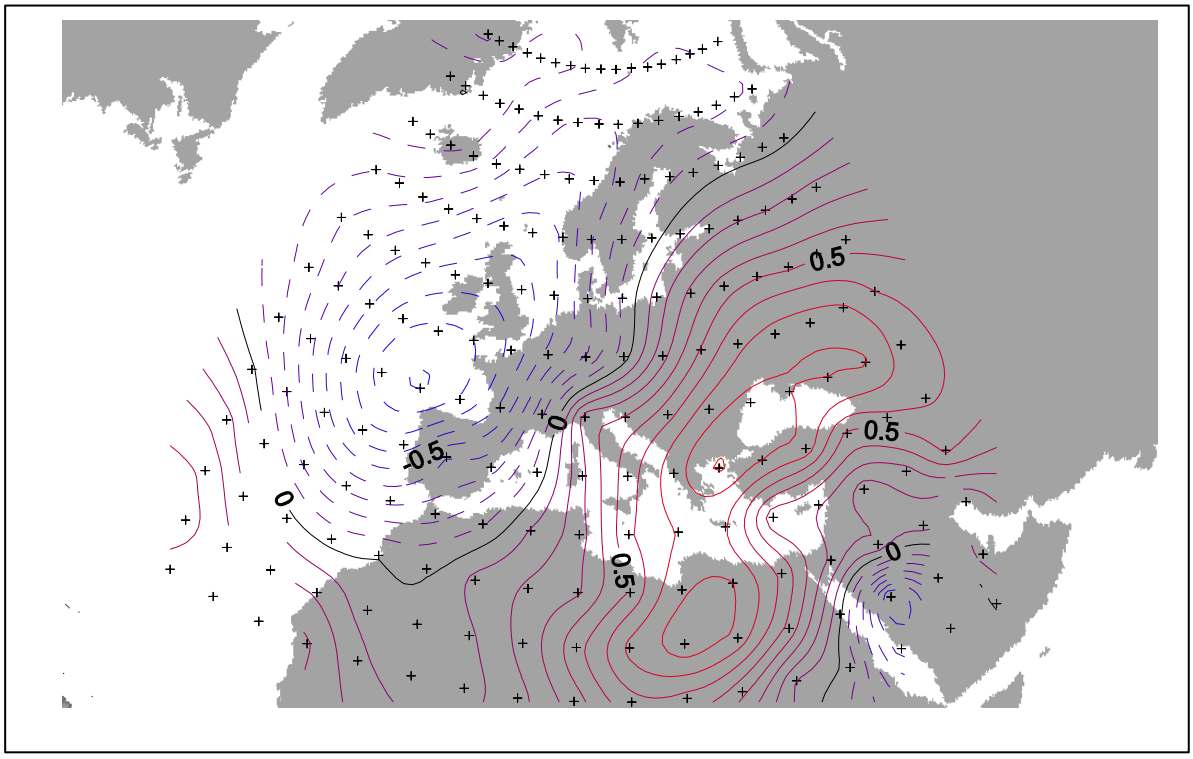

Figure 4.8 Normalized SLP anomaly map for the Ardèche Catchment (CP01). Blue dashed lines show low pressure anomalies, red solid lines show high pressure anomalies.

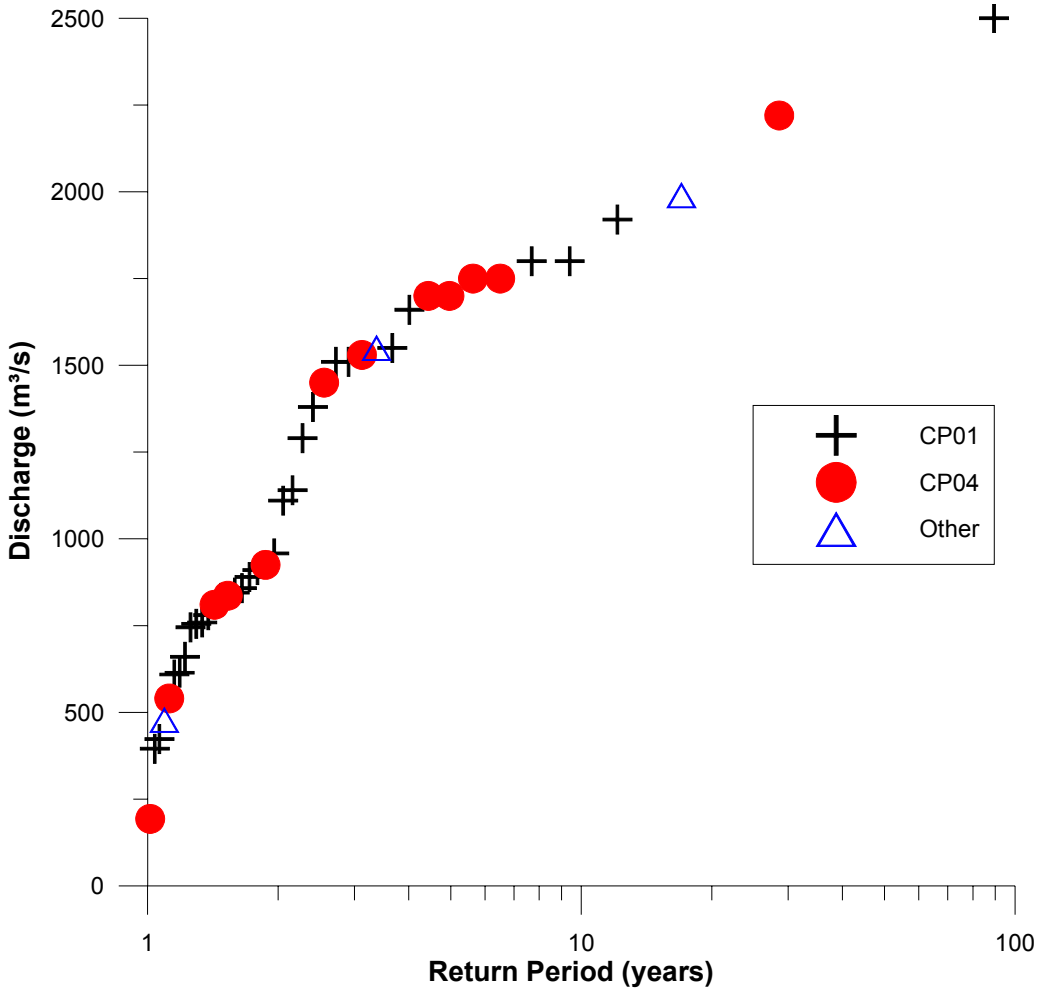

Figure 4.9 The observed annual maximum discharge versus return period and the corresponding CPs (Ardèche-St. Martin, 1955-1997).

Figure 4.10 shows the occurrence frequency of the wettest CPs (CP01) in the Ardéche. High wet CP frequencies indicate periods with high flood risk. As seen in the diagram, the occurrence of CP01 shows temporal variations in the range between 2-14 % without indicating any clear trend within the instrumental period. In addition, it should be considered that the instrumental period is quite short for detecting trends.

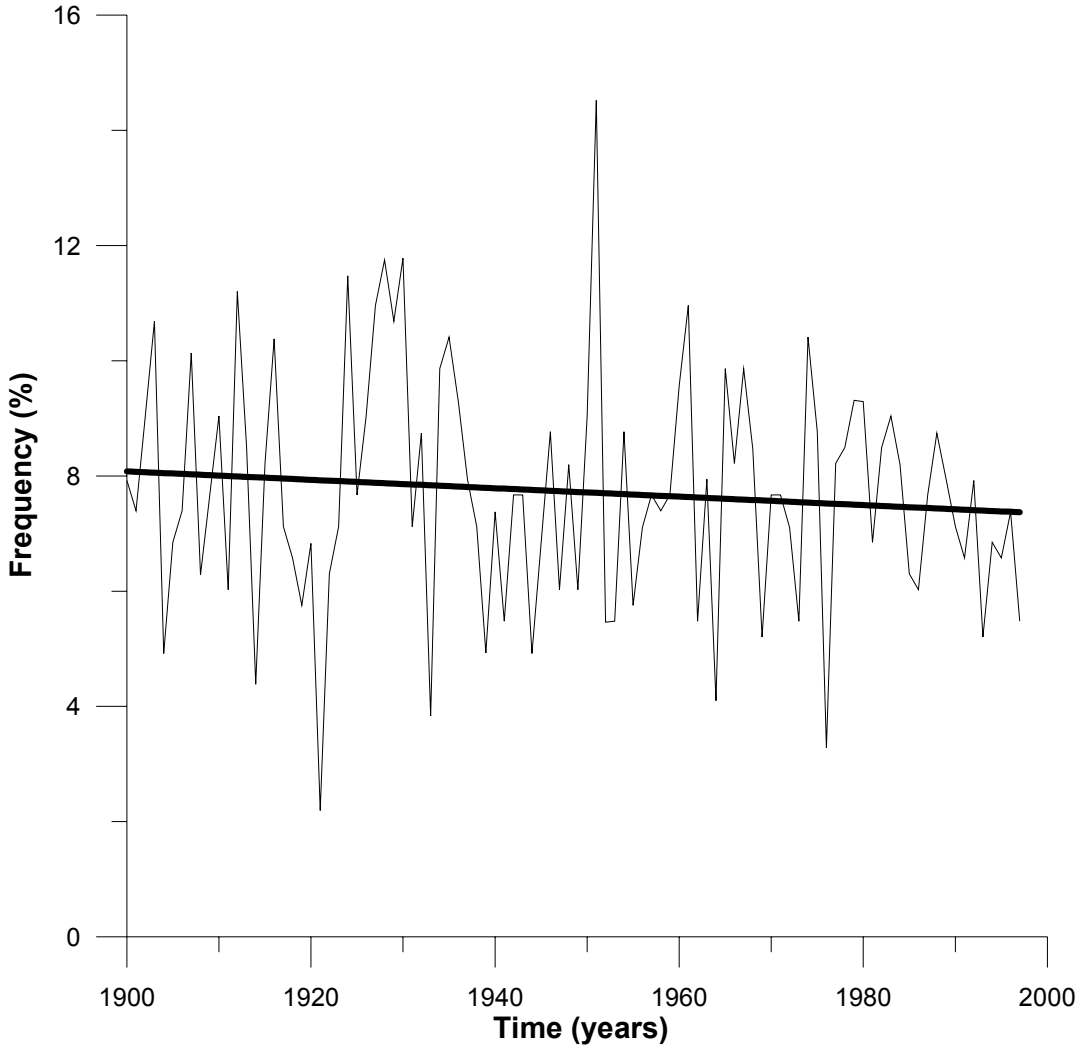

Figure 4.10 The occurrence frequency of CP01 with a linear fit in the Ardèche Catchment (1900-2000).

The results for the Llobregat Catchment are similar. There, one single CP is responsible for most of the discharge increases. All others are causing fewer increases than normal. The statistics of Z(t) for days with CP09 and on the subsequent days following CP09 (1 day and 2 days after CP09) in Table 4.3 show that the influence of wet CP (CP09) ceases rapidly since the catchment reaction is fast.

As seen in Table 4.3, the most of the discharge increases in the Llobregat Basin occur on the day of CP09 which prevails partly on the following day. However, the influence of CP09 becomes much weaker after two days. The duration of flood-causing weather types is short in the Llobregat. Llasat (1997) states also that the region is under influence of flash- floods especially in autumn.

Table 4.3 Statistics of Z(t) for Llobregat Catchment showing days with CP09 and the subsequent days.

Llobregat - Martorell (September – May)						
CP	Frequency HH [%]	Probability of increase p(CP(t)) [%]	Contribution A [%]	Contribution/HH A/HH [-]	Mean m [m³/s]	Standard Deviation s [m³/s]
CP09	7.32	35.23	46.61	6.37	27.2	73.4
1 day after CP09	5.11	29.41	16.01	3.13	16.0	29.4
2 days after CP09	4.53	16.77	3.11	0.69	6.2	10.8
Other days	83.04	15.38	34.27	0.41	4.0	10.0

Figure 4.11 shows the anomaly map corresponding to the *wettest* CP for the Llobregat (CP09). The catchment is influenced by a low anomaly centered over the western part of the Mediterranean Sea, east from the Spanish coast close to Llobregat Region. In this pattern, warm air with high moisture content moves from north Africa towards central Europe. The movement of the moist air is directed to the northwest forming a low anomaly center located over the Mediterranean and the high anomaly is centered over Romania.

The annual discharge maxima in the Llobregat Basin between 1912-1990 can be seen in Figure 4.12. It can be concluded that most of the major floods in the basin were caused by the wet CP (CP09).

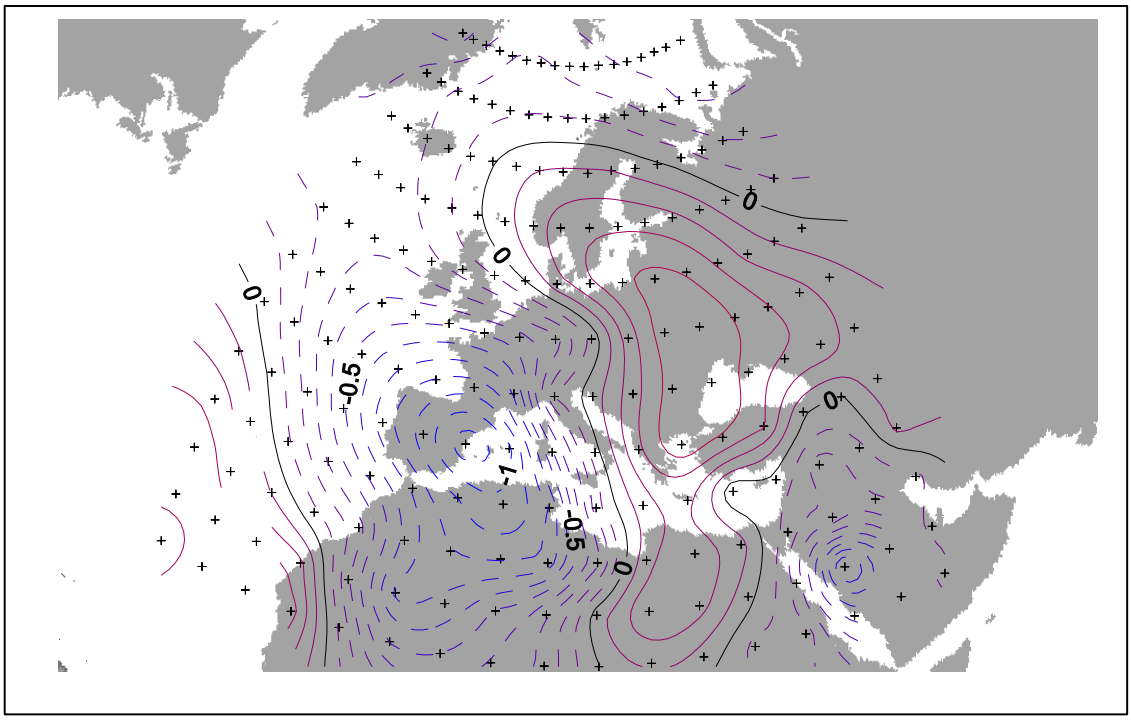

Figure 4.11 Wet CP (CP09) for the Llobregat Catchment. Blue dashed lines show low pressure anomalies, red solid lines show high pressure anomalies.

The analysis of longer CP time series should allow one to specify the role of climate in the occurrence of floods throughout the Study Areas. Therefore, the classification period was expanded up to 100 years (1900-2000) in order to investigate the variability in the CP frequencies within a longer period then the observation period.

Figure 4.12 shows the occurrence frequencies of all wet CPs for Ardèche-Saint Martin during the last 100 years (cumulative frequency of CP01, CP04 and CP05). The cumulative frequency should indicate an overall behavior of the wet CPs within the observation period. Again, the frequency of wet CPs show fluctuations in the range of 9-30 % of CP occurrence in the Ardèche basin. Within this period, the 10-year moving average indicates a slight trend of decrease in the wet CP occurrence in the Ardèche.

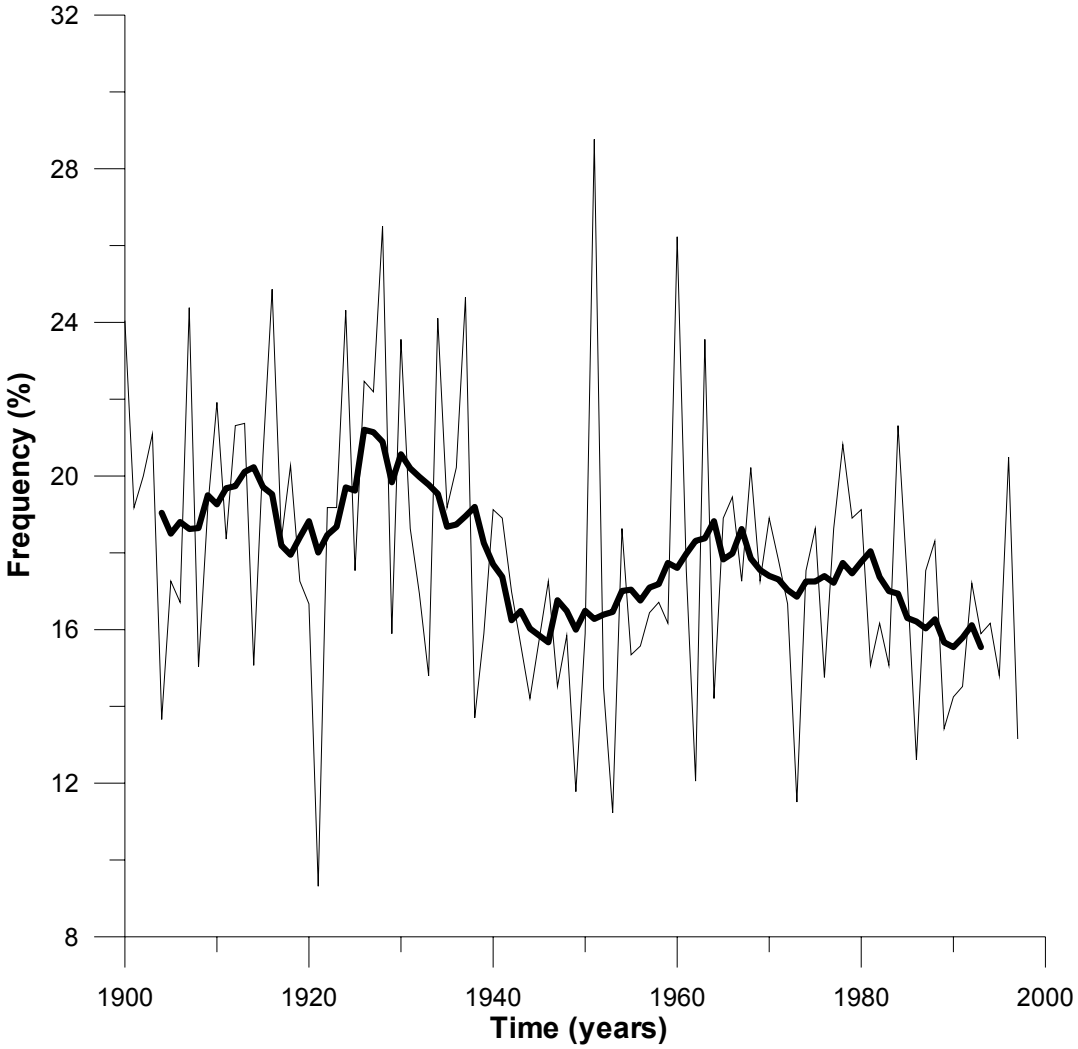

Figure 4.12 Cumulative frequency of wet CPs (CP01, CP04 and CP05) with a 10-year moving average in the Ardèche Catchment (1900-2000).

In the Llobregat Basin at Martorell, the occurrence frequency of wet CP (CP09) for the same time period (1900-2000) looks different as shown in Figure 4.13. Here the magnitude of the fluctuations are smaller, but the trend seems to be positive indicating a slight increase of the wet CP in the recent years in the Llobregat Region (10-year running average). In the diagram, black line shows the frequency of the wet CP and the red line represents the 10-year running average.

In the analysis of long CP series in the Study Areas, there have been slight changes observed in the occurrence of flood events and also in the frequency of flood-producing CPs, but in the overall evaluation, these did not show clear trends. The changes in the frequency of CPs occur more or less in a random manner.

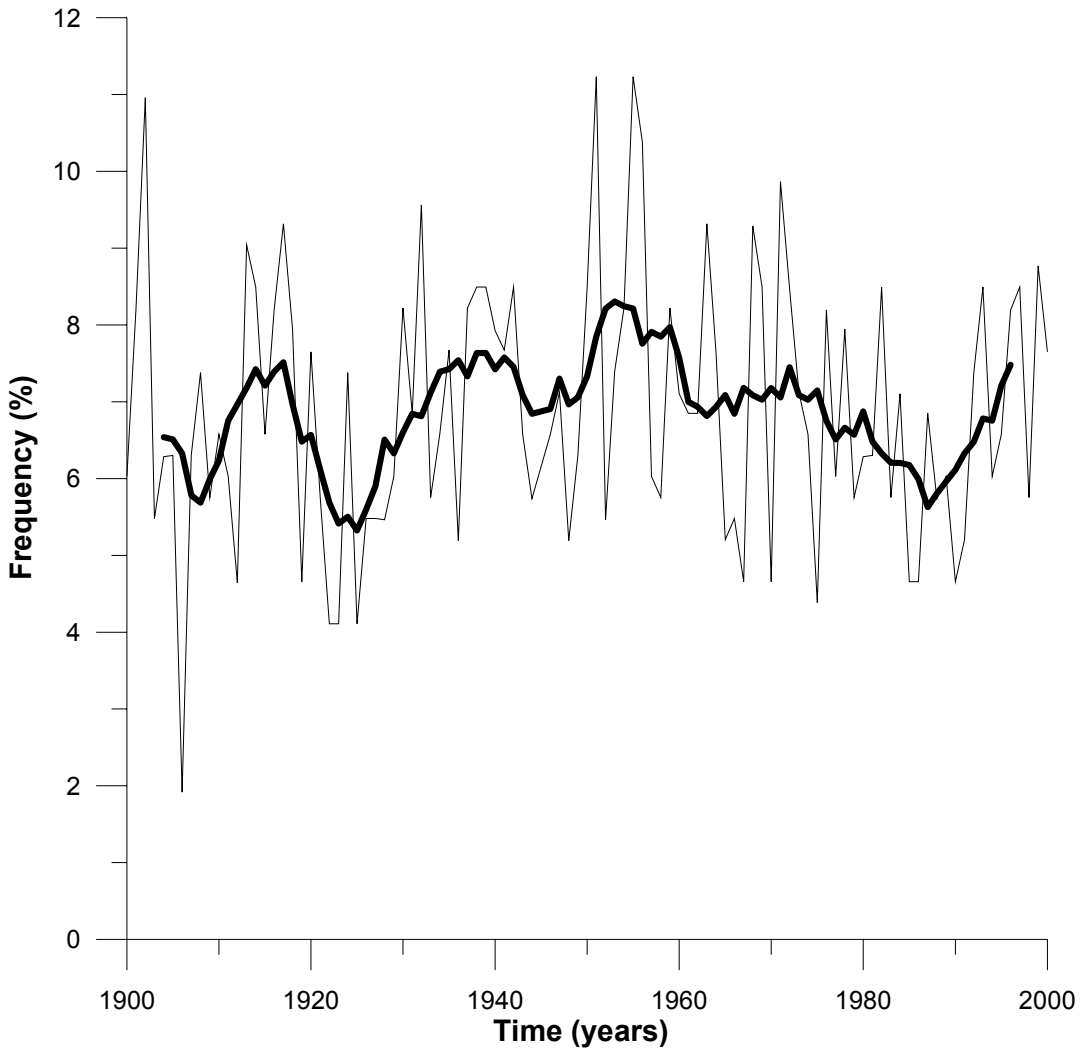

Figure 4.13 Frequency of wet CPs (CP09) with a 10-year moving average in the Llobregat Catchment at Martorell (1900-2000).

In order to see whether the peak flood discharges in the Llobregat were caused by the wet CP (CP09) which was identified by the classification, the observed annual maximum discharge series within 1912-1990 and their return periods are shown in Figure 4.14.

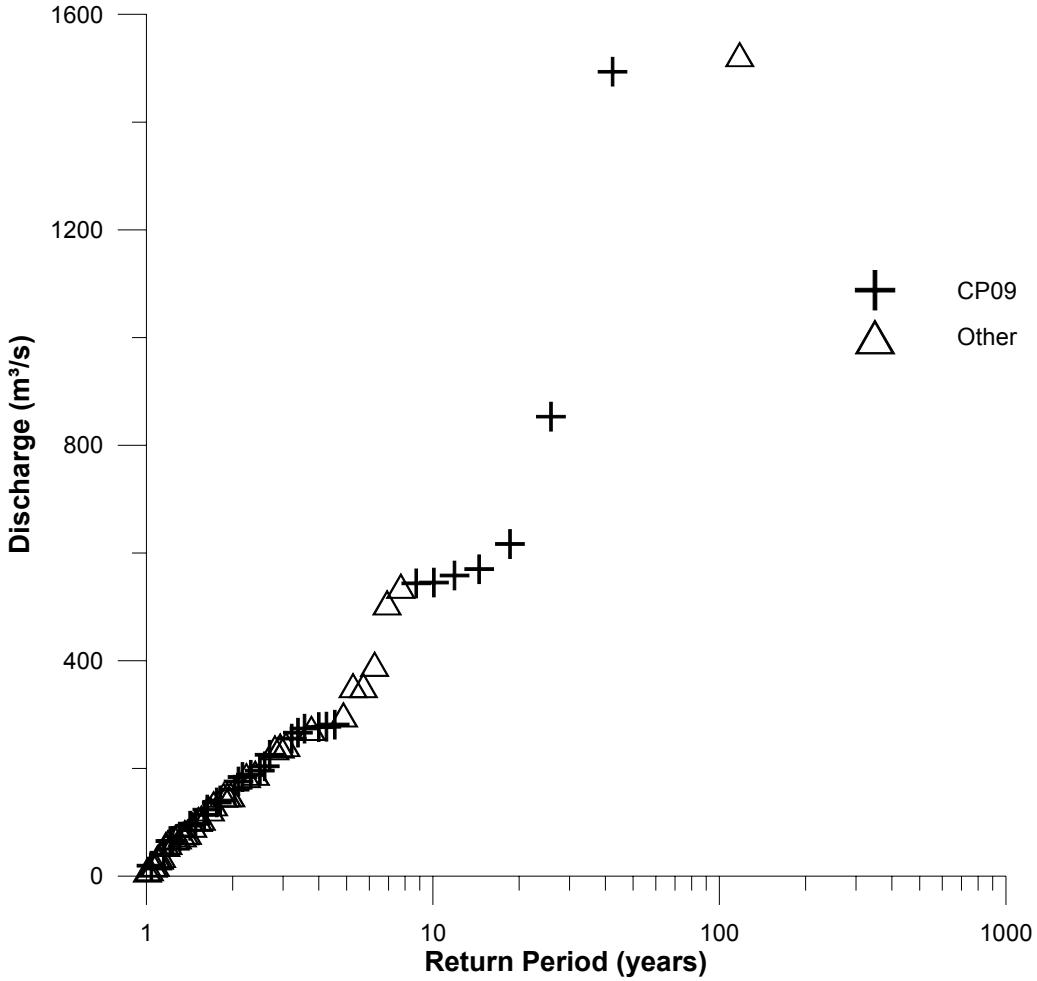

Figure 4.14 Observed annual discharge maxima for the Llobregat Catchment and their recurrence periods and the corresponding CPs.

Table 4.4 shows an overview of the wet CP occurrence frequencies and the frequencies of wet CPs corresponding high discharge amounts in the Ardèche and in the Llobregat Catchments. As an indicator of major floods, threshold values for discharge which correspond to 1 % exceedance probabilities were chosen in each basin. For the Ardèche, flood discharges corresponding 1 % exceedance probability lie around 500 m³/s and for the Llobregat about 80 m³/s. The purpose of the table is to give a rough impression of the relative frequencies of wet CPs and the relative occurrence frequencies of wet CPs corresponding to high discharge values.

Table 4.4 Relative frequencies of wet CPs in the Ardèche and in the Llobregat Catchments and the frequencies of wet CPs corresponding high discharge amounts $Q_{Ardèche\text{-}St.Martin}$ = 500 m³/s and $Q_{Llobregat}$ = 80 m³/s with. 1% exceedance probability.

Ardèche St. - Martin					Llobregat - Martorell
Wet CP	CP01	CP04	CP05	All wet CPs	CP09
Relative frequency of wet CP [%]	7.52	7.93	1.61	17.06	6.85
Q = 500 m³/s with 1 % exceedance probability					Q = 80 m³/s with 1 % exceedance probability
Relative frequency of wet CP [%] corresponding Q	0.25	0.51	0.06	0.82	0.25

In the overall evaluation of CP occurrencies in the Ardèche, the relative frequency of wet CPs (CP01, CP04 and CP05) contributed to 17 % during the observation period (1955-1997). In the Ardèche only 1 % of discharge values exceed 500 m³/s during this time period. The mean discharge during recording time is 34.88 m³/s in the Ardèche. Therefore, $Q_{Ardèche\text{-}St.Martin}$ = 500 m³/s was chosen as a discharge threshold value (as indicated above) which is supposed to indicate major floods in the basin. Then, wet CPs corresponding to discharge values which were equal or greater than the threshold discharge were counted. In the Ardèche 0.82 % of total days match wet CPs with a considerable discharge amount.

The same was done for the Llobregat Basin. The relative frequency of wet CP (CP09) contributes 6.84 % to the overall CP occurrence. $Q_{Llobregat}$ = 80 m³/s was determined to indicate major floods in the Llobregat (1 % exceedance probability). The average discharge of Llobregat River is 7.52 m³/s (1912-1990). Only 0.25 % of the total days correspond to CP09 with discharge values equal or above $Q_{Llobregat}$ = 80 m³/s.

This indicates that the occurrence of wet CPs does not have to lead to major floods since this is only a necessary condition but not a sufficient one.

Chapter 5

Discharge Downscaling Method

5.1 Introduction

Discharge is one of the most important elements of the hydrologic cycle. The estimation of discharge plays a major role in the assessment of water resources and for the design of flood protection measures. River flooding and the prediction of its occurrence has always been an essential and challenging task in hydrology.

In most countries, there are usually plenty of rainfall records, but the more elaborate and expensive streamflow measurements are often inadequate in their length and limited in their availability for a particular river under investigation. Therefore evaluating discharge from rainfall has been the inspiration of many researchers over the recent years and a number of numerical modeling approaches has been developed.

Other than what has been done before, a discharge downscaling method has been developed within the current research which enables generating discharge time series from circulation patterns in mesoscale catchments. Thus, it is direct downscaling of discharge from large-scale atmospheric information. This approach should provide a better understanding of the influences of climate on floods in the Study Areas.

The discharge downscaling method is a statistical downscaling method which belongs to the weather pattern-based approach as revised in Chapter 3. The aim of this method is to determine an empirical link between the large-scale meteorological features and the discharge directly without rain and rainfall-runoff modeling. A schematic comparison of discharge downscaling and the conventional downscaling of discharge with rainfall-runoff modeling can be seen in Figure 5.1.

The main idea behind linking atmospheric circulation patterns to discharge is based on the fact that rainfall and discharge increases show similar characteristics regarding their discrete nature and both include rapid increases and gradual decreases depending on the storm event as demonstrated earlier in Chapter 4 (Figure 4.4 and Figure 4.5). Another possible advantage of considering discharge is that it is less influenced by the local precipitation variability since discharge integrates the precipitation falling over a large area.

The statistical downscaling consists of four steps as described in von Storch et al., 1993:

- A large-scale parameter should be found which controls the local parameter
- Determination of the statistical relationship between large and local scale parameters within the training period
- Validation of this relationship with independent data (in the validation period)
- Given a successful validation, the local parameter can be estimated with the large-scale parameter

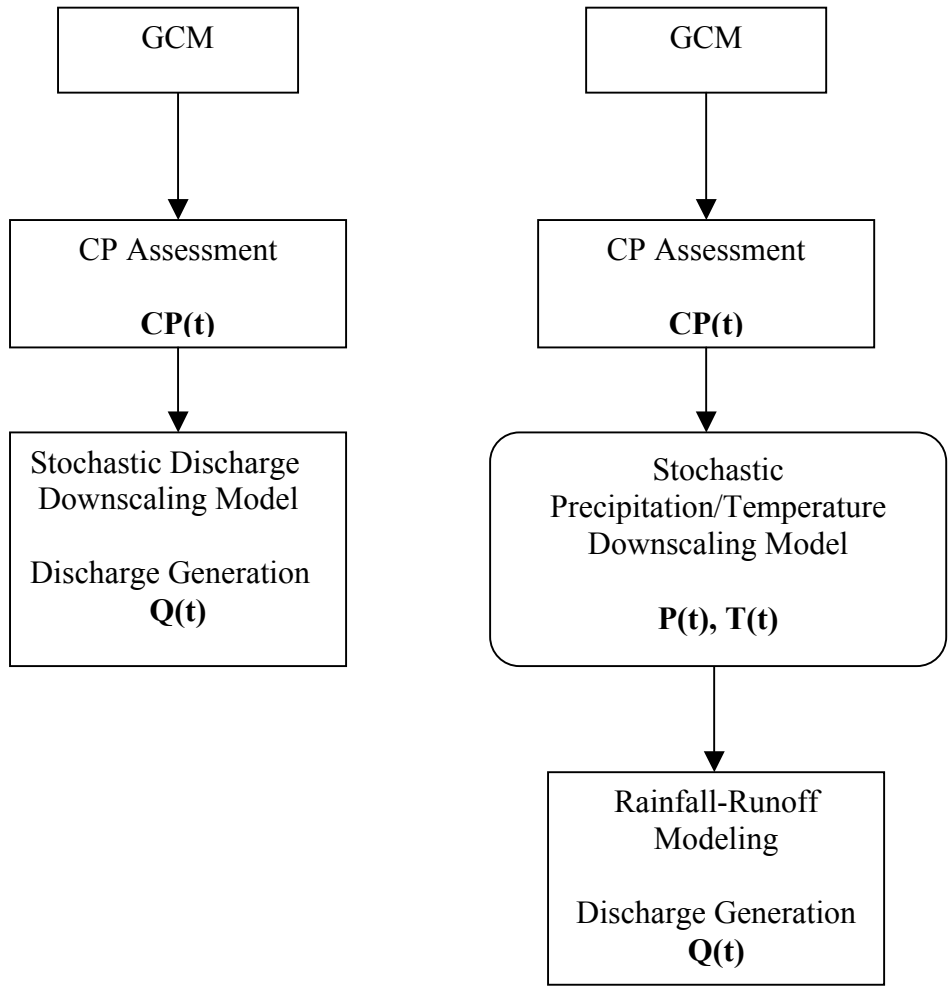

Figure 5.1 Schematic comparison of discharge downscaling introduced within the present study (left) and the conventional downscaling (right).

In this study, the large-scale information is first classified using a fuzzy rule-based optimization method as presented in Chapter 4, and for the linkage of the CPs to discharge in the distinct basins, a stochastic discharge downscaling model is developed. Within the downscaling procedure, stochastic model parameters which depend on the circulation pattern (CP) types are used. In this case, the non-linearity is captured by the CPs each of which has a specific relationship with the surface variables (such as precipitation or temperature, here: discharge). In the following section, the details of the discharge downscaling model will be discussed.

5.1.1 Stochastic Discharge Downscaling Model

The discharge downscaling model should enable the linkage of CPs to discharge in daily temporal resolution in the distinct basins. The classification of the atmospheric circulation patterns was carried out on daily time resolution which resulted in wet CPs in each Study Area. Figure 5.2 shows a schematic summary of linking atmospheric circulation to discharge directly with SLP data is shown.

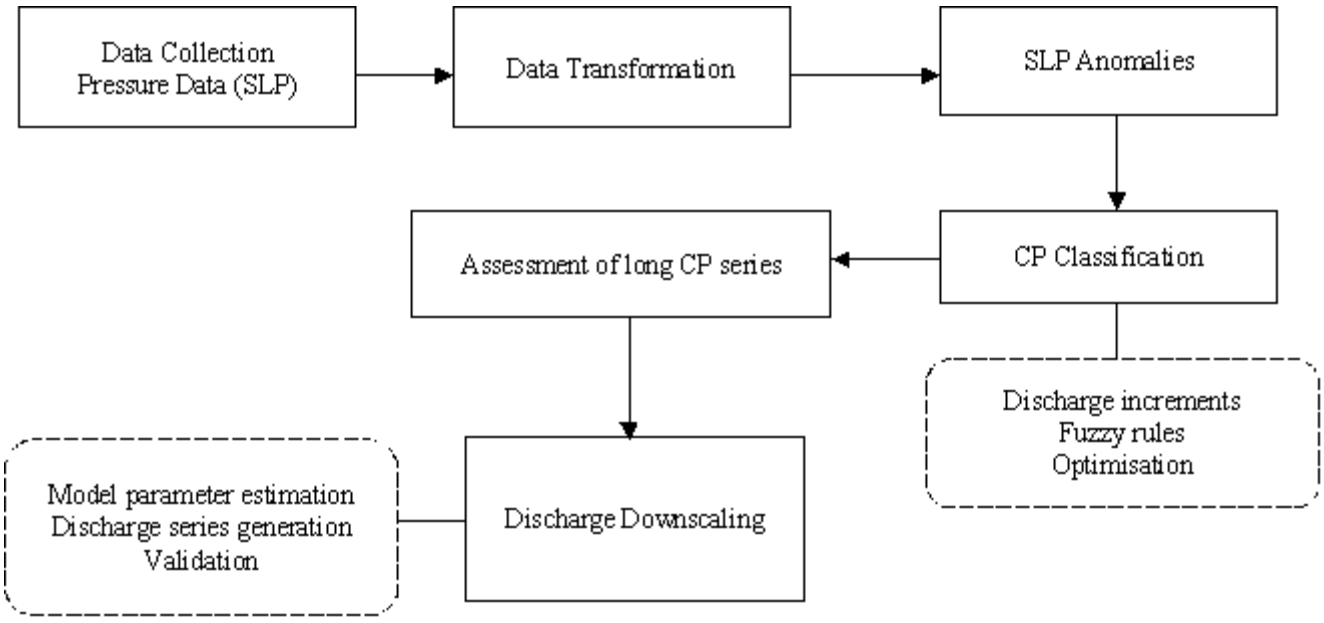

Figure 5.2 A schematic summary of linking atmospheric circulation to discharge directly using SLP data.

The discharge downscaling model describes the changes in discharge in order to yield a direct link between CPs and discharge on a daily time basis. Therefore positive and negative

changes - in other words, increases and decreases of discharge - are modeled separately. The increases of discharge are modeled as a stochastic process coupled with atmospheric circulation by using conditional model parameters and the discharge decreases are modeled by a linear reservoir approach. The model was applied successfully to the Study Areas which are affected by different climatic situations.

For the discharge downscaling model, first the discharge increments series $\Delta Q(t)$ are first calculated as in Equation (4.1). Then $\Delta Q(t)$ series are separated into positive $\Delta Q^{+}(t)$ and negative $\Delta Q^{-}(t)$ components:

$$\Delta Q(t) = \Delta Q^{+}(t) - \Delta Q^{-}(t) \tag{5.1}$$

The positive part of the discharge series is the result of precipitation which shows random characteristics. Therefore, positive changes, $\Delta Q^{+}(t)$, are linked to CPs directly considering the actual CP of the day, $CP(t)$, and the CPs of the previous day(s), denoted as $CP(\Delta t)$, depending on the time window, Δt, which represents the lag time.

$$\begin{aligned} &\Delta Q^{+}(t) = F(CP(t), CP(\Delta t)) \\ &\Delta Q^{+}(t) \geq 0 \end{aligned} \tag{5.2}$$

The negative component of discharge $\Delta Q^{-}(t)$ namely the decreases in discharge are modeled according to the linear reservoir approach which depends on the recession constant k_r as follows:

$$\Delta Q^{-}(t) = k_r \cdot Q(t - \Delta t) \tag{5.3}$$

For the discharge increases, Bernoulli random variables ($I_1(t), I_2(t)$) are introduced with values of 0 or 1 (random numbers with given probabilities) as shown in Equation (5.4). Due to the discrete nature of increases of discharge, $I_1(t)$ is used to determine the case of *increase/no increase* of discharge on a given day. In case, discharge increases on the given day, then the magnitude of the increase will be determined by $I_2(t)$.

Two different distribution functions are initiated to model the increases due to the magnitude of the increase. The first one is $X(t)$ which represents the slight increases distributed with the Beta distribution function, and the second is $Y(t)$ which models high discharge increases with the Weibull distribution function. Details related to the distribution functions and the estimation of the model parameters will be discussed in the next section.

For the total daily discharge changes, $\Delta Q(t)$, positive and negative components are added. Substitution of both components of positive and negative changes of discharge yields $\Delta Q(t)$ as follows:

$$\Delta Q(t) = \underbrace{I_1(t)}_{\substack{Increase \\ or \\ no\ increase}} \cdot \overbrace{\{\underbrace{I_2(t) \cdot X(t)}_{\text{Beta}} + \underbrace{(1 - I_2(t)) \cdot Y(t)}_{\text{Weibull}}\}}^{\Delta Q^+(t)} + \overbrace{k_r \cdot Q(t - \Delta t)}^{\Delta Q^-(t)} \tag{5.4}$$

with parameters:

$I_1(t), I_2(t)$	: Bernoulli random variables (0 or 1 with probabilities depending on CP)
$X(t)$	: Beta distributed random variable in [0, x_0]
$Y(t)$	: Weibull distributed random variable with parameters depending on CP
k_r	: Recession constant dependent on the catchment

In order to estimate the model parameters, discharge observations were analyzed. In the following section, the details of the discharge downscaling model are given.

5.1.2 Model Parameter Estimation

In order to explain flood events in the Study Areas, discharge series, especially discharge increases, have been thoroughly investigated. In terms of flood investigation, the occurrence frequency and the magnitude of high discharge increases are very important.

For the stochastic discharge downscaling model-set up, the following steps were taken:

1. The selection of the probability distribution function which is the most representative to the observations
2. Parameter estimation of the selected probability distribution function
3. Testing the quality of the fit of the distribution function

Since high-magnitude discharge increases are important in terms of floods, it was preferred to introduce two different distribution functions. The reason for this is to achieve a better fit of the distribution to the low frequency-high magnitude data (the tail of the distribution function) in order to model flood peak discharges well. This helps to model high discharge increases, which occur rarely other than usual medium and low-magnitude discharge increases, more realistically. Therefore small discharge increases which can be regarded as insignificant for floods are modeled with the Beta distribution function, whereas higher discharge increases are distributed according to the Weibull distribution function.

The separation of the two different distribution functions is achieved by introducing a discharge threshold value x_0 which is catchment dependent. The Beta parameters (α_b, β_b) are estimated for each catchment (instead of for each CP) as the discharge increases between $0 < \Delta Q^+(t) < x_0$ are minor compared to floods (discharge increases below x_0 can be considered as a noise effect). However Weibull parameters (λ_w, β_w) are estimated for each CP separately (or for each CP group) in order to link the significant discharge increases that are greater than x_0 ($\Delta Q^+(t) > x_0$) to CPs directly. Beta and Weibull distribution functions were chosen since they both performed the best-fit to the observed discharge increases. Both Beta and Weibull are two-parameter probability distribution functions. Detailed information on the distribution functions is provided in a later section.

Several threshold values were tested for the Study Areas by comparing the quality of the fit of the two distribution functions. The parameter x_0 was determined to be 30 m³/s for the Ardèche Basin and 50 m³/s for the Llobregat Basin for which the best fit was achieved.

Table 5.1 gives a brief summary of the parameters of the discharge downscaling model that are to be estimated. The parameters are listed in two groups according to their relevance either to the catchment or to the circulation patterns (CPs).

The probabilities of discharge increases are estimated from the observations in each basin. Since discharge increases are modeled by two different probability functions, the probabilities of increases are divided into three groups as follows:

- p_1 is the estimated probability of days with no increase of discharge, $\Delta Q^+(t) = 0$
- p_2 is the estimated probability of discharge increases within $[0, x_0]$ modeled by the Beta distribution function, $0 < \Delta Q^+(t) < x_0$
- p_3 is the estimated probability of discharge increases modeled by the Weibull distribution function, which yields to p3 = 1-(p1+ p2), $\Delta Q^+(t) > x_0$

According to this, the occurrence of discharge increases depend on the following conditions:

- If $I_1(t) < p_1$ then $\Delta Q^+(t) = 0$ no increase of discharge
- If $p_1 < I_1(t) \leq p_1 + p_2$ then $0 < \Delta Q^+(t) < x_0$ Beta distributed
- If $I_1(t) > 1 - p_3$ then $\Delta Q^+(t) > x_0$ Weibull distributed

In case discharge increases on a given day, the magnitude of the increase is determined by $I_2(t)$ which will be distributed either by the Beta or the Weibull distribution function.

As stated before, discharge decreases are the natural reaction of the catchment and serve to conduct the excess water out of the watershed. Related to this, the concentration time Δt (lag time between the atmospheric signal and the hydrological response of the catchment), and the recession constant k_r are estimated individually for each basin.

Table 5.1 Model parameters to be estimated according to their relevance.

Parameters of the Discharge Downscaling Model	
Catchment specific	**Circulation pattern (CP) specific**
$\Delta Q^-(t)$: decrease in discharge [m³/s]	$\Delta Q^+(t)$: increase in discharge [m³/s]
k_r: recession constant [-]	Weibull distribution parameters (λ_w, β_w)
Δt: concentration time / lag time [day]	$I_1(t)$, $I_2(t)$: Bernoulli variables dependent on time
x_0: discharge threshold value [m³/s] Beta distribution range $0 < \Delta Q^+(t) < x_0$ Weibull distribution range $\Delta Q^+(t) > x_0$	p_1: Probability of *no* increase in discharge $\Delta Q^+(t) = 0$ p_2: Probability of $0 < \Delta Q^+(t) < x_0$ p_3: Probability of $\Delta Q^+(t) > x_0$ $p_3 = 1-(p_1+p_2)$
Beta distribution parameters (α_b, β_b)	

5.1.2.1 Beta Distribution

The Beta distribution models a random variable (x) that takes values in the interval by 0 to 1. The distribution plays a special role in decision methods. It can be used to model the distribution of a quantity that is known to vary between lower and upper boundaries.

Definition. The Beta probability distribution function (pdf) is given by

$$f_x(x,\alpha_b,\beta_b) = \frac{1}{B(\alpha_b,\beta_b)} x^{\alpha_b-1}(1-x)^{\beta_b-1} \quad for \quad 0<x<1, \quad \alpha_b>0, \quad \beta_b>0$$
$$f_x(x,\alpha_b,\beta_b) = \quad 0 \qquad\qquad\qquad\qquad otherwise. \tag{5.5}$$

The expression

$$B(\alpha_b,\beta_b) = \int_0^1 x^{\alpha_b-1}(1-x)^{\beta_b-1}dx = \frac{\Gamma(\alpha_b)\Gamma(\beta_b)}{\Gamma(\alpha_b+\beta_b)} \tag{5.6}$$

denotes the Beta function with parameters α_b and β_b (index *b* denotes Beta).

The Gamma function is:

$$\Gamma(r) = \int_0^\infty t^{r-1} e^{-t}\, dt \qquad for \quad r > 0$$
$$\Gamma(r) = 0 \qquad\qquad otherwise \tag{5.7}$$

For the discharge downscaling model, Beta distribution parameters α_b and β_b are estimated for all CPs which correspond to discharge increases in [0, x_0] for winter and summer separately. As stated in the beginning, the Beta distribution function takes values between [0, 1]. In order to expand this interval to [0, x_0], the following linear transformation has been carried out so that the discharge values of range [0, x_0] are distributed between 0 and 1.

$$x_t = \frac{x}{x_0} \tag{5.8}$$

with

x_t : Transformed discharge value

x : Discharge value before transformation

x_0 : Threshold value for the modeling discharge increases

The parameters are estimated with Maximum Likelihood Method (Stedinger and Martins, 2000) to fit the distribution function to the observations. The principle of the Maximum Likelihood Method (MLM) is that the parameters of the function are estimated so that the observed values are the most probable ones. The Likelihood functions include the occurrence probabilities of the observations and therefore the function will be maximized. The quality of the fit with the estimated parameters has been tested with the Kolmogorov-Smirnov Goodness of Fit Test (KS) (Chakravart, Laha, and Roy, 1967). The KS test is a non-parametric test that is used to decide whether a sample comes from a population with a specific distribution. Details about the KS test can be found in Plate (1993), Kottegoda and Rosso (1997) and in Hartung (1984). A short summary of the estimated model parameters for the Ardèche and Llobregat Catchments are given in Table 5.2 and Table 5.3 respectively.

5.1.2.2 Weibull Distribution

The Weibull distribution provides a close approximation to the probability laws of many natural phenomena. It has been used to model, for example, the time to failure of electrical and mechanical systems. In reliability engineering, attention is often focused on a threshold level below which a system or component or basic material has an acceptably low probability of failure. The Weibull distribution is also of the asymptotic distributions of General Extreme Value Theory (Gumbel, 1954) and offers great flexibility.

Definition. The two-parameter Weibull pdf with parameters β_w and $\lambda_w>0$ (subscript *w* denotes Weibull) is given by

$$f_x(x-x_0) = \frac{\beta_w}{\lambda_w}\left(\frac{x-x_0}{\lambda_w}\right)^{\beta_w-1} exp\left[-\left(\frac{x-x_0}{\lambda_w}\right)^{\beta_w}\right] \quad for \quad x-x_0>0, \qquad (5.9)$$

$$f_x(x-x_0) = 0 \quad otherwise.$$

The cumulative density function takes the form

$$F_x(x-x_0) = 1-exp\left[-\left(\frac{x-x_0}{\lambda_w}\right)^{\beta_w}\right] \quad for \quad x-x_0>0, \qquad (5.10)$$

$$F_x(x-x_0) = 0 \quad otherwise.$$

Maximum Likelihood Procedure has been applied for both distribution functions to estimate the parameters. For the Weibull distribution, the parameters for each CP have been determined sepatarely and tested with Kolmogorov-Smirnov Goodness of Fit Test (KS). It is also possible to estimate the model parameters for CP groups which are formed according to their wetness characteristics (i.e. wet, normal and dry CP groups). Estimated Weibull parameters λ_w and β_w are given in Table 5.1 and 5.2 for the Study Areas.

The decreases of discharge are modeled according to the linear reservoir approach which is presented in the next section.

5.1.2.3 The Linear Reservoir Approach

Due to the fact that the negative changes of discharge are due to the mostly deterministic reaction of the catchment to excess water, they are modeled according to the linear reservoir approach. In order to define the catchment-dependent recession constant k_r, the direct runoff in the Study Areas has to be assessed. The hydrograph of discharge against time has two main components, the area under the hump, labelled *surface runoff* (which is produced by a volume of water derived from the storm event), and the broad band near the time axis, representing *baseflow* contributed from groundwater. A rainfall and river hydrograph can be seen in Figure 5.3.

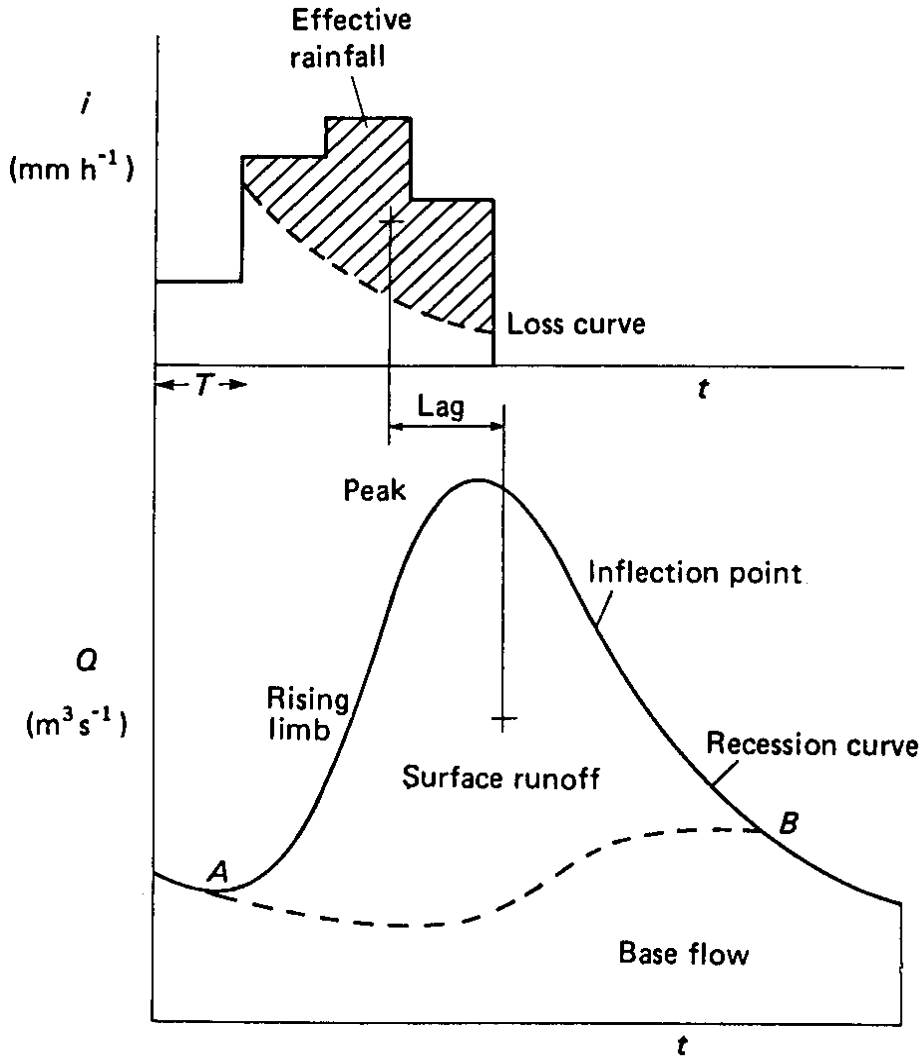

Figure 5.3 Rainfall and a river hydrograph *Source: Shaw, 1994.*

The volume of surface runoff, represented by the area under the hydrograph minus the baseflow as seen in Figure 5.3, can be considered in two main subdivisions to simplify the

complex water movements over the surface and in the ground. The effective rainfall makes the immediate contribution to the rising limb from A to the peak of the hydrograph and, even when the rainfall ceases, continues to contribute until the *inflection point*. Beyond this point, it is generally considered that the flow comes from the water temporarily stored in the soil. This flow continues to provide the flow of the *recession curve* until the water from the total effective rainfall is completely depleted at B.

For the separation of baseflow from the storm runoff, there are several methods available (see Figure 5.4). The simplest separation would be given by a horizontal line to *a* from the start of the rise of the hydrograph. This would assume that the storm has no effect on or makes no contribution to groundwater. The more realistic separation is curve *c*, which shows a marked storm effect peaking some time after the peak of the stream flow. However, the shape of this curve would be quite subjective, and differing answers would be produced by different analysts. The straight line to point *b* on the recession is assumed to become exponential, and is fixed uniquely on the semi-logarithmic plot as shown in Figure 5.4. This is a satisfactory compromise and the method is straightforward and gives consistent results.

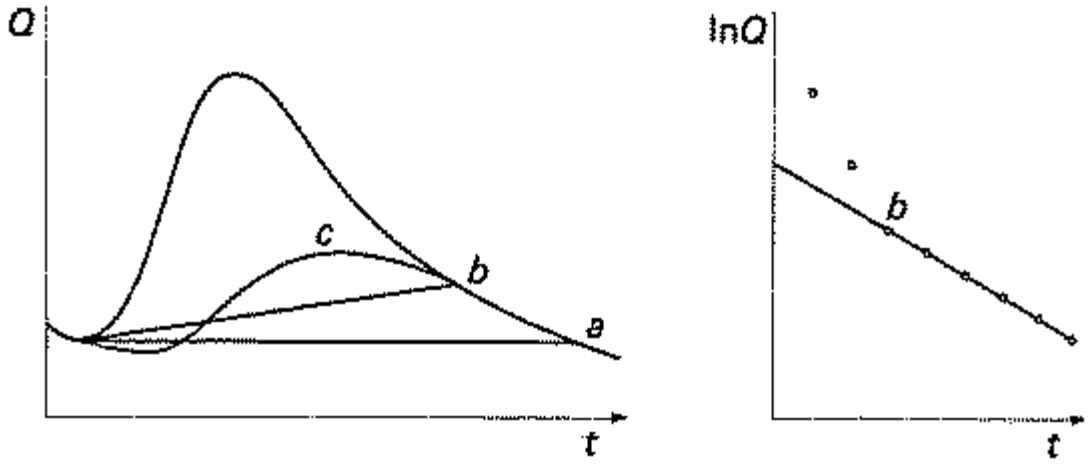

Figure 5.4 Separation of baseflow.

For the determination of the baseflow in the Study Areas, 10-day minima of the discharge series were linearly connected to estimate the baseflow as seen in Figure 5.5. This simplified baseflow separation method is applied since the contribution of baseflow to the total runoff hydrograph is insignificant in both Study Areas (especially if floods are considered) depending on the geological structure and the composition of the basin.

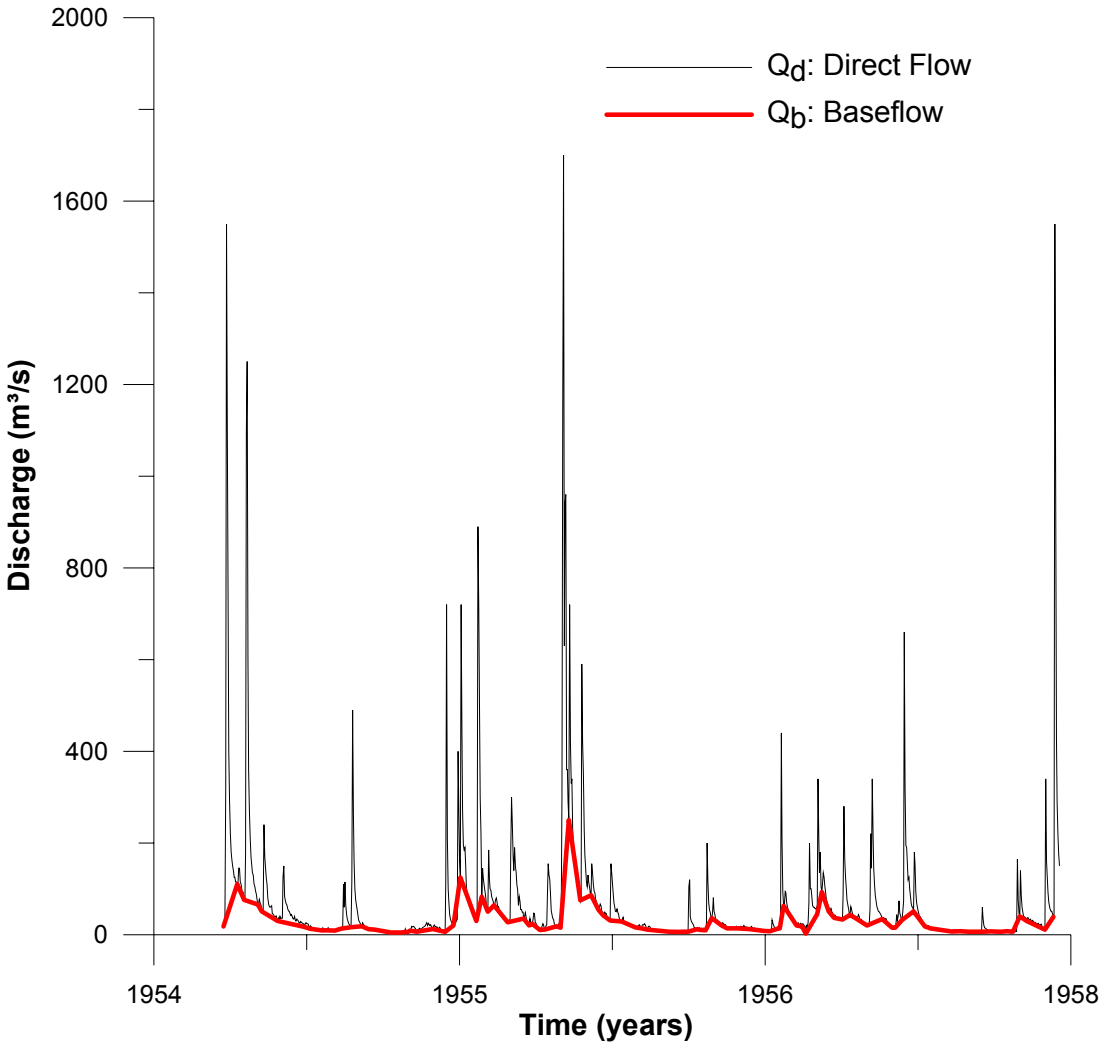

Figure 5.5 The determination of baseflow in the Ardèche Catchment representing the time period of 1955-1958. Black represents the direct discharge (Q_d), and red represents the estimated baseflow (Q_b).

Once the direct flow is assessed, the recession constant k_r can be determined as follows:

$$Q(t) = Q(t_0)e^{-k_r(t-t_0)} \tag{5.11}$$

$Q(t)$: Total flow

$Q(t_0)$: Flow where recession starts

t : Time

t_0 : Time when recession starts

This equation is linear in the semi-log domain:

$$\ln Q(t) = -k_r (t - t_0) + \ln Q(t_0) \tag{5.12}$$

which results in

$$k_r = -\left(\frac{\ln\left(\frac{Q(t)}{Q(t_0)} \right)}{t - t_0} \right) \tag{5.13}$$

For the estimation of the recession constant k_r in the Study Areas, discharge decreases are plotted against discharge of the previous day (assuming Δt = 1 day) as a scatter diagram shown in Figure 5.6 in order to gain an overall view of the possible value-range of k_r. It can be observed from the diagram that the recession constant k_r shows linear characteristics since the data points lie within a linear band. In estimating k_r, the main aim was to consider and to include the majority of the possible decreases in discharge. In Figure 5.6, the negative changes $\Delta Q^{-}(t)$ and discharge of the previous day $Q(t - \Delta t)$ (here Δt = 1 day thus $Q(t-1)$) in the Ardéche basin are shown. k_r -value was assumed to be k_r = 0.95 for both basins which indicates a high recession rate.

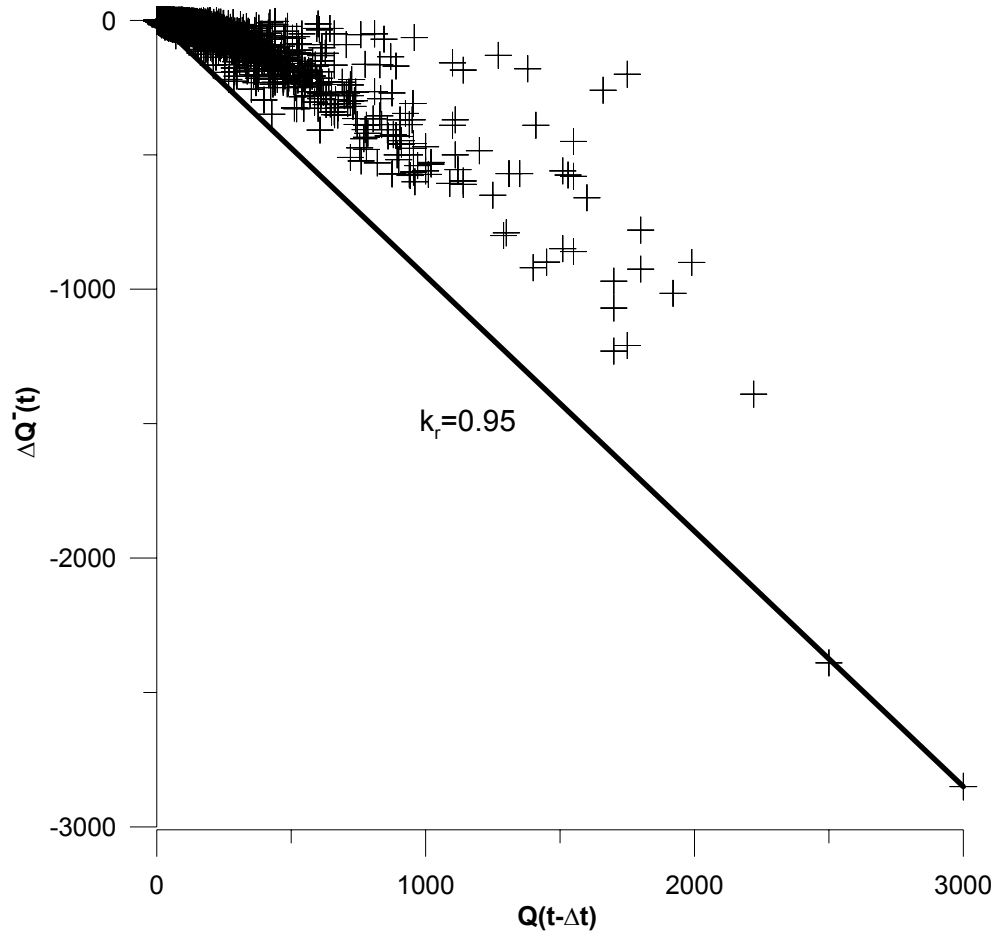

Figure 5.6 Determination of the recession constant k_r for Ardèche-Saint Martin.

Table 5.2.a shows a list of the estimated model parameters for the discharge increases in the Ardèche Catchment for winter and summer seasons separately. The threshold for the discharge increases was determined as $x_o = 30$ m³/s for the Ardèche since it delivered a better model performance. Table 5.2.b gives the estimated probabilities of discharge increases for all CPs in the Ardèche Basin.

Table 5.2.a Estimated parameters of Beta and Weibull distribution functions at Ardèche Saint Martin with $x_o = 30$ m³/s.

Ardèche Saint Martin (1955-1997), $x_o = 30$ m³/s					
		winter		summer	
	CP	λ_w	β_w	λ_w	β_w
Weibull Distribution	CP01	0.726	156.20	0.609	57.00
	CP02	0.815	80.90	0.784	92.30
	CP03	0.668	48.80	0.673	87.20
	CP04	0.750	202.30	0.686	123.50
	CP05	0.626	124.40	0.664	193.00
	CP06	0.724	66.60	0.986	36.90
	CP07	0.746	54.20	0.729	70.80
	CP08	0.708	42.00	0.862	27.10
	CP09	0.758	54.50	0.964	41.10
	CP10	0.755	57.00	0.793	55.60
	Unclassified	0.768	60.10	0.921	27.10
Beta Distribution	All CP	α_b	β_b	α_b	β_b
		0.840	1.420	0.610	2.580

Table 5.2.b Estimated probabilities of discharge increases at Ardèche Saint Martin, $x_o = 30$ m³/s
p_1: probability of no discharge increase, p_2: probability of discharge increase in $[0, x_o]$,
p_3: probability of discharge increase above x_o.

Ardèche Saint Martin (1955-1997), $x_o = 30$ m³/s						
	winter			summer		
CP	p_1	p_2	p_3	p_1	p_2	p_3
CP01	0.219	0.385	0.396	0.219	0.683	0.10
CP02	0.103	0.546	0.351	0.134	0.779	0.09
CP03	0.133	0.602	0.265	0.222	0.676	0.101
CP04	0.190	0.363	0.447	0.207	0.617	0.176
CP05	0.250	0.340	0.410	0.196	0.753	0.052
CP06	0.181	0.553	0.266	0.174	0.743	0.083
CP07	0.125	0.652	0.223	0.188	0.778	0.034
CP08	0.125	0.682	0.193	0.134	0.833	0.033
CP09	0.111	0.618	0.272	0.142	0.792	0.065
CP10	0.136	0.584	0.280	0.176	0.770	0.054
Unclassified	0.114	0.578	0.310	0.141	0.806	0.052

For the Llobregat Catchment, 3 CP groups have been formed in order to classify CPs with similar characteristics and estimate the model parameters for the CP groups separately. As it can be seen from Table 5.3.a, the majority of the CPs comprised one group having the same model parameters whereas CP03 and CP09 were treated separately due to their wet characteristics. CP09 was defined as *critical CP* for the Llobregat Basin in Chapter 4.

Forming groups of CPs is also advisable in order to avoid having an insufficient number of samples per each CP type for the model parameter estimation if this is the case. Assigning similar CPs into one group increases the sample size which enables a better estimation of the model parameters.

In Table 5.3.a CP-groups for the Weibull parameters are defined as:

1. CP Group: CP01, CP02, CP04, CP05, CP06, CP08, CP10, CP11, CP12, Unclassified
2. CP Group: CP03
3. CP Group: CP09

Table 5.3.a Estimated parameters of Beta and Weibull distribution functions at Llobregat-Martorell with $x_o = 50$ m³/s.

Llobregat Martorell (1912-1990), $x_o = 50$ m³/s					
		winter		summer	
	CP	λ_w	β_w	λ_w	β_w
Weibull Distribution	1. CP Group	0.673	66.692	0.660	39.271
	2. CP Group	0.806	121.304	0.788	44.779
	3. CP Group	0.756	90.052	0.788	44.779
Beta Distribution	All CP	α_b	β_b	α_b	β_b
		0.60	4.32	0.63	4.20

In Table 5.3.b the estimated probabilities of discharge increases are given separately for summer and winter seasons in the Llobregat Basin.

Table 5.3.b Estimated probabilities of discharge increases at Llobregat-Martorell, $x_o = 50$ m³/s
p_1: probability of no discharge increase, p_2: probability of discharge increase in $[0, x_o]$,
p_3: probability of discharge increase above x_o.

Llobregat-Martorell (1912-1990), $x_o = 50$ m³/s						
	winter			summer		
CP	p_1	p_2	p_3	p_1	p_2	p_3
CP01	0.408	0.585	0.007	0.440	0.554	0.006
CP02	0.389	0.593	0.018	0.307	0.690	0.004
CP03	0.434	0.539	0.026	0.319	0.647	0.034
CP04	0.409	0.560	0.031	0.363	0.619	0.018
CP05	0.349	0.632	0.019	0.324	0.660	0.016
CP06	0.263	0.718	0.019	0.337	0.654	0.009
CP07	0.351	0.637	0.012	0.354	0.641	0.005
CP08	0.481	0.507	0.013	0.534	0.459	0.007
CP09	0.422	0.517	0.061	0.410	0.560	0.030
CP10	0.262	0.727	0.012	0.172	0.818	0.010
CP11	0.367	0.621	0.012	0.275	0.709	0.016
CP12	0.470	0.508	0.026	0.413	0.574	0.013
Unclassified	0.577	0.416	0.008	0.395	0.596	0.009

Discharge series in the Ardèche Catchment at Saint Martin were simulated for the period between 1955-1997. Figure 5.7 shows a part of the simulation (1955-1960). The simulation of discharge shows good agreement with the observations in terms of variability and amplitude of floods.

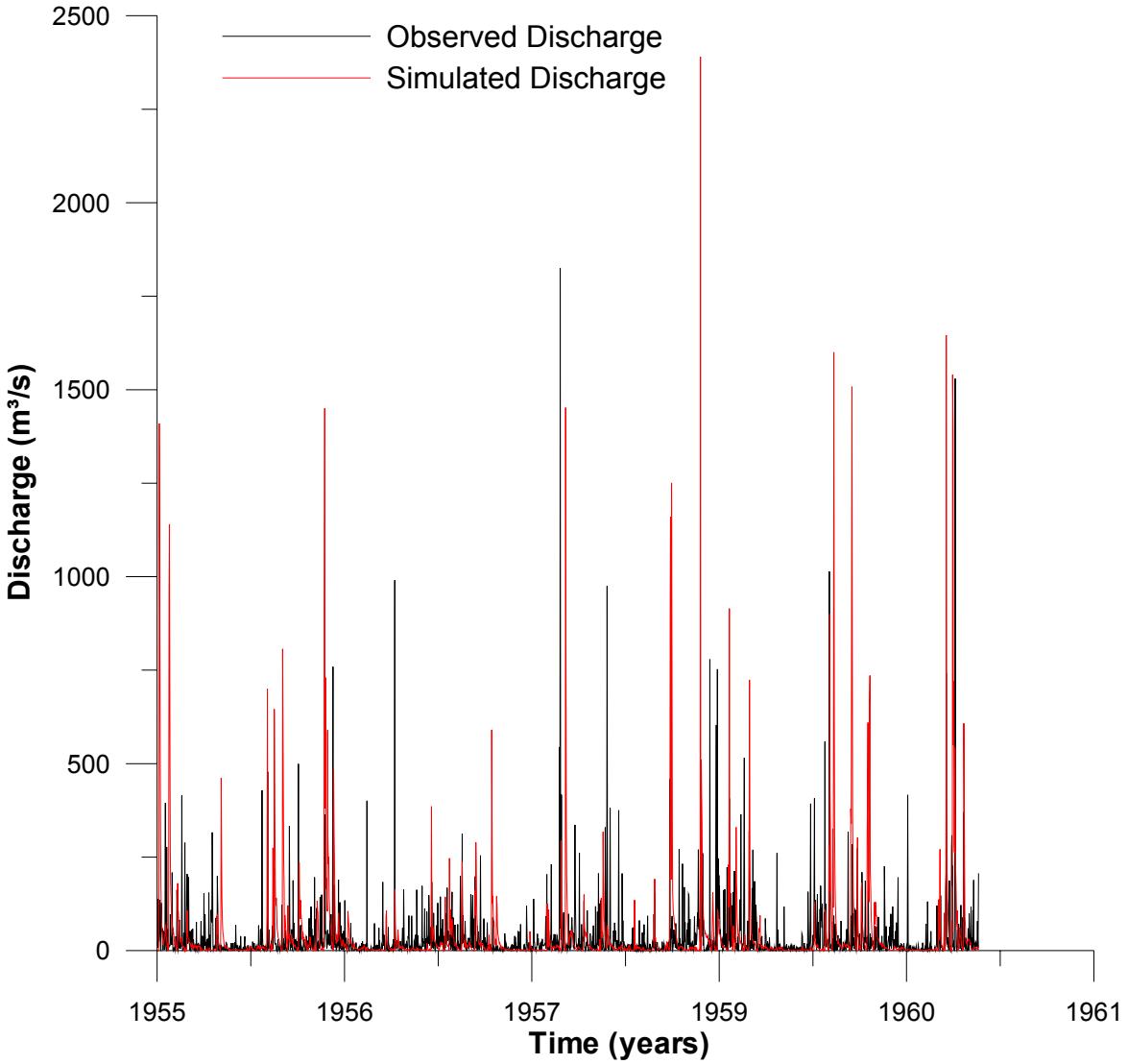

Figure 5.7 Observed and simulated discharge time series for the Ardèche at St.-Martin (1955-1960).

In the simulated discharge time series presented above, high discharges were caused by the CPs which were identified as *wet* according the discharge observations. Table 5.4 gives an overview of the statistics of simulated and observed discharge series in the Ardèche Catchment. Both observed and simulated discharge series are compared in terms of mean, standard deviation and the discharge values at the 25 %, 50 %, 75 %, 90 % and the 99 % quantiles. Thus, the simulation is tested in two ways: The first test is the non-parametric KS test, and the second test is the comparison of the statistical parameters with the observed ones. The model delivers good results in both cases.

Table 5.4 Statistics of discharge downscaling and the observations in the Ardèche Basin during the observation period between 1955-1997.

Ardèche - Saint Martin								
Discharge Series	Discharge		Quantiles					
	Mean	St Dev	25%	50%	75%	90%	95%	99%
Simulated	37.34	96.81	2.51	10.64	29.66	87.27	162.62	447.41
Observed	34.88	105.48	1.06	7.34	25.00	74.00	145.73	511.97

According to Table 5.4, the simulated discharge series could capture the main characteristics of the observations. The mean, standard deviation of both series are comparably similar as well as the distribution of the discharge values at different quantiles of the distribution. One can see that within the simulation presented above, the 95 % quantile is being overestimated by the simulation compared to observed values whereas the 99 % quantile is slightly underestimated. The results obtained from the simulation remain satisfactory.

It should be considered that the results of the simulation are strongly dependent on the generation of random numbers and therefore each simulation is different from another one representing *one possible realization*. A large number of simulations have been carried out in order to eliminate the randomness of the results and to consider the overall model performance.

Another point which should be mentioned here is that the model is supposed to serve a better understanding of flood-producing atmospheric conditions for the selected catchments by using the data available for the observation period. This means that the flood features (occurrence frequency and magnitude) in the selected catchment will be simulated, whereas the time when flood occurs will be determined by a random function. The model is therefore not meant to be used for flood-forecasting purposes, but for explaining the link between flood-prone atmospheric conditions and floods in mesoscale catchments.

The same procedure was applied for the Llobregat Basin. The discharge was simulated for the time period between 1900-2000 for the Llobregat Catchment. Figure 5.8 presents the simulated and observed discharge series for the period between 1950-1990. The statistical comparison of simulated and observed discharge series are presented in Table 5.5. As can be

seen in the figure, the model captured the mean features of the discharge behavior also in the Llobregat Basin as well.

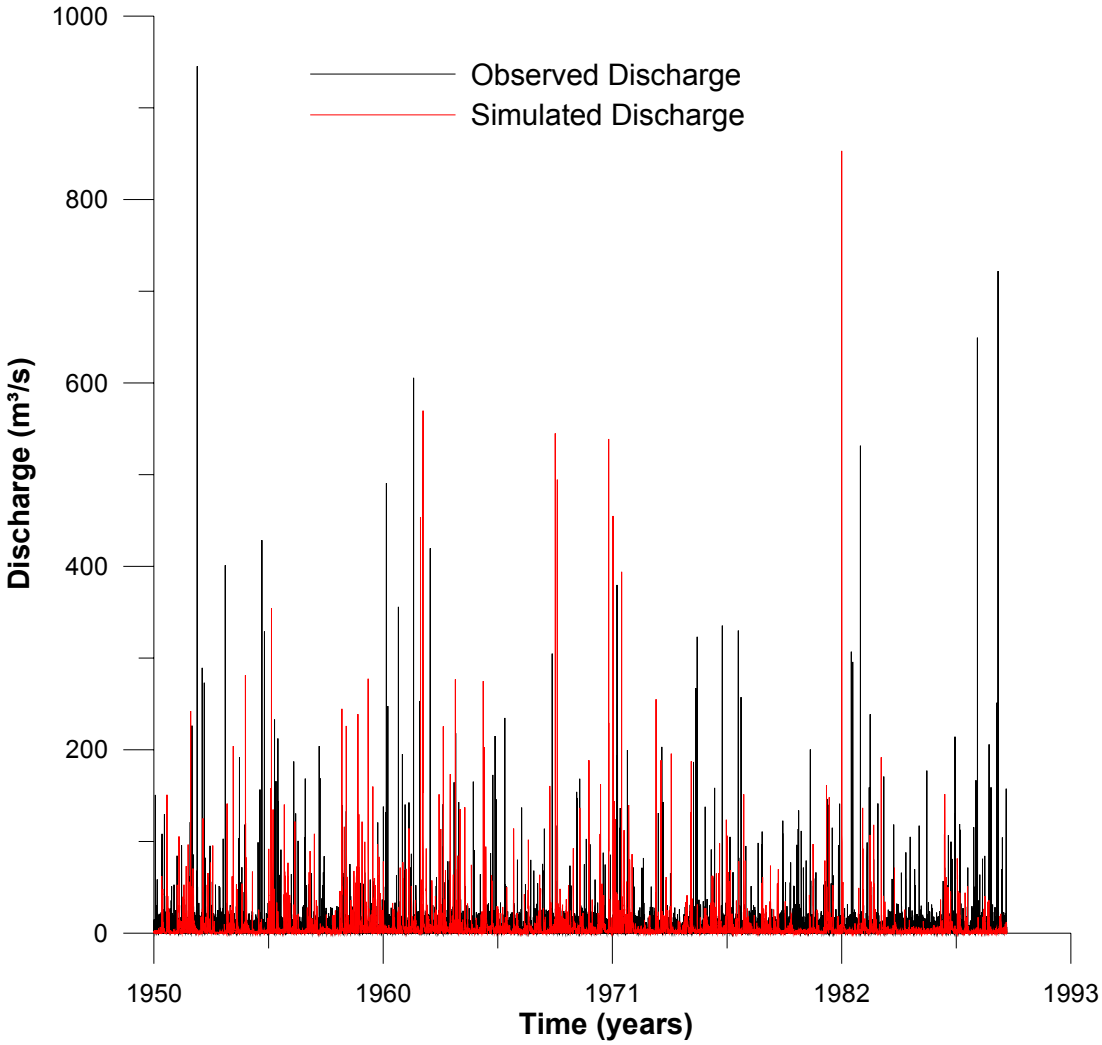

Figure 5.8 Observed and simulated discharge time series for the period between 1950-1990 in the Llobregat at Martorell.

Table 5.5 Statistics of discharge downscalings and observations in the Llobregat Basin 1912-1990.

Llobregat-Martorell								
Discharge Series	Discharge		Quantiles					
	Mean	St Dev	25%	50%	75%	90%	95%	99%
Simulated	6.41	23.49	0.13	1.18	6.31	14.35	20.84	79.50
Observed	7.50	30.70	0.23	1.75	5.20	15.27	27.45	85.75

In the simulated discharge time series presented above, peak discharges were caused by the wet CP (CP09).

In order to analyze the variability of the observed and the generated discharge behavior in both Study Areas, the observed and simulated annual maximum discharges were investigated. The annual maximum discharge value is the largest discharge amount registered in a year.

Figure 5.9 illustrates the observed annual maximum discharge in the Ardèche at Saint Martin between 1955-1997. The 5-year moving average indicates a high variability in the magnitude of annual peaks in the Ardèche. In order to have a look at the annual discharge peaks in a longer period than the observation period, the annual maxima of discharge series were simulated as shown in Figure 5.10 (1900-2000). The magnitude of the annual discharge peaks differs in the range of approximately 500-2500 m³/s in the Ardèche.

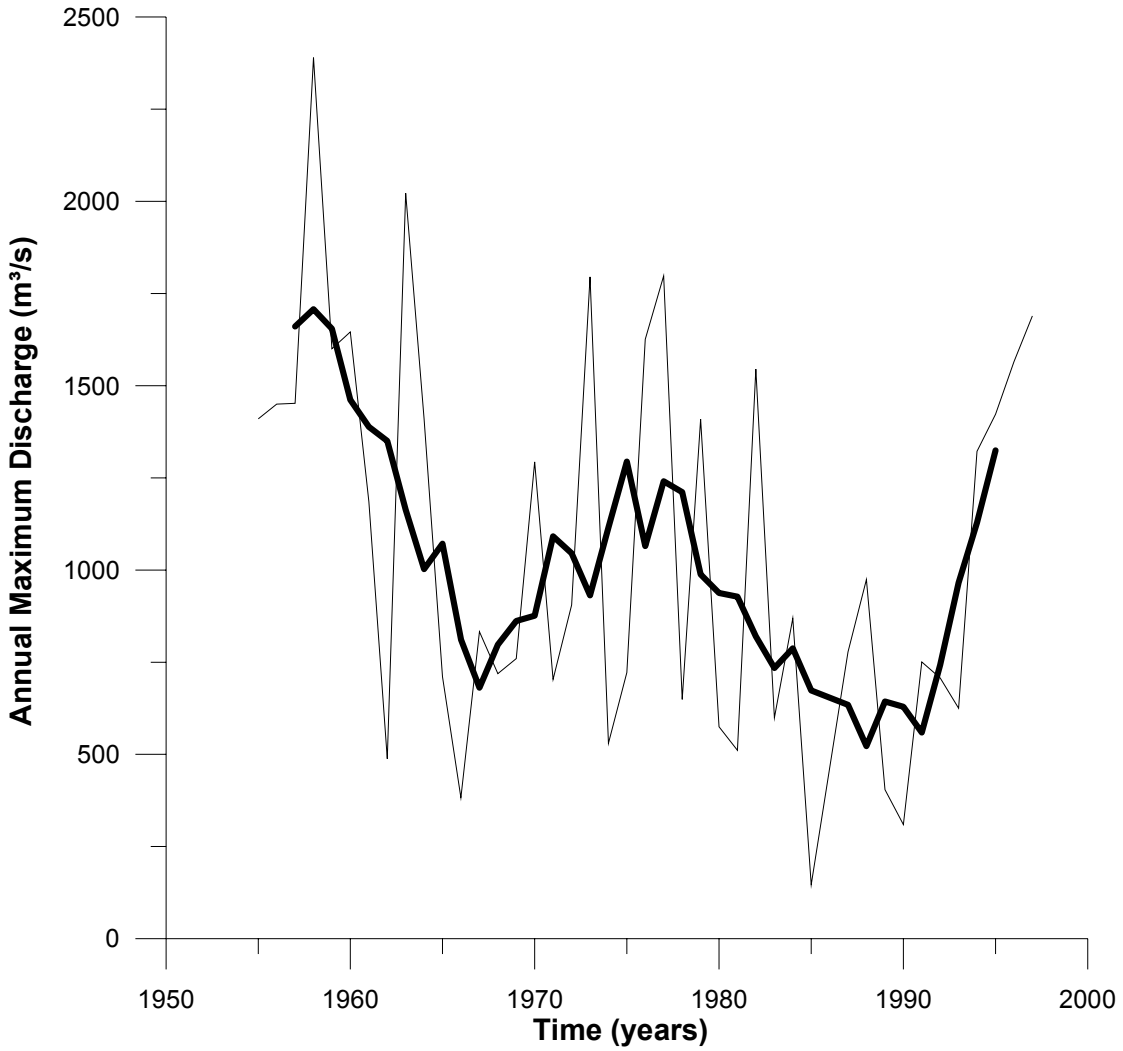

Figure 5.9 Observed annual maximum discharge between 1955-1997 in the Ardèche-Saint Martin with a 10-year moving average.

In general, the annual maximum discharge series might indicate an increase or decrease in the magnitude of large floods over longer time periods. In the Ardèche, there was no significant trend observed.

In Figure 5.10 the simulated annual maxima of discharge are illustrated in Ardèche-Saint Martin between 1900-2000. The behavior of the annual peak discharges varies significantly in time including periods with high annual maxima which are followed by rather low discharges. The long-term variability of simulated annual peak discharges shows no statistically significant monotonic trends.

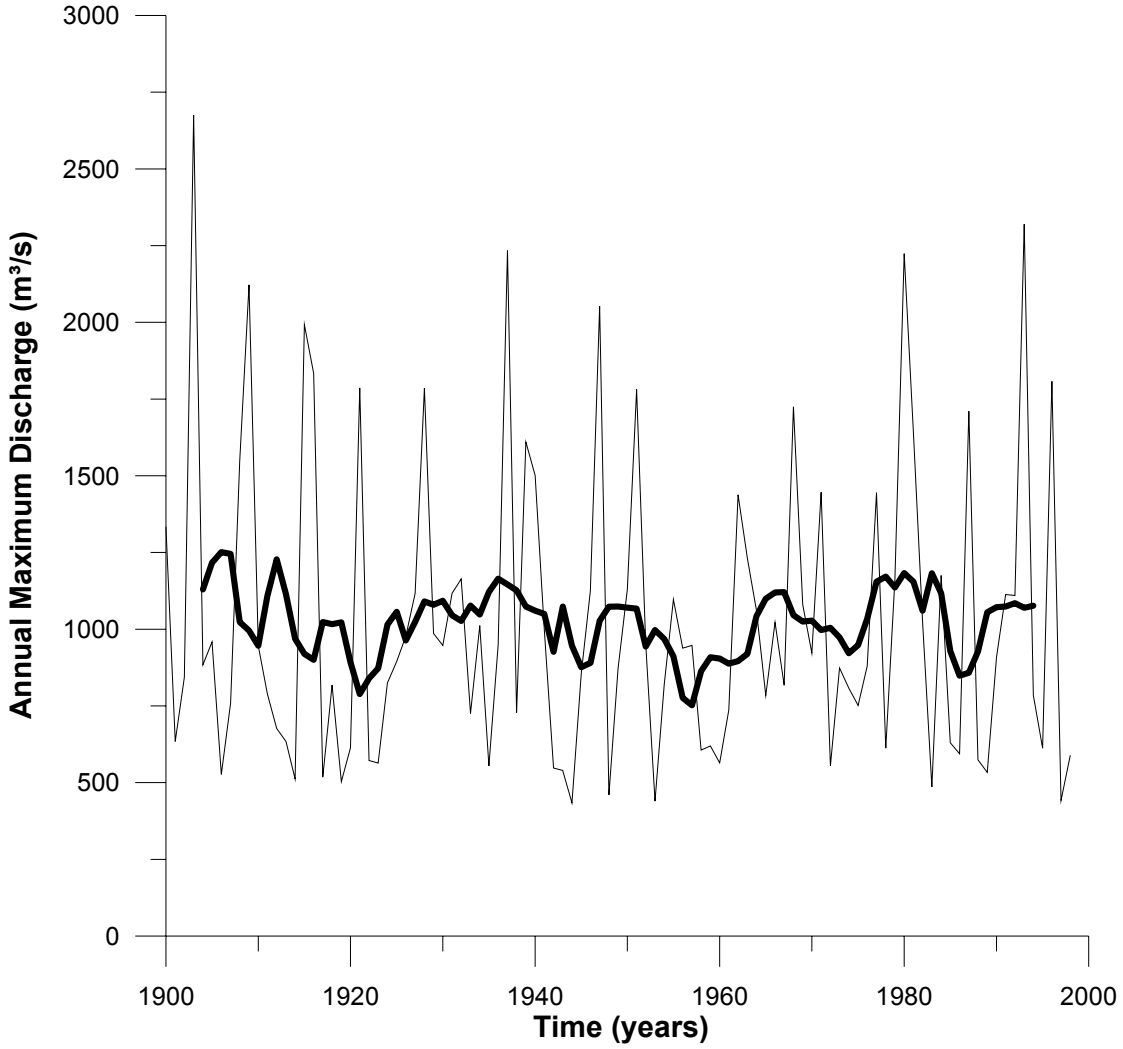

Figure 5.10 Simulated annual maximum discharge between 1900-2000 in the Ardèche-Saint Martin with a 10-year moving average.

The same analysis was applied to the Llobregat Basin. Figure 5.11 and Figure 5.12 show the observed (1912-1990) and the simulated annual maximum discharge series (1900-2000) in the

Llobregat at Martorell respectively. The observed annual peak discharges vary between approximately 50-1600 m³/s (see Figure 5.11).

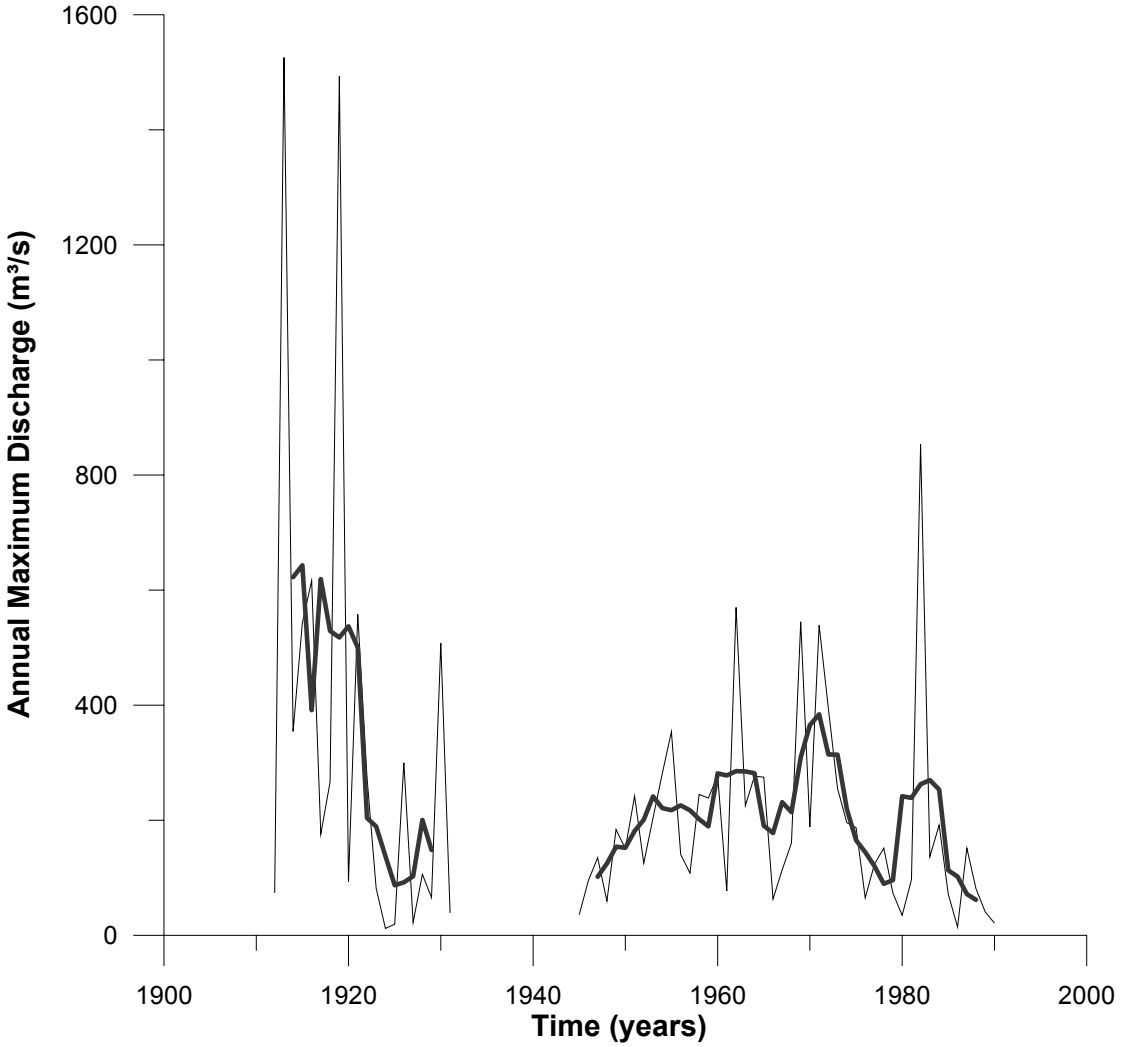

Figure 5.11 Observed annual maximum discharge between 1912-1990 in the Llobregat-Martorell with a 5-year moving average (for the period between 1932-1944, the observations are not available).

After investigating the observed maximum discharges, the simulated discharges between 1900-2000 were analyzed. The same structure of the variability of maximum discharges in time over the whole period can be recognized in the simulated annual maxima series without indicating a clear trend (see Figure 5.12). The range of maximum annual peak simulated values is comparable to the observed values (approximately 60-1500 m³/s).

Regarding the investigation of possible trends within the annual maximum discharge series, it should be considered that one single simulation cannot be adequate for such an analysis since each simulation strongly depends on the random numbers used for the simulation. In order to

investigate the possible trends in the annual peaks, a large number of simulations should be run and the average behavior of these simulations should be investigated.

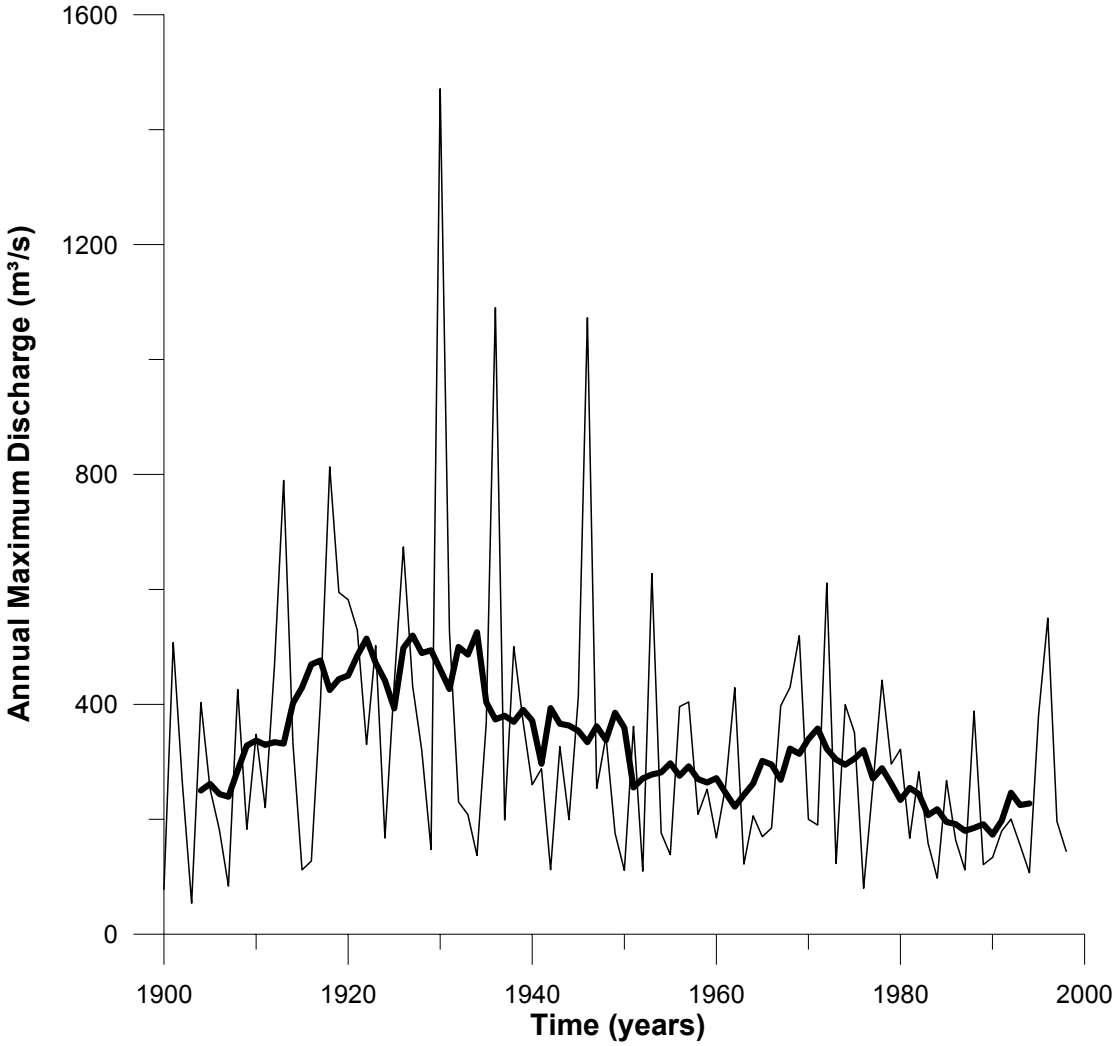

Figure 5.12 Simulated annual maximum discharge in Llobregat-Martorell between 1900-2000 with a 10-year moving average.

For the evaluation of the hydrological sensitivity of the discharge downscaling model, i.e. whether the model can reproduce *wet* and *dry* conditions, wet and dry years in the Study Areas were assessed. This was achieved by analyzing the occurrence frequency of wet CPs (see Chapter 4: Figure 4.13 and Figure 4.14). High occurrence frequency of wet CPs indicates wet periods whereas low frequency of wet CPs signifies dry periods. According to this, for the Ardèche Basin, the "wet year" was selected as 1951 with a cumulative wet CP occurrence of 30 % and the "dry year" was 1921 corresponding wet CP frequency of 9 %. The same was applied in the Llobregat. 1951 was indicated as the wet year with wet CP frequency of 11 % whereas the dry year 1906 showed only 2 % of wet CP frequency. In order to make the wet and dry characteristics significant over a longer time period, it was assumed that these wet

and dry years conditions prevailed 100 years by repeating themselves in the CP sequence. Finally a wet 100 year CP series and a dry 100 year CP series were obtained for each basin and the discharge downscaling model was run within the given wet and dry conditions. The results of the model at Ardèche-Saint Martin are shown in the Figure 5.13. Simulated discharge series for wet conditions are illustrated in red and the dry conditions are shown in blue. One can conclude that the model produces much higher discharge series for wet conditions than the ones representing dry conditions (see the 10-year moving average smoothing). This indicates that the discharge downscaling model is capable of differentiating wet and dry condition very well.

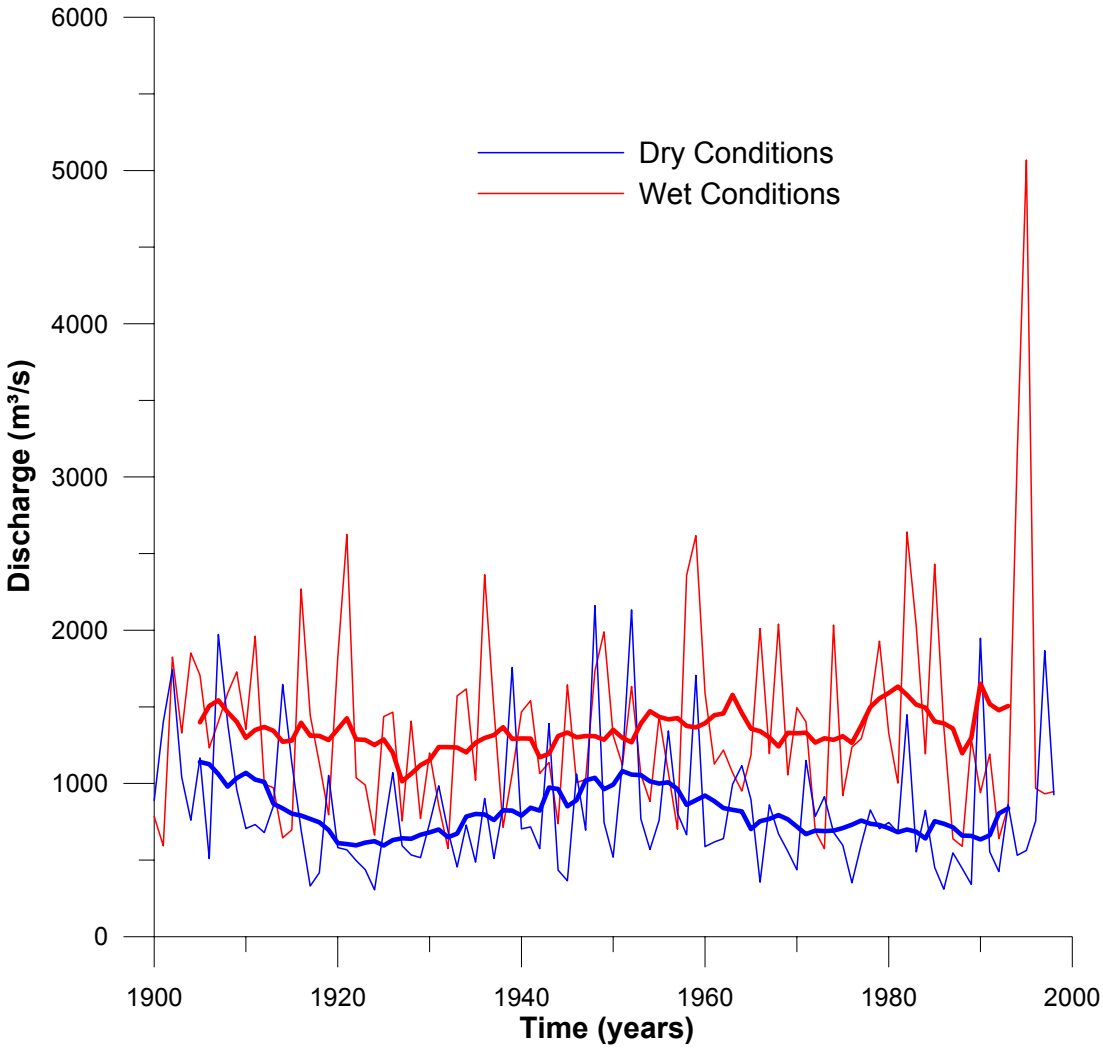

Figure 5.13 Simulated annual maximum discharge for the period between 1900-2000 based on dry and wet conditions for the Ardèche Basin at Saint Martin. Both dry and wet runs simulations are smoothed with a 10-year moving average.

The results of the simulation of discharge series in both wet and dry conditions in the Llobregat Catchment provided similar results. Here, again wet conditions produced higher discharges and dry conditions lower discharges in the average as shown in Figure 5.14.

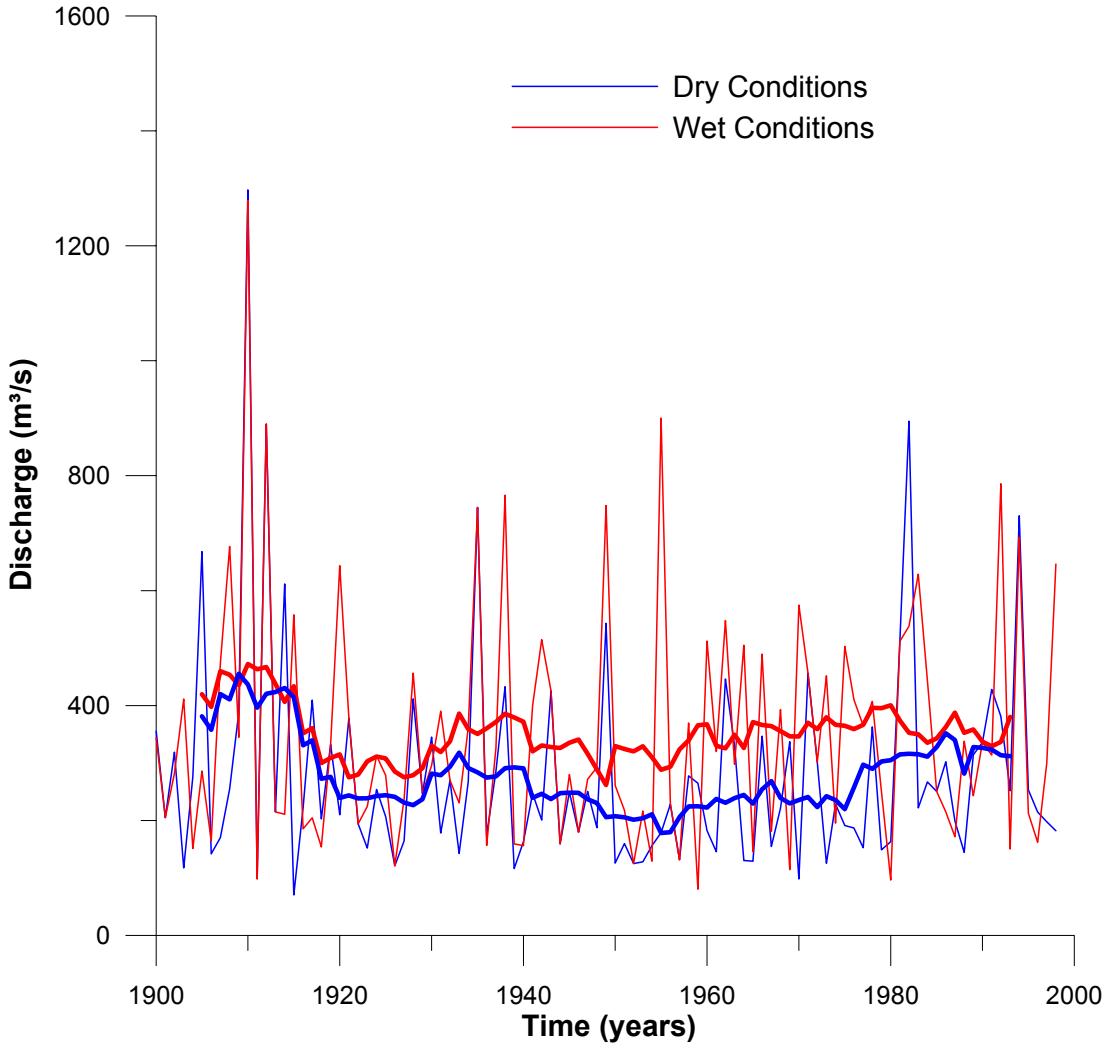

Figure 5.14 Simulated annual maximum discharge for the period between 1900-2000 based on dry and wet conditions for the Llobregat Basin at Martorell. Both dry and wet runs simulations are smoothed with a 10-year moving average.

The results of the discharge downscaling model have been validated by fitting Generalised Extreme Value (GEV) distribution such as Method of Moments (MM) and Maximum Likelihood Method (MLM). The frequency and the magnitude of the simulated discharges show good agreement with the observed ones during the intrumental record period in both Study Areas. This can be seen in Figure 5.15 for the Ardèche, where the annual peak of observed and ten simulated discharge series in the Ardèche-St. Martin are shown. The red symbols in the figure show the extrapolation of simulated annual maxima up to 1000 years using the same CP series which was fitted to GEV; the black symbols show the observed

annual maxima. The discharge downscaling model reproduces the extreme value statistics very well, since the simulated discharges cover the observed maxima for the whole time period of extrapolation (for 2, 5, 10, 20, 25, 50, 100, 200, 500, 1000 years corresponding return periods). It should still be considered that the quality of the fit of the extreme-value distribution depends on the selected distribution function and its parameters.

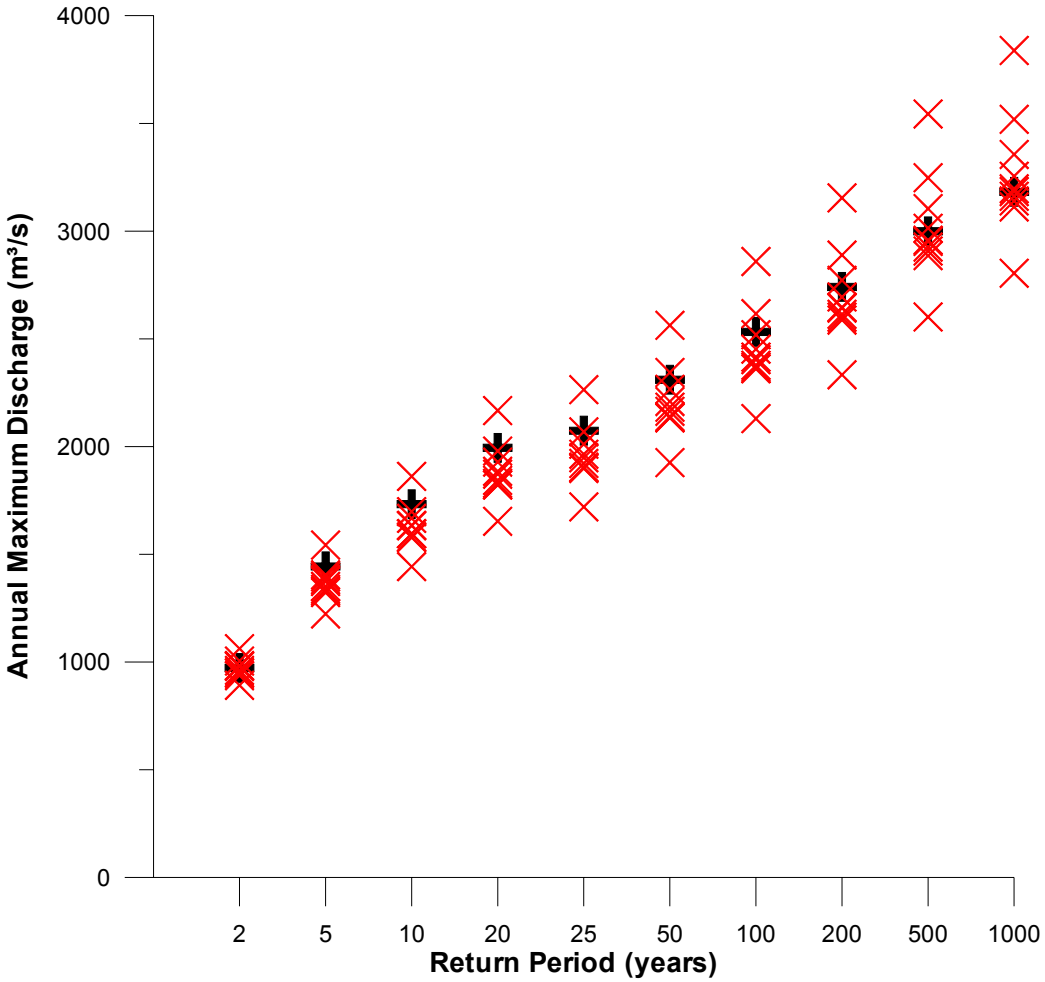

Figure 5.15 Return period of annual maxima of the observed and ten simulated discharge series in the Ardèche Basin. Red symbols show the downscaled simulated annual maxima and black symbols represent the extrapolated downscaled annual maxima.

The validation of the results of the discharge downscaling model in the Llobregat at Martorell can be seen in Figure 5.16. The model produces satisfying results in the Llobregat as well.

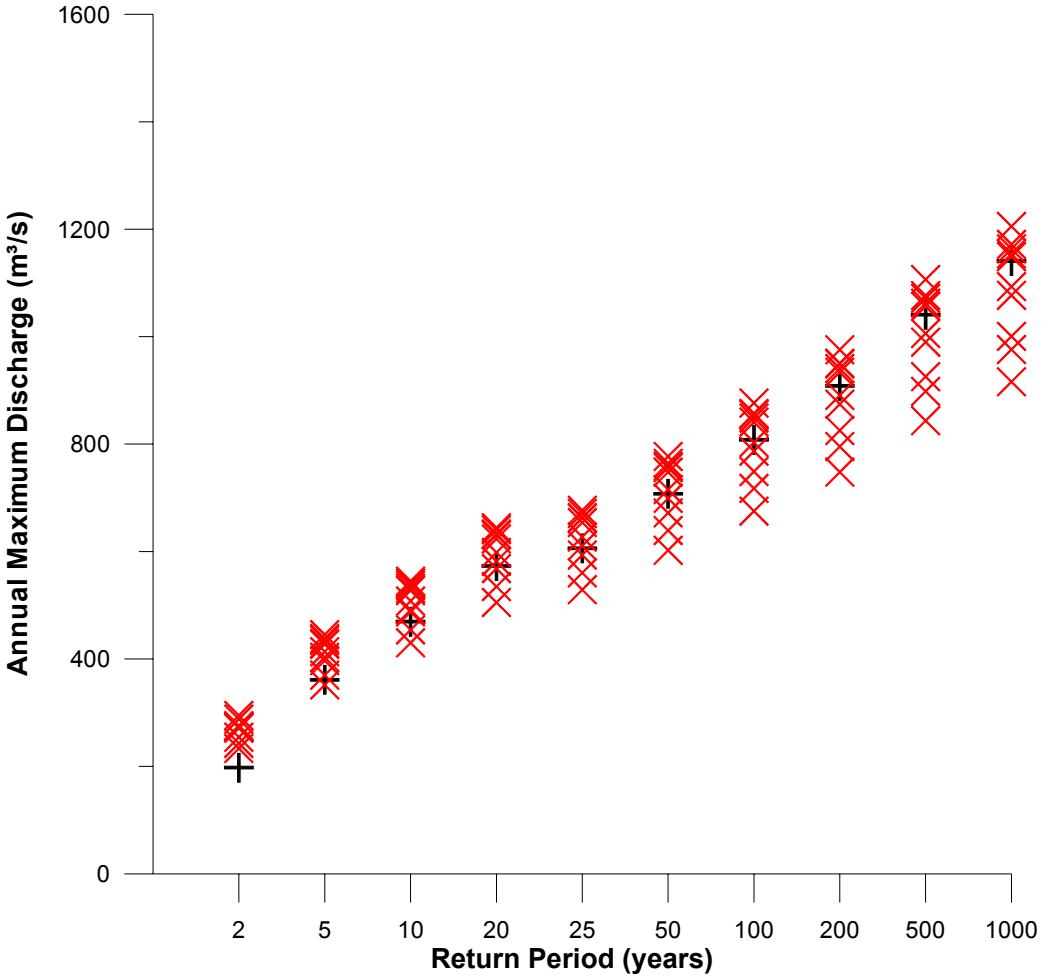

Figure 5.16 Return period of annual maxima of the observed and ten simulated discharge series in the Llobregat Basin. Red symbols show the downscaled simulated annual maxima and black symbols represent the downscaled observed annual maxima.

Chapter 6

Application of the Discharge Downscaling Method to Historical Climate Scenarios

6.1 Introduction

Climate scenarios are required to assess the climate change impacts and describe possible future developments in the climate. Despite of the fact that scenarios are the main tools in this scope, they are often not predictable and have high scientific uncertainties. A scenario is not a forecast, but an alternative illustration of what might happen. A set of scenarios is often adapted to reflect the range of uncertainty in projections as well as possible.

For understanding and modeling current and future climate trends, it is crucial to know more about past climate variability. The climate model projections provide estimates for many of the climatic variables and a key framework for assessing the impacts of climate change.

The strategy for providing climate scenarios for regional and national impact assessment is based on several key needs:

- A historical climate record is needed in order to have basis for assessing the importance of climate and climate change.
- The range of future climates used in the assessment process must be sufficiently broad to reflect the levels of uncertainty in models and in the projections.
- The assessment must reflect the range and character of natural variability of climate.
- The period of model predictions must overlap with the period of historical observations in order to evaluate the capabilities of the models.
- The assessment process should include opportunities to determine thresholds or limits in human and ecosystem adaptability.

Each climate simulation is based on models that include both the ocean and the atmosphere, and for which the atmospheric greenhouse gas concentrations and sulfate emissions evolve with time.

The study focused on historical climate scenarios, since the context of this research comprises the investigation of past climate variability and its possible consequences on past floods. Therefore historical climate scenarios were used for the analysis and the generation of past flood peaks. The analysis of flood hazards was combined with a flood frequency model to assess the effects of variability changes. Several monthly data sets for historical time series are available; however, they were not appropriate for this study since daily temporal resolution was required to analyze floods. For the investigation of possible past floods and their magnitudes, several datasets in daily time resolution have been provided.

- Daily Sea Level Pressure Observations from different stations:

  i.e. Cadiz, Milan, Padua, Reykjavik, Uppsala, Stockholm from IMPROVE Project (IMPROVE - Improved understanding of past climatic variability from early daily European instrumental sources, research project funded by European Community)
- Daily Sea Level Pressure Point Data from following stations:

  Barcelona, Prague, Budapest, Sion, Bern
- Daily Temperature Point Data from following stations:

  Belgium, Cadiz, Stockholm, St. Petersburg, Uppsala (IMPROVE)
- Daily GCM fields for reconstructed climate for the period between 1500-1990 from KIHZ Project (KIHZ – Natural climate variations from 10000 years to the present day, German research project funded by HGF-Hemholtz-Gemeinschaft Deutscher Forschungszentren)

Using the data listed above, several classifications have been carried out. Among observed daily gridded SLP data (1899-2003), observed daily historical point pressure and temperature data (1773-1991) and daily historical GCM data (1500-1990) have been classified to reproduce longer discharge time series. The results of the application of discharge downscaling on the historical data will be the subject of this chapter. In the next section, the classification of the historical climate data will be presented.

6.2 Classification of Historical Circulation Patterns Based on the Nearest Neighbor Method

The classification of daily historical pressure records from the previously listed stations was achieved by gridding using the Nearest Neighbor (NN) method.

The Nearest Neighbor Method attempts to compare similar situations in the past with current data and assume that similar events are likely to occur in similar conditions. The main principle of the method is to find the most similar days (clusters) in the past to the observations and compare the resulting events. The Nearest Neighbor Method is quite practical, since it is quite intuitive in its operation and the data requirements are relatively modest. Details are provided in Appendix 4.

The distances were calculated according to

- Euclidean distance (without covariances)
- Mahalanobis distance (with covariances)

For a distance between two *p*- dimensional observations

$$x = (x_1, x_2, ..., x_p) \quad \text{and} \quad y = (y_1, y_2, ..., y_p)^T \tag{6.1}$$

Euclidean distance is calculated as:

$$d_E(x, y) = \left[(x - y)^T (x - y)\right]^{\frac{1}{2}} \tag{6.2}$$

whereas Mahalanobis distance accounts for covariances as follows:

$$d_E(x, y) = \left[(x - y)^T S^{-1} (x - y)\right]^{\frac{1}{2}} \tag{6.3}$$

The variables are:

d_E : Euclidean distance

d_M : Mahalanobis distance with covariances

x : observations of air pressure

y : observations of air temperature

S^{-1} : the inverse of S (the covariance matrix)

p : Number of variables

Distances are composed of the sum of air pressure and temperature after Mahalanobis distances since air pressure and air temperature are correlated with each other. Further, air pressure data of the previous and subsequent days are taken into account within the calculation of the distances as follows:

$$d_p(t_1,t_2) = d_M(\mathbf{x}(t_1),\mathbf{x}(t_2)) + \alpha \cdot d_M(\mathbf{y}(t_1),\mathbf{y}(t_2) + \beta \cdot d_M(\mathbf{x}(t_1-1),\mathbf{x}(t_2-1)) + \beta \cdot d_M(\mathbf{x}(t_1+1),\mathbf{x}(t_2+1)) \quad (6.4)$$

$\mathbf{x}(t)$: Vector of air pressure

$\mathbf{y}(t)$: Vector of air temperature

The classification of the historical record has been done by assigning a grid to a day *"t"* from the observed period which minimizes the distance.

$$d_P(t,t^*) \rightarrow min$$
$$t^* \in T \ (= \text{days with gridded data - 1900})$$

The classification quality has been assessed via the Jackknife method:

- For each day in the gridded period, the nearest neighbor from the other days is chosen (min 183 days apart)
- Spatial correlation between the grids is calculated (in daily and monthly means)
- Agreement with existing classification is checked

The classification quality assessed by the Jackknife method can be seen in Figure 6.1 where the spatial correlation in daily and monthly means is shown. The Jackknife method introduced by Quenouille (1949) is a resampling technique which is generally used for bias and standard error estimation. Details are given in Appendix 5.

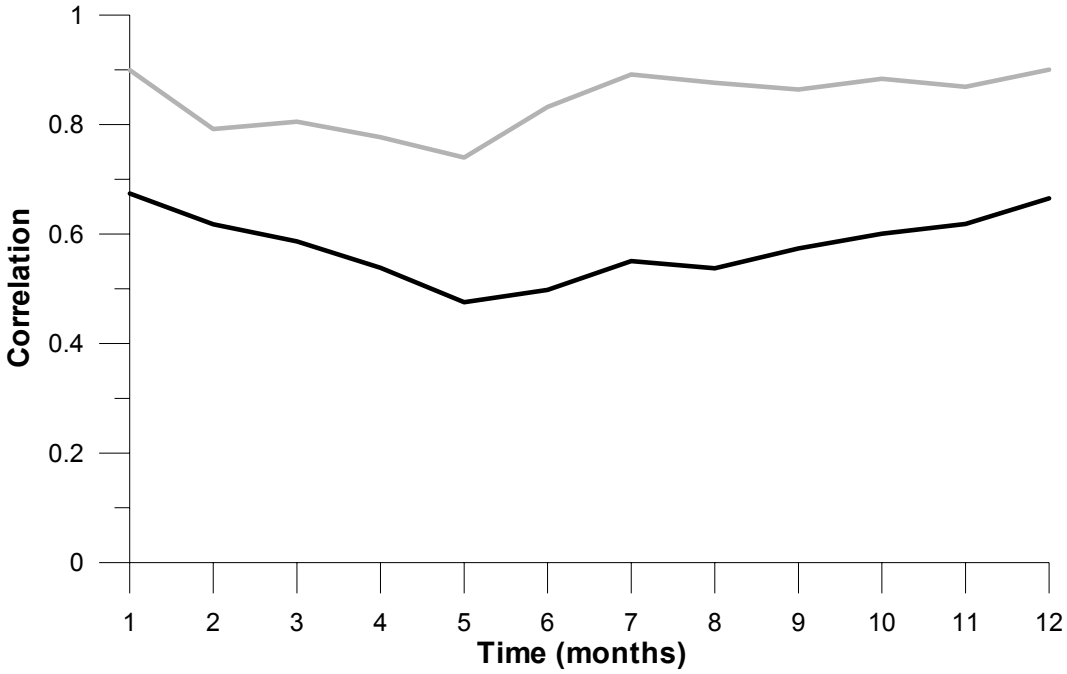

Figure 6.1 Classification quality via the Jackknife method. Gray line represents the daily spatial correlation between the grids and black line shows the monthly correlation.

According to the results, 30 % of the patterns have the same class as in the existing classification of gridded SLP data which is significantly higher than would be obtained from random data, and the classification turns out to be different from the original (existing classification of gridded SLP data – long series between 1899-2003).

The results of the discharge simulation resulting from the NN classification in the Ardèche Vogue (1774-1900) can be seen in Figure 6.2. The model can reproduce the variability of high discharge events in frequency and magnitude. The statistics of the simulated and observed discharge series can be seen in Table 6.1. The results of the simulation show very good agreement with the observed values in terms of statistical parameters, although the simulation period is much longer than the observation period.

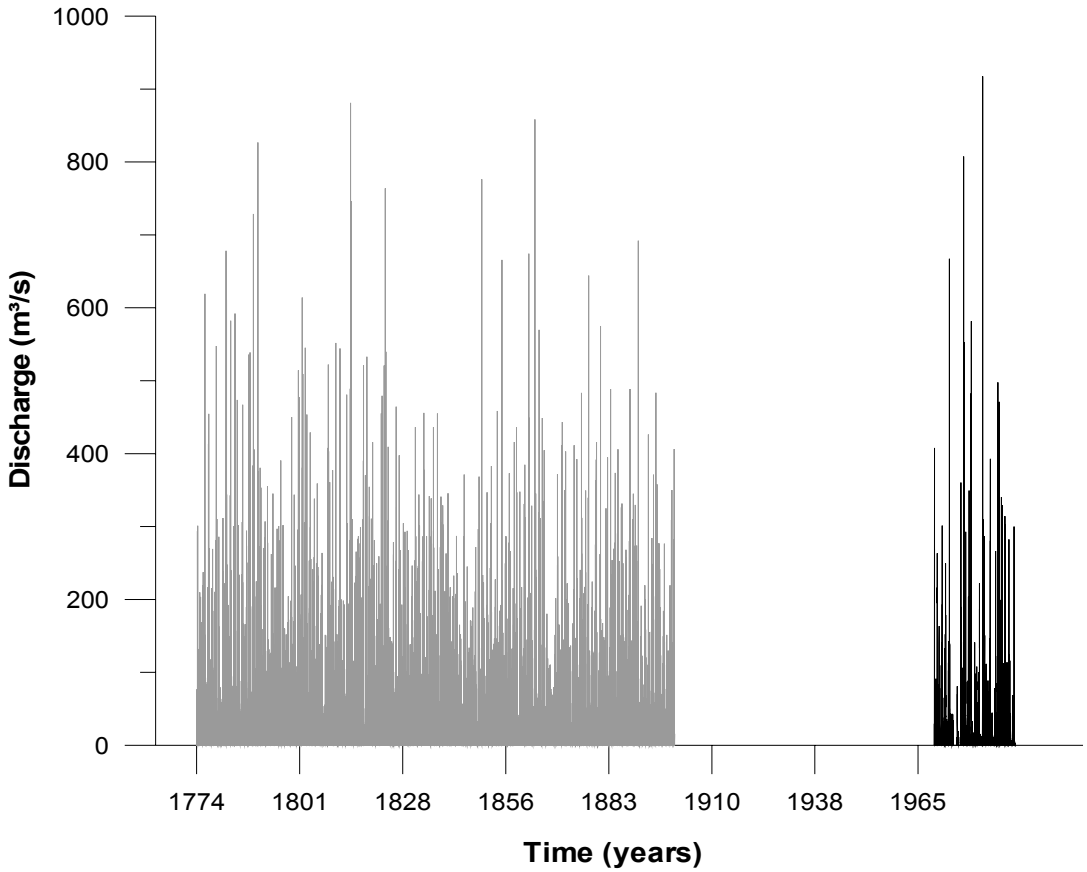

Figure 6.2 Observed (black) and simulated (gray) discharge time series for the Ardèche at Vogue (1774-1900) using NN-based classification.

Table 6.1 Statistics of discharge simulated and observed in the Ardèche Basin at Vogue between 1774-1900.

Ardèche-Vogue								
Discharge Series	Discharge		Quantiles					
	Mean	St Dev	25%	50%	75%	90%	95%	99%
Simulated	14.21	38.07	0.69	4.06	12.82	27.54	55.22	189.58
Observed	13.86	38.80	0.60	3.70	12.21	29.80	54.50	163.41

The same analysis was done for the historical flood simulations using historical NN-based data in the Ardèche-St.Martin. Figure 6.3 illustrates 100-year flood discharges calculated on the basis of 30-year discharge data by shifting the time windows and their median between 1774-1990. The natural variability of the occurrence of historical floods could be observed clearly again. One can see that the occurrence of high floods vary in time significantly (see the median of the simulated peak discharges). The magnitude of simulated floods varies in the range of approximately 1500-3500 m³/s in the Ardèche Basin.

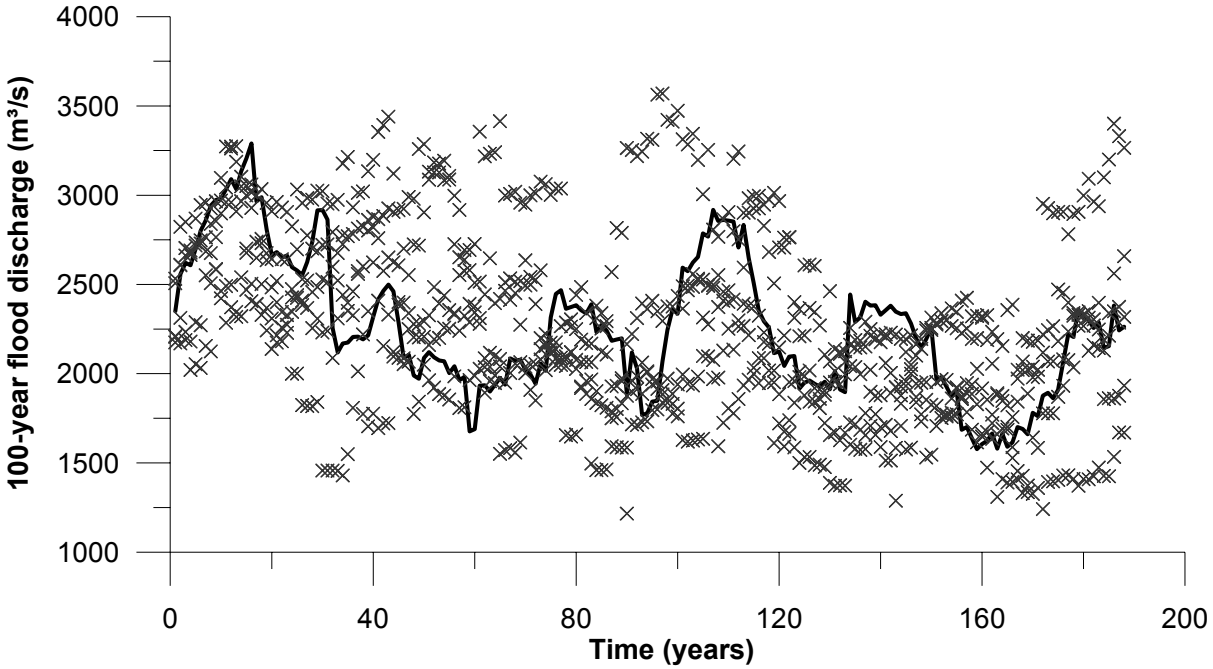

Figure 6.3 100-year flood discharges (cross symbols) for Ardèche-St.Martin between 1774-1990 based on historical NN-based data and their median (black line).

It is also interesting to see how the frequency of certain CPs in the Ardèche and in the Llobregat Basin changed during the historical period. For this, the occurrence frequency of CP01 in the Ardèche is shown in Figure 6.4 which resulted from the NN-based classification. As observed in the diagram, the occurrence frequency of CP01 reached approximately 12 % in about 1800 and then began decreasing gradually. Since the 1850s, the frequency of CP01 has been fluctuating in the range of 4-8 %.

Figure 6.5 indicates the occurrence frequency of CP04 in the Ardèche which shows smoother fluctuations during the same time period compared to CP01. CP04 occurred within the range of approximately 1-7 % occurrence frequency.

Regarding the CP09 in the Llobregat, its frequency shows similar characteristics compared to CP01 in the Ardèche (see Figure 6.4 and Figure 6.6 for a comparison). The occurrence frequency of CP09 in the Llobregat is illustrated in Figure 6.6. CP09 seems to have occurred more often in the beginning of 1800 showing a negative trend towards 1850. Since then, the frequency of CP09 varied without showing significant changes.

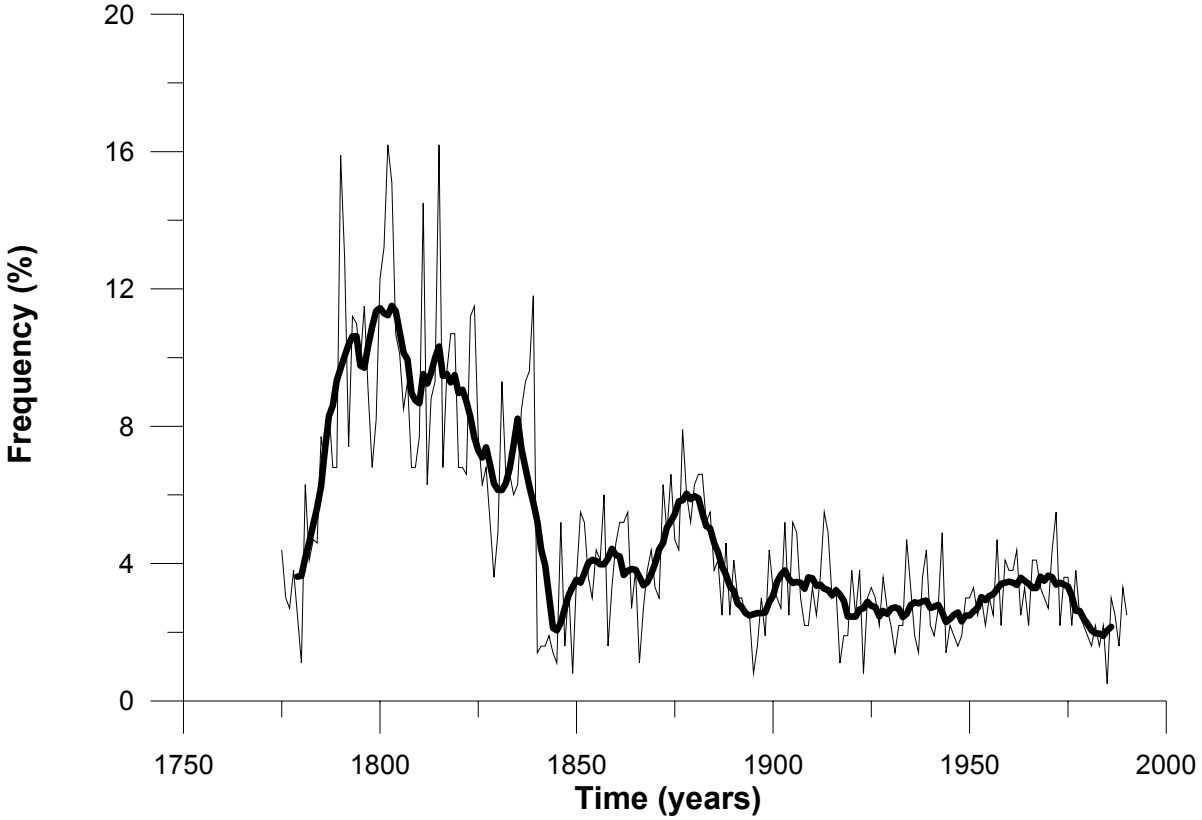

Figure 6.4 The occurrence frequency of CP01 in the Ardèche with NN-based classification (1774-1990) and a 10-year moving average.

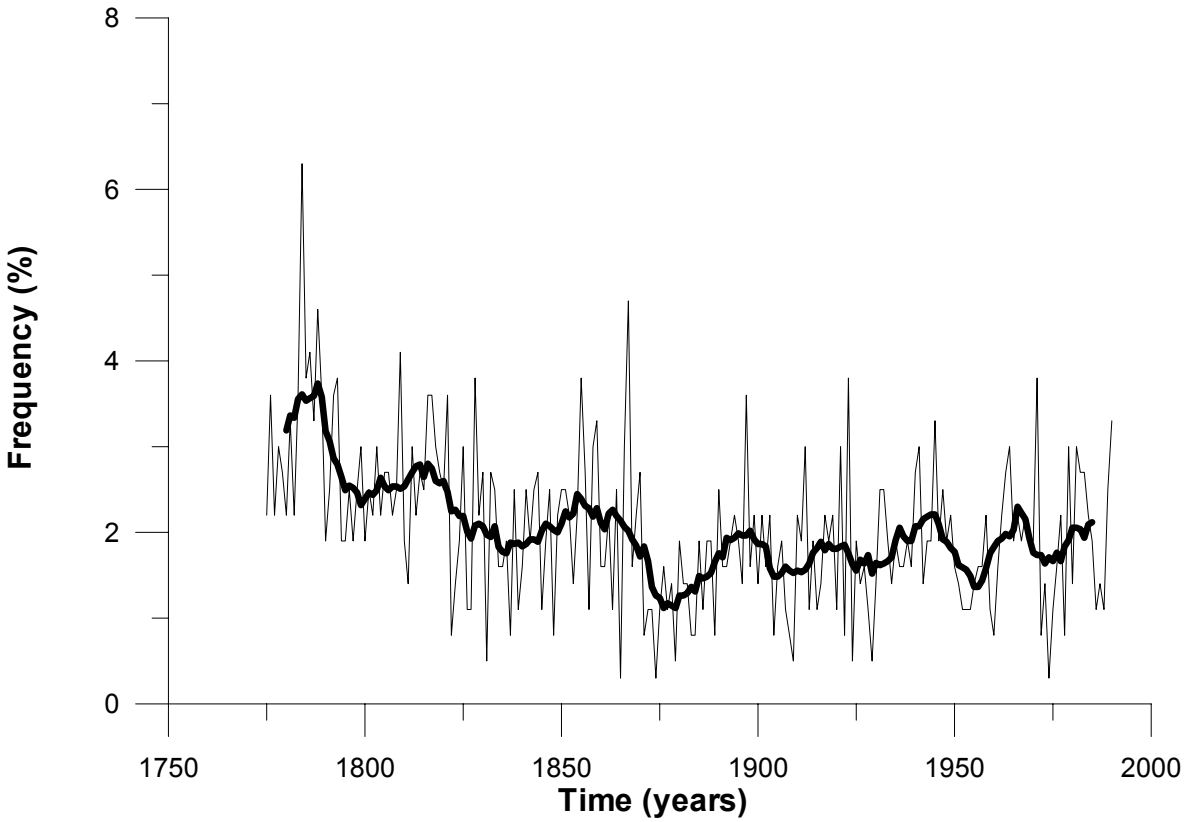

Figure 6.5 The occurrence frequency of CP04 in the Ardèche with NN-based classification (1774-1990) and a 10-year moving average.

The validation of the results of the discharge downscaling model using NN-based classification has been assessed by fitting Generalized Extreme Value GEV distribution with Method of Moments (MM) and Maximum Likelihood Method (MLM) for both Study Areas. The results of the annual maximum discharge and the corresponding return periods are demonstrated in Figure 6.7 for Ardèche-Saint Martin. In the figure, black symbols show the extrapolated observed values whereas red symbols show the extrapolation simulated annual maxima series up to 1000 years of recurrence period using the same CP series which was fitted to GEV. For the whole extrapolation period the frequency and the magnitude of the simulated discharges show a good agreement with the observed ones. In case of NN-based classification of the atmospheric circulation patterns, the discharge downscaling model reproduces the extreme value statistics very well, since the simulated discharges cover the observed maxima for the whole time period of extrapolation (for 2, 5, 10, 20, 25, 50, 100, 200, 500, 1000 years corresponding return periods). It should still be considered that the quality of the fit of the extreme-value distribution depends on the selected distribution function and its parameters.

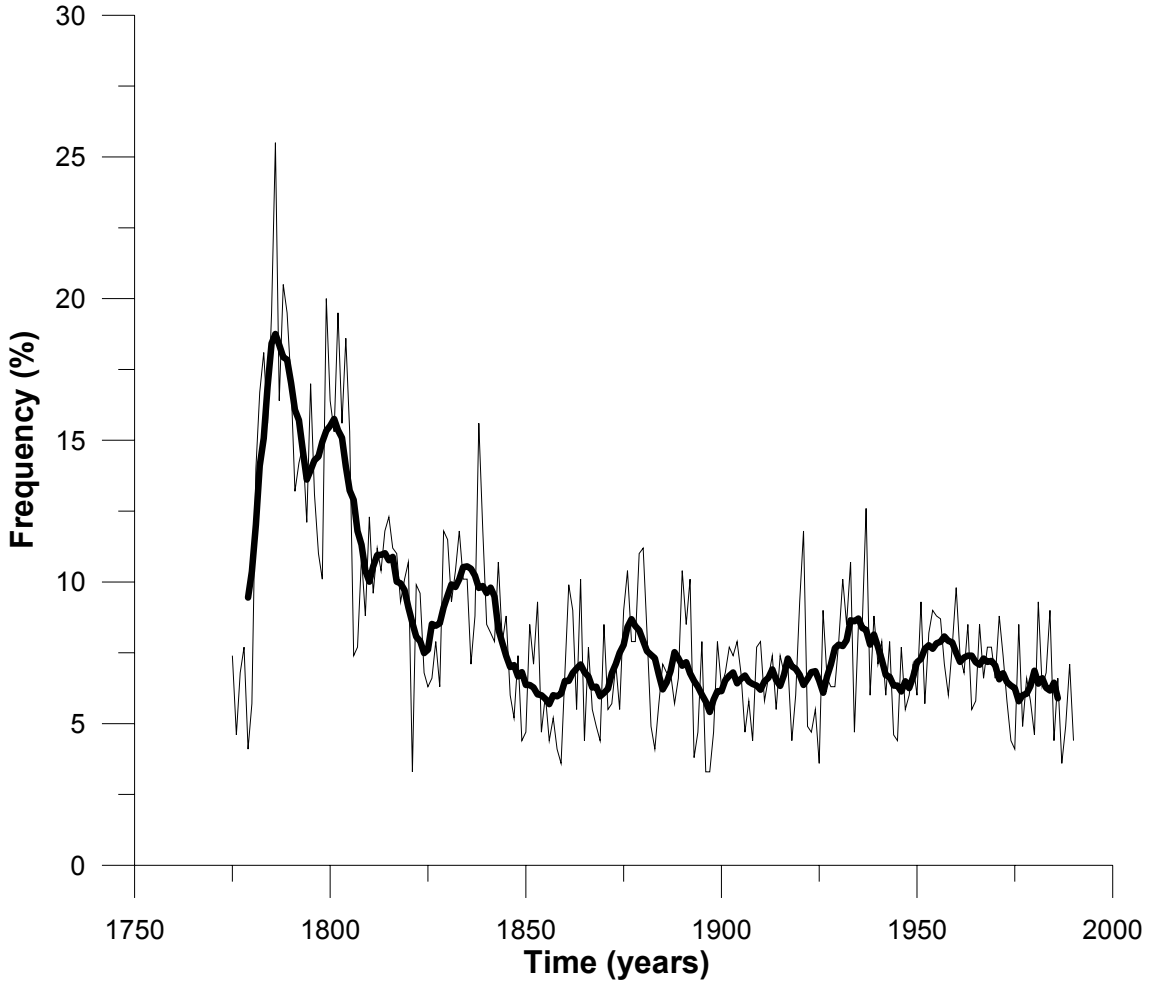

Figure 6.6 The occurrence frequency of CP09 in the Llobregat with NN-based classification (1774-1990) and a 10-year moving average.

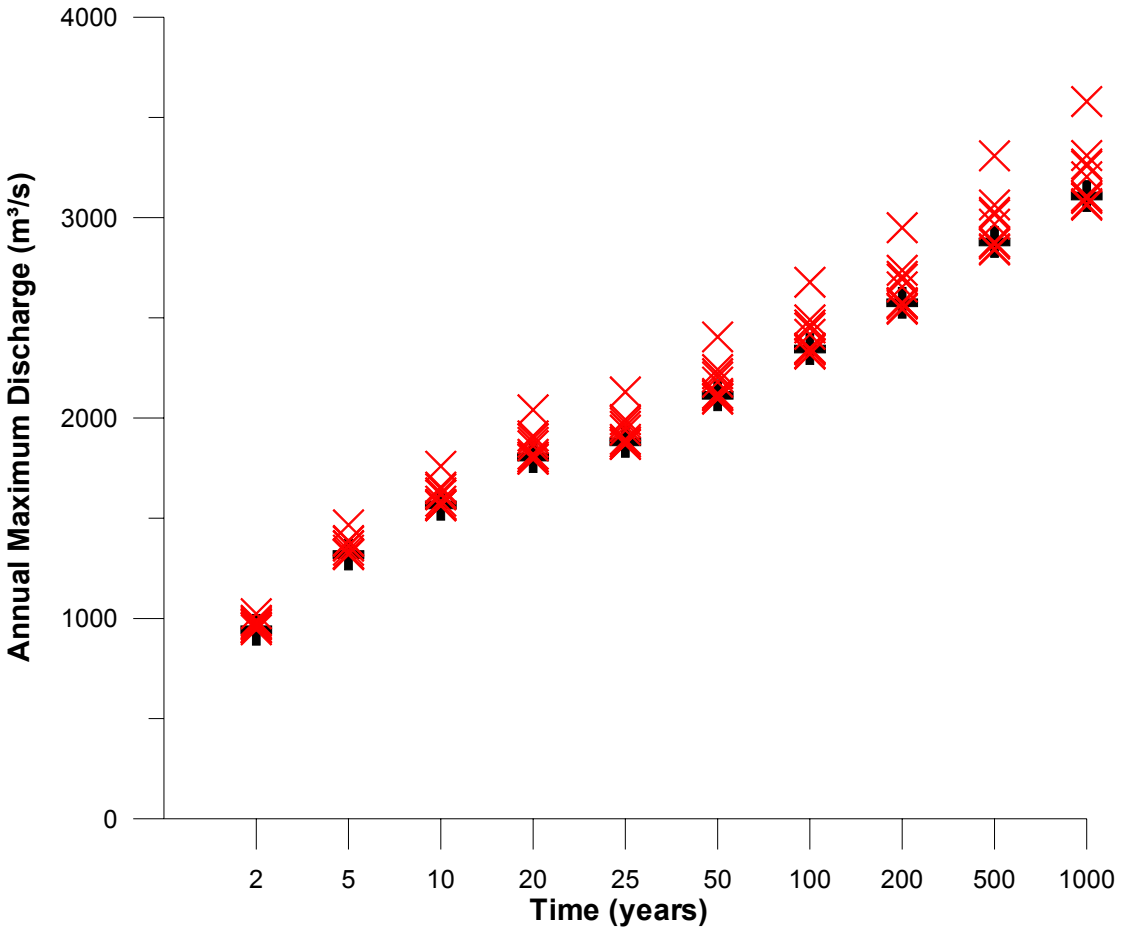

Figure 6.7 Return period of annual maxima of observed (1774-1990) and ten simulated discharge series based on the NN method for Ardèche-St.Martin. Red symbols show the downscaled simulated annual maxima and black symbols represent the downscaled observed annual maxima (1955-1997).

6.3 Classification of Historical Circulation Patterns Based on the Historical Climate Reconstructions

The application of historical GCM runs for the reconstructed climate data will be presented in this section.

The global climate in the last 2000 years was reconstructed globally with simulations with a global climate model forced by external driving factors, such as solar variability, atmospheric concentrations of greenhouse trace gases, volcanic aerosols and variations of orbital parameters within the research project KIHZ (Natural climate variability in historical times). Additionally, the model was constrained by a large set of proxy data sets from drilling cores, tree rings, polen records and instrumental records, through a scheme of data assimilation. The results represent a dynamical consistent global interpolation of the observations to the high resolution of the climate model (about 250 km). It allows

for an estimation of the natural climate variability at the local and regional scale. More information about the data used and methods applied can be obtained at http://www.gfz-potsdam.de/pb3/pb33/kihzhome/kihz00 oder Zorita et. al (2003).

The classification of historical atmospheric circulation patterns was achieved by applying the same fuzzy rule sets that were assessed for the long SLP observations (1899-2003) as presented in Chapter 4 so that for each day a CP could be assigned using daily GCM SLP fields between 1500-1990 for each Study Area. Figure 6.8 demonstrates a schematic flow diagram of the application.

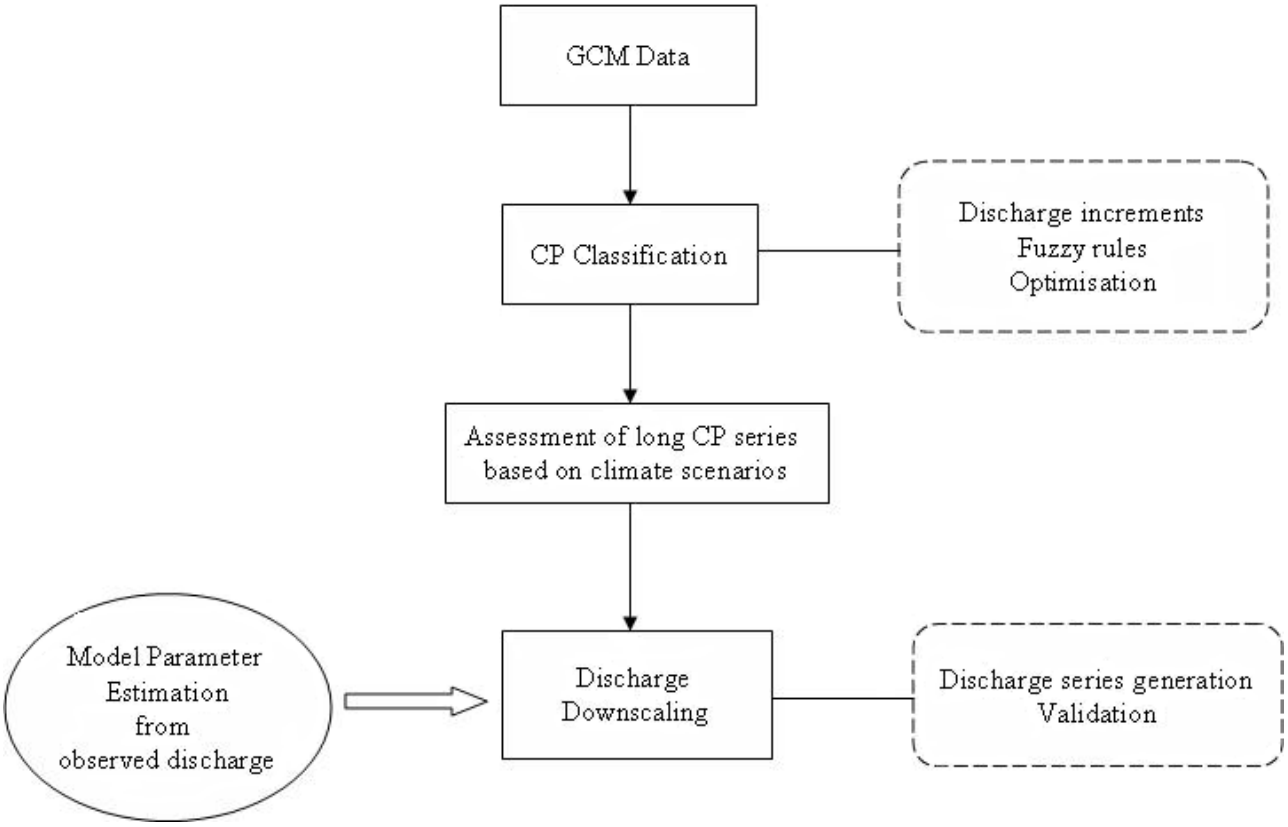

Figure 6.8 A schematic summary of linking atmospheric circulation to discharge directly for the flood simulation based on different climate scenarios. Once the model parameters are set using the observations, discharge series can be generated using long CP series based on climate scenarios.

After the assessment the CP series from the historical GCM fields, the classification should be validated. This was achieved by comparing the frequency of the historical CP assessed with the observed frequency of CPs. The comparison can be seen in Figure 6.9. As it can be observed from the diagram clearly, the atmospheric circulation patterns obtained from GCM output (in blue) do not match with the patterns which originate from the observations (in red).

Since it is of interest to use the long historical GCM SLP-series in order to analyze the long-term variability of the past climate related to past floods, a frequency correction factor was initiated in order to remove the bias which was observed in the frequencies. Bias indicates a systematic error in the frequency.

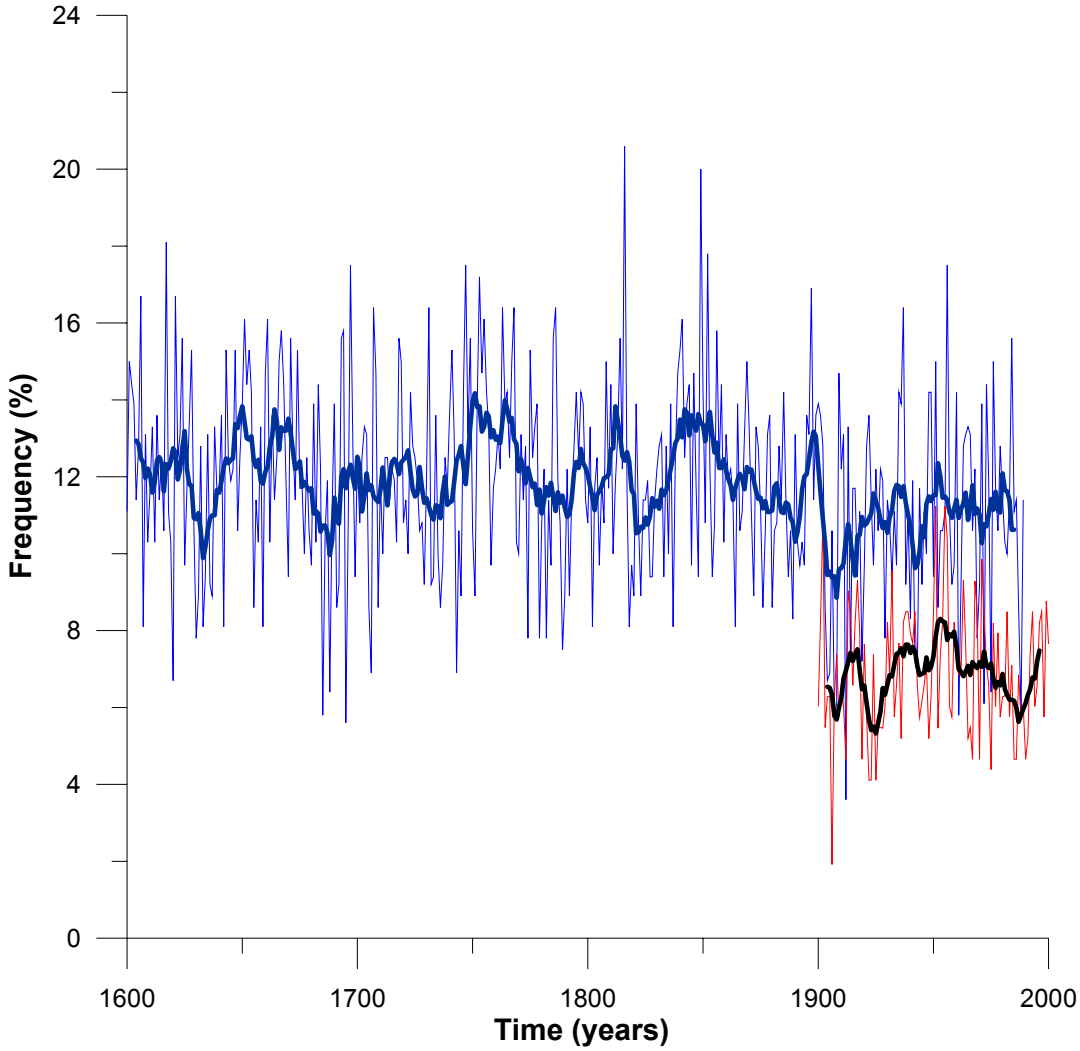

Figure 6.9 CP frequencies for CP09 (frequencies resulting from GCM fields are shown in blue, frequencies from observed data in red).

The frequency correction was achieved by reclassifying ambiguous patterns having very similar occurrence frequencies according to the following condition (slight differences within the CP frequencies might result in different CPs):

$$\mu_1(t), \mu_2(t), \cdots, \mu_K(t) \rightarrow \mu_1^*(t), \mu_2^*(t), \cdots, \mu_K^*(t)$$
$$\mu_k^*(t) = \nu_k \cdot \mu_k(t) \qquad (6.5)$$

$\mu_k(t)$: Membership grade corresponding to rule k

$\mu^*_k(t)$: Membership grade corresponding to rule k after the reclassification

ν_k : Correction factor for the rule k obtained by using an optimization method

For a certain time period the differences in the frequencies will be minimized:

$$\sum \frac{(H_k - H_k^*)^2}{H_k} \rightarrow min \tag{6.6}$$

H_k : The observed frequency of the CP k

H_k^* : Corrected frequency of the CP k after reclassification

Figure 6.10 shows the occurrence frequency of the circulation patterns after the frequency correction. The 10-year moving average of the original CP frequencies (red line) shows a better correspondance with the one after the correction (blue line).

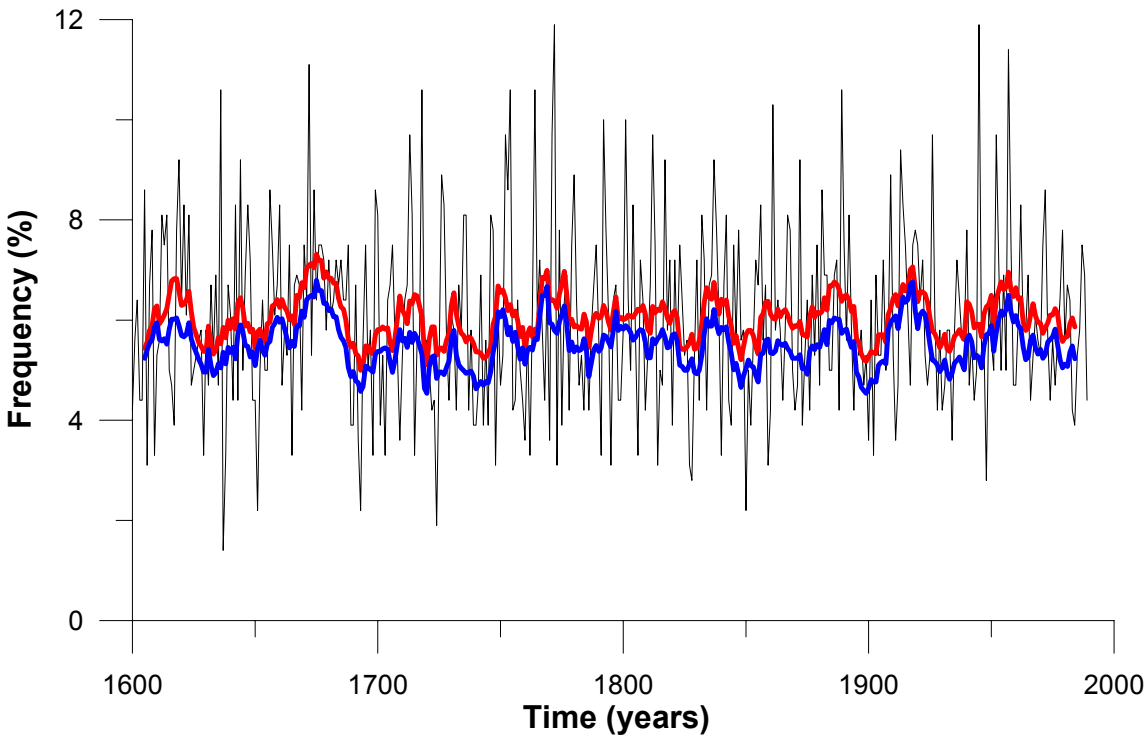

Figure 6.10 Corrected frequencies for CP01 (red line indicates 10-year moving average and blue line indicates 10-year moving average after the frequency correction).

Once the historical CP time series are assessed, the historical discharge time series can be simulated. There have been several simulations done for the time period between 1500-1990. Due to the high volume of data of the long simulation period, which corresponds to almost 500 years, the simulation results are presented in three continuous time intervals (1500-1650; 1651-1800; 1801-1990) for both Study Areas.

Figures 6.11, 6.12, and 6.13 show the results of the simulated discharge series in the Llobregat Basin for three different simulation periods. The statistical comparison of the simulated and observed discharge series is indicated in the following tables after each simulation. The first simulation was done for the period between 1500-1650 and is shown in Figure 6.11. Similarly as in the observation period, high discharges occur rarely and in a random manner.

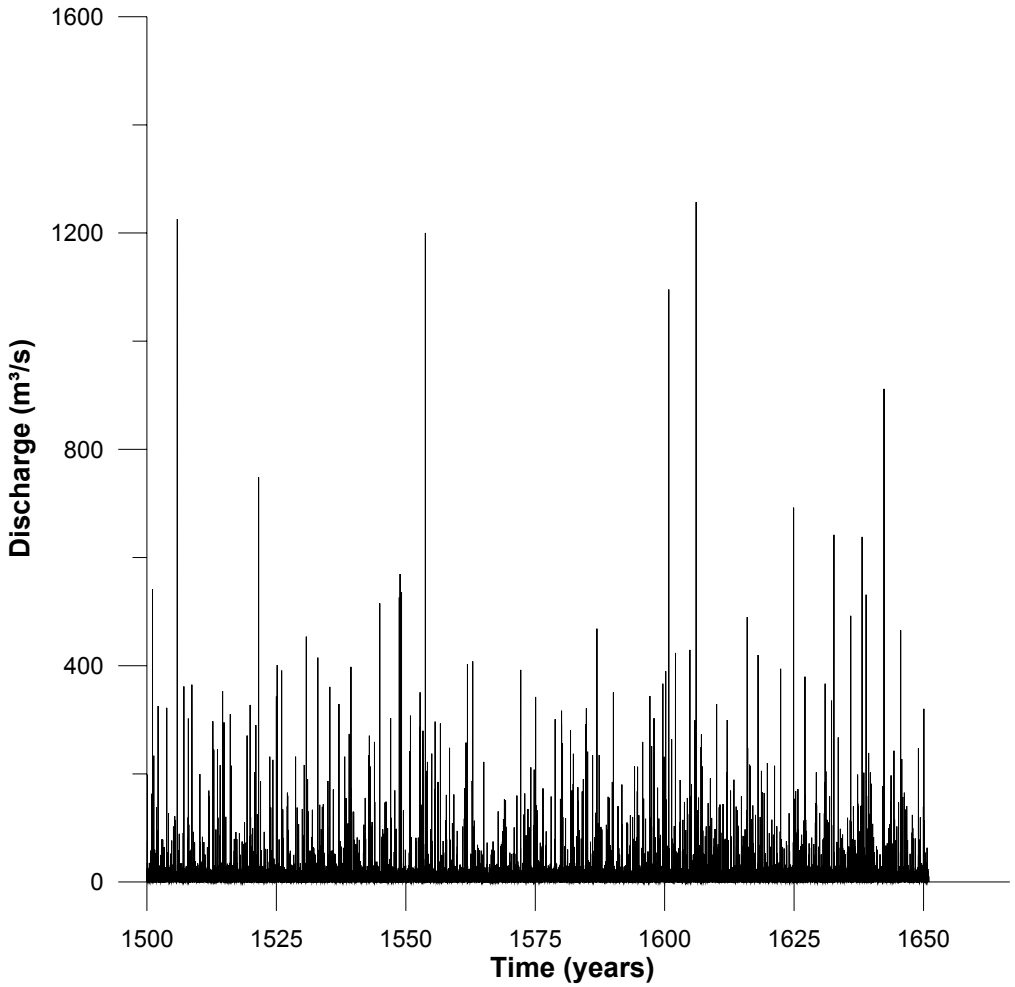

Figure 6.11 Simulated discharge for the Llobregat Basin based on the historical GCM data (KIHZ) for the period between 1500-1650.

The statistics for the simulated and the observed discharge series are given in Table 6.2. The simulated discharge series (1500-1650) and the observed discharge series (1912-1990) show

similar characteristics. The frequency and the magnitude of the peak discharges are successfully reproduced by the discharge downscaling model.

Table 6.2 Statistics of historical discharge simulation (1500-1650) and discharge observations (1912-1990) in the Llobregat Basin.

Llobregat-Martorell								
Discharge Series	Discharge		Quantiles					
	Mean	St Dev	25%	50%	75%	90%	95%	99%
Simulated	5.88	22.17	0.12	1.10	6.04	13.87	19.98	61.06
Observed	7.50	30.70	0.23	1.75	5.2	15.27	27.45	85.76

The simulated discharge series (1651-1800) and the statistics of the simulated discharge compared with the observations are presented next (Figure 6.12 and Table 6.3):

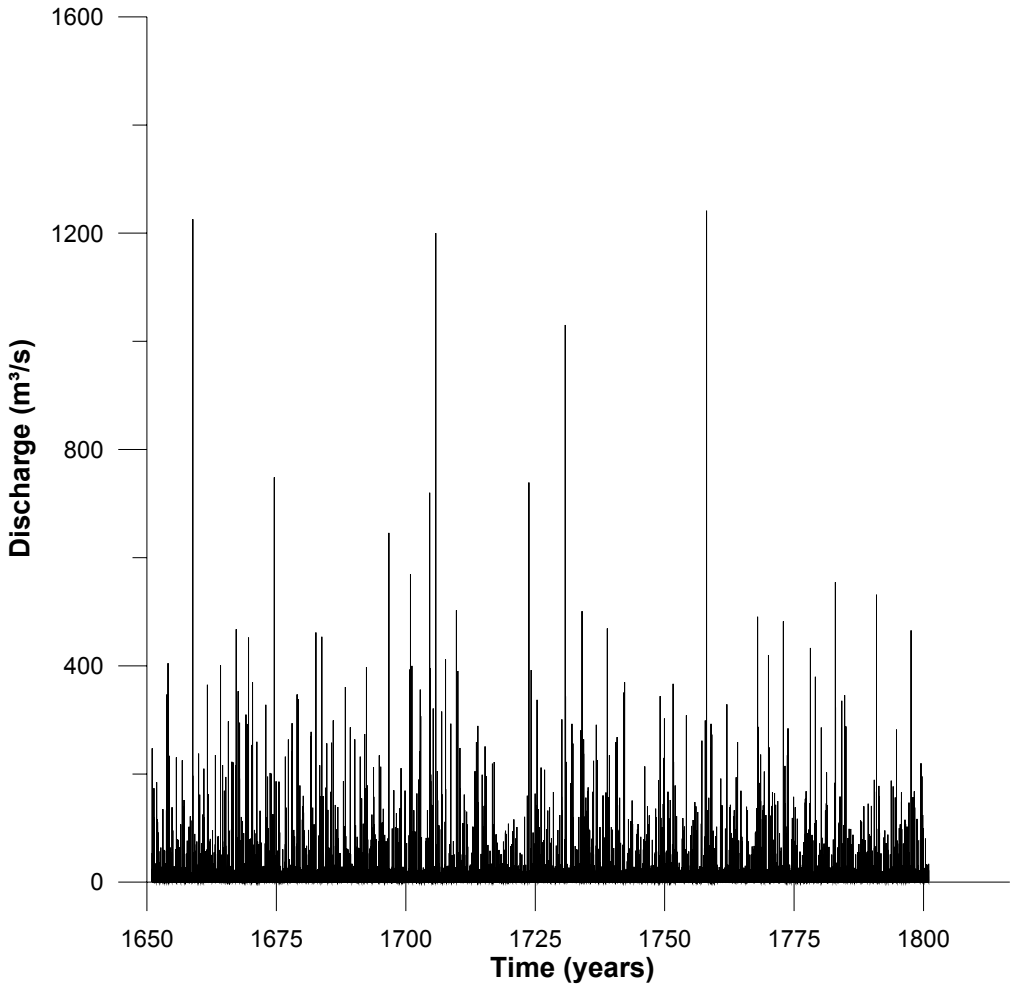

Figure 6.12 Simulated discharge for the Llobregat Basin at Martorell based on the historical GCM data (KIHZ) for the period between 1651-1800.

As seen in Table 6.3, the statistical characteristics of the observed discharge are captured within the simulated discharge.

Table 6.3 Statistics of historical discharge simulations (1651-1800) and discharge observations (1912-1990) in the Llobregat Basin.

Llobregat- Martorell								
Discharge Series	Discharge		Quantiles					
	Mean	St Dev	25%	50%	75%	90%	95%	99%
Simulated	6.41	24.86	0.10	1.08	5.99	13.87	20.22	82.78
Observed	7.50	30.70	0.23	1.75	5.20	15.27	27.45	85.75

The same applies to the simulated discharge for the last period between 1801-1990, as shown in Figure 6.13. It can be concluded that the simulated discharge shows statistical similarity with the observed one in all simulations performed (see also Table 6.4 for the statistical comparison of the simulated and observed discharge series).

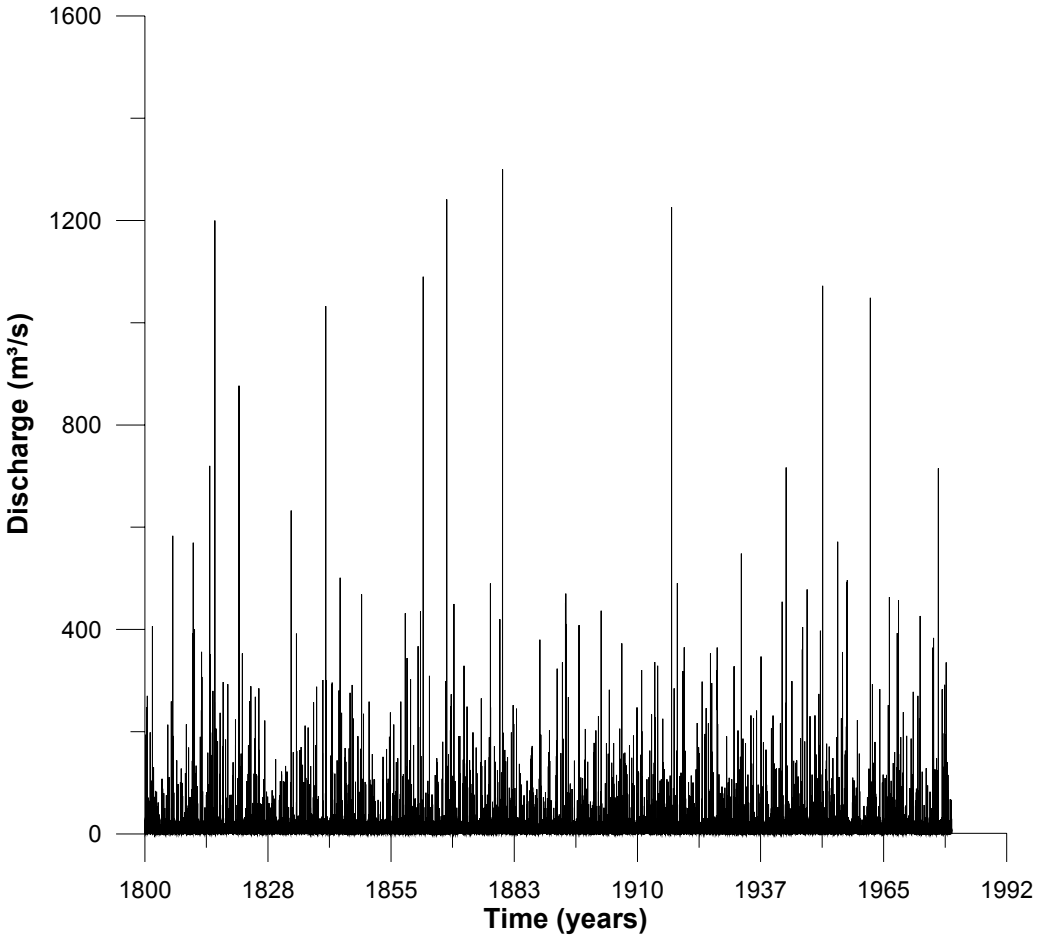

Figure 6.13 Simulated discharge for the Llobregat Basin at Martorell based on the historical GCM data (KIHZ) for the period between 1801-1990.

Table 6.4 Statistics of historical discharge simulations (1801-1990) and the observations (1912-1990) in the Llobregat Basin.

Llobregat-Martorell								
Discharge Series	Discharge		Quantiles					
	Mean	St Dev	25%	50%	75%	90%	95%	99%
Simulated	6.37	24.33	0.13	1.19	6.29	14.25	20.63	76.48
Observed	7.50	30.70	0.23	1.75	5.20	15.27	27.45	85.75

It can be concluded that the simulated discharge and the observations show reasonable agreement in the overall evaluation. A better performance was observed in the simulation of extreme discharge values which was the main objective of the model. The simulation was done using the classification based on corrected KIHZ GCM-fields for the reconstructed climate for Spain and France. In this context, it was of interest mainly to observe the long-term natural variability related to floods and to gain an idea of the dynamics of the statistical features.

The results for the Ardèche Catchment are similar. In Figure 6.14, the simulated discharges between 1500-1650 are shown. One can see that the variability of the frequency and the magnitude of the high discharges in the simulated discharge series are comparable to the ones in the observed discharge series (see Table 6.5). Further simulations of the discharge series and the statistical comparison between the simulated and observed discharge series are presented below for the period between 1651-1800 (in Figure 6.15 and Table 6.6) and 1801-1990 (as shown in Figure 6.16 and Table 6.7) in the Ardéche Basin.

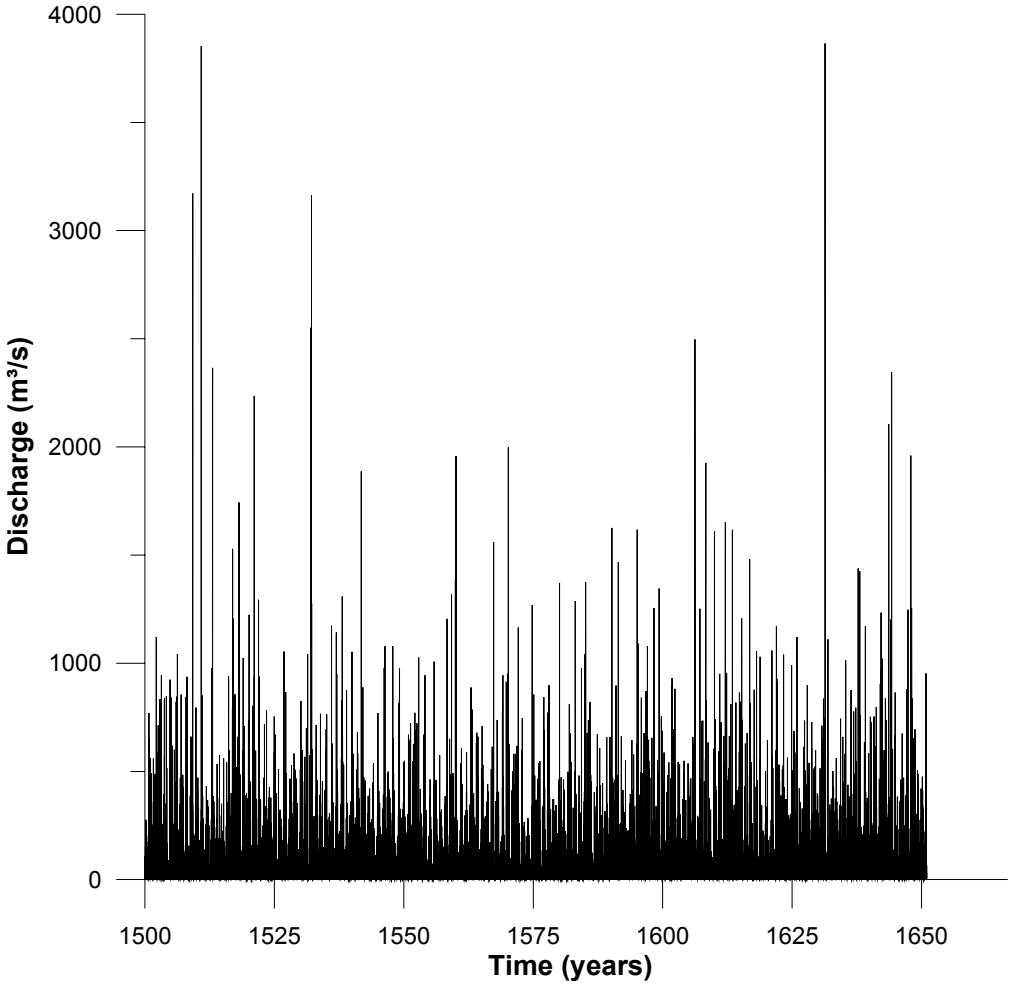

Figure 6.14 Simulated discharge for the Ardèche Basin at Saint Martin based on the historical GCM data (KIHZ) for the period between 1500-1650.

Table 6.5 Statistics of historical discharge simulations (1500-1650) and discharge observations (1955-1997) in the Ardèche Basin.

Ardèche-Saint Martin								
Discharge Series	Discharge		Quantiles					
	Mean	St Dev	25%	50%	75%	90%	95%	99%
Simulated	42.86	86.35	3.77	14.90	46.01	108.54	176.00	389.55
Observed	34.88	105.48	1.06	7.34	25.00	74.00	145.73	511.97

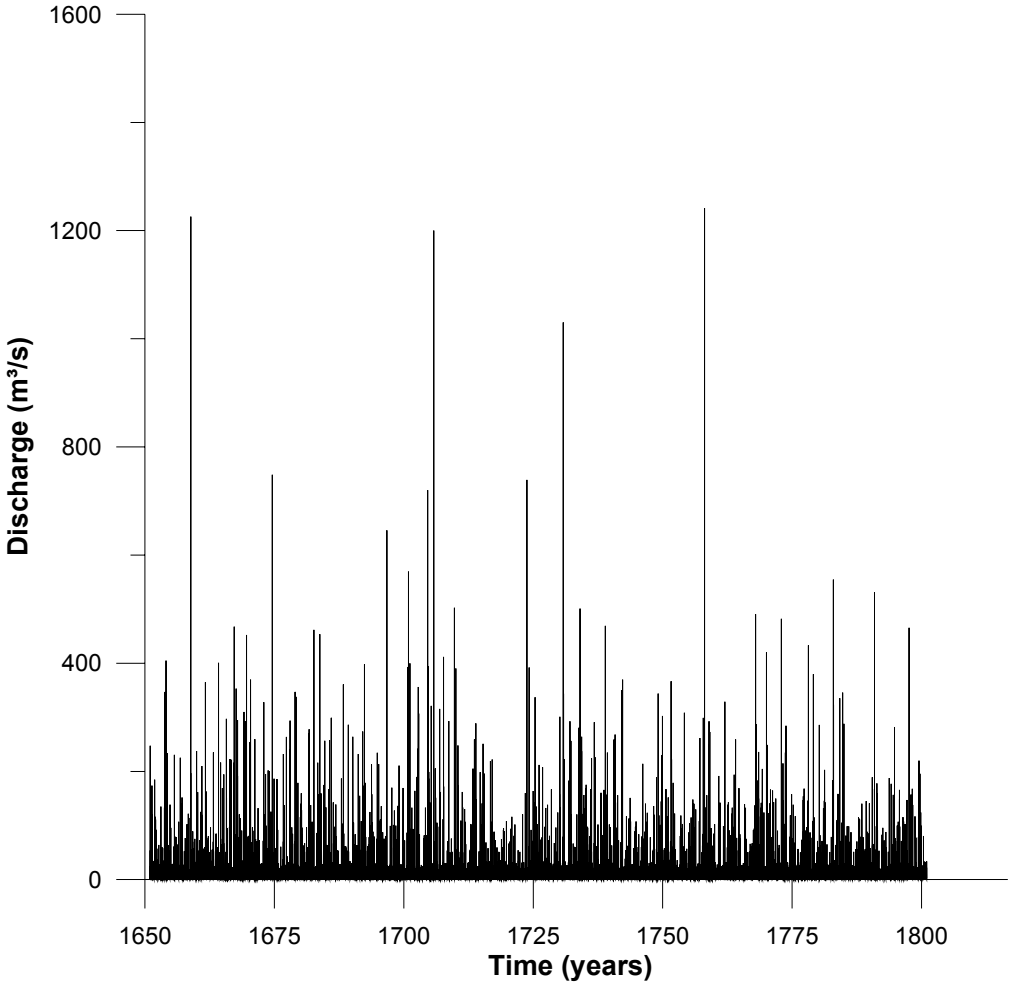

Figure 6.15 Simulated discharge for the Ardèche Basin at Saint Martin based on the historical GCM data (KIHZ) for the period between 1651-1800.

Table 6.6 Statistics of historical discharge simulations (1651-1800) and discharge observations (1955-1997) in the Ardèche Basin.

Ardèche-Saint Martin								
Discharge Series	Discharge		Quantiles					
	Mean	St Dev	25%	50%	75%	90%	95%	99%
Simulated	50.23	97.99	4.83	19.86	55.19	119.27	192.89	451.59
Observed	34.88	105.48	1.06	7.34	25.00	74.00	145.73	511.97

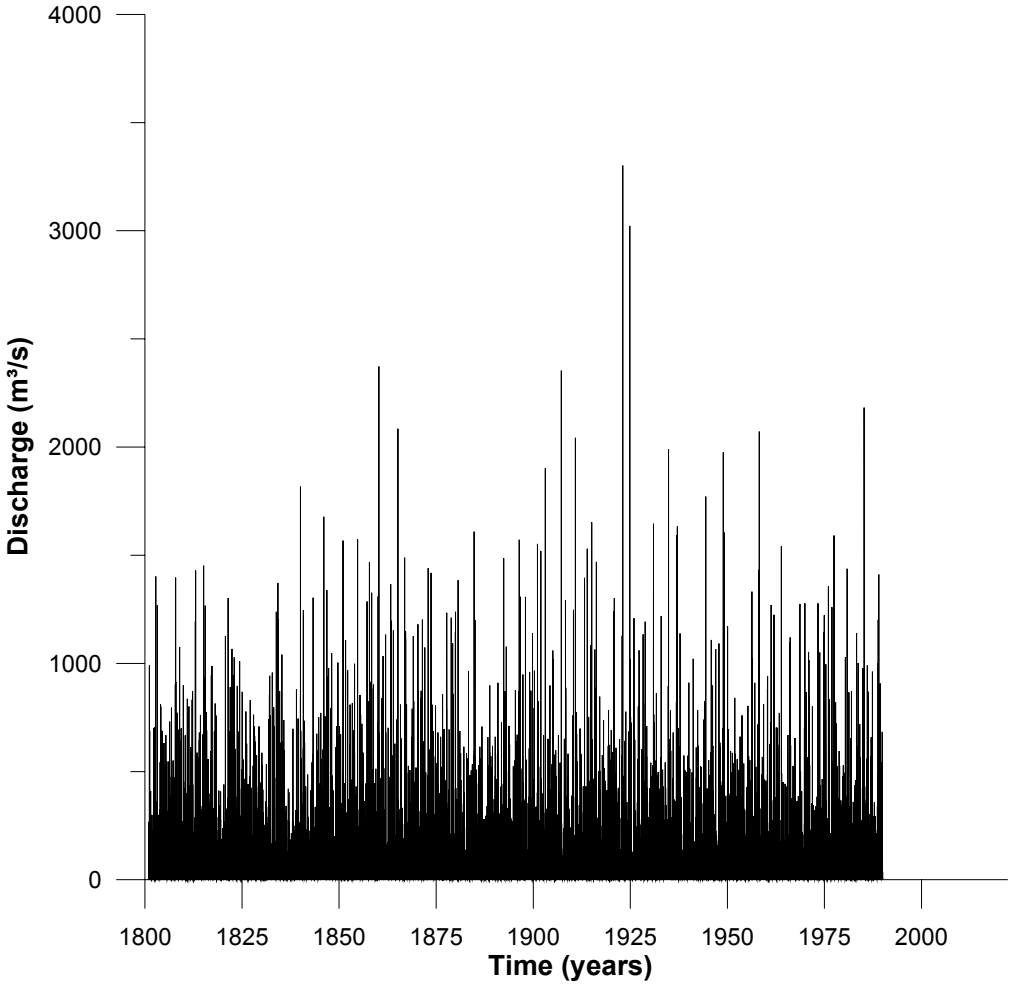

Figure 6.16 Simulated discharge for the Ardèche Basin at Saint Martin based on the historical GCM data (KIHZ) for the period between 1801-1990.

Table 6.7 Statistics of historical discharge simulations (1801-1990) and discharge observations in the Ardèche Basin.

Ardèche-Saint Martin								
Discharge Series	Discharge		Quantiles					
	Mean	St Dev	25%	50%	75%	90%	95%	99%
Simulated	49.80	99.57	4.78	19.56	54.38	118.77	192.09	448.71
Observed	34.88	105.48	1.06	7.34	25.00	74.00	145.73	511.97

The simulations for the period 1500-1990 in the Ardèche-Saint Martin also delivered reasonable results compared to observations. This is evident from the statistical comparison of simulated and observed discharge series as presented above. Statistical parameters such as mean, standard deviation and the discharge values at different quantiles were comparable for simulated and observed values.

In the following, only the simulated annual maximum discharge values which resulted from the GCM data and the 25-year moving average are presented for the same period in the Ardèche (1500-1990). Low frequency-high magnitude floods (flood peaks) can be observed in Figure 6.17. They reach up to 4000 m³/s, which is considerably higher than the discharge maxima observed during the instrumental period. The moving average shown in red deviates between 500-1500 m³/s.

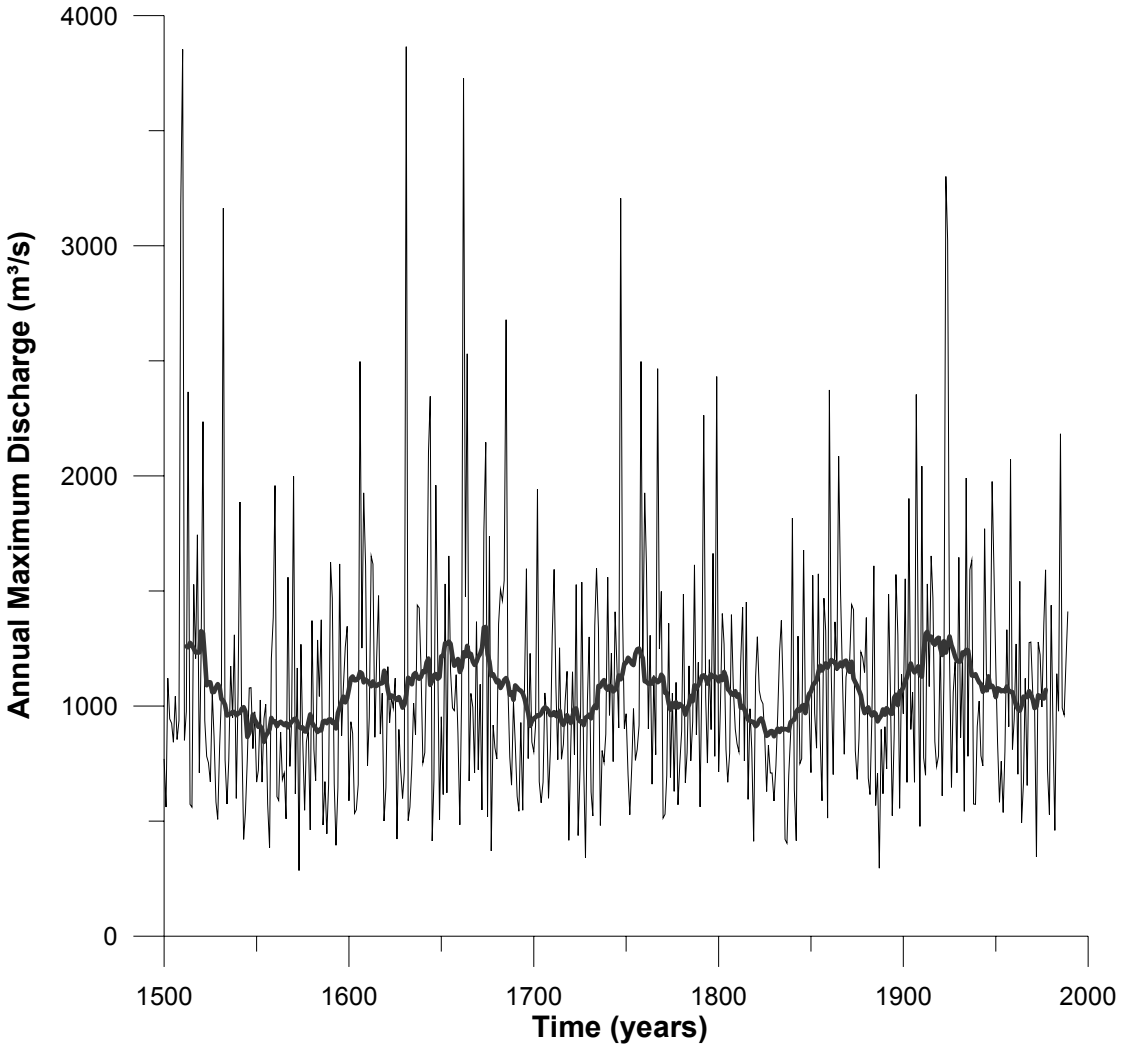

Figure 6.17 Simulated annual maximum discharge based on the historical GCM data (KIHZ) for the period between 1500-1990 with a moving average of 25 years for the Ardèche Basin at Saint Martin.

One can see that there is a high variability in the frequency and the magnitude of the annual peak discharges. The same applies for the Llobregat Basin. Figure 6.18 shows the simulated annual maximum discharge series and the 25-year running average in the Llobregat.

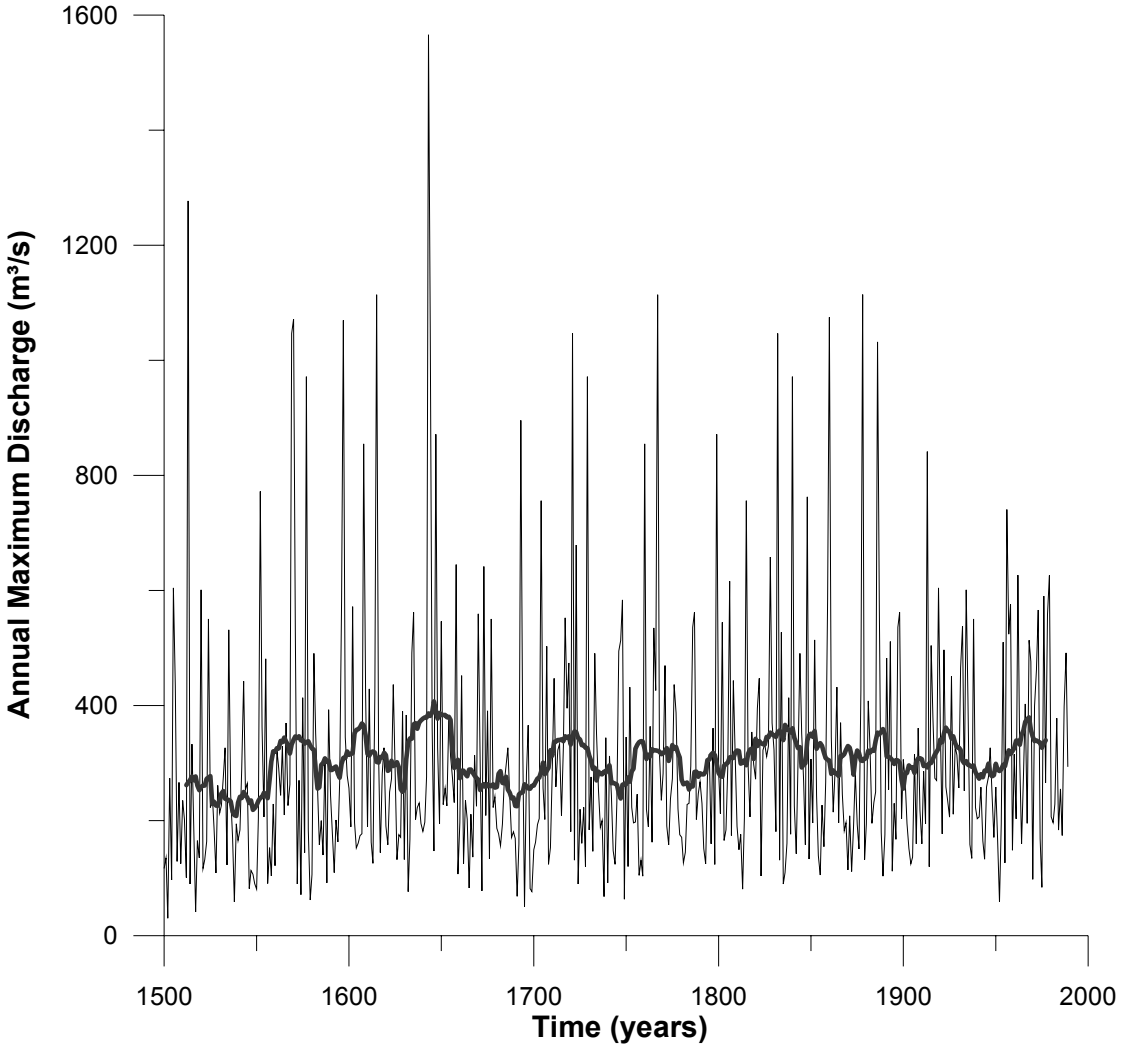

Figure 6.18 Simulated annual maximum discharge based on the historical GCM data (KIHZ) for the period between 1500-1990 with a moving average of 25 years for the Llobregat Basin at Martorell.

As an overall evaluation, the application of historical flood simulation from GCM fields between 1500-1990 shows interesting results. Figure 6.19 shows the annual peak of observed and simulated discharge series in the Ardèche-Saint Martin. The red symbols show the 100-year flood which yield from fitting the 30-year simulated annual maxima (with a moving time window) to the GEV distribution and the black symbols show the median of these 100-year flood values. It can be concluded that the possible extreme floods show considerable fluctuations (with high discharge differences in magnitude) in longer time periods and this could be observed with GCM data for the reconstructed climate. This indicates that there is a significant natural variability in flood frequencies over longer time periods.

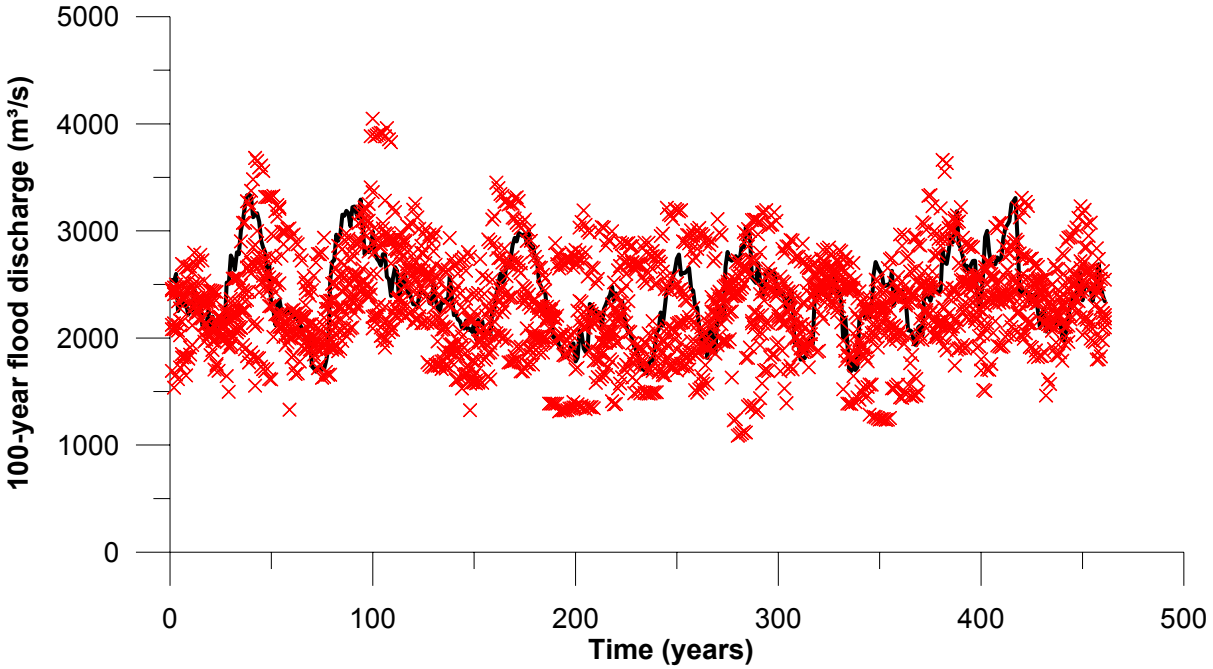

Figure 6.19 100-year flood discharges (red symbols) for Ardèche-St.Martin between 1500-1990 based on the GCM fields and their median (black symbols).

Chapter 7

Discussion and Conclusions

7.1 Discussion

This chapter includes some remarks on the methodology applied and the results obtained and presents the important conclusions of the study.

The main goal of the research was to investigate the links between climate and floods in mesoscale catchments in order to provide insight of the governing meteorological influences on the flood phenomenon.

First of all, the methods introduced within the context of the study can be used in any mesoscale catchment with a size of a few hundred to a few thousand squared kilometers. Within this range, catchments usually show quick response to rainfall and, thus the link between the atmospheric surface variables and discharge can be established on a daily time scale.

For a better linkage of climate and floods, discharge increases were involved in the definition of circulation patterns. This way, positive changes in discharge which are triggered by changing meteorological conditions can be detected more conveniently.

Due to the lower spatial variability of discharge when compared to precipitation, discharge is more appropriate for downscaling purposes from large-scale atmospheric features.

This approach works well in catchments with fast reactions to precipitation depending on the close relationship between precipitation and discharge. For larger catchments with slower reactions, discharge increments have to be related to more than one days' weather in order to consider the delayed hydrological response of the basin. This lag time can be involved in the

classification of CPs within the optimization of the fuzzy rules. The rules are optimized by measuring the performance of the classification regarding the probability of the occurrence of a positive increment within the time lag which is catchment specific. Further, artificial factors which might affect the river flow can be considered in case if their consequences are significant for the investigation of floods.

The automatic derivation of fuzzy rules led to meteorologically reasonable CPs. For the Ardèche catchment, 10 CPs were asssessed. 12 CPs were defined to represent the atmospheric conditions in the Llobregat. The CPs derived from discharge increments can be used to explain the effective precipitation behaviour of the catchments (Zehe and Bárdossy, 2002). A split sampling approach shows that CPs can be derived from using 10 years of observed discharge and SLP anomalies which can reproduce the occurrence variability of the CPs. Most of the annual discharge maxima were preceded by one or two critical CPs.

As quoted in the beginning, many authors have reported that beyond SLP data, the differentiation of significant changes in flow from insignificant ones can be achieved by using geopotential heights, specific humidity and derived indices like vorticity and flow direction. However in this study, the preference was given to SLP data due to its availability from the beginning of 19th century in order to analyze longer time series.

The developed methodology can be used to investigate long series of CP occurrences with respect to flooding in the selected catchments. This way, possible non-stationarities of the series of extremes can be investigated and detected. The understanding of flood-producing circulation might have an influence on extreme value statistics, as different mechanisms might produce different extremes. Further research is needed to investigate this possibility in detail.

The proposed methodology can be used in catchments without an important influence of ice and snow. The reason for that is that catchments where snowmelt contributes significantly to flooding show a different precipitation-discharge characterization. The increases in discharge during snowmelting are not necessarily corresponding to wet CPs, but warming temperatures. Therefore a different approach is needed to link discharge and CP in this case. The approach can also be applied for reconstructing pre-instrumental flood frequencies and to downscale future flood events for different climate scenarios.

In order to analyze the present and the possible past flood events in the Study Areas, a discharge downscaling method was established. The purpose of discharge downscaling is to generate reasonable daily discharge series from CP sequences. For this purpose, a stochastic discharge simulation model was developed which simulates daily discharge changes. It is composed of positive and negative components. Thus, the increases being related to weather and decreases that are dependent on the catchment characteristics can be simulated separately.

The increases in discharge are modeled with two different probability distribution functions with parameters depending on each CP. Particular interest is given to the modeling of high increases since floods are under investigation. Decreases of discharge being a result of the deterministic reaction of the catchment are modeled according to the linear reservoir approach.

The discharge downscaling model delivered reasonable results in the Study Areas. The statistical characteristics of the observed data could be captured within the model so that realistic flood peaks could be produced. The dynamics of the flood occurrences will be reproduced well by the model.

The performance of the model was tested twice, first by a non-parametric KS Test was applied and then by a statistical comparison between the simulation and the observation in terms of statistical parameters such as mean, standard deviation and the values at certain quantiles was made. The results of the simulation were comparable with the observations.

Long discharge series could be generated in the past using historical SLP and temperature observations GCM scenarios were available. For the last 500 years, discharge simulations showed a high variability in the flood frequencies and magnitudes. This could be recognized even using GCM output. The validation of the simulation results for the past period was done by using extreme value statistics.

Reliable estimates of flood peak discharges can be obtained if the recurrence intervals of these discharges do not significantly exceed the lengths of measured peak discharge series. As covered in Chapter 6, the model reproduced the extreme value statistics well for the return periods between 2 and up to 1000 years. However, it should be noted that due to the

uncertainty, the extrapolation period should not be much longer than the observation period since the estimations that are made for such long periods in the future become less reliable. Another remark concerning extreme value statistics is that it requires subjective decisions on the part of the analyst, which could possibly influence the results. Therefore different techniques should be applied and results should be compared.

Due to the fact that climate models still remain to be uncertain, the studies involving climate model output should be interpreted with care. The results presented in this study should be therefore considered as possible flood scenarios. This counts as a limitation of this research study.

The model can also be applied using future climate projections for the prediction of possible future floods i.e including climate impact studies. This aspect is important especially in terms of flood protection measures i.e assessment of design flood discharges, probable maximum flood (PMF) estimation.

It is also worth noting that for solution of many hydrological and environmental problems, it is important to know about not only the probable maximum flood peak discharges, but also the probable maximum flood hydrographs (Kutchment and Gelfan, 2001).

7.2 Conclusions

The main objectives of this study were based on the needs to investigate the meteorological causes of floods in mesoscale catchments. The methodologies and the results achieved and presented in the previous chapters lead to the following conclusions:

- Critical circulation patterns could be defined for the Ardèche and Llobregat Basins which are under different climatic regimes. These wet CPs caused most of the major floods in the Study Areas.

- The link between large-scale surface variables and local parameters can be achieved by using daily sea level pressure observations and daily discharge series in mesoscale

catchments. Since floods are rare events, it is of importance to analyze long time observations. Therefore, SLP series were preferred due to the longer availability of data (1899-2003).

- Discharge observations provided a good indication of flood conditions. The key element of discharge downscaling was linking the CPs to *discharge increases* which is the result of changing atmospheric conditions. In this way, it was possible to establish a direct link between atmospheric conditions and floods in the selected catchments.

- For the application of the model in larger catchments with slower reactions, the lag time window should be expanded up to a few days in order to consider the delayed hydrological response of the catchment to precipitation.

- Long CP time series are obtained by reconstructing historical SLP fields based on point SLP and temperature observations (IMPROVE Project) using NN classification (1774-1990) for Europe. The past GCM scenarios obtained from KIHZ Project were used for the classification of daily atmospheric circulation for the last 500 years (1500-1990). Both classifications showed good performance and could explain flood-prone weather situations in the Study Areas.

- There were no non-stationarities observed in the occurrence of critical CPs during the investigation period throughout the Study Areas. Within the analysis of historical flood peaks, the stochastic links between atmospheric circulation and discharge (predictors and predictands) were assumed to be stationary over the whole time period.

- The downscaling model is based on stochastic methods and is supposed to simulate the occurrence frequency and the magnitude of floods. However, the time when flood occurs will be determined by a random function. Therefore, the model finds application for flood analysis and provides information about the flood generation, but is not appropriate for flood forecasting purposes.

- The performance of the model can be increased by involving pre-event information (i.e. Sea Surface Temperature - SST data) within the downscaling model.

- The classification of circulation patterns can also be done by involving absolute pressure values instead of pressure anomalies.

- Further research is required for catchments in which snowmelting contributes to flooding significantly. In this case, warming temperatures should be considered. This can be achieved by downscaling the temperature additionally.

- The approach can also be applied for reconstructing pre-instrumental flood frequencies and to downscale future flood events for different climate scenarios.

References

Aarts, E., Korst, J. (1989): Simulated Annealing and Boltzmann Machines. John Wiley & Sons.

Anderson, M. G., Bates, P. D. (2001): Model Validation: Perspectives in Hydrological Science / edited by M. G. Anderson and P. D. Bates. John Wiley & Sons, Ltd., Chichester.

Bandemer, H., Gottwald, S. (1993): Einführung in Fuzzy-Methoden: Theorie und Anwendung unscharfer Mengen. Akademie Verlag GmbH, Berlin.

Bardossy, A., Caspary, H.J. (1990): Detection of climate change in Europe by analyzing European atmospheric circulation patterns from 1881 to 1989, Theoretical and Applied Climatology, 42: 155-167.

Bárdossy, A., Plate, E. J. (1992): Space-time model of daily rainfall using atmospherforic circulation patterns. Water Resour. Resources, 28, 1247-1259.

Bárdossy, A. (1993): Stochastische Modelle zur Beschreibung der raum-zeitlichen Variabilität des Niederschlages. Diss. Univ. Karlsruhe, zugleich: Institut für Hydrologie und Wasserwirtschaft, Universität Karlsruhe, H. 44.

Bárdossy, A., Matyasovsky, I., Bogárdi, I. (1994): Knowledge based classification of circulation patterns for stochastic precipitation modelling. In Hipel edited by K. W. McLeod, A. W. Panu, U. S. and Singh, V. P. Stochastic and statistical methods in hydrology and environmental enginering, Vol 3, Kluwer, Dordrecht.

Bárdossy, A. (1995): Anwendung und Anwendbarkeit der Geostatistik im Rahmen der Regionalisierung. In: Methoden der Regionalisierung - Materialien. München edited by H.-B. Kleeberg (unpublished.).

Bárdossy, A., Duckstein, L., Bogardi, I. (1995): Fuzzy Rule-Based Classification of Atmospheric Circulation Patterns. International Journal of Climatology, 15:1087-1097.

Bárdossy, A. (1999): Stochastic downscaling methods to assess the hydrological impacts of climate change on river basin hydrology. Keynote Paper 1, ECLAT-2, KNMI Workshop, Potsdam.

Bárdossy, A., Caspary, H. J. (1999): Detection of climate change in Europe by analyzing European atmospheric circulation patterns from 1881 to 1989. Theoretical and Applied Climatology, 42: 155-167.

Bárdossy, A. (2000): Fuzzy rule-based flood forecasting. Proceedings European Conference on Advances in Flood Research, Potsdam Institute for Climate Impact Research: 494-503.

Bárdossy, A., van Mierlo, J. M. C. (2000): Regional precipitation and temperature scenarios for climate change. Hydrological Sciences-Journal des Sciences Hydrologiques, 45, 4: 559-575.

Bárdossy, A., Stehlik, J., Caspary, H. J. (2002): Automated objective classification of daily circulation patterns for precipitation and temperature downscaling based on optimized fuzzy rules. Climate Research, 23:11-22.

Bárdossy, A., Filiz, F. (submitted): Identification of flood producing atmospheric circulation patterns. Journal of Hydrology, accepted paper.

Barry, R. G., Chorley R. J. (1998): Atmosphere, Weather & Climate. Routledge, London and New York.

Baur, F., Hess, P., Nagel, H. (1944): Kalender der Grosswetterlagen Europas 1881-1939. Bad Homburg: 35 pp.

Benito, G., Sánchez-Moya, Y., Sopeña, A. (2003): Sedimentology of high-stage flood deposits of the Tagus River, Central Spain, Sedimentary Geology, 157: 107-132.

Berger, A. (1981): Climatic Variations and Variability: Facts and Theories / edited by A. Berger. D. Reidel Publishing Company, Dordrecht, Boston, London.

Berger, A., Schneider, S., Duplessy, J. Cl. (1988): Climate and Geosciences: A Challenge for Science and Society in the 21st Century / edited by A. Berger, S. Schneider and J.Cl. Duplessy. Kluwer Academic Publishers, Dordrecht, Boston, London.

Beven, K., Kirkby, M. (1979). A physically based, variable contributing area model of basin hydrology. Bulletin of Hydrolic Sciences, 24:43-69.

Beven, K. J., Lamb, R., Quinn, P., Romanovicz, R., and Freer, J. (1995): TOPMODEL edited by Singh, V. P. Computer Models of Watershed Hydrology. Water Resources Publications: 627-668.

Biewer, B. (1997): Fuzzy-Methoden: Praxisrelevante Rechenmodelle und Fuzzy-Programmiersprachen. Springer-Verlag, Berlin.

Bronstert, A. (1995): River Flooding in Germany: Influenced by Climate Change?. Physics and Chemistry of the Earth, 20, 5-6: 445-450.

Bronstert, A. (2000): Menschenwerk oder Laune der Natur. Antrittsvorlesung an der Universität Potsdam, PUTZ –Potsdamer Universitätszeitung, http://www.uni-potsdam.de/u/putz/jan01/bron.htm.

Bronstert, A., Niehoff, D., Bürger, G. (2002): Effects of climate and land-use change on storm runoff generation: present knowledge and modelling capabilities. Hydrological Processes, 16: 509-529.

Bronstert, A. (2003): Floods and Climate Change: Interactions and Impacts. Risk Analysis, 23: 545-557.

Brown, R. A. (1991): Fluid Mechanics of the Atmosphere. International Geophysics Series, Volume 47, Academic Press, Inc., San Diego.

Budyko, M. I. (1982): The Earth´s Climate: Past and Future. International Geophysics Series, Volume 29, Academic Press, Inc., New York.

Burroughs, W. J. (1991): Watching the World´s Weather. Cambridge University Press, Cambridge.

Bürger, K. (1958): Zur Klimatologie der Großwetterlagen. Berichte des Deutschen Wetterdienstes, 45, 6, Selbstverlag des Deutschen Wetterdienstes, Offenbach am Main.

Bürger, G. (1996): Expanded downscaling for generating local weather scenarios. Climate Research, 7, 2: 111-128.

Bürger, G. (2002): Selected precipitation scenarios across Europe. Journal of Hydrology, 262: 99-110.

Caspary, H. J. (1996): Die Winterhochwasser 1990, 1993 und 1995 in Südwestdeutschland - Signale einer bereits eingetretenen Klimaänderung? In: Klimaänderung und Wasserwirtschaft. Internationales Symposium am 27./28. November 1995 im Europäischen Patentamt in München. Tagungsband. Institut für Wasserwesen, Heft 56:169-183.

Casti, J. (1992): Searching for certainty: what science can know about the future, Scribners.

Cawley, G.C., Dorling, S.R. (1996): Reproducing a Subjective Classification Scheme for Atmospheric Circulation Patterns over the United Kingdom using a Neural Network. Proceedings of the International Conference on Artificial Neural Networks (ICANN '96): 281-286.

Chakravarti, I. M, Laha, R. G., Roy, J. (1967): Handbook of Methods of Applied Statistics. Volume I, John Wiley and Sons, pp. 392-394.

Christensen, J. H., Räisänen, J., Iversen, T., Bjørge, D., Christensen, O. B., Rummukainen, M. (2001): A synthesis of regional climate change simulations –A Scandinavian perspective. Geophysical Research Letters, 28, 1003-1006.

Coles, S. (2001): An Introduction to Statistical Modeling of Extreme Values. Springer-Verlag, London Limited. London, Berlin, Heidelberg.

Davie, T. (2003): Fundamentals of Hydrology. Routledge Fundamentals of Physical Geography, London and New York.

de Villalta, M. F., Benito, G. (2001): Historical flood data analysis using a GIS: the Palaeotagus database, The Use of Historical Data in Natural Hazard Assessment edited by T. Glade, P. Albini, F. Francés: 101-112.

Dzerdzeevskii. B. (1962): Fluctuations of climate and general circulation of the atmosphere in extra-tropical latitudes of the Northern Hemisphere and some problems of dynamic climatology. Tellus, 14: 328-336.

Dobrovolski, S. G. (2000): Stochastic Climate Theory: Models and Applications. Springer, Berlin.

DOE (1996): Department of Environment 1996. Review of the potential effects of climate change in the United Kingdom. HMSO, London.

Dubois, D., Prade, H. (1980): Fuzzy Sets and Systems: Theory and Applications. Academic Press, Inc., New York.

Duckstein, L., Bárdossy, A. Bogardi, I. (1993): Linkage between the occurrence of daily atmospheric circulation patterns and floods: an Arizona case study, Journal of Hydrology, 143: 413-428.

Dyck, S., Peschke, G. (1995): Grundlagen der Hydrologie. Verlag für Bauwesen, Berlin.

Ehret, U. (2003): Rainfall and Radar Nowcasting in Small Catchments using Weather Radar. Dissertation, Mitteilungsheft 121, Institut für Wasserbau, Universität Stuttgart.

Elliott, R. D. (1949): The weather types of North America. Weatherwise 2:15-18, 40-43, 64-67, 86-88, 110-113, 136-138.

Fisher, R.A., Tippett, L. H. C. (1928): Limiting forms of the frequency distribution of the largest or smallest member of a sample. Cambridge Philosophical Society, 24: 180-190.

Frakes, B., Yarnal, B. (1997): A Procedure for Blending Manual and Correlation-Based Synoptic Classifications. International Journal of Climatology, 17: 1381-1396.

Gamble, D. W., Meentemeyer, V. G. (1997): A Synoptic Climatology of Extreme Unseasonable Floods in the Southeastern United States, 1950-1990. Physical Geography, 18, 6: 496-524.

Giorgi, F., Bates, G. T. (1989): On the climatological skill of a regional model over complex terrain. Monthly Weather Review, 117: 2325-2347.

Giorgi, F. (1990): Simulation of regional climate using a limited area model nested in a general circulation model. Journal of Climate, 3,9: 941-963.

Giorgi, F., Marinucci, M. R., Visconti, G. (1990): Use of a limited-area model nested in a general circulation model for regional climate simulation over Europe. Journal of Geophysical Research, 95, 18413-31.

Giorgi, F., Mearns, L. O. (1991): Approaches to the Simulation of Regional Climate Change: A Review. Reviwe of Geophysics, 29, 2: 191-216.

Giorgi, F., Bates, G. T., Hostetler, S.W., Shields Brodeur, C., Marinucci, R., Hirakuchi, H. (1993): Recent nested modeling experiments with the NCAR Regional Climate Model (RegCM). American Geophysical Union Fall Meeting, San Francisco, 6-10 December, 171.

Giorgi, F., Hostetler, S., Shields Brodeur, C. (1994): Analysis of the Surface Hydrology in a Regional Climate Model. Quarterly Journal of the Royal Meteorological Society, 120:161-184.

Gleick, P. H. (1987): Regional hydrologic consequences of increases in atmospheric CO2 and other trace gases. Climate Change, 10: 137-161.

Gonzakes-Rouco, F., Zorita, E., Heyen, H. Valero, F. (1999): Testing the Validity of a Statistical Downscaling Method in Simulations with Global Climate Models. GKSS-Forschungszentrum Geesthacht GmbH, Geesthacht.

Goodess C. M, Palutikof, J. P. (1998): Development of daily rainfall scenarios for southeast Spain using a circulation-type approach to downscaling. International Journal of Climatology, 18:1051-1083.

Gottschalk, L., Olivry, J. C. (1999): Hydrological Extremes: Undertstanding, Predicting, Mitigating /edited by L. Gottschalk and J. C. Olivry, International Association of Hydrological Sciences, IAHS Press, Oxfordshire.

Graedel, T. E., Crutzen, P. J. (1995): Atmosphere, Climate and Change. Scientific American Library, New York.

Gregory J.M., Wigley T.M.L., Jones P.D. (1993): Application of Markov models to area-average daily precipitation series and interannual variability in seasonal totals. Climate dynamics, 8: 299-310.

Grotch, S.L., MacCracken, M. C. (1991): The Use of General Circulation Models to Predict Regional Climatic Change. Journal of Climate, 4: 578-588.

Gumbel, E. J. (1954): Statistical Theory of Extreme Values and Some Practical Applications, National Bureau of Standards Applied Mathematics Series 33, U.S. Government Printing Office, Washington, D.C.

Gumbel, E. J. (1958): Statistics of Extremes, Columbia University Press, New York: 245.
Hartung, J. (1984): Statistik: Lehr- und Handbuch der angewandten Statistik. Oldenburg Verlag, München, Wien.

Hay, L.E., McCabe, G.J., Wolock, D.M., Ayers, M.A. (1991): Simulation of precipitation by weather type analysis, Water Resources Research 27, 493-501.

Hellström, C., Chen, D., Achberger, C., Räisänen, J. (2001): Comparison of climate change scenarios for Sweden based on statistical and dynamical downscaling of monthly precipitation. Climate Research, 19: 45-55.

Hess, P., Brezowsky, H. (1969): Katalog der Großwetterlagen Europas. Berichte des Deutschen Wetterdienst 113, 15, 2 neu bearbeitete und ergänzte Auflage, Selbstverlag des Deutschen Wetterdienst, Offenbach am Main.

Hewitson, B.C. Crane, R.G. (1996): Climate downscaling techniques and applications. Climate Research, 7: 85-95.

Hostetler, S.W. Giorgi, F. (1992): Use of a regional atmospheric model to simulate lake-atmosphere feedbacks associated with pleistocene lakes Lahontan and Bonneville. Climate Dynamics, 7: 39-44.

Hostetler, S.W., Bates, G.T., and F. Giorgi (1993): Interactive nesting of a lake thermal model within a regional climate model for climate change studies. Journal of Geophysical Resources, 98, 5045-5057.

Houze, R. A., Jr. (1993): Cloud Dynamics. International Geophysics Series, Volume 53, Academic Press , Inc., San Diego.

Hulme, M., Barrow, E. (1997): Climate of the British Isles: present, past and future, edited by M. Hulme and E. Barrow, Routledge, London: 454pp.

Hupfer, P., Kuttler, W. (1998): Witterung und Klima herausgegeben von P. Hupfer und W. Kuttler, Teubner, Stuttgart.

IPCC (1996): Climate Change 1995. Impacts, Adaptations and Mitigations of Climate Change: Scientific-Technical Analysis, Cambridge University Press, Cambridge Contribution of Working Group I to the Second Assessment Report of the Intergovernmental Panel on Climate Change.

IPCC (2001): Climate Change 2001. The Scientific Basis - Contribution of Working Group I to the Third Assessment Report of the Intergovernmental Panel on Climate Change.

Jacob, D. Podzun, R. (1997): Sensitivity Studies with the Regional Climate Model REMO. Meteorology and Atmospheric Physics. 63: 119-129.

Jacob, D. (2001): A note to the simulation of the annual and inter-annual variability of the water budget over the Baltic Sea drainage basin. Meteorology and Atmospheric Physics, 77: 61–73.

Jacob, D., Andrae, U., Elgered, G., Fortelius, C., Graham, L. P., Jackson, S. D., Karstens, U., Koepken, Chr., Lindau, R., Podzun, R., Rockel, B., Rubel, F., Sass, H.B., Smith, R.N.D. R.N.D., Van den Hurk, R.N.D., Yang, X. (2001): A Comprehensive Model Intercomparison Study Investigating the Water Budget during the BALTEX-PIDCAP Period. Meteorology and Atmospheric Physics, 77, 1-4: 19-43.

Jenkins G.S., Barron, E. J. (1997): Global climate model and coupled regional climate model simulations over the Eastern United States: GENESIS and RegCM2 simulations. Global and Planetary Change, 15: 3-32.

Jenkinson, A.F., Collison, F.P. (1977): An initial climatology of gales over the North Sea. Synoptic Climatology Branch Memorandum No. 62, Meteorological Office, Bracknell.

Jones P.D., Hulme, M. Briffa, K.R. (1993): A comparison of Lamb Circulation Types with an objective classification derived from grid-point mean-sea-level pressure data.. International Journal of Climatology,13: 665-663.

Jones P.D., Goodess, C. M., Davies, T.D. (2000): ACCORD –Atmospheric Circulation Classification and Regional Downscaling. Final Report to the European Commision (DGXII), Brussels.

Jones, R.G., Murphy, J.M., Noguer, M. (1995): Simulations of climate change over Europe using a nested regional climate model. I: Assessment of control climate, including sensitivity to location of lateral boundaries. Quarterly Journal of the Royal Meteorological Society, 121: 1413–1449.

Kaleris, V., Papanastasopoulos, Lagas, G. (2001): Case study on impact of atmospheric circulation changes on river basin hydrology: uncertainty aspects. Journal of Hydrology, 245: 137-152.

Karl, T.R., Wang, W. C., Schlesinger, M.E., Knight, R. W., Portman, D. (1990): A method of relating general circulation model simulated climate to observed local climate. Part I: Seasonal statistics. Jounal of Climate, 3: 1053-1079.

Katz, R.W. (1996): The use of stochastic models to generate climate change scenarios. Climate Change, 32: 237-255.

Kim, J.-W., Chang, J.-T., Baker, N.L., Wilks, D.S., Gates, W.L.: (1984): The statistical problem of climate inversion: Determination of the relationship between local and large-scale climate, Monthly Weather Review, 112: 2069-2077.

Kirkpatrick, S., Jr., C. G., Vecchi, M. (1983): Optimization by simulated annealing. Science, 220.

Krick I. P. (1943): Synoptic weather types of North America. Californian Institute of Technology, Pasadena, CA.

Kottegoda, N. T, Rosso, R. (1997): Statistics, Probability, and Reliability for Civil and Environmental Engineers. The McGraw-Hill Companies, Inc. New York, London, Sydney, Tokyo.

Koutsoyiannis, D., Onof, C. (2001): Rainfall disaggregation using adjusting procedures on a Poisson cluster model. Journal of Hydrology, 246: 109-122.

Kutchment, L. S., Gelfan, A. N. (2001): Dynamic-Stochastic Model of Snowmelt Runoff Generation and Its Application for Estimating Extreme Floods. 58th Eastern Snow Conference, Ottawa, Ontario, Canada.

Lahiri, S. N. (2002): On the Jackknife-After-Bootstrap Method for Dependent Data and Its Consistency Properties. Economic Theory, 18: 79-96.

Lamb, H. H. (1972): British Isles Weather types and a register of daily sequence of circulation patterns, 1861-1971. Geophysical Memoir 116, HMSO, London: 85pp.

Lamb, H. H. (1977): Climate – Present, Past and Future, Volume 2: Climatic history and the future. Methuen & Co Ltd, London.

Land, C. (1999): The ECHAM4.L39(DLR) Atmosphere GCM: Technical Description and Model Climatology. Deutsches Zentrum für Luft- und Raumfahrt e.V., Köln.

Leiner, B. (1998): Grundlagen de Zeitreihenanalyse. Oldenburg Verlag, München, Wien.

Leavesley, G.H. (1994): Modeling the effects of climate change on water resources - A review, Assessing the Impacts of Climate Change on Natural Resource Systems edited by K.D. Frederick and N. Rosenberg, Kluwer Academic Publishers, Dordrecht: 179-208.

Lepistö A., Kivinen Y. (1997): Effects of climatic change on hydrological patterns of a forested catchment: a physically based modeling approach. Boreal Environment Research 2: 19-31.

Liljequist, G. H., Cehak, K. (1984): Allgemeine Meteorologie. Friedr. Vieweg & Sohn, Braunschweig, Wiesbaden.

Linacre, E. (1992): Climate Data and Resources: A Reference and Guide. Routledge, London and New York.

Llasat, M.C. (1997): Meteorological conditions of heavy rains, FRIEND Projects H-5-5 and 1.1, UNESCO: 269-276.

Lorenz, P.; Richter, K.-G.; Jacob, D.; Ludwig, K.; Gerlinger, K. (2003): Regional climatic modeling with the coupled model system REMO-LARSIM. Oral Presentation, EGS-AGU-EUG Joint Assembly, Nice-France, 6-11 April 2003.

Maak, K., von Storch, H. (1996): Statistical Downscaling of Monthly Mean Air Temperature to the Beginning of the Flowering of Snowdrops in Northern Germany. GKSS-Forschungszentrum Geesthacht GmbH, Geesthacht.

Maheras, P. (1988): The synoptic weather types and objective delimitation of the winter period in Greece, Weather, 43: 40 – 45.

Maheras, P. (1989): Delimitation of the summer dry period in Greece according to the frequency of weather-types. Theoretical & Applied Climatology, 39: 171 – 176.

Mamassis, N., Koutsoyiannis, D. (1996): Influence of atmospheric circulation types on space-time distribution of intense rainfall. Journal of Geophysical Research, 101, D21, 26267-76.

Maniak, U. (1997): Hydrologie und Wasserwirtschaft: Eine Einführung für Ingenieure, Springer-Verlag, Berlin, Heidelberg.

Martins, E. S., Stedinger, J. R. (2000): Generalized Maximum Likelihood GEV Quantile Estimators for Hydrologic Data. Water Resources Research, 36, 3: 737-744.

McCuen, R. H. (1989): Hydrologic Analysis and Design. Prentice Hall, New Jersey, 867 pp.

McElroy, M. B. (2002): The Atmospheric Environment: Effects of Human Activity. Princeton University Press, Princeton, New Jersey.

Menzel, L., Niehoff, D., Bürger, G., Bronstert, A. (2002): Climate change impacts on river flooding: A modelling study of three meso-scale catchments. Climatic Change: Implications for the Hydrological Cycle and for Water Management edited by M. Beniston, Kluwer Academic Publishers, Netherlands: 249-269.

Metropolis, N., Rosenbluth, A.W., Rosenbluth, M. N., Teller, A.H. and Teller, E. (1958): Equations of State Calculations by Fast Computing Machines, Journal of Chemical Physics, 21: 1087- 1092.

Mielke, P.W., Johnson, E. S. (1974): Some Generalized Beta Distributions of the Second Kind Having Desirable Application Features in Hydrology and Meteorology. Water Resources Research, 10, 2:223-226.

Miller, R.G. (1974): The Jackknife a review, Biometrika, 61, 1 15.

Palmen, E., Newton, C. W. (1969): Atmospheric Circulation Systems: Their Structure and Physical Interpretation. International Geophysics Series, Volume 13, academic Press, Inc., New York and London.

Panofsky, H. A., Dutton, J. A.(1984): Atmospheric Turbulence: Models and Methods for Engineering Applications. John Wiley & Sons, Inc, New York.

Pearce, R. P. (2002): Meteorology at the Millennium, International Geophysics Series, Volume 83, Academic Press, Inc., San Diego, San Francisco, New York, Boston, London.

Pfeifer, D. (1989): Einführung in die Extremwertstatistik, Teubner, Stuttgart.

Pincus, M. (1970): A Monte Carlo method for the approximate solution of certain types of constrained optimization problems, Oper. Res., 18: 1225-1228.

Plate, E. (1982): Engineering Meteorology: Fundamentals of Meteorology and Their Applicationto Problems in Environmental and Civil Engineering / edited by E.Plate. Elsevier Scientific Publishing Company, Amsterdam, Oxford, New York.

Plate, E. J. (1993): Statistik und angewandte Wahrscheinlichkeitslehre für Bauingenieure, Ernst Verlag für Architektur und technische Wissenschaften, Berlin.
Pollock, D.S.G. (1999): A Handbook of Time-Series Analysis, Signal Processing and Dynamics, Academic Press, Inc. Cambridge.

Pongrácz R., Bogardi I., Duckstein L. (1999): Drought Forecasting Using Atmospheric Circulation and ENSO Information. In: Hydraulic Engineering for Sustainable Water Resources Management at the Turn of the Millennium: Proceedings (szerk: M.N. Abbott et al.), CD-ROM, 8p. Graz, Austria.

Quenouille, M.H. (1956): Notes on bias in estimation. Biometrika 43: 353-360.

Rao, T. S., Priestley, M. B., Lessi, O. (1997): Applications of Time-Series Analysis in Astronomy and Meteorology, Chapman & Hall, London.

Richardson, C. W. (1981): Stochastic simulation of daily precipitation, temperature and solar radiation. Water Resources Research, 17: 182-190.

Robinson, P.J., P.L. Finkelstein (1991): The development of impact-oriented scenarios. Bulletin of American Meteorological Society, 4: 481-490.

Roth, G. D. (1995): Wetterkunde für Alle: Wolkenbilder und andere Wetterphänomene, Großwetterlagen, Wettervorhersage, BLV Verlagsgesellschaft mbH, München.

Ruddiman, W. F. (2001): Earth´s Climate: Past and Future, W. H. Freeman and Company, New York.

Rummukainen, M. (1997): Methods for statistical downscaling of GCM simulations. SMHI – Swedisch Meteorological and Hydrological Institute, Reports Meteorology and Climatology, SWECLIM –Swedish Regional Climate Modelling Programme, Norrköping.

Samaniego, L. (2003): Hydrological Consequences of Land Use/Land Cover and Climatic Changes in Mesoscale Catchments. Instituts für Wasserbau, Universität Stuttgart, Mitteilungsheft 118.

Shaw, E. M. (1994): Hydrology in Practice, Chapman & Hall, London.

Singh, V. P. (1987): Flood Hydrology: Proceedings of the International Symposium on Flood Frequency and Risk Analyses / edited by V. P. Singh. D. Reidel Publishing Company, Dordrecht.

Stahl, K., Demuth, S. (1999): Linking streamflow drought to the occurrence of atmospheric circulation patterns. Hydrological Sciences –Journal-des Sciences Hydrologiques, 44, 3: 467-482.

Stedinger, J. R., Martins, E. S. (2000): Generalized Maximum Likelihood GEV Quantile Estimators for Hydrologic Date. Water Resources Research, 36, 737-744.

Stehlík, J., Bárdossy, A. (2002): Multivariate stochastic downscaling model for generating daily precipitation series based on atmospheric circulation. Journal of Hydrology, 256:120-141.

Stehlík, J., Bárdossy, A. (2003): Circulation pattern classification for climate change studies. Poster Presentation, EGS-AGU-EUG Joint Assembly, Nice-France, 6-11 April 2003.

Stoyan, D., Stoyan, H., Jansen, U. (1997): Umweltstatistik: Statistische Verarbeitung und Analyse von Umweltdaten, B. G. Teubner Verlagsgesellschaft, Stuttgart, Leipzig.

Tanaka, K. (1997): An Introduction to Fuzzy Logic for Practical Applications, Springer, New York, Berlin, Tokyo.

Thorndycraft, V. R., Benito, G., Barriendos, M., Llasat, M. C. (2003): Palaefloods, Histrical Data and Climatic Variability: Applications in Flood Risk Assessment edited by V. R. Thorndycraft, G. Benito, M. Barriendos, M. C. Llasat. Centro de Ciencias Medioambientales (CSIC), Madrid.

USCE (1996): U.S. Army Corps of Engineers. 1996. Annual Flood Damage Report to Congress for Fiscal Year 1995. Washington, DC,U.S. Army Corps of Engineers: 17.

von Storch, H., Zorita, E., Cubasch, U. (1993): Downscaling of global climate change estimates to regional scales: an application to Iberian rainfall in wintertime. Journal of Climate, 6: 1161-71.

von Storch, H., Bruce, H., Mearns, L. (1999): Review of Empirical Downscaling Techniques. GKSS Research Center, Institute of Hydrophysics, Germany. Online: http//www.nilu.no/regclim/rapport_4/presentation02/presentation02.htm

Velleman, P. F., Hoaglin, D. C. (1981): Applications, Basics, and Computing of Exploratory Data Analysis. Duxbury Press, Boston, MA.

Westervelt, J. (2001): Simulation Modeling for Watershed Management. Springer-Verlag New York, Inc., New York.

Ward, R.C., Robinson, M. (2000): Principles of Hydrology. McGraw-Hill Publishing Company, London.

Wigley, T. M. L., Jones, P. D., Briffa, K. R., Smith, K. R. (1990): Ontaining sub-grid scale information from coarse resolution general circulation model output. Journal of Geophysical Research, 95,: 1443-53.

Wilby, R. L. (1992): The use of atmospheric circulation patterns as drought indicators. British Hydrological Society Drought Workshop, Loughborough University of Technology, UK.

Wilby, R. L., Greenfield, B., Glenny, C. (1994): A coupled synoptic-hydrological model for climate change impact assessment. Journal of Hydrology, 153: 265-290.

Wilby, R. L. (1995): Greenhouse hydrology. Progress in Physical Hydrology 19, 3: 351-369.

Wilby, R. L. (1997): Contemporary Hydrology edited by R. L. Wilby. John Wiley & Sons, New York.

Wilby, R.L. (1997): Statistical downscaling using atmospheric circulation indices. Workshop on Statistical Downscaling, National Center for Atmospheric Research, Boulder, Colorado, USA.

Wilby, R. L., Wigley (1997): Downscaling general circulation model output: a review of methods and limitations. Progress in Physical Geography, 21, 4: 530-548.

Wilby, R. L., Hassan, H., Hanaki, K. (1998): Statistical downscaling of hydrometeorological variables using general circulation model output. Journal of Hydrology, 205, 1-19.

Wilby, R. L., Wigley, M. L., Conway, D., Jones, P. D., Hewitson, B. C., Main, J., Wilks, D. S. (1998): Statistical downscaling of general circulation model output: A comparison of methods. Water Resources Research, 34, 11: 2995-3008.

Wilby, R. L., Hay, L. E., Leavesley, G. H. (1999): A comparison of downscaled and raw GCM output: implications for climate change scenarios in the San Juan River basin, Colorado. Journal of Hydrology, 225: 67-91.

Wilks, D. S. (1989): Conditioning stochastic daily precipitation models on total monthly precipitation. Water Resources Research, 25: 1429-1439.

Wilks, D.S. (1992): Adapting stochastic weather generation algorithms for climate change studies. Climatic Change 22: 67-84.

Wilks, D. S. (1995): Statistical Methods in the Atmospheric Sciences: *An Introduction*. Academic Press, New York.

Wilson, L., Lettenmaier, D.-P., Skyllingstad E. (1992): A hierarchical stochastic model of large-scale atmospheric circulation patterns and multiple station daily rainfall. Journal of Geophysical Research, 97, ND3, 2791-2809.

Woth, K. (2001): A Methodology for Spatial Data Selection for Statistical Downscaling Purposes: A case study of Precipitation in Southwestern Europe, GKSS-Forschungszentrum Geesthacht GmbH, Geesthacht.

Xu, C.-Y. (1999): From GCMs to river flow : a review of downscaling methods and hydrologic modelling approaches. Progress in Physical Geography, 23, 2: 229-249.

Yakowitz, S. (1987): Nearest-neighbour methods for time series analysis. Journal of Time Series Analysis, 8:235-247.

Yarnal, B. (1984): A Procedure for the Classification of Synoptic Weather Maps from Gridded Atmospheric Pressure Surface Data. Computers & Geosciences, 10, 4: 397-410.

Yarnal, B. (1993): Synoptic climatology in environmental analysis: a primer. Belhaven Press, London. 10, 4: 397-410.

Yarnal, B., Frakes, B. (1997): Using Synoptic Climatology to Define Representative Discharge Events. International Journal of Climatology, 17: 323-341.

Zadeh, L. A. (1965): Fuzzy Sets. Information and Control, 8: 338-353.

Zadeh, L. A. (1973): Outline of a new approach to the analysis of complex systems and decision process. IEEE Transactions SMC-3, 1: 1585-1588.

Zadeh, L. A. (1987): A Fuzzy-Algorithmic Approach to the Definition of Complex or Imprecise Concepts. Fuzzy sets and applications: selected papers by L. A. Zadeh edited by R.R. Yager, A Wiley-Interscience publication, John Wiley & Sons, New York.

Zehe, E., Bárdossy, A (2002): Hydrological Impact of Climate Change on The River Rhine. Towards Sustainable Flood Risk Management in the Rhine and Meuse River basins, Final Report of the IRMA-SPONGE Umbrella Program, NCR publication No 18.

Zimmermann, H. J. (1996): Fuzzy Set Theory and its Application. 3rd rev.edition, Kluwer Academic Publishers, Bonston, Dodrecht, London.

Zimmermann, H. J. (1996): Fuzzy Logic. Anwendungen. Band 2, (with C. v. Altrock), Oldenbourg Verlag München Wien.

Zorita, E., Kharin, V., von Storch, H (1992): The atmospheric circulation and sea surface temperature in the North Atlantic area winter: their interaction and relevance for Iberian precipitation. Journal of Climate, 5: 1097-1108.

Zorita, E., von Storch, H. (1997): A Survey of Statistical Downscaling Techniques. GKSS-Forschungszentrum Geesthacht GmbH, Geesthacht.

Zorita, E., von Storch, H., Gonzales-Rouco, F. J., Cubasch, U., Luterbacher, J., Legutke, S., Fischer-Bruns, I., Schlese, U. (2003): Simulation of the Climate of the Last Five Centuries. GKSS-Forschungszentrum Geesthacht GmbH, Geesthacht.

Appendix 1

European Circulation Patterns according to Hess and Brezowsky (1969).

Major Type	Sub-type	No.	Description	Abbreviation
Zonal circulation	W	1	West, anticyclonic	Wa
		2	West, cyclonic	Wz
		3	Southern, West	WS
		4	Angleformed West	WW
Mixed circulation	SW	5	Southwest, anticyclonic	SWa
		6	Southwest, cyclonic	SWz
	NW	7	Northwest, anticyclonic	NWa
		8	Nortwest, cyclonic	NWz
	HM	9	Central European high	HM
		10	Central European ridge	BM
	TM	11	Central European low	TM
Meridional circulation	N	12	North, anticyclonic	Na
		13	North, cyclonic	Nz
		14	North, Iceland high, anticyclonic	HNa
		15	North, Iceland high, cyclonic	HNz
		16	British Isles high	HB
		17	Central European trough	TRM
	NE	18	Northeast, anticyclonic	NEa
		19	Northeast, cyclonic	Nez
	E	20	Fennoscandian high, anticyclonic	HFa
		21	Fennoscandian high, cyclonic	HFz
		22	Norwegian Sea-Fennoscandian high, anticyclonic	HNFa
		23	Norwegian Sea-Fennoscandian high, cyclonic	HNFz
		24	Southeast, anticyclonic	SEa
		25	Southeast, cyclonic	SEz
	S	26	South, anticyclonic	Sa
		27	South, cyclonic	Sz
		28	British Isles low	TB
		29	Western Europe trough	TRW
Unclassified	U	30	Classification not possible	U

Appendix 2

Comparison of statistical downscaling approaches *(modified and adapted from Xu, 1999)*

Common assumptions

1) Local scale parameters are a function of synoptic forcing
2) The GCM used to derive downscaled relationships is valid at the scale used
3) The relationship derived remains valid under greenhouse forcing

Regression method

Procedures

1) Identify a large scale predictor G, which controls the local parameter L
2) Find a statistical relationship between L and G
3) Validate the relationship with independent data
4) If the relationship is confirmed, G can be derived from GCM experiments to estimate L

Advantages and shortcomings

1) Simple, less computationally demanding
2) Application is limited to the sites, variables and seasons when the local climate is related well to the conditions in the free troposphere
3) Very long observation series needed

Examples of applications

1) Large scale predictors and local scale predictands are the same variables
2) Large scale predictors and local scale predictands are different variables
3) Use of artificial neural network (ANN) approaches

Circulation-based method

Procedures

2) Classify atmospheric circulation pattern into limited number of classes
2) Simulate weather types through the use of stochastic models
3) Link the likelihood of rainfall occurring to weather type using conditional probabilities
4) Simulate rainfall and/or other hydrometeorological processes using weather types

Advantages and shortcomings

1) Possible to generate daily sequences of precipitation at a point for any number of days based on limited historic data sets
2) Weather classification schemes are somehow parochial and/or subjective. There is a need for more general classification systems

Examples of applications

1) Relating regional rainfall to synoptic weather patterns
2) Relating long term temperature fluctuations to synoptic weather patterns
3) Relating precipitation chemistry to synoptic weather patterns
4) Relating river flow to synoptic weather

Weather generator method

Procedures

1) Use observed daily rainfall data to determine the probability of the state of a day
2) Use exponential (or other) distribution to fit and estimate the amount of rainfall on a wet day
3) Condition other weather variables (temperature, radiation, etc.) on the wet/dry status of the day

Advantages and shortcomings

1) Able to generate realistic, statistical characteristics of daily rainfall series
2) Relies on GCM predicted changes in mean precipitation, which are known to be unreliable – a problem that is of primary importance to hydrology and that is yet to be resolved

Examples of applications

1) Use of stochastic weather generators for the present climate
2) Use of stochastic weather generators for climate change and impacts studies

Appendix 3

Simulated Annealing Algorithm

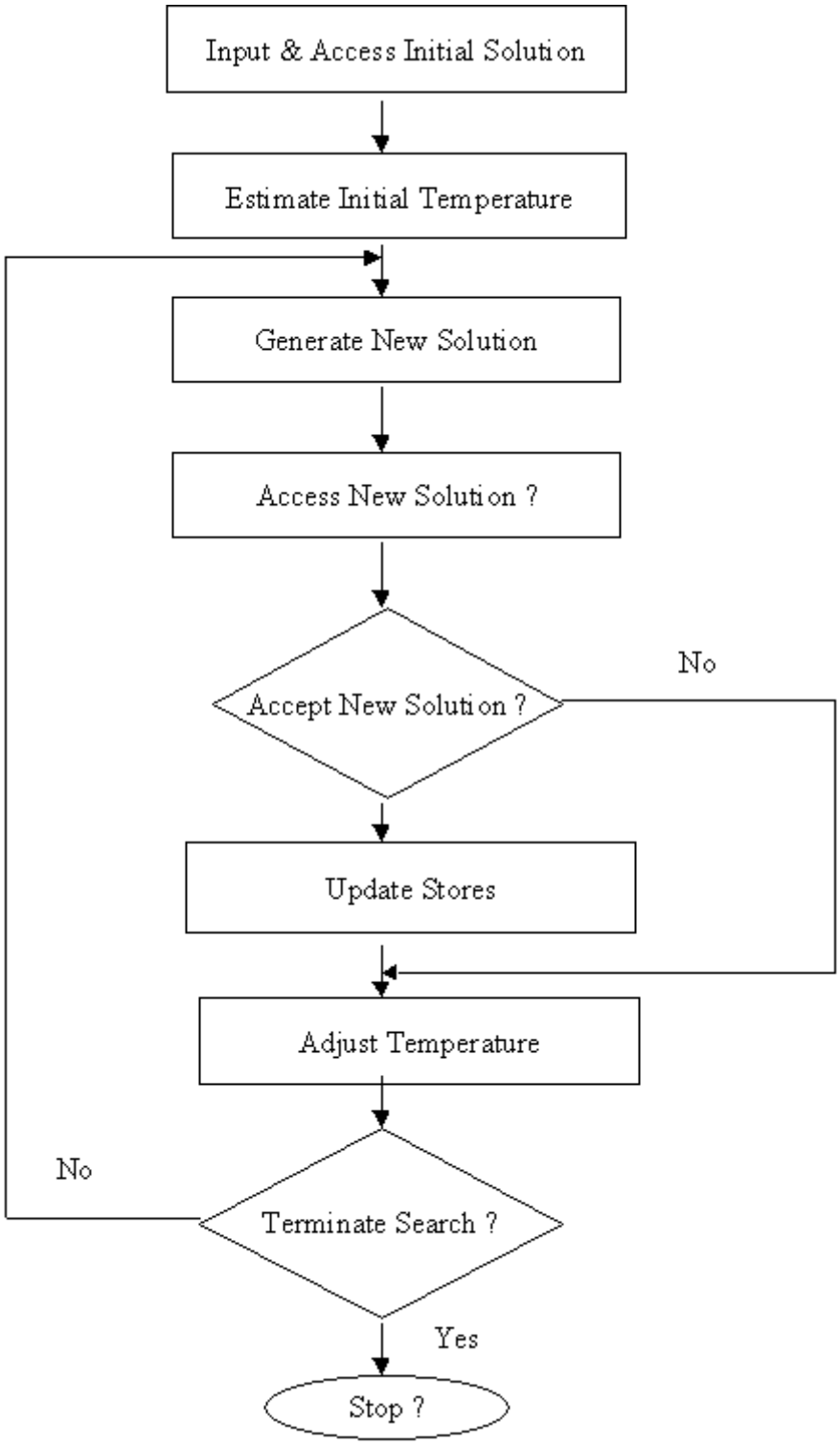

Appendix 4

The Nearest Neighbor Method

The Nearest Method also called Single Linkage Clustering is a Cluster Analysis (CA) which suggests how to *organize* observed data into meaningful structures. The Nearest Neighbor is a useful classification method which uses the dissimilarities or distances between objects when forming the clusters.

Definition.

A dataset D of P training points is given by

$D = \{\mathbf{x}^{\mu}, c^{\mu}\}, \quad \mu = 1,..., P.$

The aim is for a given $\mathbf{x}$, to return the "correct" class of $c(\mathbf{x})$ using the Nearest Neighbor method. The following steps should be taken:

- The dissimilarity of the test point $\mathbf{x}$ to each of the stored points, $d^{\mu} = d(\mathbf{x}, \mathbf{x}^{\mu})$ should be calculated (depending on the problem i.e. Euclidean or Mahalanobis distances).
- The training point $\mathbf{x}^{\mu^*}$ should be found such that $d^{\mu^*} < d^{\mu}$ for all $\mu = 1,..., P$.
- Class label $c(\mathbf{x}) = c^{\mu^*}$ is assigned.

In the case that there are two or more "equidistant" (or equi-dissimilar) points with different class labels, the most numerous class is chosen. If there is no one single most numerous class, the *k*-nearest neighbors method can be applied. The reader is referred to the related literature for further details (Yakowitz, 1987).

Appendix 5

The Jackknife Method

Quenouille (1956) suggested an original method of adjusting for bias that John W. Tukey termed as *jackknife*, which means a "useful tool" by implication. Miller (1974) provides a mathematical review.

Definition.

If $t_{n-1}^{(i)}$ is the estimator of a parameter based on a sample of size (n-1) obtained by omitting the i^{th} observation, the **jackknife estimator** is given by

$$J = nt_n - \frac{(n-1)}{n}\sum_{i=1}^{n} t_{n-1}^{(i)}$$

The bias in the jackknife estimator is not more than $1/n^2$ if an estimator of the same parameter based on the complete sample of size n has a bias of the order of 1/n (Kottegoda and Rosso 1997).

Appendix 6

Fulya Filiz

Curriculum Vitae

Personal Details	Date of birth	22. Juli 1975	
	Place of birth	Adana-Turkey	
Education	High School	ISTEK Experimental High School, Istanbul	09/1987 – 06/1993
	University	Technical University Yildiz, Istanbul Environmental Engineering Bachelor Degree	09/1993 – 06/1997 06/1997
	Master´s	Universität Stuttgart Master of Science Program in Water Resources Engineering and Management (WAREM)	09/1997 – 10/1999
	PhD	Universität Stuttgart Linking Large Scale Meteorological Conditions to Floods in Mesoscale Catchments	since 03/2000
Work Experience	Research Assistant	100-online Project Geostatistics and Stochastic Modeling EU Research Projectt SPHERE – Systematic, Palaeflood and Historical Data for the Improvement of Flood Risk Estimation	03/2000 – 12/2003

Institut für Wasserbau
Universität Stuttgart

Pfaffenwaldring 61
70569 Stuttgart (Vaihingen)
Telefon (0711) 685 - 4717/41/52 o. - 4679
Telefax (0711) 685 - 7020 o. 4746 o. 4681
email: iws@iws.uni-stuttgart.de
http://www.iws.uni-stuttgart.de

Verzeichnis der Mitteilungshefte

1 Röhnisch, Arthur: *Die Bemühungen um eine Wasserbauliche Versuchsanstalt an der Technischen Hochschule Stuttgart*, und
Fattah Abouleid, Abdel: *Beitrag zur Berechnung einer in lockeren Sand gerammten, zweifach verankerten Spundwand*, 1963

2 Marotz, Günter: *Beitrag zur Frage der Standfestigkeit von dichten Asphaltbelägen im Großwasserbau*, 1964

3 Gurr, Siegfried: *Beitrag zur Berechnung zusammengesetzter ebener Flächentragwerke unter besonderer Berücksichtigung ebener Stauwände, mit Hilfe von Randwert- und Lastwertmatrizen*, 1965

4 Plica, Peter: *Ein Beitrag zur Anwendung von Schalenkonstruktionen im Stahlwasserbau*, und Petrikat, Kurt: *Möglichkeiten und Grenzen des wasserbaulichen Versuchswesens*, 1966

5 Plate, Erich: *Beitrag zur Bestimmung der Windgeschwindigkeitsverteilung in der durch eine Wand gestörten bodennahen Luftschicht*, und
Röhnisch, Arthur; Marotz, Günter: *Neue Baustoffe und Bauausführungen für den Schutz der Böschungen und der Sohle von Kanälen, Flüssen und Häfen; Gestehungskosten und jeweilige Vorteile*, sowie Unny, T.E.: *Schwingungsuntersuchungen am Kegelstrahlschieber*, 1967

6 Seiler, Erich: *Die Ermittlung des Anlagenwertes der bundeseigenen Binnenschiffahrtsstraßen und Talsperren und des Anteils der Binnenschiffahrt an diesem Wert*, 1967

7 *Sonderheft anläßlich des 65. Geburtstages von Prof. Arthur Röhnisch mit Beiträgen von* Benk, Dieter; Breitling, J.; Gurr, Siegfried; Haberhauer, Robert; Honekamp, Hermann; Kuz, Klaus Dieter; Marotz, Günter; Mayer-Vorfelder, Hans-Jörg; Miller, Rudolf; Plate, Erich J.; Radomski, Helge; Schwarz, Helmut; Vollmer, Ernst; Wildenhahn, Eberhard; 1967

8 Jumikis, Alfred: *Beitrag zur experimentellen Untersuchung des Wassernachschubs in einem gefrierenden Boden und die Beurteilung der Ergebnisse*, 1968

9 Marotz, Günter: *Technische Grundlagen einer Wasserspeicherung im natürlichen Untergrund*, 1968

10 Radomski, Helge: *Untersuchungen über den Einfluß der Querschnittsform wellenförmiger Spundwände auf die statischen und rammtechnischen Eigenschaften*, 1968

11 Schwarz, Helmut: *Die Grenztragfähigkeit des Baugrundes bei Einwirkung vertikal gezogener Ankerplatten als zweidimensionales Bruchproblem*, 1969

12 Erbel, Klaus: *Ein Beitrag zur Untersuchung der Metamorphose von Mittelgebirgsschneedecken unter besonderer Berücksichtigung eines Verfahrens zur Bestimmung der thermischen Schneequalität*, 1969

13 Westhaus, Karl-Heinz: *Der Strukturwandel in der Binnenschiffahrt und sein Einfluß auf den Ausbau der Binnenschiffskanäle*, 1969

14 Mayer-Vorfelder, Hans-Jörg: *Ein Beitrag zur Berechnung des Erdwiderstandes unter Ansatz der logarithmischen Spirale als Gleitflächenfunktion*, 1970

15 Schulz, Manfred: *Berechnung des räumlichen Erddruckes auf die Wandung kreiszylindrischer Körper*, 1970

16 Mobasseri, Manoutschehr: *Die Rippenstützmauer. Konstruktion und Grenzen ihrer Standsicherheit*, 1970

17 Benk, Dieter: *Ein Beitrag zum Betrieb und zur Bemessung von Hochwasserrückhaltebecken*, 1970

18 Gàl, Attila: *Bestimmung der mitschwingenden Wassermasse bei überströmten Fischbauchklappen mit kreiszylindrischem Staublech*, 1971, vergriffen

19 Kuz, Klaus Dieter: *Ein Beitrag zur Frage des Einsetzens von Kavitationserscheinungen in einer Düsenströmung bei Berücksichtigung der im Wasser gelösten Gase*, 1971, vergriffen

20 Schaak, Hartmut: *Verteilleitungen von Wasserkraftanlagen*, 1971

21 *Sonderheft zur Eröffnung der neuen Versuchsanstalt des Instituts für Wasserbau der Universität Stuttgart mit Beiträgen von*
Brombach, Hansjörg; Dirksen, Wolfram; Gàl, Attila; Gerlach, Reinhard; Giesecke, Jürgen; Holthoff, Franz-Josef; Kuz, Klaus Dieter; Marotz, Günter; Minor, Hans-Erwin; Petrikat, Kurt; Röhnisch, Arthur; Rueff, Helge; Schwarz, Helmut; Vollmer, Ernst; Wildenhahn, Eberhard; 1972

22 Wang, Chung-su: *Ein Beitrag zur Berechnung der Schwingungen an Kegelstrahlschiebern*, 1972

23 Mayer-Vorfelder, Hans-Jörg: *Erdwiderstandsbeiwerte nach dem Ohde-Variationsverfahren*, 1972

24 Minor, Hans-Erwin: *Beitrag zur Bestimmung der Schwingungsanfachungsfunktionen überströmter Stauklappen*, 1972, vergriffen

25 Brombach, Hansjörg: *Untersuchung strömungsmechanischer Elemente (Fluidik) und die Möglichkeit der Anwendung von Wirbelkammerelementen im Wasserbau*, 1972, vergriffen

26 Wildenhahn, Eberhard: *Beitrag zur Berechnung von Horizontalfilterbrunnen*, 1972

27 Steinlein, Helmut: *Die Eliminierung der Schwebstoffe aus Flußwasser zum Zweck der unterirdischen Wasserspeicherung, gezeigt am Beispiel der Iller*, 1972

28 Holthoff, Franz Josef: *Die Überwindung großer Hubhöhen in der Binnenschiffahrt durch Schwimmerhebewerke*, 1973

29 Röder, Karl: *Einwirkungen aus Baugrundbewegungen auf trog- und kastenförmige Konstruktionen des Wasser- und Tunnelbaues*, 1973

30 Kretschmer, Heinz: *Die Bemessung von Bogenstaumauern in Abhängigkeit von der Talform*, 1973

31 Honekamp, Hermann: *Beitrag zur Berechnung der Montage von Unterwasserpipelines*, 1973

32 Giesecke, Jürgen: *Die Wirbelkammertriode als neuartiges Steuerorgan im Wasserbau*, und
Brombach, Hansjörg: *Entwicklung, Bauformen, Wirkungsweise und Steuereigenschaften von Wirbelkammerverstärkern*, 1974

33 Rueff, Helge: *Untersuchung der schwingungserregenden Kräfte an zwei hintereinander angeordneten Tiefschützen unter besonderer Berücksichtigung von Kavitation*, 1974

34 Röhnisch, Arthur: *Einpreßversuche mit Zementmörtel für Spannbeton - Vergleich der Ergebnisse von Modellversuchen mit Ausführungen in Hüllwellrohren*, 1975

35 *Sonderheft anläßlich des 65. Geburtstages von Prof. Dr.-Ing. Kurt Petrikat mit Beiträgen von*: Brombach, Hansjörg; Erbel, Klaus; Flinspach, Dieter; Fischer jr., Richard; Gàl, Attila; Gerlach, Reinhard; Giesecke, Jürgen; Haberhauer, Robert; Hafner Edzard; Hausenblas, Bernhard; Horlacher, Hans-Burkhard; Hutarew, Andreas; Knoll, Manfred; Krummet, Ralph; Marotz, Günter; Merkle, Theodor; Miller, Christoph; Minor, Hans-Erwin; Neumayer, Hans; Rao, Syamala; Rath, Paul; Rueff, Helge; Ruppert, Jürgen; Schwarz, Wolfgang; Topal-Gökceli, Mehmet; Vollmer, Ernst; Wang, Chung-su; Weber, Hans-Georg; 1975

36 Berger, Jochum: *Beitrag zur Berechnung des Spannungszustandes in rotationssymmetrisch belasteten Kugelschalen veränderlicher Wandstärke unter Gas- und Flüssigkeitsdruck durch Integration schwach singulärer Differentialgleichungen*, 1975

37 Dirksen, Wolfram: *Berechnung instationärer Abflußvorgänge in gestauten Gerinnen mittels Differenzenverfahren und die Anwendung auf Hochwasserrückhaltebecken*, 1976

38 Horlacher, Hans-Burkhard: *Berechnung instationärer Temperatur- und Wärmespannungsfelder in langen mehrschichtigen Hohlzylindern*, 1976

39 Hafner, Edzard: *Untersuchung der hydrodynamischen Kräfte auf Baukörper im Tiefwasserbereich des Meeres*, 1977, ISBN 3-921694-39-6

40 Ruppert, Jürgen: *Über den Axialwirbelkammerverstärker für den Einsatz im Wasserbau*, 1977, ISBN 3-921694-40-X

41 Hutarew, Andreas: *Beitrag zur Beeinflußbarkeit des Sauerstoffgehalts in Fließgewässern an Abstürzen und Wehren*, 1977, ISBN 3-921694-41-8, vergriffen

42 Miller, Christoph: *Ein Beitrag zur Bestimmung der schwingungserregenden Kräfte an unterströmten Wehren*, 1977, ISBN 3-921694-42-6

43 Schwarz, Wolfgang: *Druckstoßberechnung unter Berücksichtigung der Radial- und Längsverschiebungen der Rohrwandung*, 1978, ISBN 3-921694-43-4

44 Kinzelbach, Wolfgang: *Numerische Untersuchungen über den optimalen Einsatz variabler Kühlsysteme einer Kraftwerkskette am Beispiel Oberrhein*, 1978, ISBN 3-921694-44-2

45 Barczewski, Baldur: *Neue Meßmethoden für Wasser-Luftgemische und deren Anwendung auf zweiphasige Auftriebsstrahlen*, 1979, ISBN 3-921694-45-0

46 Neumayer, Hans: *Untersuchung der Strömungsvorgänge in radialen Wirbelkammerverstärkern*, 1979, ISBN 3-921694-46-9

47 Elalfy, Youssef-Elhassan: *Untersuchung der Strömungsvorgänge in Wirbelkammerdioden und -drosseln*, 1979, ISBN 3-921694-47-7

48 Brombach, Hansjörg: *Automatisierung der Bewirtschaftung von Wasserspeichern*, 1981, ISBN 3-921694-48-5

49 Geldner, Peter: *Deterministische und stochastische Methoden zur Bestimmung der Selbstdichtung von Gewässern*, 1981, ISBN 3-921694-49-3, vergriffen

50 Mehlhorn, Hans: *Temperaturveränderungen im Grundwasser durch Brauchwassereinleitungen*, 1982, ISBN 3-921694-50-7, vergriffen

51 Hafner, Edzard: *Rohrleitungen und Behälter im Meer*, 1983, ISBN 3-921694-51-5

52 Rinnert, Bernd: *Hydrodynamische Dispersion in porösen Medien: Einfluß von Dichteunterschieden auf die Vertikalvermischung in horizontaler Strömung*, 1983, ISBN 3-921694-52-3, vergriffen

53 Lindner, Wulf: *Steuerung von Grundwasserentnahmen unter Einhaltung ökologischer Kriterien*, 1983, ISBN 3-921694-53-1, vergriffen

54 Herr, Michael; Herzer, Jörg; Kinzelbach, Wolfgang; Kobus, Helmut; Rinnert, Bernd: *Methoden zur rechnerischen Erfassung und hydraulischen Sanierung von Grundwasserkontaminationen*, 1983, ISBN 3-921694-54-X

55 Schmitt, Paul: *Wege zur Automatisierung der Niederschlagsermittlung*, 1984, ISBN 3-921694-55-8, vergriffen

56 Müller, Peter: *Transport und selektive Sedimentation von Schwebstoffen bei gestau tem Abfluß*, 1985, ISBN 3-921694-56-6

57 El-Qawasmeh, Fuad: *Möglichkeiten und Grenzen der Tropfbewässerung unter besonderer Berücksichtigung der Verstopfungsanfälligkeit der Tropfelemente*, 1985, ISBN 3-921694-57-4, vergriffen

58 Kirchenbaur, Klaus: *Mikroprozessorgesteuerte Erfassung instationärer Druckfelder am Beispiel seegangsbelasteter Baukörper*, 1985, ISBN 3-921694-58-2

59 Kobus, Helmut (Hrsg.): *Modellierung des großräumigen Wärme- und Schadstofftransports im Grundwasser*, Tätigkeitsbericht 1984/85 (DFG-Forschergruppe an den Universitäten Hohenheim, Karlsruhe und Stuttgart), 1985, ISBN 3-921694-59-0, vergriffen

60 Spitz, Karlheinz: *Dispersion in porösen Medien: Einfluß von Inhomogenitäten und Dichteunterschieden*, 1985, ISBN 3-921694-60-4, vergriffen

61 Kobus, Helmut: *An Introduction to Air-Water Flows in Hydraulics*, 1985, ISBN 3-921694-61-2

62 Kaleris, Vassilios: *Erfassung des Austausches von Oberflächen- und Grundwasser in horizontalebenen Grundwassermodellen*, 1986, ISBN 3-921694-62-0

63 Herr, Michael: *Grundlagen der hydraulischen Sanierung verunreinigter Porengrundwasserleiter*, 1987, ISBN 3-921694-63-9

64 Marx, Walter: *Berechnung von Temperatur und Spannung in Massenbeton infolge Hydratation*, 1987, ISBN 3-921694-64-7

65 Koschitzky, Hans-Peter: *Dimensionierungskonzept für Sohlbelüfter in Schußrinnen zur Vermeidung von Kavitationsschäden*, 1987, ISBN 3-921694-65-5

66 Kobus, Helmut (Hrsg.): *Modellierung des großräumigen Wärme- und Schadstofftransports im Grundwasser*, Tätigkeitsbericht 1986/87 (DFG-Forschergruppe an den Universitäten Hohenheim, Karlsruhe und Stuttgart) 1987, ISBN 3-921694-66-3

67 Söll, Thomas: *Berechnungsverfahren zur Abschätzung anthropogener Temperaturanomalien im Grundwasser*, 1988, ISBN 3-921694-67-1

68 Dittrich, Andreas; Westrich, Bernd: *Bodenseeufererosion, Bestandsaufnahme und Bewertung*, 1988, ISBN 3-921694-68-X, vergriffen

69 Huwe, Bernd; van der Ploeg, Rienk R.: *Modelle zur Simulation des Stickstoffhaushaltes von Standorten mit unterschiedlicher landwirtschaftlicher Nutzung*, 1988, ISBN 3-921694-69-8, vergriffen

70 Stephan, Karl: *Integration elliptischer Funktionen*, 1988, ISBN 3-921694-70-1

71 Kobus, Helmut; Zilliox, Lothaire (Hrsg.): *Nitratbelastung des Grundwassers, Auswirkungen der Landwirtschaft auf die Grundwasser- und Rohwasserbeschaffenheit und Maßnahmen zum Schutz des Grundwassers*. Vorträge des deutsch-französischen Kolloquiums am 6. Oktober 1988, Universitäten Stuttgart und Louis Pasteur Strasbourg (Vorträge in deutsch oder französisch, Kurzfassungen zweisprachig), 1988, ISBN 3-921694-71-X

72 Soyeaux, Renald: *Unterströmung von Stauanlagen auf klüftigem Untergrund unter Berücksichtigung laminarer und turbulenter Fließzustände*,1991,ISBN 3-921694-72-8

73 Kohane, Roberto: *Berechnungsmethoden für Hochwasserabfluß in Fließgewässern mit überströmten Vorländern*, 1991, ISBN 3-921694-73-6

74 Hassinger, Reinhard: *Beitrag zur Hydraulik und Bemessung von Blocksteinrampen in flexibler Bauweise*, 1991, ISBN 3-921694-74-4, vergriffen

75 Schäfer, Gerhard: *Einfluß von Schichtenstrukturen und lokalen Einlagerungen auf die Längsdispersion in Porengrundwasserleitern*, 1991, ISBN 3-921694-75-2

76 Giesecke, Jürgen: *Vorträge, Wasserwirtschaft in stark besiedelten Regionen; Umweltforschung mit Schwerpunkt Wasserwirtschaft*, 1991, ISBN 3-921694-76-0

77 Huwe, Bernd: *Deterministische und stochastische Ansätze zur Modellierung des Stickstoffhaushalts landwirtschaftlich genutzter Flächen auf unterschiedlichem Skalenniveau*, 1992, ISBN 3-921694-77-9, vergriffen

78 Rommel, Michael: *Verwendung von Kluftdaten zur realitätsnahen Generierung von Kluftnetzen mit anschließender laminar-turbulenter Strömungsberechnung*, 1993, ISBN 3-92 1694-78-7

79 Marschall, Paul: *Die Ermittlung lokaler Stofffrachten im Grundwasser mit Hilfe von Einbohrloch-Meßverfahren*, 1993, ISBN 3-921694-79-5, vergriffen

80 Ptak, Thomas: *Stofftransport in heterogenen Porenaquiferen: Felduntersuchungen und stochastische Modellierung*, 1993, ISBN 3-921694-80-9, vergriffen

81 Haakh, Frieder: *Transientes Strömungsverhalten in Wirbelkammern,* 1993, ISBN 3-921694-81-7

82 Kobus, Helmut; Cirpka, Olaf; Barczewski, Baldur; Koschitzky, Hans-Peter: *Versuchseinrichtung zur Grundwasser und Altlastensanierung VEGAS, Konzeption und Programmrahmen*, 1993, ISBN 3-921694-82-5

83 Zang, Weidong: *Optimaler Echtzeit-Betrieb eines Speichers mit aktueller Abflußregenerierung*, 1994, ISBN 3-921694-83-3, vergriffen

84 Franke, Hans-Jörg: *Stochastische Modellierung eines flächenhaften Stoffeintrages und Transports in Grundwasser am Beispiel der Pflanzenschutzmittelproblematik*, 1995, ISBN 3-921694-84-1

85 Lang, Ulrich: *Simulation regionaler Strömungs- und Transportvorgänge in Karstaquiferen mit Hilfe des Doppelkontinuum-Ansatzes: Methodenentwicklung und Parameteridentifikation*, 1995, ISBN 3-921694-85-X, vergriffen

86 Helmig, Rainer: *Einführung in die Numerischen Methoden der Hydromechanik*, 1996, ISBN 3-921694-86-8, vergriffen

87 Cirpka, Olaf: *CONTRACT: A Numerical Tool for Contaminant Transport and Chemical Transformations - Theory and Program Documentation* -, 1996, ISBN 3-921694-87-6

88 Haberlandt, Uwe: *Stochastische Synthese und Regionalisierung des Niederschlages für Schmutzfrachtberechnungen*, 1996, ISBN 3-921694-88-4

89 Croisé, Jean: *Extraktion von flüchtigen Chemikalien aus natürlichen Lockergesteinen mittels erzwungener Luftströmung*, 1996, ISBN 3-921694-89-2

90 Jorde, Klaus: *Ökologisch begründete, dynamische Mindestwasserregelungen bei Ausleitungskraftwerken*, 1997, ISBN 3-921694-90-6

91 Helmig, Rainer: *Gekoppelte Strömungs- und Transportprozesse im Untergrund - Ein Beitrag zur Hydrosystemmodellierung-*, 1998, ISBN 3-921694-91-4

92 Emmert, Martin: *Numerische Modellierung nichtisothermer Gas-Wasser Systeme in porösen Medien*, 1997, ISBN 3-921694-92-2

93 Kern, Ulrich: *Transport von Schweb- und Schadstoffen in staugeregelten Fließgewässern am Beispiel des Neckars*, 1997, ISBN 3-921694-93-0

94 Förster, Georg: *Druckstoßdämpfung durch große Luftblasen in Hochpunkten von Rohrleitungen 1997*, ISBN 3-921694-94-9

95 Cirpka, Olaf: *Numerische Methoden zur Simulation des reaktiven Mehrkomponententransports im Grundwasser*, 1997, ISBN 3-921694-95-7

96 Färber, Arne: *Wärmetransport in der ungesättigten Bodenzone: Entwicklung einer thermischen In-situ-Sanierungstechnologie*, 1997, ISBN 3-921694-96-5

97 Betz, Christoph: *Wasserdampfdestillation von Schadstoffen im porösen Medium: Entwicklung einer thermischen In-situ-Sanierungstechnologie*, 1998, ISBN 3-921694-97-3

98 Xu, Yichun: *Numerical Modeling of Suspended Sediment Transport in Rivers*, 1998, ISBN 3-921694-98-1, vergriffen

99 Wüst, Wolfgang: *Geochemische Untersuchungen zur Sanierung CKW-kontaminierter Aquifere mit Fe(0)-Reaktionswänden,* 2000, ISBN 3-933761-02-2

100 Sheta, Hussam: *Simulation von Mehrphasenvorgängen in porösen Medien unter Einbeziehung von Hysterese-Effekten*, 2000, ISBN 3-933761-03-4

101 Ayros, Edwin: *Regionalisierung extremer Abflüsse auf der Grundlage statistischer Verfahren*, 2000, ISBN 3-933761-04-2, vergriffen

102 Huber, Ralf: *Compositional Multiphase Flow and Transport in Heterogeneous Porous Media*, 2000, ISBN 3-933761-05-0

103 Braun, Christopherus: *Ein Upscaling-Verfahren für Mehrphasenströmungen in porösen Medien*, 2000, ISBN 3-933761-06-9

104 Hofmann, Bernd: *Entwicklung eines rechnergestützten Managementsystems zur Beurteilung von Grundwasserschadensfällen*, 2000, ISBN 3-933761-07-7

105 Class, Holger: *Theorie und numerische Modellierung nichtisothermer Mehrphasenprozesse in NAPL-kontaminierten porösen Medien,* 2001, ISBN 3-933761-08-5

106 Schmidt, Reinhard: *Wasserdampf- und Heißluftinjektion zur thermischen Sanierung kontaminierter Standorte*, 2001, ISBN 3-933761-09-3

107 Reinhold Josef:, *Schadstoffextraktion mit hydraulischen Sanierungsverfahren unter Anwendung von grenzflächenaktiven Stoffen*, 2001, ISBN 3-933761-10-7

108 Schneider, Matthias: *Habitat- und Abflussmodellierung für Fließgewässer mit unscharfen Berechnungsansätzen*, 2001, ISBN 3-933761-11-5

109 Rathgeb, Andreas: *Hydrodynamische Bemessungsgrundlagen für Lockerdeckwerke an überströmbaren Erddämmen*, 2001, ISBN 3-933761-12-3

110 Lang, Stefan: *Parallele numerische Simulation instätionärer Probleme mit adaptiven Methoden auf unstrukturierten Gittern*, 2001, ISBN 3-933761-13-1

111 Appt, Jochen; Stumpp Simone: *Die Bodensee-Messkampagne 2001, IWS/CWR Lake Constance Measurement Program 2001*, 2002, ISBN 3-933761-14-X

112 Heimerl, Stephan: *Systematische Beurteilung von Wasserkraftprojekten,* 2002, ISBN 3-933761-15-8

113 Iqbal, Amin: *On the Management and Salinity Control of Drip Irrigation,* 2002, ISBN 3-933761-16-6

114 Silberhorn-Hemminger, Annette: *Modellierung von Kluftaquifersystemen: Geostatistische Analyse und deterministisch-stochastische Kluftgenerierung,* 2002, ISBN 3-933761-17-4

115 Winkler, Angela: *Prozesse des Wärme- und Stofftransports bei der In-situ-Sanierung mit festen Wärmequellen,* 2003, ISBN 3-933761-18-2

116 Marx, Walter: *Wasserkraft, Bewässerung, Umwelt - Planungs- und Bewertungsschwerpunkte der Wasserbewirtschaftung,* 2003, ISBN 3-933761-19-0

117 Hinkelmann, Reinhard: *Efficient Numerical Methods and Information-Processing Techniques in Environment Water,* 2003, ISBN 3-933761-20-4

118 Samaniego-Eguiguren, Luis Eduardo: *Hydrological Consequences of Land Use / Land Cover and Climatic Changes in Mesoscale Catchments*, 2003, ISBN 3-933761-21-2

119 Neunhäuserer, Lina: *Diskretisierungsansätze zur Modellierung von Strömungs- und Transportprozessen in geklüftet-porösen Medien*, 2003, ISBN 3-933761-22-0

120 Paul, Maren: *Simulation of Two-Phase Flow in Heterogeneous Poros Media with Adaptive Methods*, 2003, ISBN 3-933761-23-9

121 Ehret, Uwe: *Rainfall and Flood Nowcasting in Small Catchments using Weather Radar*, 2003, ISBN 3-933761-24-7

122 Haag, Ingo: *Der Sauerstoffhaushalt staugeregelter Flüsse am Beispiel des Neckars - Analysen, Experimente, Simulationen -,* 2003, ISBN 3-933761-25-5

123 Appt, Jochen: *Analysis of Basin-Scale Internal Waves in Upper Lake Constance,* 2003, ISBN 3-933761-26-3

124 Hrsg.: Schrenk, Volker; Batereau, Katrin; Barczewski, Baldur; Weber, Karolin und Koschitzky, Hans-Peter: *Symposium Ressource Fläche und VEGAS - Statuskolloquium 2003, 30. September und 1. Oktober 2003,* 2003, ISBN 3-933761-27-1

125 Omar Khalil Ouda: *Optimisation of Agricultural Water Use: A Decision Support System for the Gaza Strip,* 2003, ISBN 3-933761-28-0

126 Batereau, Katrin: *Sensorbasierte Bodenluftmessung zur Vor-Ort-Erkundung von Schadensherden im Untergrund*, 2004, ISBN 3-933761-29-8

127 Witt, Oliver: *Erosionsstabilität von Gewässersedimenten mit Auswirkung auf den Stofftransport bei Hochwasser am Beispiel ausgewählter Stauhaltungen des Oberrheins*, 2004, ISBN 3-933761-30-1

128 Jakobs, Hartmut: *Simulation nicht-isothermer Gas-Wasser-Prozesse in komplexen Kluft-Matrix-Systemen*, 2004, ISBN 3-933761-31-X

129 Li, Chen-Chien: *Deterministisch stochastisches Berechnungskonzept zur Beurteilung der Auswirkungen erosiver Hochwasserereignisse in Flussstauhaltungen,* 2004, ISBN 3-933761-32-8

130 Reichenberger, Volker; Helmig, Rainer; Jakobs, Hartmut; Bastian, Peter; Niessner, Jennifer: *Complex Gas-Water Processes in Discrete Fracture-Matrix Systems Upscaling, Mass-Conservative Discretization and Efficient Multilevel Solution,* 2004, ISBN 3-933761-33-6

131 Hrsg.: Barczewski, Baldur; Koschitzky, Hans-Peter; Weber, Karolin; Wege, Ralf: *VEGAS - Statuskolloquium 2004,* 5. Oktober 2004, 2004, ISBN 3-933761-34-4

132 Asie, Kemal Jabir: *Finite Volume Models for Multiphase Multicomponent Flow through Porous Media*. 2005, ISBN 3-933761-35-2

133 Jacoub, George: *Development of a 2-D Numerical Module for Particulate Contaminant Transport in Flood Retention Reservoirs and Impounded Rivers,* 2004, ISBN 3-933761-36-0

134 Nowak, Wolfgang: *Geostatistical Methods for the Identification of Flow and Transport Parameters in the Subsurface,* 2005, ISBN 3-933761-37-9

135 Süß, Mia: *Analysis of the influence of structures and boundaries on flow and transport processes in fractured porous media*, 2005, ISBN 3-933761-38-7

136 Jose, Surabhin Chackiath: *Experimental Investigations on Longitudinal Dispersive Mixing in Heterogeneous Aquifers,* 2005, ISBN: 3-933761-39-5

137 Filiz, Fulya: *Linking Large-Scale Meteorological Conditions to Floods in Mesoscale Catchments,* 2005, ISBN 3-933761-40-9

138 Qin, Minghao: *Wirklichkeitsnahe und recheneffiziente Ermittlung von Temperatur und Spannungen bei großen RCC-Staumauern*, 2005, ISBN 3-933761-41-7

139 Kobayashi, Kenichiro: *Optimization Methods for Multiphase Systems in the Subsurface - Application to Methane Migration in Coal Mining Areas*, 2005, ISBN 3-933761-42-5